CRANFIELD UNIVERSITY

N. Qazi

MODELLING OF AN AXIAL FLOW COMPACT SEPARATOR USING NEURAL NETWORK

SCHOOL OF ENGINEERING

PHD THESIS

CRANFIELD UNIVERSITY

School of Engineering
Department of Process and Systems Engineering

PHD THESIS

Academic Year 2008 - 2009

Nadeem Qazi

Modelling of an axial flow compact separator using neural network

Supervisor: Dr. H. Yeung

May 2009

This thesis is submitted in partial fulfilment of the requirements for the degree of Doctor of Philosophy

Abstract

A novel design axial flow cyclonic separator called I-SEP was tested with an extensive set of experiments using air-water two phase flow mixture at atmospheric pressure. These experiments provided valuable data on the separation efficiency and pressure drop under different inlet conditions. The performance parameters i.e. Gas Carry Under (GCU) and Liquid Carry Over (LCO) were found to be non-linearly related to the inlet operating conditions. However it was found that resistance on the tangential outlet of the I-SEP affects the GCU and that manipulating the pressure difference between the two outlets and the inlet of the I-SEP through manual control valves, the GCU could be controlled.

The separator was also extensively tested and compared with a gravity separator, when they were placed at the exit of a riser, in severe slugging condition frequently encountered in the production pipe work from some oil fields. The tests revealed that the I-SEP has better tendency to suppress severe slugging as compared to the gravity separator.

A framework for neural network based on multiple types of input was also developed to model the separation performance of the I-SEP. Mutual Information (one of the key elements of the information theory) was applied to select the appropriate candidate input variables to the neural network framework. This framework was then used to develop a neural network model based on dimensionless input parameters such as pressure coefficient. This neural network model produced satisfactory prediction on unseen experimental data.

The inverse function of a trained neural network was combined with a PID controller in a closed loop to control the GCU and LCO at a given set point by predicting the manipulating variable i.e. pressure at the I-SEP outlets. This control scheme was simulated using the test data. Such controller could be used to assist the operator in maintaining and controlling the GCU or LCO at the I-SEP outlets.

The work performed during this study also includes the development of a data repository system to store and query the experimental result. An internet based framework is also developed that allows remote access of the experimental data using internet or wireless mobile devices.

Acknowledgements

I would like to take this space to extend my appreciation and gratitude to the following people as without their constant support and guidance I may very well not have written this thesis.

First and foremost, I am very much indebted to my research project supervisor Dr Hoi Yeung for his advice and support in this research. Great Credit should go to him as his encouragement has kept me focused throughout my research.

My special thanks for Dr. Yi Cao for his valuable and helpful technical suggestions. I really appreciate his help and time whenever it is needed. He has been very helpful in completion of this thesis.

I am also thankful to Department of Process and System Engineering, Cranfield University and Iqbal Charity trust for funding my research studies

I want to give my sincere thanks to Sam Skears in the Department of PASE. I also want to thank my fellow doctoral students.

I am indebted to my little angel Humd who has been a source of happiness for me during my studies. My sincere thanks to my wife Shazia for her cooperation and support during the study. Finally, many thanks to my family including my Amee and Abu uncle, brothers and sisters for their prayers.

List of Figures

List of Tables

Nomenclature

A. Symbols

a	Scalar output of neuron
a_c	Centrifugal acceleration
A	Area of cross section (m^2)
A^{inlet}	Inlet area of I-SEP (m^2)
b	Bias
d	Diameter of the particle (mm)
$d_{d,\min}$	Minimum diameter of the separated droplet (m)
D	Diameter of the separator (mm)
D_{vf}	Diameter of the vortex finder (mm)
f	Transfer function
F	scale factor in ANN
F_l	Amount of the liquid fraction coming out from the underflow (%)
F_g	Amount of the gas fraction coming out from the underflow (%)
g	Acceleration due to gravity (m/s^2)
G	Mass flux (kg/m^2-s)
G_UF	Percentage of gas coming out of tangential outlet in single phase gas flow (%)
G_OF	Percentage of gas coming out of axial outlet in single phase gas flow (%)
h	Height (m)
h_n	Hidden neuron
H	Total height of separator (m)
H_{GS}	Distance it travelled before falling (m)
K_{12}	Loss coefficient between inlet and axial outlet in single phase flow
L	Characteristic length of I-SEP (m)
L_{GS}	Horizontal distance travelled by the liquid droplet in gravity separator (m)
L_OF	Percentage of liquid coming out of axial outlet in single phase liquid flow (%)

L_UF Percentage of liquid coming out of tangential outlet in single phase liquid flow (%)

m mass flow of the gas or liquid at the outlet of the separator (kg/s)

m_t^g mass flow rate of gas at tangential outlet of the separator (kg/s)

m_t^l Mass flow rate of liquid at tangential outlet of the separator (kg/s)

m_a^g Mass flow rate of gas at axial outlet of the separator (kg/s)

m_a^l Mass flow rate of liquid at axial outlet of the separator (kg/s)

M molecular weight of the gas

M_{sg} mass flow rate of the liquid observed during the cycle (kg/s)

n number of moles

N total number of the participant neural network in the combined model

N_e Number of turns

N_s Number of the spiral turns particle take on its way towards exit of the cyclone

p Pressure (bar)

P_k Process component vector of the combined output vector

P_{inlet} Pressure at inlet of separator (bar)

P_a Pressure at the axial outlet of the I-SEP (bar)

P_t Pressure at the tangential outlet of the I-SEP (bar)

P_{12} Pressure drop between inlet and tangential outlet of the I-SEP (bar)

P_{13} Pressure drop between inlet and axial outlet of the I-SEP (bar)

Q Volumetric flow rate in (m^3/s)

Q_a^g Volumetric flow rate of the gas at axial outlet of the I-SEP (m^3/s)

Q_t^g Volumetric flow rate of the gas at tangential outlet of the I-SEP (m^3/s)

Q_t^l Volumetric flow rate of the liquid at tangential outlet of the I-SEP (m^3/s)

Q_{ta}^l Actual liquid flow rate measured at tangential outlet of HISEP (m^3/s)

r Radius within the cyclone (mm)

r^{inlet} Inlet radius of I-SEP (mm)

r_{vf} Radius of vortex finder (mm)

R	Gas Constant
S	Minimum separation parameter
Stk	Stokes Number
t	Time of the severe slugging cycle (s)
T	Temperature (K)
T_a	Temperature at the axial outlet of the I-SEP (Kelvin)
T_t	Temperature at the tangential outlet of the I-SEP (Kelvin)
U_{GS}	Superficial gas velocity in the gravity separator (m/s)
U_{LS}	Superficial liquid velocity in the gravity separator (m/s)
v	Voltage measured by the sensing device (volts)
v_f	final value of voltage corresponding to last value of physical quantity (volts)
vi	Initial value of the voltage observed at given initial value of the physical Vin inlet velocity (volts)
V_g	Volume of gas in separator measured in (m3)
V_g	Average velocity of the gas at inlet (m/s)
V_{in}	Inlet velocity (m/s)
V_r	Radial velocity component (m/s)
V_t	Tangential velocity component (m/s)
V_{tmix}	Tangential mixture velocity (m/s)
V	Measurement White noise vector.
W	Width of the inlet duct (m)
W	Process White noise vector
w_n	Weights of neurons
x_n	inputs
X_{50}	Cut size diameter of heavier particle (μm)
y	Measured output in ANN
Y	Physical quantity being measured
Y_c	Output vector of the combined model
Y_i	Initial value of the physical quantity

Y_f Final value of the physical quantity used during the calibration of the device.

Z_o Vortex length or effective cyclone length

$I(X;Y)$ Mutual information of random variable X and Y

$p(a,b)$ Joint probability distribution function of X and Y

$p(a)$ Marginal probability distribution functions of X.

$p(b)$ Marginal probability distribution functions of X

ρ Density (kg/m^3)

ρ_p Density of the particle (kg/m^3)

ρ_f Density of the fluid i.e. gas in this case (kg/m^3)

ρ_g Density of gas measure (kg/m^3)

μ Viscosity of the fluid (Pa-s)

ϕ Two phase multiplier obtained using the homogeneous flow model

η_l Liquid separation efficiency (%)

η_g Gas separation efficiency (%)

ΔP Pressure drop between inlet and outlet of the separator (bar)

B. Subscripts

a axial
g gas
l liquid
t tangential
gin gas in
gout gas out
inlet inlet area of I-SEP
lin liquid in
lout liquid out
GS superficial gas velocity
LS superficial liquid velocity
vf vortex finder

C. Acronyms

ACF Auto Correlation Function

AFC Axial Flow Cyclone

ANN	Artificial Neural Network
ANNs	Artificial Neural Networks
AAPE	Absolute Average Percentage Error
CAPEX	Capital Expenditure
CFB	Circulating Fluidized Bed
CFD	Computational Fluid Dynamics
CV	Control Valve
DAQ	Data Acquisition System
DP	Differential Pressure
Eu	Euler Number
FAD	Free Air Delivery
FM	Flow Meter
GCU	Gas Carry Under
GCV	Gas Control Valve
G-L	Gas-Liquid
GLCC	Gas-Liquid Cylindrical Cyclone
GVF	Gas Volume Fraction
HI-SEP	Gravity Separator
ID	Internal Diameter
I-SEP	Compact Axial Flow Separator
KM	KALMAN FILTER
LCO	Liquid Carry Over
LCV	Liquid Control Valve
MD	Mass Difference
MLP	Multi-Layer Preceptron
MI	Mutual Information
NSS	Non Severe Slugging
OPEX	Operational Expenditure
PCA	Process Component Analysis
PDF	Probability Density Function
P&ID	Process and Instrumentation Diagram

PSD	Power Spectral Density
PSDF	Power Spectral Density Function
PVT	Pressure Volume Temperature
RBP	Riser Base Pressure
RFC	Reverse-flow or tangential cyclonic separator
SCADA	Supervisory, Control and Data Acquisition
SD	Standard Deviation
SNR	Signal Noise Ratio
SS	Severe Slugging
SSE	Sum of Square Error
WAP	Wireless Access Protocol
WEB	World Wide Web
UK	United Kingdom
VASPS	Vertical Annular Separation and Pumping System

Chapter 1

Introduction

1.1 Background

As the oil and gas industry exploration moves into deeper waters, the necessity to recover hydrocarbon efficiently is getting more challenging. On the other hand the conventional multiphase flow separation equipments such as gravity separators, are centrifugal separators, are expensive especially for offshore operations. They require low design pressures due to the limitation in the maximum wall thickness in high pressure applications. This requires the choking of produced fluids for sufficient pressure drop before entering the gravitational separator causing the lost of energy from the system. Therefore design and operation of such conventional bulky topside multiphase separation systems are expensive in terms of CAPEX and OPEX, making them economically unattractive for deep waters. The issues of capital and operational costs, equipment weight and space utilisation have led the industry to explore more economically viable options. One such option is the use of compact separators with acceptable separation efficiency. However, the technology is still at the emerging stage with limited field experience in comparison to the conventional separators. Thus the major challenge to the application of compact separators has been to be able to demonstrate that the technology is not only well understood but is also able to deliver the optimised solution to the challenge emphasised above.

1.2 The Novel Design Compact Separator I-SEP

The “I-SEP” shown in Figure 1.1 is the name given to a newly design axial-flow cyclonic separator and is patented by its inventors Caltech Ltd. (UK). It is simple, compact, light weight and less expensive gas-liquid, liquid-liquid and solid-liquid separator suited for wide range applications but mainly targeted to the deep shore oil

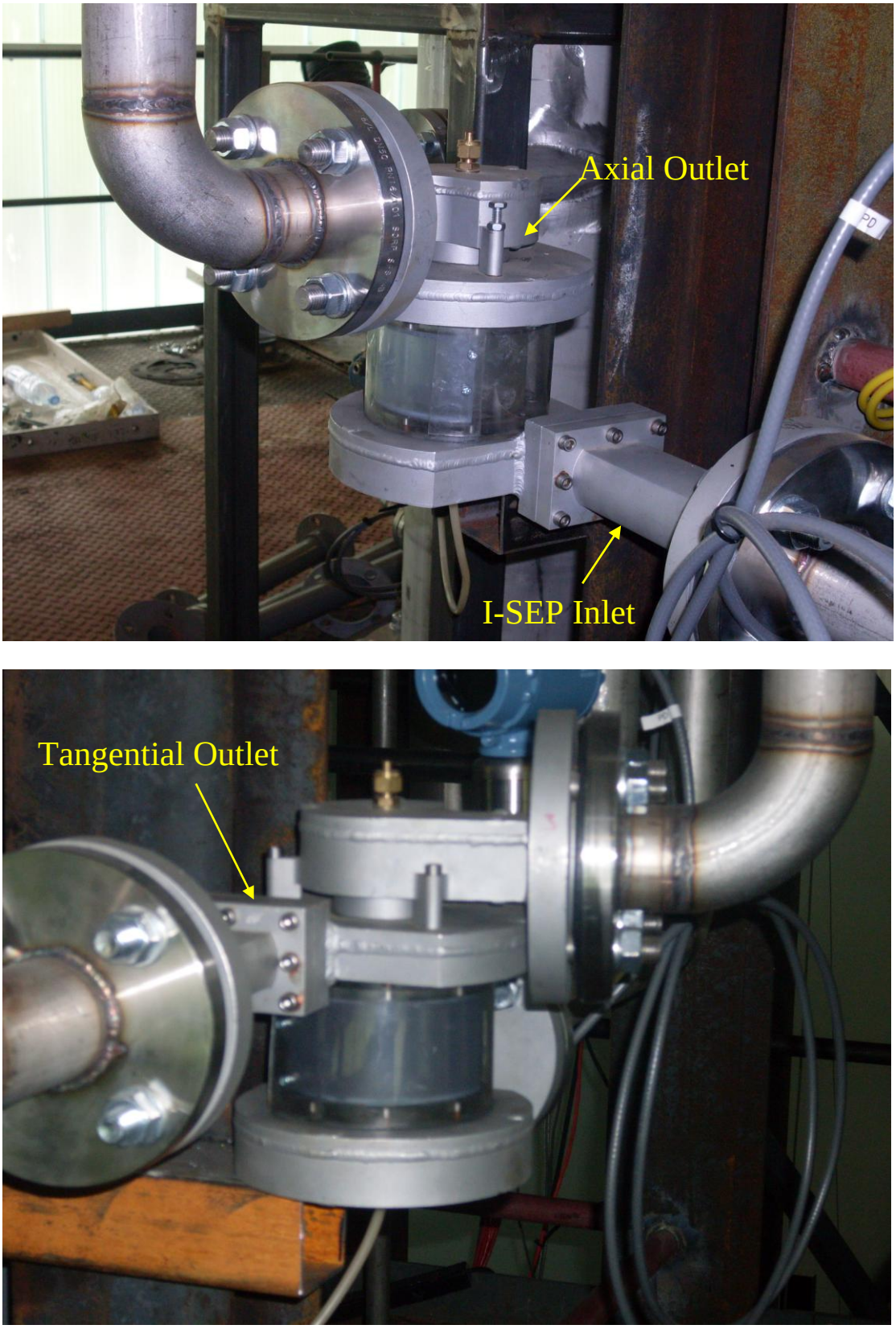

Figure 1.1 A Novel Design Axial Flow Cyclonic Separator

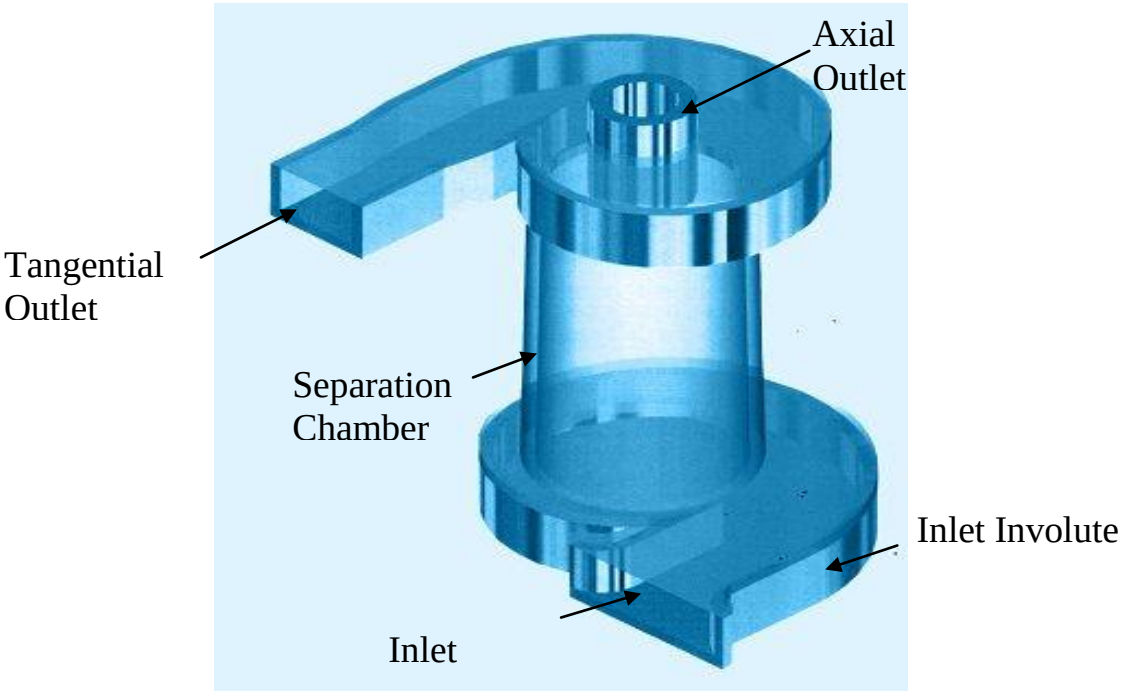

Figure 1.2 Pictorial Representation of I-SEP

and gas industry. It requires very little or no maintenance as it does not have any moving parts.

The pictorial representation of the I-SEP is shown in Figure 1.2. It can be seen that it is composed of a specially design separation chamber between a compact dual involute converting rotational energy into centrifugal force to separate particle of different density from air, water and oil. It allows both the light and dense phases to spin and move uniaxially unlike its counter reverse flow based separators in which after the tangential entry of the fluid into separator, the lighter phase moves upwards and exits via top axial outlet, whereas the denser phase spins downwards and exits the bottom outlet maintaining its tangential velocity. There is no reversal of the fluids within I-SEP, unlike the gas liquid compact separator (GLCC) and thus it benefits lower pressure drop.

I-SEP is different from other axial flow cyclones as it uses inlet involute to produces the swirl inside the separator. In detail, the fluid enters the I-SEP through an involute inlet path where it is made to spin producing high ‘g’ forces, which makes it progress

up to the separating chamber. In separating chamber, the gas-liquid separation takes place and heavier fluid moves radially outwards through tangential outlet (also referred as underflow), while lighter fluid moves axially upward towards other outlet, also known as overflow. Here the separated gas get collected via vortex finder and leaves the separator. The application of I-SEP includes:

- Full/Partial gas-liquid separation
- Knock-out liquid from wet gas
- Solid separation from gas or liquid phase
- Partial oil-water separation
- Subsea applications
- Multiphase metering
- Well testing, well clean out.

The I-SEP has successfully been used in Hoover's new vortex bagless vacuum cleaners current available in the market (Sarshar and Najam, 2001). The first underbalanced drill application of I-SEP was tested in 2000 in North Sea. It is a double I-SEP skid-mounted unit having a footprint of 2.2 **x** 2.2 meters and an overall height of six meters. After its successful trial the unit was moved offshore and was installed on Shell UK's Skiff platform for its maiden UBD operation. (Sarshar and Najam, 2001).

Another example of the I-SEP application is at wellhead where it can operate upstream of the wellhead chokes under typical pressure rating values of 5000 to 10,000 psig (Sarshar and Najam, 2001).

The separation efficiency of I-SEP is defined as a ratio of mass flow rate of the lighter and heavier phase at axial and tangential outlet respectively to the total input mass of the both liquid and gas. The separation efficiency and hence the performance of the separator is thus measured by proportion of the liquid coming out along gas through the axial outlet commonly called as Liquid Carry Over (LCO) and proportion of gas

coming along liquid through tangential outlet commonly called as Gas Carry Under (GCU). The performance of I-SEP is limited by these two phenomena, which further depends upon the gas volume fraction of the inlet mixture, mixture velocity, inlet pressure, and inlet flow regime.

The pressure drop across I-SEP inlet is another criteria used to define the separation performance of the I-SEP a lower value of which means higher separation performance.

1.3 The Problem

The performance of the I-SEP depends upon the operating pressure and volumetric flow rate of the incoming liquid and gas phases. It is one of the major requirements to be able to predict the efficiency of the I-SEP at different inlet operating conditions in order to size and design the system for a particular application.

It is known that the performance of the I-SEP can be improved by controlling the proportion of the gas in the liquid stream i.e. GCU% through throttling the control valves attached to the tangential and axial outlet of the I-SEP. This throttling of the valve creates a pressure difference between the tangential and axial outlet. The GCU % is related to this pressure difference, and a particular value of this pressure difference is required to achieve a desired GCU% under different inlet operating condition. The present Caltec `s approach to solve this problem is manual during which control valve attached to the tangential outlet of the I-SEP is manually manipulated to achieved the pressure difference for a required GCU%. However, it is a difficult and time consuming job and depends upon the operator experience as GCU % is found to be very sensitive to a small change in the pressure difference between tangential and axial outlet of I-SEP. A robust method to adjust or control these valves is needed.

Severe slugging in multiphase pipe lines connecting the platforms and subsea wells is a major and expensive problem in offshore oil production system. It results in poor separation and limits the production capacity. There are many active and passive

remedies to suppress the severe slugging. Separators have been used as a slug mitigating both as active and passive device to eliminate or reduce the severe slugging. I-SEP is now being employed in platforms such as North Sea and it is important that the performance of the I-SEP under severe slugging conditions is established.

For efficient operation, it is desirable to be able to monitor and control I-SEP performance remotely. The latest information technology tools such as internet and pocket devices such as mobiles offer this possibility.

1.4 Thesis Objectives

The aim of the research reported in the thesis was to develop solutions to the problems mentioned in section 1.3. As I-SEP is a novel compact separator not very much literature is available for the modelling of separator of this type. Thus experimental testing was required to gain some understanding of the device. With this knowledge methods of predicting and controlling its performance were sought. The objectives of the research were to:

1. Undertake experimental data collection:
    - To determine the performance of the I-SEP under different inlet condition.
    - To determine the effect of back pressure in reducing GCU in the liquid outlet stream.
    - To investigate the I-SEP behaviour during severe slugging.
2. To develop a model based on artificial neural network that could be used to predict the separation efficiency and pressure drop across the I-SEP under different inlet conditions.
3. To demonstrate the use of neural network for controlling the I-SEP performance i.e.GCU and LCO.
4. To develop a data repository system for storing all the raw data as well as performing all the calculations such as gas and liquid separation efficiency, GCU, LCO, loss coefficient, pressure drop across the I-SEP, liquid and gas superficial

velocity, mixture velocity along with gas density at all the three location of the I-SEP.

5. To develop a software platform that may be used to monitor and control the I-SEP performance remotely using wireless and wired Internet. The software platform should be able to display the performance information of the I-SEP to remote user graphically and numerically.

Figure 1.3 displays the thesis roadmap which illustrates the links in the research work carried out to fulfil above objectives.

1.5 Thesis Outline

This thesis is organized in seven chapters:

- Chapter 2 presents a state of art literature covering the gas liquid separators with their potential applications, mechanistic modelling and control studies. The second part of this literature review covers neural networks techniques used to develop forecasting model using stacked neural network.

- Chapter 3 describes the Compact separator rig, methods to infer the separation efficiency of I-SEP. It also discusses the data acquisition system along with development of a data repository system for managing the experimental data, performing calculations and displaying result. Development of internet application to access the compact separator rig remotely is also briefly discussed in this chapter. The detail about the internet application is given in Appendix A of this thesis. Additionally experiment methodology of single phase experiments along experimental analysis is also discussed in this chapter
- Chapter 4 describes the experiments performed to study the effect of operational variable such as inlet pressure, gas volume fraction of mixture and mixture velocity to investigate their effect on the separation efficiency. A

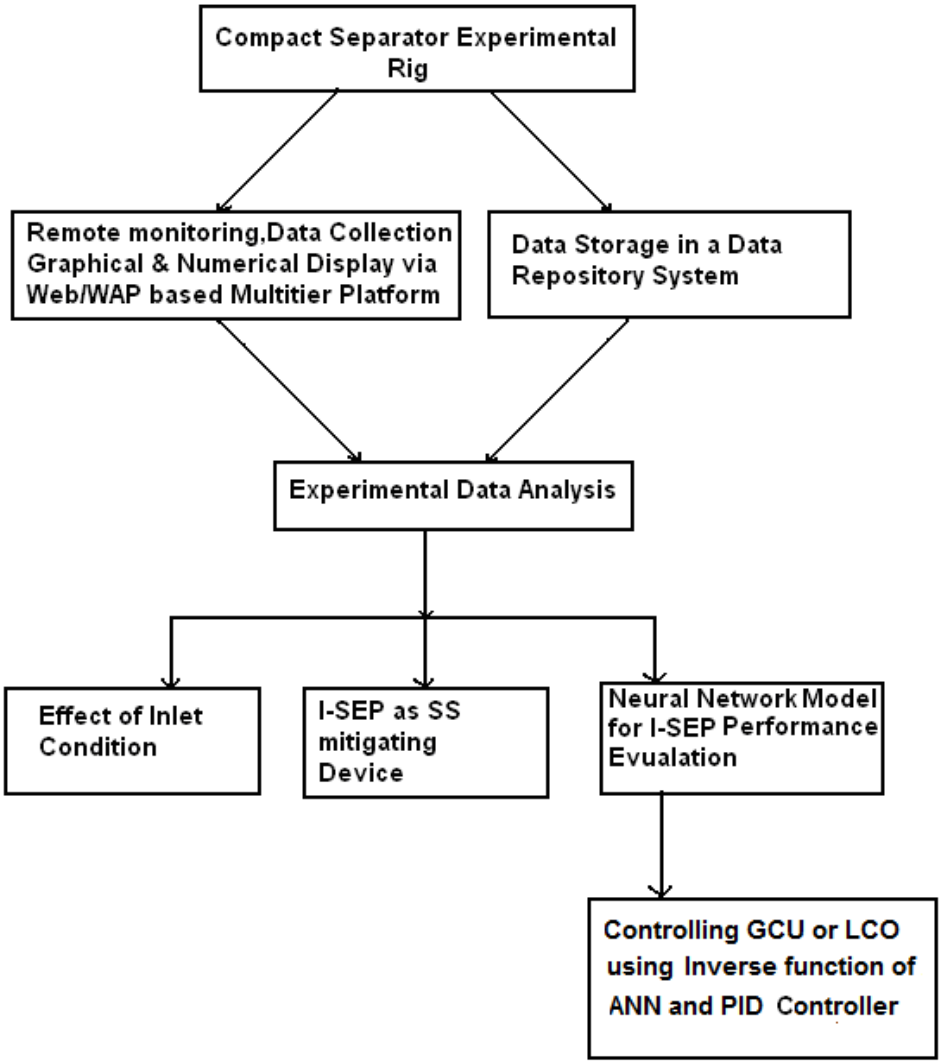

Figure 1.3 Thesis Route Map

detailed statistical analysis of the experimental result is performed to establish the performance of the I-SEP. the degree of separation of the I-SEP is established in this chapter. This chapter also compares the pressure drop comparison of I-SEP with t-junction.

- Chapter 5 discusses the experiments performed to investigate the I-SEP performance in severe slugging condition. The role of I-SEP as a topside separator on a 2 inch riser is compared with a gravity separators.

- Chapter 6: presents the development of a neural network framework to predict the separation efficiency and pressure drop of the I-SEP using stacked neural network. The chapter begins with the input feature selection and explores all the possible input candidates that could be used as input to the neural network. The model is tested both on the experimental data and synthetic data to check the accuracy of the model. This chapter also discusses the combination of inverse function of trained neural network with a PID controller in a close loop to control the GCU or LCO by predicting the manipulated variable i.e. pressure at the I-SEP outlets.
- Chapter 7: Finally concludes the thesis and discusses the future work.

Chapter 2

Literature Review

According to the requirement of the thesis work these literature review covers three different but interlink topics. First part of the literature review deals with the design and operation of compact separator followed by the methods and techniques that has been in use for identifying the flow regime in pipes, followed by control strategies used to improve the performance of the gas liquid cyclonic separator. The later section of this literature review covers neural networks techniques used to develop forecasting model using stacked neural network.

2.1 Introduction

Separation of dense phase in multiphase flow is one of the major challenging tasks in oil and gas industry. It is because crude oil emerging from the well also contains natural gas, water and some time sand. Each of these needs to be separated out for economics reason before being transported to their destination. The separation technology of heavy vessels has proved costly especially for the offshore production operations. Like any other technology, the separation technology in the 21st century is taking its shape and exploring new alternatives to the vessel type separators. Davies and Watson (1979) Davies (1984) and Oranje (1990) studied compact separators for offshore production. They showed several advantages of using a cyclone separator instead of a conventional separator. The advantages included reduction in size, weight, cost and improvement of separation performance. These compact separators can also operate on high pressure and temperature having low maintenance cost. These attributes lead to adopt the compact or inline separator as one of the suitable alternative of the bulky gravity separators.

The concept of compact separator is being applied in design of many systems for example Vertical Annular Separation and Pumping System (VASPS) which is a

patent application by the British Petroleum designed for gas- liquid subsea separation, the Gas–Liquid Cylindrical Cyclone (GLCC) which is a joint product of Chevron Petroleum Technology and Tulsa University (USA). It is a vertical pipe having tangential inlet and outlet for liquid and gas. This device offer a vast application covering from partial separation to the multiphase metering as described by Kouba and Shoham (1996)

Separators cover a vast area of application in oil and gas industry. They have used in multiphase flow metering. In this configuration the separated gas and liquid phase is metered by a single-phase flow meter installed in respective outlets of the separator. The gas and liquid legs are recombined downstream of the meters to form, two-phase flow. Pumps and desanders, portable well-testing equipment, flare gas scrubbers, slug catchers are other potential applications of gas liquid cyclone Chirinos et al. (2000). They have also been used for sub sea separation and pumping facilities Baker and Entress (1992) and in handling of slug flow in off shore platform Cowie (1992). Kvaener Process Systems and Statoil developed a compact cyclone multiphase meter. This unit, together with a microwave water-cut, coriolis flow and density measurement, and appropriate gas measurement, provided a complete well testing system in oil fields in North and South America. Another Compact separator device named as Compact separator by its developer Petrobras and the State University of Campinas (Brazil), is being used as a part of subsea boosting technology for oil production from deep water fields and can also be used as slug catcher as mentioned by Rosa et al (2001).

However the compact separation is an emerging technology and very little literature is available on the optimum design and performance of compact separators. The next section begins with the brief explanation of the related concepts in the separation technology followed by the description on mechanistic modelling of reverse flow cyclonic separator and control strategies to improve the performance of the reverse flow cyclonic separators.

2.2 Gas Liquid Separation Mechanisms

The droplet of liquid is separated from the gas stream in multiphase flow when it encounters an obstacle in the gas flow or it hits the wall of the separator. This mechanism requires application of external forces large enough to separate it from the gas stream during its residence time in the separator. The gas-liquid separation methods can be categorized in three categories:

- Sedimentation or Gravity Settling
- Diffusion
- Inertia

2.2.1 Sedimentation or Gravity Settling

This simplest form of gas-liquid separation use gravity as the main agent to separate the droplet from the gas stream. Larger slow moving particles in the gas stream are overcome by the gravity and separated from the gas. The methods require a large vessel and need high residence time for separation process. Gravity settling chambers separate droplet utilising this mechanism.

2.2.2 Diffusion

The Brownian motion show in Figure 2.1 occurs when small aerosols (less than 0.1 μm) collide with gas molecules. These collisions cause the aerosols to deviate from the fluid flow path around barriers increasing the likelihood of the aerosols striking a fibre surface and being removed. This method is generally used in separating the mixture with low liquid concentration and small particle diameter usually (<1 μm).

Figure 2.1 Brownian Motion

2.2.3 Inertia

Inertial forces are also one of the agents used in separation techniques. The liquid being heavier than gas posses more inertia offering more resistance to any change in its flow direction and hence whenever an obstacles is engineered into the flow path

as shown in Figure 2.2, separation of the phases can be achieved. Following are the different ways to achieve this type of separation.

- Meshes
- Vanes
- Centrifugal Force

Figure 2.2 Inertial Impaction

2.2.3.1 Meshes

This method uses wire mesh as an obstruction in the direction of the flow, which causes to change in the flow direction. The gas being lighter more readily changes its direction while liquid being heavier impinge on the surface. The droplets due to the coalescence grow in the numbers and eventually flow down towards a liquid line due to gravity.

2.2.3.2 Vanes

A series of parallel plates are used as obstruction, which causes the gas to change the flow path due to bends in the plate when the mixture of the gas and liquid flows between these plates. Liquid drops however being heavier impinge with the plates. This continues until enough droplets have combined to give them sufficient weight to fall out of the gas stream.

2.2.3.3 Centrifugal Force

This is most exciting and ingenious inertial method of separation causing to produce a circular motion in the particles by exerting centrifugal force on them. The centrifugal force can be several times greater than gravitational force and causes the particles to separate from gas. The centrifugal force required for this method may be generated by an external mechanical device such as swirl generator, or by the fluids. The GLCC uses tangential inlet nozzle to produce centrifugal force. The I-SEP used in this study uses novel dual involutes to produce the same effect.

2.3 Type of Separators

Based on the principles defined in earlier section below are four major types of separators.

2.3.1 Gravity Separators

All oil, gas, water and sand separation applications in the industry mostly use gravity separators for the separation. Gravity separators are vessels that work on the principle of density difference and utilize gravity for separating dense phase from the relatively lighter phases. According to (Rousseau, 1987) gravity separator could not be used to separate the droplet greater than 70 micron.

Conventional gas-liquid separators are generally categorized in horizontal and vertical separators as shown in Figure 2.3. Vertical separators occupy less space than horizontal separators and should be preferred over horizontal separators in situation where gas-liquid ratio is high. Horizontal separators are larger than vertical separators and are mostly used at gas well and are preferred over vertical separators in low gas-liquid ratio.

A gravity separator either horizontal or vertical mainly consists of four main sections as shown in the Figure 2.3. The bulk separation of gas from the liquid is achieved in the first section due to impact and change in momentum. Momentum breaker in the form of a plate or vanes is used for this purpose near the inlet to reduce the high velocity of entering fluid. The gas flows to the upper part of the separator while liquid flows towards the lower part of the separator.

The second section of the separator is a settling chamber, during which the gas velocity is lowered and heaver droplet of liquid is settle down and separated from the gas. The un-separated fine droplets of liquids in the gas stream move upward and are finally removed in the mist elimination section of the separator. The last section of the separator is called as liquid collection section where liquid is collected and retained for sufficient time to let the bubble escape before the liquid is discharged from the separator. The proper control of liquid level in the liquid collection section controls the efficiency of the separation avoiding the gas bubble to exit through the liquid outlet of the separator.

2.3.1.1 Sizing of the Gravity Separator

(Hansen,2005) has described some basic criteria for sizing the gravity separator which are listed below:

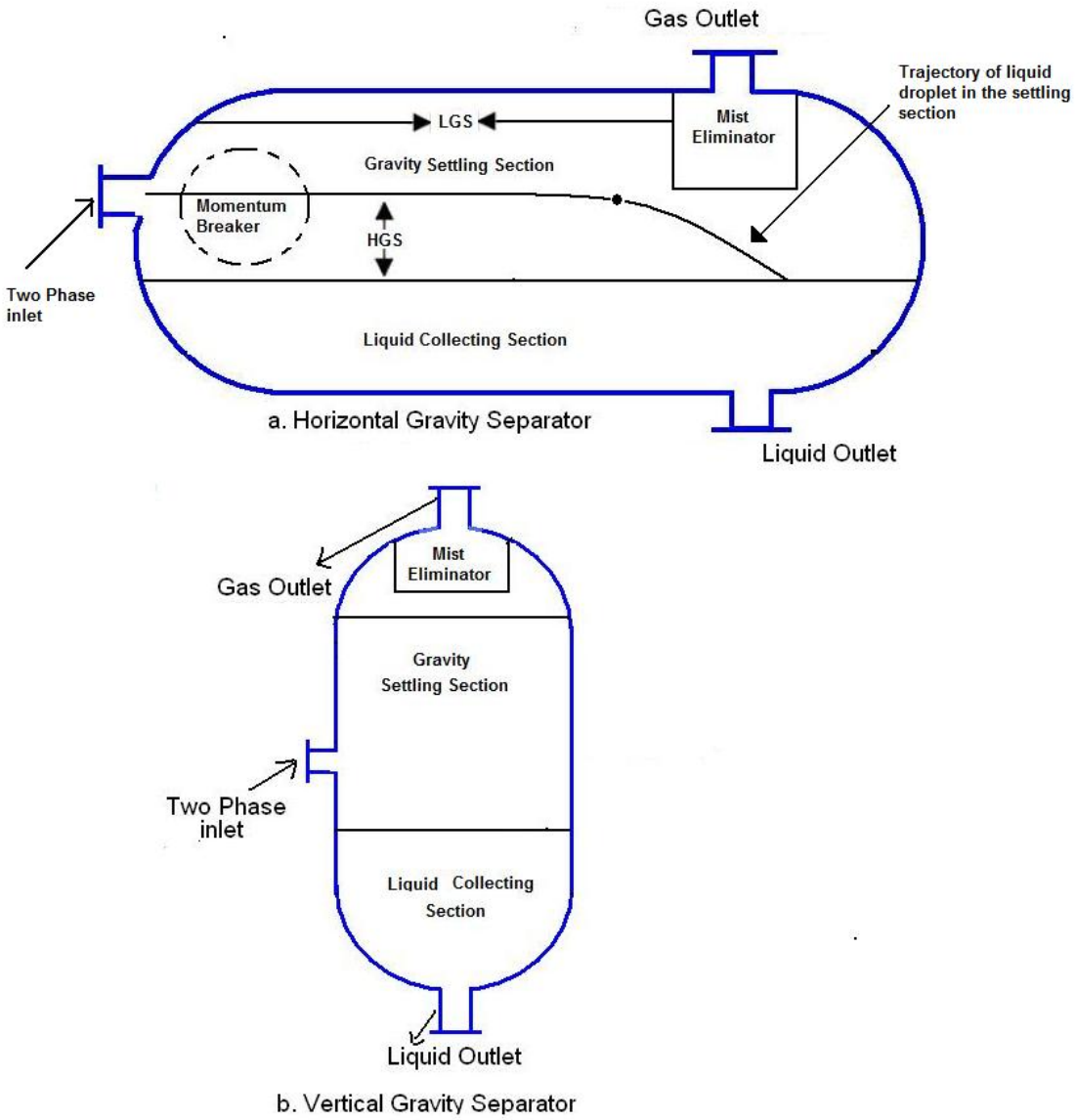

Figure 2.3 Conventional Gravity Separators

- The size of the separator should be such that it provides sufficient volume in the gas space to accommodate the rise in the liquid level caused by the surges in the liquid flow rate.

- It should provide enough time so that the immiscible gas, water and oil could be separated by the gravity.
- It should allow for variation in the flow rate of gas, oil and water into the separator without adversely affecting the separation efficiency.

The size of the gravity separator is determined based on the required gas and liquid capacity. The required gas capacity determines the diameter of the vertical separator or height and settling length of the horizontal separator. The gas velocity however is determined by the limiting droplet size that could be separated in the settling chamber of the gravity separator. According to (Perry and Green, 1989) the gas velocity or the fluid velocity should be less than terminal velocity of the droplets for efficient separation.

The liquid droplet in gravity settling section of a vertical separator is falling down against an up-flowing gas stream, however for the horizontal separator it follows a trajectory like path during its downward motion in the vessel which means it also covers horizontal distance while it is being settled down under gravity as shown in Figure 2.3a. The separation of the liquid droplet inside horizontal gravity separator is thus affected by residence time of the gas (t_{res}) and settling time of the liquid droplet (t_s). The residence time is the time for the gas to go from the inlet to the outlet covering a horizontal distance (L_{GS}) between the inlet and outlet of the horizontal separator and is given by the equation:

$$t_{res} = \frac{L_{GS}}{U_{GS}}$$

Whereas settling time is the time required for liquid droplet to settle down after covering a vertical distance (H_{GS})moving with a downward terminal velocity and is given by the equation.

$$t_s = \frac{H_{GS}}{U_t}$$

The condition that liquid droplet is separated from the gas and fall down to the gas liquid interface requires that the liquid droplet must fall to liquid surface within the

residence time of the gas. This means that settling time should be less than or equal to the residence time.

$$\frac{L_{GS}}{U_{GS}} = \frac{H_{GS}}{U_t} \qquad 2\text{-}1$$

The separation performance of the horizontal separator increases with the large residence time as then liquid droplet have more chance to get separated and fall down to the liquid surface. As the height of the liquid level inside the separator is increased the gas flow area inside the horizontal separator is decreased causing to increase the gas velocity and thus decreasing the residence time and also the distance that the droplet will fall during the residence time.

The size of the separator also affects the minimum size of the liquid droplet that can be separated during the separation in the settling section of the gravity separator. This relationship is calculated on the basis of terminal settling velocity of the liquid droplet which is determined by balancing the forces acting on liquid droplet during its downward motion. If the turbulence and surface tension effect are ignored then the droplet inside the gravity separator is acted upon by vertically downward gravitational force opposed by upward buoyancy and drag force acting opposite to the direction of the particle. Assuming the liquid drop as solid and applying the Stokes law the terminal velocity can be given by the following equation in term of the diameter of liquid droplet.

$$U_t = \sqrt{\frac{4gd_d(\rho_d - \rho_g)}{3\rho_d C_d}} \qquad (2\text{-}2)$$

From the equation (2-1) the terminal velocity can also be written in

$$U_t = \frac{H_{GS}U_{GS}}{L_{GS}} \qquad (2\text{-}3)$$

Assuming the Reynolds number of droplet is < 1 and applying the Stokes law to determine the drag coefficient the equation for the minimum droplet size can be given by the following equation

$$d_{d,\min} = \sqrt{\frac{18\mu_g H_{GS} U_{GS}}{g(\rho_d - \rho_g) L_{GS}}} \qquad (2\text{-}4)$$

Where

$d_{d,\min}$ is the minimum diameter of the separated droplet (m)

μ_g is the viscosity of gas in the gravity separator (Pa-s)

U_{GS} is gas velocity in the gravity separator (m/s)

U_t is the terminal velocity of the falling liquid droplet (m/s)

L_{GS} is the Horizontal distance travelled by the liquid droplet in gravity separator (m)

H_{GS} is the vertical distance travelled by the liquid droplet before falling to liquid surface (m)

ρ_g is density of the gas (kg/m^3)

ρ_d is density of liquid droplet (kg/m^3)

g is the acceleration (m/s^2)

The equation 2-4 indicates that if all the other physical parameters are kept constant than the droplet diameter size becomes the function of the ratio of separator height and length. Thus if this ratio is reduced the diameter of the droplet would also be reduced, however reducing the ratio of the separator height and separator length require long and low chamber which will take lot of space and is not desirable especially in offshore application.

(Abia and Thorpe, 2007) has recently evaluated the performance of a horizontal three phase separator (bucket & weir) on Alba field, situated offshore of the coast of Equatorial Guinea. The height and length for separator under study was given as 0.856m and 5.89m respectively with gas velocity of 0.805m/s and gas viscosity of 0.01 mPa-s at 391^{o}K. The equation 2-4 when used with this data produced a minimum oil droplet size of 64 micron.

One of the other finding of their work is effect of ratio residence time of heavier phase (which is oil in this case) to lighter phase (i.e. water in this case) on separation efficiency of the separator. Theoretically in oil water separation, it is required that oil

residence time should be equal or greater than the water settling time to prevent water carried in oil stream. However their recent research has shown that at low value of ratio of the residence time of oil and settling time of water such as 0.4 or more, the water percentage in the oil is lowered down to almost zero percentage. It means that the percentage of drops below 64 micron is very low. It also indicates that to design gravity separator the inlet drop size distribution should be known and the turbulence created by inlet devices such as impingement plates and plunging jets should be minimum.

2.3.2 Mesh Type Eliminators

The most common type of the demister used in the chemical process industries is the knitted mesh demister as shown in Figure 2.4. The Mesh eliminators work on the principle of the inertial impaction. Typically, mist eliminator pads, consisting of fibres or knitted meshes, can remove droplets down to 1-5 microns but the vessel containing them is relatively large because they must be operated at low velocities to prevent liquid re-entrainment. Unfortunately, these separators present some significant drawbacks when they are used in high-pressure applications or in any application in which a reduction in the diameter of the vessel containing the separator is necessary and high separation efficiency is required.

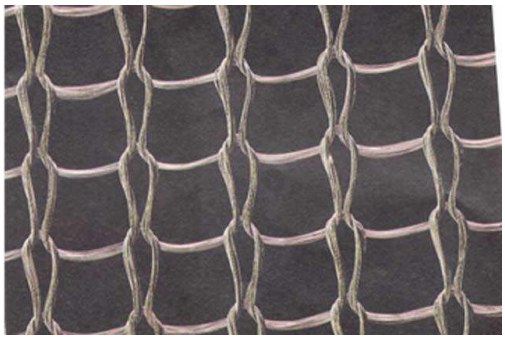

Figure 2.4 The structure of wire mesh demister

2.3.3 Filter Vane Separators

A vane separator as shown in Figure 2.5 is simply a series of baffles or plates profiled with sharp bends within a vessel work on inertial impaction principle. The vane

separators are sensitive to mass velocity for removal efficiency, but generally can operate at higher velocities than mist eliminators. However, because of the relatively large paths between the plates constituting the tortuous network, vane separator can only remove relatively large droplet sizes usually 10 microns and above.

The collection efficiency of the vane separator decreases at low gas flow rates due to decrease in the inertial impaction efficiency while at high gas flow rate the increase re-entertainment causes to decreases the collection efficiency. The pressure drop for the vane separator is low around 5-10 mbar for air-water system under atmospheric pressure.

Figure 2.5 A Vane Type Separator

2.3.4 Cyclonic Separator

The Cyclones are one of the most versatile separation techniques used to remove small particles or droplets from a gas or liquid. Initially they had been use for separating coal from the gas but in its present form are being used for separation of materials of differing density, size, and shape. They utilize centrifugal forces and low pressure created due to the induction of flow in the tangential direction into cylindrical vessel. This technique causes flow to rotate strongly inside the cyclone producing a centrifugal acceleration which then forces heavier particle to move towards outside wall where they are subsequently removed from the flow. Gas cyclones are widely used in industry for the separation of solid particles from gas and air streams Coker (1993) while water cyclones, also known as hydro cyclones, are used for the separation of fluids of differing densities Svarovsky (1984). Cyclones are also popular because they are simple and inexpensive to manufacture, require little

maintenance, contain no moving parts, and have the ability to operate at high temperatures and pressures Coker (1993).

2.4 Geometry of a Conventional Cyclonic Separator

While separators can be categorized on the basis of their shape as horizontal, vertical and spherical the basic geometry consists of three openings: these are inlet or feed and two outlets opening called as underflow and overflow are shown in the Figure 2.6. However the geometrical position of the underflow and overflow varies in different type of the cyclone separator. A conventional cyclonic separator for example is like an inverted cone having underflow and overflow in the opposite direction as can be seen in Figure 2.6. The lighter fluid comes out from overflow and heavier flow comes out from the underflow. A vortex finder is used at overflow to collect the lighter fluid. The geometry of the cyclone is usually defined by following dimensions:

- Body diameter of cyclone
- Height of the cyclone
- Diameter of vortex finder
- Length of the vortex finder
- Height and width of the inlet
- Diameter of the under and overflow

2.5 Components of a Cyclonic Separator:

For efficient and stable operation over a wide range of condition a gas liquid separator may have following sections

- Inlet Section
- Primary Separation Section
- Secondary Separation Section
- Mist Extraction Section
- Liquid Accumulation Section

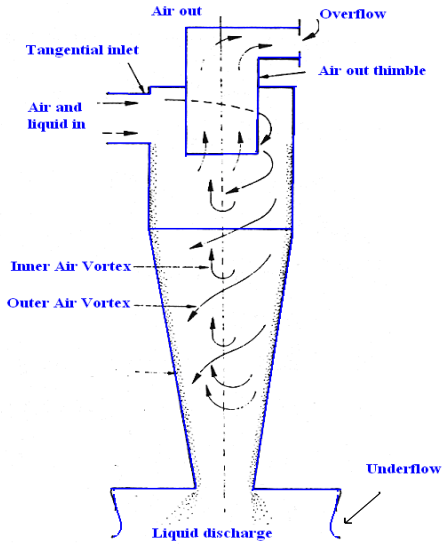

Figure 2.6 Conventional Cyclonic Separator.

2.5.1 Inlet Section

The design of inlet has been the single most redesigned component of the compact separator due to its importance in determining the incoming gas-liquid distribution and initial inlet tangential-inlet velocity in separator. Hoffmann, (2002) has described four type of inlet configuration which is circular, slotted, volute and swirl vanes types as shown in the Figure 2.7.

Nebrensky et al. (1980) developed the design parameters for the cyclone separator included a tangential rectangular inlet equipped with special vane and shroud arrangement to change the inlet area. They extended the operating range of the separator by controlling the inlet velocity independent of throughput. Cowie, (1992) acquired data on vertical slug catchers and studied their performance for radial and tangential inlet configurations. The tangential inlet provided the best liquid carry-over performance, reducing foam generation. Although conventional vertical separator uses the perpendicular inlet, however it has been seen in recent studies that inclined inlet is found more efficient in the improvement of the performance of the separator.

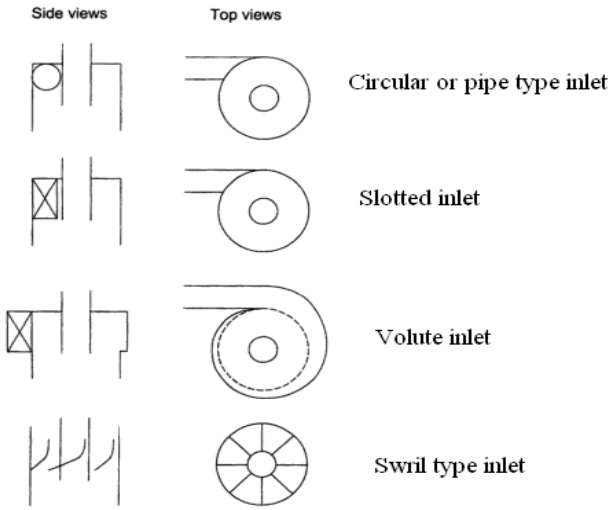

Figure 2.7 Inlet Types of Compact Separator

It is because incline inlet reduces the liquid carry over in the gas stream through two mechanisms. Firstly the downward inclination of the inlet promotes stratification and provides primary separation at the inlet nozzle. Secondly the downward inclination cause liquid stream to spiral below the inlet after one revolution, preventing the liquid from blocking the flow of the gas into upper part of the separator.

2.5.2 Primary Separation Section

This section removes bulk of the liquid from the inlet. This separation is usually accomplished by a change in direction of fluid flow. In vertical separator centrifugal force from tangential inlet quickly removes large volume of liquid and allows redistribution of gas velocity. Horizontal and spherical separators use properly shaped and positioned deflection plates to achieve the same effects. This arrangement quickly removes slugs and large droplets of liquid from the gas stream, minimizes the entrainment gas turbulence and re-entrainment of liquid particles.

2.5.3 Secondary Separation Section

This section removes maximum of smaller liquid droplets without elaborate design. It mainly occurs due to the gravity settling of the gas stream after the velocity has been drastically reduced. The efficiency in this section depends upon gas and liquid properties liquid drop size and degree of gas turbulence.

2.5.4 Mist Extraction Section

This section removes the remaining tiny liquids droplets from gas stream after it has been passed from primary and secondary section. The principle here in this section is either impingement or centrifugal force; in either case tiny liquid droplets are collected on a surface where they are drained away from gas stream or from large droplets that can fall back into primary separation section.

2.5.5 Liquid Accumulation Section

This section receives and disposes the collected liquid. It should have proper liquid level control equipment to handle liquid surge that may occur in normal operation. This section should be so arranged so that the separated liquid has a minimum disturbance from the flowing gas stream.

2.6 Reverse and Axial Flow Cyclonic Separators

It was observed during this literature survey that two types of cyclone are in practice depending upon the flow entrance in the separator. These are reverse-flow or tangential cyclonic separator (RFC) and axial flow cyclonic separator (AFC). Both separators perform same functions however the difference lies in the way the flow enters in the apparatus.

2.6.1 Reverse Flow Cyclonic Separator

The flow enters tangentially in RFC as shown in Figure 2-6 creating a strong rotation and a vortex inside, after which direction of the flow is reversed creating an outer vortex in upward axial direction. The gas or lighter phase is exited through a vortex finder installed at the overflow of the separator. The particles in the gas are pushed outward to the cyclone walls in the centrifugal field and are transported to the underflow by the downward motion of the gas. The flow in the tangential cyclone is usually highly turbulent and non-stationary, which together with the flow reversal in the cyclone result in a relatively high pressure drop across the cyclone Maynard (2000).

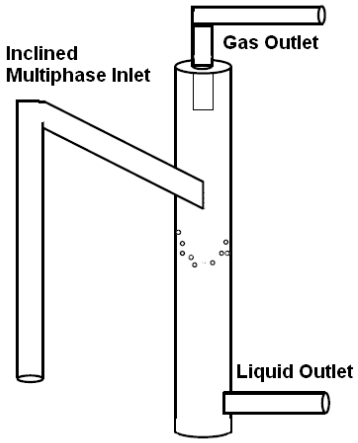

Figure 2.8 A Gas Liquid Cylindrical Cyclone (GLCC)

The GLCC is an example of the reverse flow cyclone shown in the Figure 2.8. It consists of a vertical pipe with two outlets at opposite end for gas and liquid exits. This separator uses tangential inlet to produce swirl motion inside the separator generating buoyancy and centrifugal force much higher than gravitational force. The liquid and gas are separated with liquid pushed radially outward and downward toward the liquid exit while gas is driven inward and upward toward the gas outlet.

2.6.2 Axial Flow Cyclonic Separator

The axial cyclonic separator shown in Figure 2.9, unlike RFC does not have any conical shape at the bottom. The underflow and overflow both lie at the top perpendicular to each other. This mean both denser and lighter phase exit from the same end of the cyclone thus there is no reversal of flow observed in the axial flow cyclone. I-SEP is example of an axial flow cyclonic separator. Unlike GLCC it has liquid and gas outlet in the same direction and it uses involute to generate centrifugal force. Both liquid and gas flow uniaxially upward, liquid being heavier exit through the tangential outlet and gas exit out through the axial outlet.

Many researchers have been giving theories about the tangential flow inside the cyclone since 1950 starting from Lapple (1951) to Iozia and David (1990). Kao and Tsai (2001) during their comparison work on the exiting theories on tangential flow

cyclone found that many of these theories applicable in the low range of flow Reynolds numbers. However only few researchers have studied the axial flow for example Liu and Rubow (1984) developed an axial flow cascade cyclone at a design flow rate of 30 l/min. Maynard, (2000) derived the particle penetration of the axial flow cyclone based on the assumption that particle collection mainly occurs in the vane and body sections only. According to Nieuwstadt and Dirkzwager (1995) the axial flow cyclone principally consists of pipe geometry and needs a swirl generator to produce rotation in the input flow as shown in Figure 2-5. Gas with fluid droplets enters at the bottom and flows in a swirling generator, the fluid droplet are deposited at the walls in the settling zone and both the gas and fluid are removed at the top of cyclones. The pressure drop across this AFC is very small due to much less disturbed flow as compared to tangential cyclone. Chen et al. (1999) has reported higher separation efficiency using a down-exhaust cyclone axial flow separator to separate solid from gases in circulating fluidized-bed (CFB) boilers with lower pressure drop.

Komura et al. (2002) studied the flow characteristic and gas separation efficiency in cyclone separator. They proposed the use of spiral type cyclone to improve the efficiency of the gas-liquid separator. A honey comb type swirl breaker was utilized in this experiment to improve gas separation efficiency. Their experiments showed that gas separation efficiency drops sharply in higher Reynolds number range due to sudden change in the flow pattern inside 18D long cyclonic pipe. Their experiments also revealed that for this particular axial cyclone the gas separation efficiency decreased at higher gas volume ratio of the mixture.

2.7 Cyclone Separation Theory

A number of models have been proposed to explain the separation phenomena inside the separator. However most of them discuss the separation of the solid from the gas. If droplet coalescence and surface interaction are ignored in the gas-liquid separation then we can assume a liquid droplet to behave like a solid particle in the gas in term of the forces acting on it. The well known models describing the separation phenomena are:

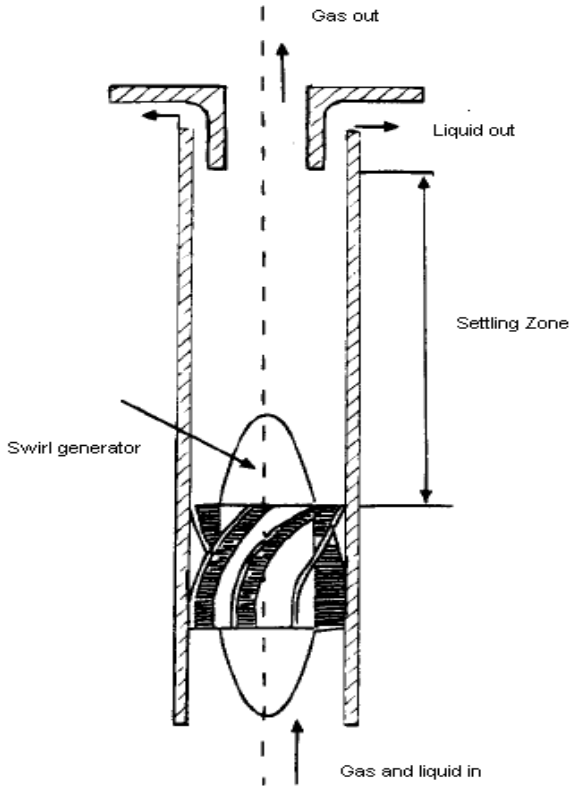

Figure 2.9 Axial Flow Separator

1. Equilibrium model
2. Time of flight model

According to equilibrium model two forces are acting on the liquid particle during its stay in the separator. This model is based on the equilibrium of these two forces acting in the opposite direction, one of this force is the drag force acting inside the vortex and is proportional to the particle size and other force is the centrifugal force which is proportional to the mass and directed outward from the cyclone surface. The large particles are thus centrifuged out to the cyclone wall and the small particles are dragged and escaped out from the vortex tube. The particle size for which these two forces are equal is called as "cut size diameter". It is the particle size that has an equal probability of being captured or escaped from the wall of the cyclone. This cut size diameter has been taken as one of the important parameter in the defining the separation efficiency of the compact separator, especially in the case of the gas solid

separation. The velocity of the fluid inside the separator during the swirl motion can be resolved into three components i.e. tangential, radial and axial as shown in the Figure 2.10. The centrifugal force on the particle is defined from the following equation:

$$F_c = \frac{\pi d^3(\rho_p - \rho_f)V_t^2}{6r} \qquad (2\text{-}6)$$

The opposite drag force is given by the following equation:

$$F_d = 3\pi\mu V_r d \qquad (2\text{-}7)$$

Where,

d is the diameter of the particle (m)

ρ_p is density of the particle (kg/m^3)

ρ_f is the density of the fluid i.e. gas in this case (kg/m^3)

V_t is the tangential velocity component (m/s)

V_r is the radial velocity component (m/s)

r is the radius of the cyclone (m)

μ is the viscosity of the gas (Pa- s)

The particle will move towards the radial direction when the centrifugal force exceeds the drag force. Since the centrifugal force is proportional to the mass and therefore to cubic power of particle diameter (d^3) in equation (2-6) this mean that heavier particle would be directed towards the underflow. While the drag force is proportional to the particle diameter (d) in equation 2-7 hence lighter particle would go to the overflow. The particle size for which the two forces are equal is called as cut-size diameter as it is particle size that stands a 50-50 chance of being captured. The cut size diameter as calculated by the Barth using the equilibrium model is given as:

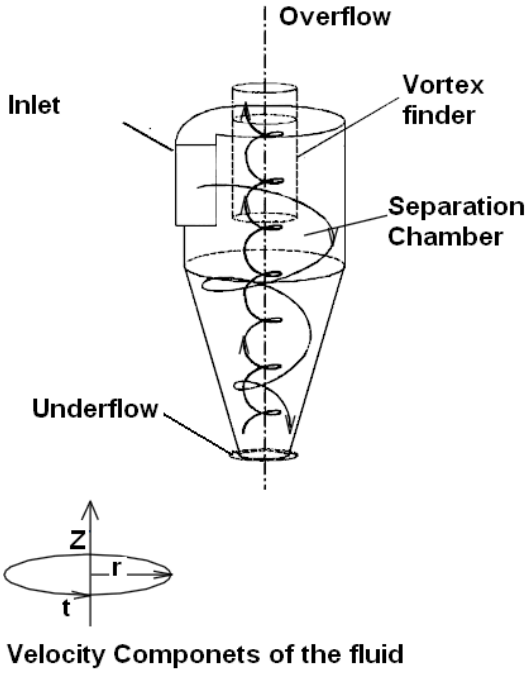

Figure 2.10 Sketch of an tangential inlet cyclone, the coordinate directions are also shown with z-axis coincide with the direction of the swirl tube, radial and tangential component of the velocity are shown by r, and t.

$$d_{50} = \sqrt{\frac{9\mu V_r D_x}{\pi \rho_p V_t^2}} \qquad (2\text{-}8)$$

According to time of flight model when a particle enters into the cyclone at a certain radial distance from the cyclone axis, it takes some time to reach the wall of the cyclone. The particle which can traverse entire width of the inlet jet before actually reaching the bottom of the cyclone is termed as smallest size particle. The cut size diameter for such a particle according to time of flight model can be given by the following equation:

$$d_{50} = \sqrt{\frac{9\mu W}{\pi N_e V_{in}(\rho_p - \rho_g)}} \qquad (2\text{-}9)$$

The number of turns N_e was empirically calculated by (Zenz, 1999) as given in equation :

$$N_e = 6.1(1 - e^{-0.66V_{in}}) \qquad (2\text{-}10)$$

Where,

V_{in} is the inlet velocity (m/s)

V_t is tangential velocity (m/s)

V_r is radial velocity (m/s)

μ is the gas viscosity (Pa-s)

W is width of the inlet duct (m)

D_x is the diameter of the vortex finder (m)

N_e is the number of turns

2.7.1 Vortex Flow inside the cyclone

The velocity and pressure profiles are important to know as these two parameters define the link between separation efficiency and the inlet conditions. The tangential velocity component of the swirl flow inside the cyclone can be determined by the type of the vortex flow. Munson (1990) has described three type of vortex, irrotational or free vortex, rotational or force vortex and combination of these two which is called as Rankine vortex. These vortexes are defined by the following equations that define tangential velocity as the function of the radius.

$$\text{Free Vortex} \quad V_t = \frac{C}{r} \qquad (2\text{-}11)$$

$$\text{Forced Vortex} \quad V_t = Cr \qquad (2\text{-}12)$$

Where, C is constant and r is the radius.

The Free vortex as can be seen from the equation 2-11 causes the tangential velocity component to decrease as the fluid element move more toward the centre due to decrease in radius. The tangential velocity profile is determined by assuming any of these vortexes. The physical measurement of the velocity distribution within the

cyclone helps researchers to better understand the behaviour of cyclone. However large information is available on this for the reverse flow cyclone but comparatively not much is written on this topic for the axial flow cyclone. Shepherd and Lapple (1939) used photographic techniques to measure the velocity distribution in reverse flow cyclone. Modern techniques allow the measurement of velocities using laser as used by Collantes et al. (2000), Modigell and Weng (2000) and Dai et al (1999). Ferrara et al,(1999) Rankine vortex are created in a conical reverse flow cyclone whereas in cylindrical cyclone forced vortex is created as a result of velocity distribution.

2.8 Separation Efficiency

There are two basic definitions used in literature to define the separation efficiency of cyclone of any type Hoffmann (2002) and Svarovsky (1984). The term total efficiency is usually coined to refer the mass fraction of fluid/solid at the inlet recovered in liquid or gas stream expressed in percentage. The other definition is based on particle/droplet size of separated particle/droplet and called as grade efficiency, a curve called grade efficiency curve is obtained by measuring the particle size of each separated particles. However in this project the former definition for the separation efficiency is used. The separation efficiency at one end depends upon the physical properties of the fluids such as density, viscosity, temperature, inlet pressure and at other end also affected by the gas volume fraction at the inlet. Hoffmann (2002) and Svarovsky (1984) reported that controlling of the underflow orifice of the hydrocyclone could also affect the separation efficiency of the separator.

2.8.1 Liquid Carry Over

Efficient operation of the separator is limited by two undesirable phenomena namely LCO and GCU. The locus of superficial liquid velocity versus the superficial gas velocity in the separator at which liquid carry over initiated is called as operational envelop for liquid carry over as shown in Figure 2.11. The area below the envelope is the region of normal operating condition where there is no carry over from separator. The region above this operational envelop gives the flow condition for continuous LCO. The shape and size of the envelope for a particular separator however depends

upon many factor. The equilibrium liquid level in the separator, separator operating pressure and fluid viscosity has been considered most important among all the factors.

In gas processing systems, high separation efficiency is crucial to be able to meet the product specifications. Hence, liquid carry-over is very costly for the gas processing industry and robust techniques are required to verify LCO. It occurs in the gas leg in the form of droplets at high gas and low liquid flow rate or as stratified flow usually at high liquid and gas flow rate Chirinos et al. (2000) The authors working on the GLCC has figured out that the mechanisms responsible for the liquid carry over are churn flow and annular flow occurring in the upper part of the separator. They also developed a mechanistic model to predict the LCO for GLCC from low to moderately high gas rates.

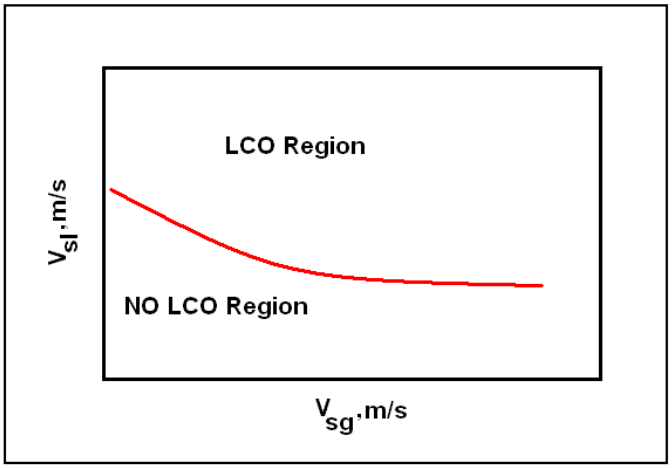

Figure 2.11 Operational Envelope for Liquid Carry Over

2.8.2 Gas Carry Under

It is one of the other important factors that affect the gas-liquid separation efficiency represents the amount of the gas which is leaving at the liquid leg of the separator. Mechanistic model has been developed to predict the GCU in the compact separator which are defined in the next section.

2.9 Pressure Drop

The separator performance is also judge by amount of the energy it takes to separate the particles from the flowing fluids. This energy appears as the pressure drop across the separator usually calculated between the inlet and overflow. The total pressure drop is still not predictable, although the Bernoulli equation says that it actually is made up from static pressure p and dynamic pressure as shown in equation:

$$\frac{p}{\rho} + gh + \frac{1}{2}v^2 = \text{constant} \qquad (2\text{-}12)$$

According to above equation both of these are interchangeable and at high velocities the static pressure would be low and vice versa but this do not occur practically and there is always a pressure drop due to the friction. This pressure drop occurs due to losses at inlet, main cyclone body and in the vortex finder. The vortex finder bears the major pressure drop Hoffmann (2002) and it is difficult to measure due to swirl inside the vortex. Therefore in order to recover the static pressure at the vortex Hoffmann (2002) proposed use of rectifier and suggested to use the pressure at the wall of outlet tube minus the inlet static pressure. Zhao (2004) developed a theoretical pressure drop model for the reverse flow cyclone using based on flow pattern and geometrical dimension of the cyclone. He proposed that total pressure drop in the cyclone is due to sum of the pressure drop in the inlet section, swirl flow, wall friction and at the outlet of the separator. However his model did not considered effect of the particle loading on the pressure drop.

Svarovsky, (1984) has defined a term loss coefficient or Euler Number to evaluate the performance of the separators.

$$Eu = \frac{\Delta P}{0.5\rho V_{in}^2} \qquad (2\text{-}13)$$

Where ΔP is the pressure drop between inlet and outlet of the separator.

ρ is the fluid density (kg/m^3)

V is the fluid velocity at inlet (m/s)

A higher value of this term means that separator requires more energy for the separation and hence less efficient.

2.10 Factor Effecting the Performance of AFC

Axial flow cyclone works on the principle of centrifugal force which increases with the increase in tangential velocity. An increase in centrifugal force means more separation, however turbulence is increased due to the increase in the velocity and causes to decreases the separation efficiency. Gomez et al. (1998) proposed that there should be an optimal velocity for any cyclone to operate and the performance of the cyclone would be affected when the inlet velocity is changed from this optimal velocity. The GCU, LCO as reported by Freston (1985) was found to be directly related with the inlet velocity for gas liquid separation.

The other important factor is the viscosity of the fluid that may affect the separation efficiency however it was reported by the King et al. (1998)that there was not significant change observed in the separation efficiency with the change in the viscosity of the fluid. An increase in LCO was reported by Mothes (1984) with the increase in viscosity. Gomez et al. (1998) on the other hand working on vertical separator has found strong dependence of inlet flow regime on separation efficiency.

2.11 Mechanistic Modelling of Reverse Flow Cyclonic Separator

The ultimate aim of the modelling work to date has been to predict the operating envelop for the compact separator with respect to LCO over in the gas stream and GCU in the liquid stream. In the recent years extensive research is done on the GLCC a patent reverse flow cyclonic separator of Tulsa University. Few mechanistic models have been proposed for predicting design optimization and performance of this separator. These models discuss the mathematical formulas to calculate the operational envelope, gas/liquid interface shape, equilibrium liquid level and pressure drops across various components. Arpandi et al. (1996) developed a mechanistic

model to predict the liquid carry over in the GLCC during churn flow. This model predicts operational envelope for LCO along with simple velocity distribution, gas liquid interface shape equilibrium liquid level, and total pressure drop. His research revealed that the churn flow at high liquid flow rate and annular flow at high gas flow rate in the upper part of GLCC upper is main cause of the LCO. His experiment further showed that the operational envelop for the LCO decreased with the increased in gas superficial velocity which mean liquid carry over was observed even at low liquid flow rate with the decrease in gas superficial velocities.

Marti et al., (1996) enhanced the mechanist model of Arpandi et al. (1996) predicting gas carry under and separation efficiency in the gas liquid cylindrical cyclone using the bubble trajectory analysis. According to this analysis the large gas bubbles are captured in the vortex region, while the homogenously distributed small bubble at the bottom of the vortex are acted upon by centripetal and drag force. These bubble will merge with gas core and go with the gas stream when the centripetal force overcomes the drag force, however otherwise the radial distance travelled by these bubble will be insufficient and will be carried by liquid stream into liquid leg exit.

Gomez et al. (2000) further enhanced the model of Arpandi et al. (1996) by incorporating the features including prediction of flow regime at the inlet, along with an analytical model for predicting the vortex characteristic. He identified that determination of the flow pattern at inlet is critical as it defines the initial tangential liquid and gas velocity which in turn determines the LCO and the GCU at their respective leg in GLCC

Movafaghian et al. (2000) studied hydrodynamic flow behaviour in compact separator theoretically and experimentally. His mechanistic model used wide range of operating condition including different inlet geometry, different set of liquid viscosities to measure data comprised of equilibrium level, zero net liquid flow hold up and operational envelope for liquid carry over. He found through his experiments

that liquid carry over envelop is extended for gas superficial velocity less than 7 m/s and reduced with the increase in the liquid viscosity.

Chirinos et al. (2000) provided experimental data and mechanistic model for predicting percentage of liquid carryover in the gas-liquid cylindrical cyclone separator. Gomez et al. (1999) used Excel and Visual Basic platform to develop a state-of-the-art computer simulator for gas-liquid cylindrical cyclone. Model enhancements include a flow pattern dependent nozzle analysis for inlet, an analytical model for the gas-liquid vortex interface shape, a unified particle trajectory model for bubbles and droplets, and a simplified model for the prediction of the separator aspect ratio. Coelho and Medronhob, (2001) developed a model predicting the efficiency performance of the solid-liquid cyclone using the dimensionless variables such as stokes number, Euler number. A mathematical model for gas-solid separation was developed by the (Zhao, 2005). This model assumes that particle concentration is varied in the radial direction and using the critical particle size separation along with the flow pattern estimate the separation efficiency of the reverse flow cyclone.

2.12 Control Strategies to Improve the Performance of the Separator

It had been identified by many researchers such as Wang et al. (1998) that performance of the gas-liquid separator such as GLCC could be enhanced by incorporating suitable control systems. Liquid and gas flow rate at separator inlet, liquid level and separator pressure have been identified as controlling parameters to improve the performance of the separator. These control strategies using either feed forward or feedback control loop hence revolve around the controlling of these variables during different flow condition approaching at the separator inlet. The control loop used in these control strategies was consisted of controller driving either liquid or a gas control valve along with liquid level and pressure sensors to measure any change in controlling parameter and then feed back or feed word this change to controller to take the appropriate action to make the system stable again. Most of the work in this domain is done by the researchers at Tulsa University in the recent past mainly working on the mathematical model for the GLCC given by Wang et al.

(1998). This model is a blue print to design the controller controlling liquid level and pressure separately using liquid and gas control valve attached at the liquid and gas leg of the GLCC. The other researches from this group then based on this model have proposed six different control strategies:

1. Liquid level control by LCV only
2. Pressure control by GCV only
3. Liquid level control by GCV only
4. Integrated liquid level control by both LCV and GCV
5. Integrated feedback and feed word control
6. Optimal Control Strategy

Wang et al., (2000) has pointed out that gas dominated flow at inlet such as annular and mist flow can be sufficiently controlled by LCV only whereas for liquid dominated flow like bubbly or churn flow the GCV alone can be used to control the liquid level inside the separator. The slug flow at the inlet however needs an integrated liquid level control both by LCV and GCV (strategy 4) so that in normal condition LCV would controlled the liquid level but would be assist by the GCV during slugging condition. The liquid level is feedback to both LCV and GCV controller in this strategy. This strategy is due to its faster response could be more effective in severe slugging.

The pressure can be maintained constant by following integrated liquid level control by LCV and pressure control by GCV (combination of strategy 1 and 2). The strategy thus uses two inputs i.e. set points for pressure and liquid level , measures any changes in these signals and feedback their error the GCV and LCV controller respectively. In this way pressure is maintained by proper closing and opening of the valve. The authors found that this strategy is ideal for reducing the pressure fluctuation in the GLCC.

Earni et al. (2003) proposed a predictive control strategy integrating both feed forward and feedback control scheme for real time control of the separator. The k controller uses the feedback signal of liquid level to compute the error with respect to set point, whereas the feed forward controller identifies the slug using proper sensor in advance, the LCV is then activated based on the error signal generated by both the feedback and feed forward controller so that the liquid level can be maintained around the set point.

2.13 Flow Regimes in Gas-Liquid Flow

The separation efficiency of the separator also depends upon the incoming flow regime as the pressure drop across the I-SEP would vary depending upon the inlet flow regime. Flow regime also plays an important parameter in defining the control strategy of the separator. Hence the knowledge of the flow regime is important for the optimal operation and correct pressure drop calculation. Therefore it is necessary to identify the flow regime at the I-SEP inlet. This flow regime may take some distance to develop and it can change with distance as the pressure, which affects the gas density, changes. The flow regime also depends on fluid properties, size of the conduit, flow rates of each of the phases and configuration of the inlet.

Hubbard and Dukler, (1966) suggested separated, intermittent and distributed flow as three basic flow pattern.

- Separated flow patterns: Both phases are continuous. Some droplets or bubbles of one phase in the other may or may not exist. Separated flow patterns include:
    - Stratified flows: Stratified smooth flow and stratified wavy flow.
    - Annular flows: Annular film flow and annular-mist flow, which entrains liquid droplets in the gas core.
- Intermittent flow patterns: At least one phase is discontinuous. These flow regimes include:

    - Elongated bubble flow.
    - Slug flow, plug flow.

- Churn or froth flow (a transition zone between slug and annular flow).

- Dispersed flow patterns: In these flow regimes, the liquid phase is continuous, while the gas phase is discontinuous. Flow patterns include:

  - Bubble flow.
  - Dispersed bubble flow, in which the finely dispersed bubbles exist in a continuous flowing liquid phase.

2.13.1 Flow Regime in Vertical Pipes

Following flow regimes are found in the vertical pipes with the change in the flow rate of the gas.

- Bubbly
- Slug
- Churn
- Wispy Annular
- Annular

The flow regimes that are obtained in vertical, upward, concurrent flow at different gas and liquid flow rates are shown in Figure 2.12. In the bubbly regime there is a distribution of bubbles of various sizes throughout the liquid. The average bubble size increases with the gas flow rate. The next regime occurs when the gas flow rate is increased to the point when many bubbles coalesce to produce slugs of gas. The gas slugs have spherical noses and occupy almost the entire cross section of the tube, being separated from the wall by a thin liquid film. Between slugs of gas there are slugs of liquid in which there may be small bubbles entrained in the wakes of the gas slugs. This well-defined flow pattern is destroyed at higher flow rates and a chaotic type of flow, generally known as churn flow, is established. Over most of the cross section there is a churning motion of irregularly shaped portions of gas and liquid. Further increase in the gas flow rate causes a degree of separation of the phases, the liquid flowing mainly on the wall of the tube and the gas in the core. Liquid drops or

droplets are carried in the core: it is the competing tendencies for drops to impinge on the liquid film and for droplets to be entrained in the core by break-up of waves on the surface of the film that determine the flow regime. The main differences between the wispy-annular and the annular flow regimes are that in the former the entrained liquid is present as relatively large drops and the liquid film contains gas bubbles, while in the annular flow regime the entrained droplets do not coalesce to form larger drops.

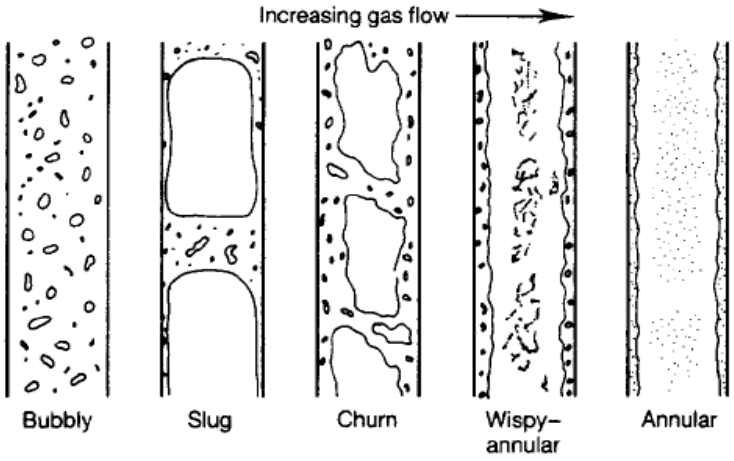

Figure 2.12 Flow Pattern in Vertical Pipe.

2.13.2 Flow Regime in Horizontal Pipes

One of the problems with the two phase flow is that a significant distance may be required for flow regime to become established and the flow regime may be changed by flow through pipe fittings and bends. Following flow regime is observed with the increasing gas velocity in the horizontal pipe.

- Bubble Flow
- Plug Flow
- Stratified flow
- Wavy Stratified flow
- Slug Flow

Concurrent gas-liquid flow in horizontal pipes displays similar patterns to those for vertical flow; however, asymmetry is caused by the effect of gravity, which is most significant at low flow rates. The sequence of flow regimes is shown in Figure 2.13. In the bubbly regime the bubbles are confined to a region near the top of the pipe. On increasing the gas flow rate, the bubbles become larger and coalesce to form long bubbles giving what is known as the plug flow regime. At still higher gas flow rates the gas plugs join into form a continuous gas layer in the upper part of the pipe. This type of flow, in which the interface between the gas and the liquid is smooth, is known as the stratified flow regime. Owing to the lower viscosity and lower density of the gas it will flow faster than the liquid. As the gas flow rate is increased further, the interfacial shear stress becomes sufficient to generate waves on the surface of the liquid producing the wavy flow regime. As the gas flow rate continues to rise, the waves, which travel in the direction of flow, grow until their crests approach the top of the pipe and, as the gas breaks through, liquid is distributed over the wall of the pipe. This is known as the slug regime and should not be confused with the regime of

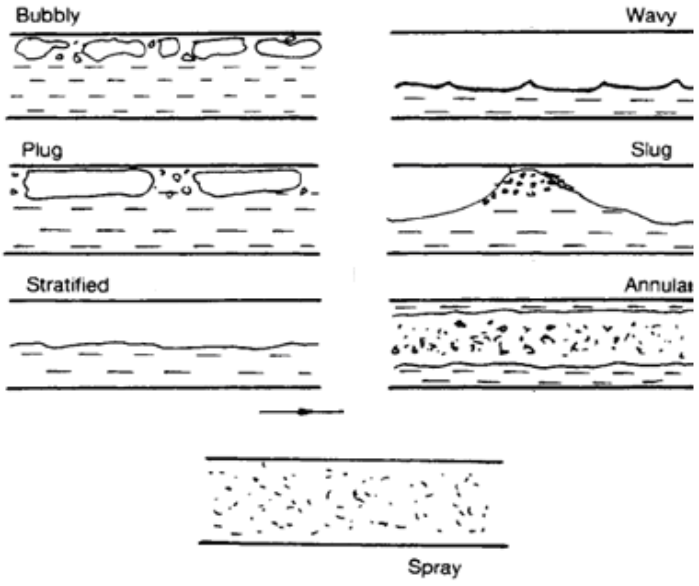

Figure 2.13 Flow Pattern in Horizontal Pipe.

the same name for vertical flow. At higher gas flow rates an annular regime is found as in vertical flow. At very high flow rates the liquid film may be very thin, the

majority of the liquid being dispersed as droplets in the gas core. This type of flow is called the spray or mist flow regime. It may be noted that similar flow regimes can be seen with immiscible liquid systems. If the densities of the two liquids are close the flow regimes for horizontal flow will more nearly resemble those for vertical flow.

2.14 Flow Regime Identification Techniques

Flow regime identification is of interest in the design, analysis and operation of many two phase flow system. Normally flow regimes are identified either by subjective judgements or by objective indication. There has been two approaches in identifying the flow regime, the direct measurement of the fluctuating quantities such as pressure and the void fraction and then application of statistical method to determine the flow pattern as done by many researchers Jones and Zuber, (1975; Shim and Jo, (2000) Costigan and Whalley, (1997) and use of visualization methods such as multi beam gamma densitometry and X-radiography as done by Abro et al. (1999). Many researchers have shown that void fraction can be used to add some objectivity to the flow regime identification. In general, such methods involve the use of the probability density function (PDF) of the void fraction signals. One of the earliest studies using this method was conducted by Jones and Zuber, (1975)while some of the more recent efforts have been reported by Costigan and Whalley, (1997). Jones and Zuber, (1975) investigated two-phase air and water flow in a vertical square channel 4.98 mm deep by 63.50 mm wide using an X-ray system to measure void fraction. They identified flow regime by plotting probability density functions (PDF) of each flow setting. Their results showed that a double peak in the PDF plot is an indicator of slug flow, while bubble and annular flows may be characterized by a single peak at low and high void fractions, respectively. Their study served as a basis for much of the work done in recent years. Franca et al. (1991), and Shim and Jo (2000) used probability density function (PDF) and power spectral density (PSD) of pressure drop fluctuations recorded by two pressure transducers to identified flow regime in gas–liquid two-phase flows. Franca et al. (1991) noted that, although PSD and PDF could not easily be used for regime identification, objective discrimination between separated and intermittent regimes might be possible by fractal techniques. Shim and

Jo (2000) based on PSD and PDF analyses, characterized bubbly, churn, and slug flow patterns in low-flow experiments in a vertical tube. However, their technique could only distinguish the bubbly flow regime at high flow rates. Some of the researchers Matsui (1984); Tutu (1984) used differential pressure techniques to acquire the PDF of void fraction. However it is found that this technique can mostly measure volumetric void or pressure fluctuation which varies with the distance of test locations. More recently (Song et al.,1995) investigated air and water flow in a 25 mm inside diameter vertical tube. They measured void fraction using an impedance sensor, and then used this data to determine several statistical parameters such as signal to noise ratio (SNR), power spectral density functions (PSDF),autocorrelation functions (ACF), and the PDF. They characterized bubble and slug flow through visual observations and examination of the PDF, SNR, and the time traces of the void signals, Their study showed that strong indicators of the bubble-to-slug transition are the shape of the PDF, a sharp increase in the SNR when the gas flow is increased, and the distinct change in apparent time scales calculated from the ACF. Merlio et al. (1977) have also used this impedance technique to identify the flow regime. This conductivity/impedance probe method works on the principle that the electrical impedance of a two-phase mixture is a function of concentration. Its popularity arises due to its low cost and almost instantaneous response. Probes of different geometries such as wire electrode Miya et al. (1971), point electrode Serizawa et al., (1975), ring electrode Andreussi and Bendiksen (1989), strip electrode Das et al. (2000),arc electrode Cheng et al. (2002) have been used widely for intrusive and no intrusive applications as well as point and global measurements. Apart from flow pattern identification, they have been adopted for measurement of different hydrodynamic parameters namely bubble size, frequency and velocity in bubbly flow, liquid film thickness in annular flow etc. Fossa, (2003) did the statistical analysis of the instantaneous cross sectional averaged void fraction obtained by the means of ring impedance probes. He calculated the main intermittent flow parameters such as slug frequency and length time average void fraction, minimum and average liquid film height.

2.15 Artificial Neural Network as Modelling Tool

The literature survey so far revealed that although there has been quite extensive work to model the gas liquid cyclonic separator but most of them cover large dimension reverse flow cyclones, while the compact gas liquid cyclone used in this study is an axial flow cyclone and due to its geometry the existing models are in appropriate to predict its performance.

Artificial neural network is a fairly new predicting and forecasting tool has successfully been used in solving problems related to function approximation, classification, pattern recognition and automatic control. Their applications cover research in multiphase flow metering Yeung and Baleny, (2007), aerospace Kim and Calise, (2008),banking Anandarajan et al. (2001), defence Lupo, (1989), Medical Eberhardt, (1999), Robotics Rao (1995), speech recognition Zhang Li-Peng et al. (1993), and telecommunications Altiparmak et al., (2009). However this technology has not been applied so far in the field of multiphase flow separation to describe the separation performance of the separator. This thesis adopts this non linear technique to model the separation efficiency of the compact gas liquid separator. Therefore it would be worth while to investigate the contribution of the artificial neural network in gas and petroleum industry. A brief literature survey in this direction revealed that this technology is occupying its place in solving problems related to oil and gas industry. The prediction of porosity and permeability in gas reservoir Olson (1998), the prediction of PVT properties for crude oil system Gharbi et al. (1999) and zone identification in complex reservoir White et al. (1995) are one of the few examples in this domain. In addition to these flow regime identification have also been done successfully using the neural network. Sun and Zhang (2008) identified flow regime based on frequency domain analysis of vortex flow using neural network.

2.15.1 Structure of Artificial Neural Network

An Artificial neural network (ANN) is collection of neurons arranged in layers. A single neuron as shown in Figure 2.14 is made up of following components:

- Weight
- Bias

- Net input
- Transfer function

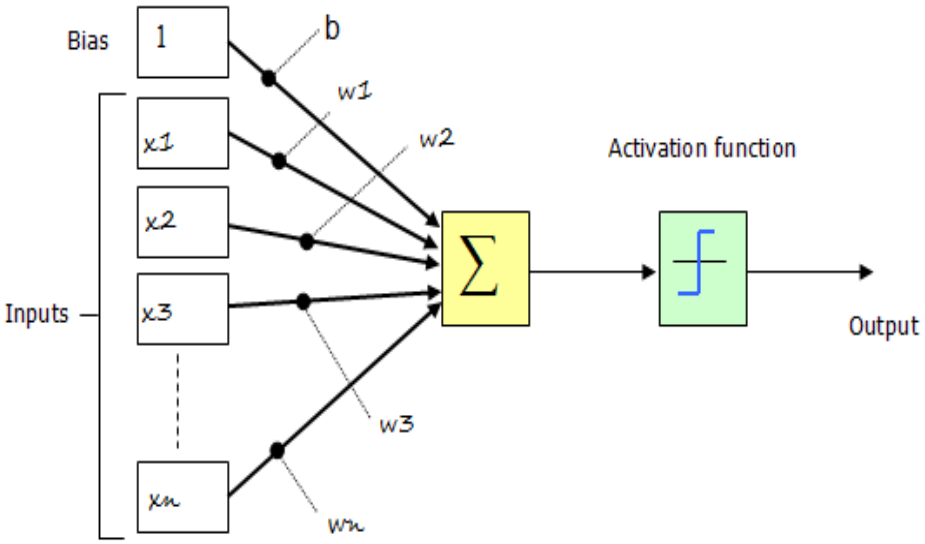

Figure 2.14 Mathematical Representation of a Neuron.

The function of the weights is to reduce the error between desired output and actual output. A neuron multiplies the input with weight to form the product (w_p). The sum of this product and bias (b) is then fed to a transfer function (f)which produces a scalar output a of the neuron. Thus mathematically the output of a single neuron can be written as:

$$a = f(w_p + b) \qquad (2\text{-}14)$$

The total input on a single neuron can be calculated from the following equation

$$t = w_1 x_1 + w_2 x_2 + w_3 x3 + \ldots\ldots\ldots w_n x_n \quad (2\text{-}15)$$

Where

$w_1 \ldots . w_n$ are the weights of neurons

$x_{1.} \ldots\ldots x_n$ are the associated inputs.

These neurons are group together to form layers. The first and last layer is called as input and output layer respectively while the intermediate layers are called as hidden layers. Each layer includes the weight matrix, the summers, the bias vector, the transfer function boxes and output vector for every neuron in the layer.

2.15.2 Feed-Forward Neural Network

On the basic of the connection of the neuron with the layers the ANNs have been classified as feed-forward and recurrent neural network. Feed-forward ANNs tend to be straight forward networks that associate inputs with outputs in forward direction only without any feed back connection as shown in the Figure 2.15. However the recurrent neural networks do contain feedback connection and are generally used to capture the dynamic character static of the process. The feed-forward neural network can be further sub classified into multi-layer perceptron radial basis function and

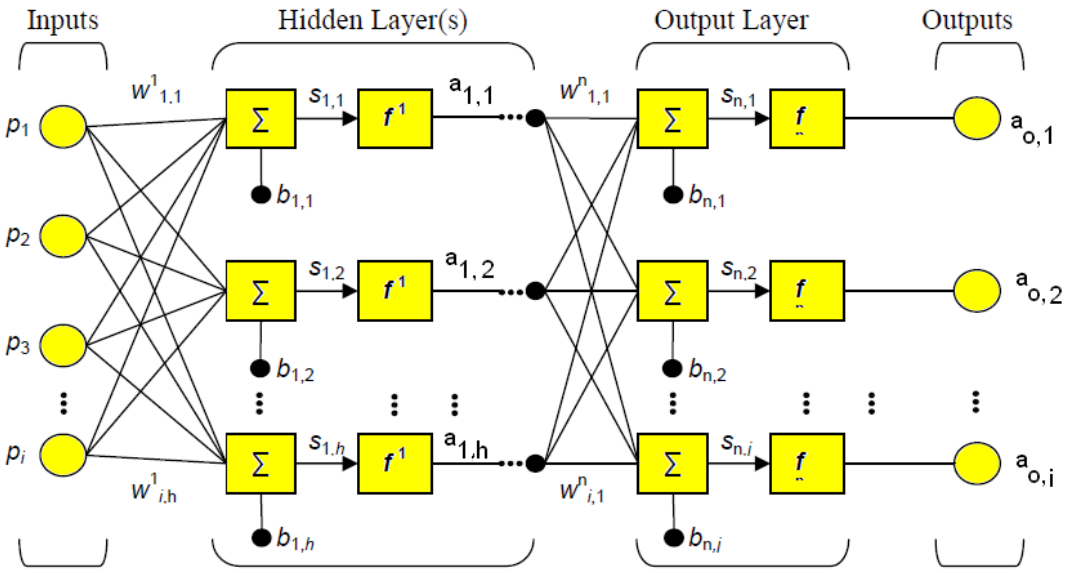

Figure 2.15 Feed-Forward Neural Network

Kohonen Self Organizing Map. This study uses the multi layer perception network with the back propagation to predict the separator efficiency of a compact separator.

The output from a single layer following the equation 2-14 can be given by the following equation:

$$a_{1,h} = f^{1}\left(\sum_{i=1}^{I} w_{i,h}^{1} p + b_{1,h}\right) \qquad (2\text{-}16)$$

The output from a two layer neural network thus can be given from the following equation:

$$a_{o,j} = f^{2}\left(\sum_{h=1}^{H}\left(w_{h,j}^{2}\left(f^{1}\left(\sum_{i=1}^{I} w_{i,h}^{1} p + b_{1,h}\right)\right) + b_{2,j}\right)\right) \qquad (2\text{-}17)$$

2.15.3 Training Neural Network

The philosophy of neural network revolves in training these neurons by adjusting the weights using any of suitable algorithms such as back propagation. A series of input and targets are passed to the network, during which neural network learns from the data capturing any linear or non linear complex trends in the data. Once trained the neural network provides reliable prediction for new unseen situations. Supervised and unsupervised learning are two most commonly used training schemes. A set of input along with the target set is presented to network in supervised learning to make them learn the relationship between the variables. On the other hand unsupervised learning used in Kohonen self-organizing map does not use any known target data set rather the network self-organizes itself to identify the salient properties of the input data set.

2.15.4 Back Propagation Training Algorithm

Several different training algorithms are available for the feed-forward neural network. The best-known examples are back propagation algorithm and relatively faster modern second-order algorithms such as conjugate gradient descent and Levenberg-Marquardt. The back-propagation is a core supervised learning algorithm, in which error for an output variable is calculated as the difference between the target output (t) and network output (a_o) which is then propagated back from output nodes

to the inner nodes. The sum of square error function is usually used as an error function.

$$SSE = \frac{1}{2}\sum_{j=1}^{N}(a_0 - t)^2 \qquad (2\text{-}18)$$

The back-propagation actually works in two phases, the forward and reverse pass. The algorithm starts with the initialization of weight of each neurons in the forward phase .The output at each layer of the neural network is then calculated by summing the product of input to each neuron with their respective weight which is then fed to the activation function which generates the final output of the layer, the output of the first layer becomes the input to second layer and so on. The final output of the neural network is then compared to actual output and then error in the form of mean square error i.e. (actual-target)^2 is propagated back from output layer to the input layer through the hidden layers. The weights are modified as the error is back propagated through the networks. This represents the first iteration or the epoch. This process is then repeated until the error between neural network output and the actual output is minimized.

The back propagation algorithm uses gradient descent method to minimize the error function with respect to modified network weights. A learning rate or a step size ranging from 0 to 1 is usually specified which determines the magnitude of the weights changes. A value of small learning rate slows down the process while a large value may cause network oscillation in weight space. This problem is usually tackled by introducing an additional momentum parameter which results faster convergence. The values of learning rate and momentum parameter are usually determined through trial and error.

One of the disadvantages of this algorithm is that training time increases with the size of the network and a global minimum is not guaranteed. One technique that is used to speed up learning is the use of conjugate-gradient algorithm which uses the second order derivate of the error function.

2.15.5 Generalization or Over-fitting

Generalization is one of the critical issues in developing a neural network. Over-fitting problem or poor generalization capability happens when a neural network over learns during the training period. This generalization error is too large when the input training sample is less than network parameter size. Early stopping and Bayesian regularization are two widely used approaches suggested in literature to overcome this problem. The early stopping or cross validation technique is implemented by dividing the sample data into training, validation and testing sub sets. The training set is used to train a neural net. The validation set is used to produce the validation error of a neural network on patterns that are trained during learning. The overall performance of the neural net is checked with the test sub set of the data which is not used during training. The validation set error is continuously monitored and training is stopped when validation error is increased continuously for a given set of iteration. The further training beyond this point will over trained the network so this weight and bias at the minimum validation error should be used for testing the network with the unseen test data set.

The Bayesian regularization on the other hand involves modifying the performance function, which is normally chosen to be mean of the sum of squares of the errors. This term when added to the performance function causes network to have smaller weight and bias producing less chance of over fitting.

Chapter 3

Compact Separator Rig

3.1 Introduction

I-SEP is the name given to a novel gas liquid axial flow compact separator by its inventor Caltec Ltd. A two phase air-water flow rig shown in Figure 3.1 was established incorporating I-SEP with a gravity separator hereafter will be referred as (HI-SEP) in the Process and System Engineering department of Cranfield University for the performance evaluation of this device. This chapter starts with the description of this rig followed by the data acquisition system (DAQ) used for recording and storing measurements in the system. It then discusses direct and inferred method to calculate the separation efficiency of the two separators (I-SEP and HI-SEP) used in the rig followed by single phase experimental analysis.

Figure 3.1 Compact Separator Rig

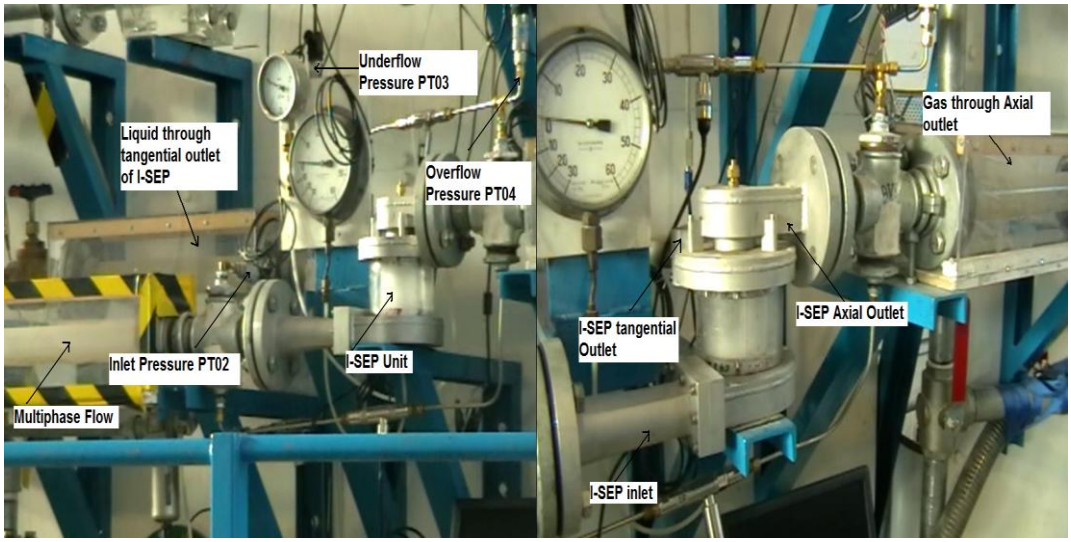

Figure 3.2a I-SEP unit with Pressure tapping at Inlet, Underflow and Overflow

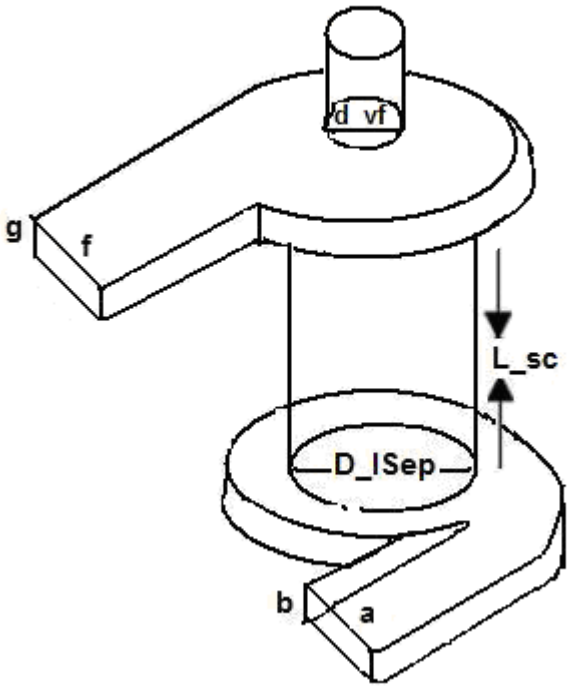

Figure 3.2b Engineering Diagram of I-SEP

Table 3-1 I-SEP Geometrical Dimension

I-SEP Dimensions	Description	Value
a	Inlet involute width	41mm
b	Inlet involute height	19mm
D_ISep	Internal Diameter of I_SEP	70 mm
L_sc	Separating chamber Length	10.1 cm
f	Tangential outlet involute width	41mm
g	Tangential outlet involute height	19mm
d_vf	Vortex finder Diameter	14mm

3.2 The I-SEP

The dimension of the I-SEP is shown in Table 3-1, while Figure 3.2a and Figure 3.2b represents the pictorial and engineering diagram of I-SEP respectively. It can be seen from this figures that it is a dual involutes compact separator that converts rotational energy into centrifugal force to separate particle of different density from air, water and oil. It is different from other axial flow cyclones as it uses inlet involute to produces the swirl inside the separator. The fluid is entered in I-SEP through an involute device where it is made to spin producing high g-force, then it progress up to a short separating chamber where after separation heavier phase moves radially outwards to the tangential outlet or underflow, while lighter fluid is moved towards axial outlet or overflow and collected via a vortex finder.

3.3 The Compact Separator Rig

The compact separator rig mainly consists of two separators; a fixed geometry I-SEP connected serially on its axial end with a gravity separator HI-SEP of 202 mm ID as shown in process and instrumentation diagram (P&ID) of the rig in Figure 3.3a. The

HI-SEP was used as knock out vessel which is assumed to completely separate the remaining liquid coming with gas stream exiting from the axial outlet of the I-SEP. The I-SEP and HI-SEP connection is shown in more detail in Figure 3.4. The introduction of air into this rig was achieved through Cranfield University owned fully automated high pressure multiphase flow test facility, which is being used for flow assurance, multiphase metering and control system research. This facility is designed for maximum operating pressure of 20 barg with air, water and oil as testing fluids. It is being controlled by latest Field bus based supervisory, control and data acquisition (SCADA) software named as DeltaV by Emerson Process Management.

The air was supplied from bank of two compressors connected in parallel capable of producing maximum air flow rate of 2550m^3/hr @ 7 barg. The air flow rate into the rig was controlled through automatic control valve handled by DeltaV system. The water was pumped from water tank to the rig; the flow rate of the water was controlled using a manual control valve named as CV2 in P&ID shown in Figure 3.3. The detail about the instrumentation used is given in the Table 3-2. Single phase V-cone flow meters were used to measured volumetric flow rate of the gas at the inlet of the rig, while the volumetric flow rate of the liquid was measured by the magnetic flow meters named as FM02, FM04, FM03 and FM09 in the P&ID show in Figure 3.3. Two control valves CV3 and CV4 were attached to axial and tangential outlet of the I-SEP respectively to study the effect of the backpressure on separation efficiency due to the throttling of these valves. After metering the gas and liquid inlet streams separately by a V-cone gas flow meter (FM01) and liquid flow meter (FM02), they were then commingled to form a gas-liquid (G-L) inlet mixture. The G-L inlet mixture before entering into I-SEP was passed through a straight 50.8mm pipe about 15 meters long to fully develop the flow regime(L/D=297). After passing through I-SEP this mixture was separated into a liquid-rich stream and gas-rich stream at

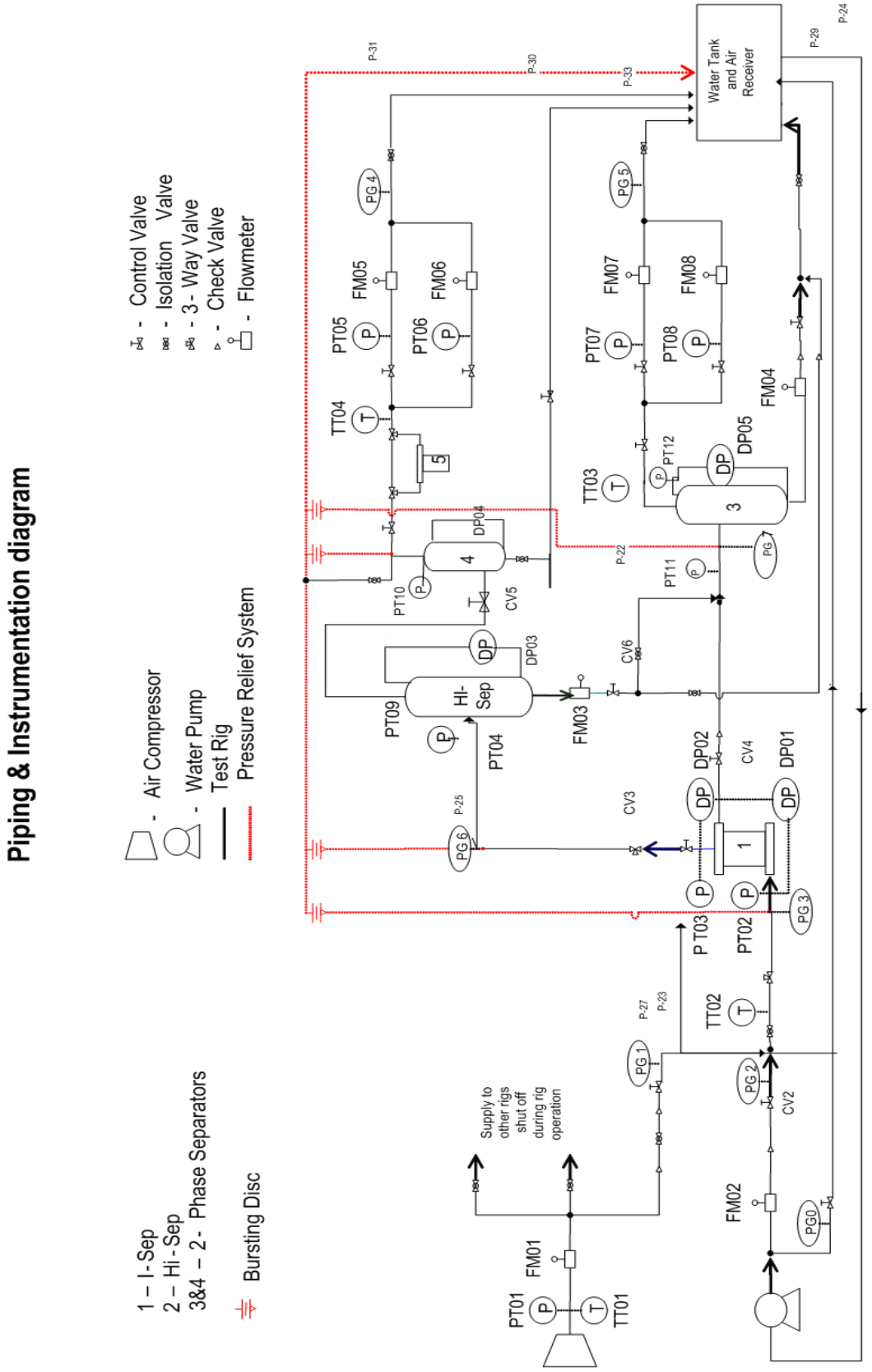

Figure 3.3a Process & Instrumentation Diagram of Compact Separator Rig

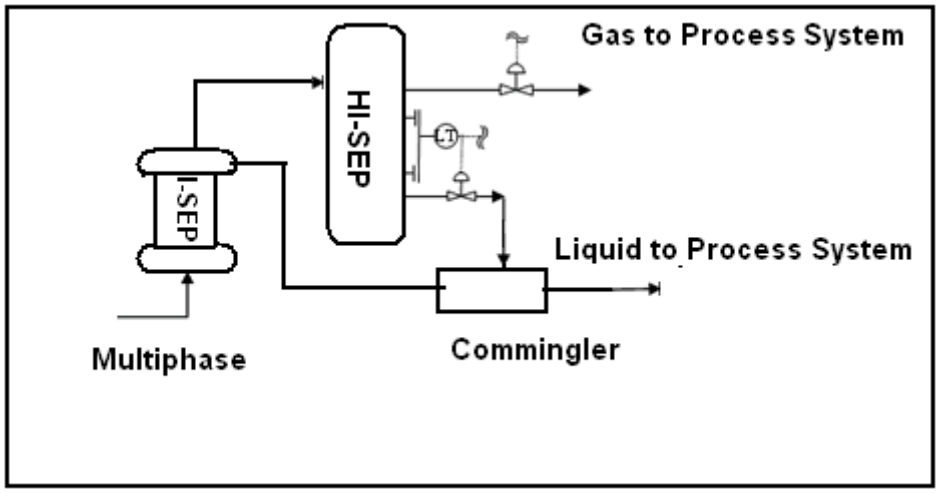

Figure 3.3b I-SEP & HI-SEP Connection

tangential and axial outlet respectively. The gas in liquid stream at tangential outlet of the I-SEP was measured after passing through another gravity separator named as unit 3 via gas flow meters FM07 and FM08.

The gas-rich mixture at axial outlet was sent to HI-SEP for further separation, which purifies the gas before measurement through gas flow meters named as FM05 and FM06 as shown in P&ID in Figure 3.3.The liquid in the this gas–rich mixture was measured through a liquid flow meter(FM04) connected at the liquid outlet of HI-SEP. This mean that liquid coming out through the axial outlet of I-SEP was not directly measured; it was actually measured after further separation through the HI-SEP. Similarly gas exiting though the both ends of the I-SEP, was actually measured after further separation through the two gravity separators.

Liquid and gas after separation through both I-SEP and HI-SEP were then sent back to the supply/receiver tank. It should also be noted that the gas flow meters FM08, FM06 were connected to one inch pipe while FM05 and FM07 were connected to 3 and 2 inch pipe respectively. The detail of all the gas and liquid flow meters and

pressure transducers including model, manufacturer, range and accuracy is given in the Table 3-3.

3.3.1 Data Acquisition of Process Variables

Pressure transducers from PTX/PMP 1400 series of Druck were used for measuring pressure, while PMP4110 series were used for measuring differential pressure at different location in the rig. Table 3-3 shows the name of the flow meters and pressure transducers used in the instrumentation. All of these measuring devices i.e. pressure transducer, flow meters etc use sensor for measurement. These sensors produced electrical signals in the form of voltage corresponding to the physical quantity being measured. However these devices need to be properly calibrated for the accurate measurement of physical quantities. Therefore these sensing devices

Table 3-2 Gas flow meter specifications

Tag #	Measures
FM01	Inlet gas volumetric flow rate
FM02	Inlet liquid volume
FM03	Liquid volumetric flow rate exiting HI-SEP
FM04	Liquid volumetric flow rate exiting HI-SEP
FM09	Liquid volumetric flow rate exiting Unit3
FM05	Gas flow meter used exiting at Hi-SEP
FM06	Gas flow meter used exiting at Hi-SEP
FM07	Gas flow meter used exiting at I-SEP tangential Outlet
FM08	Gas flow meter used exiting at I-SEP tangential Outlet
DP01	differential pressure between tangential out let and I-SEP in let.
DP02	Differential pressure between tangential out let and axial out let of I-SEP
DP03	Liquid level inside Hi-SEP
DP04	Liquid level inside Unit 4
DP05	Liquid level inside Unit 3
PT01	Inlet gas pressure
PT02	Mixture Pressure at I-Sep inlet
PT03	Mixture Pressure at I-Sep axial outlet
PT04	Mixture Pressure at Hi-Sep inlet
PT05	Pressure of gas existing Unit 4
PT06	Pressure of gas existing Unit 4
PT07	Pressure of gas existing Unit 3
PT08	Pressure of gas existing Unit 3
PT09	Pressure inside Hi-Sep
PT10	Pressure inside Unit 4
PT11	Mixture Pressure at Unit 3 inlet
PT12	Pressure inside Unit 3
PT20	Pressure at tangential outlet of I-SEP.

were first calibrated by plotting a calibration curve between the physical quantities i.e. pressure or flow rate and their corresponding voltage. The calibration curve showed a linear relation between voltage and physical quantity. The calibration curves are given in Appendix C. Following formula can be used to convert the voltage in corresponding physical quantity.

$$Y = Y_i + m(V - V_i) \qquad (3\text{-}1)$$

Where m is the slope or the gain calculated from the following formula:

Table 3-3 Flow meters & Pressure Transducers Details

Tag #	Model	Manufacturer	Range	Error
FM01	V-Cone Meter		75-450 Sm^3/hr	
FM02	MagFlow Meter	Dunfoss	0.05-9.8 l/s	≤ 1% (call manuf.)
FM03	MagFlow Meter	Endress+Hauser	0.05-2.4 l/s	≤ 1% for Q≥0.1 l/s
FM04	MagFlow Meter	Endress+Hauser	0-6.283 l/s	≤ 1% for Q≥0.2 l/s
FM09	MagFlow Meter		0-9.8 l/s	
FM05	3" Wafer Cone	McCrometer	104-1047.68 Sm^3/hr	±0.5%
FM06	1" V-Cone	McCrometer	17.46-174.62 Sm^3/hr	±0.5%
FM07	2" Wafer-Cone	McCrometer	52.38-523.85 Sm^3/hr	±0.5%
FM08	1" V Cone	McCrometer	8.73-87.31 Sm^3/hr	±0.5%
FM05*	3" Wafer Cone	Fuji	4.26-528.45(mbar)	±0.1%
FM06*	1" V-Cone	Fuji	1.56-168.74(mbar)	±0.1%
FM07*	2" Wafer-Cone	Fuji	5.38-729.70(mbar)	±0.1%
FM08*	1" V Cone	Fuji	1.24-130.69(mbar)	±0.1%
DP01	PMP 4100	Druck	0-3.5 bar	±0.04%
DP02	PMP 4100	Druck	0-2.0 bard	±0.04%
DP03	PMP 4100	Druck	0-3.5bar	±0.04%
DP04	PMP 4100	Druck	0-70 mbar	±0.04%
DP05	PMP 4100	Druck	0-3.5bar	±0.04%
PT01	PTX 1400	Druck	0-6 bar	±0.15%
PT02	PMP1400	Druck	0-6 bar	±0.15%
PT03	PMP1400	Druck	0-6 bar	±0.15%
PT04	PMP1400	Druck	0-6 bar	±0.15%
PT05	PMP1400	Druck	0-4 bar	±0.15%
PT06	PMP1400	Druck	0-4 bar	±0.15%
PT07	PMP1400	Druck	0-4 bar	±0.15%
PT08	PMP1400	Druck	0-4 bar	±0.15%
PT09	PMP1400	Druck	0-6 bar	±0.15%
PT10	PMP1400	Druck	0-6 bar	±0.15%
PT11	PMP1400	Druck	0-6 bar	±0.15%
PT12	PMP1400	Druck	0-6 bar	±0.15%
PT20	PMP1400	Druck	0-6 bar	±0.15%

$$m = \frac{Y_f - Y_i}{V_f - V_i} \qquad (3\text{-}2)$$

Y is Physical quantity being measured, it may be pressure, differential pressure or flow rate. Y_i is the initial value of the physical quantity which may be pressure or flow rate of liquid and gas. V_i is the initial value of the voltage observed at given initial value of the physical quantity. V is the corresponding voltage measured by the sensing device such as pressure transducer, flow meter, differential pressure transducer. Y_f is the final or last value of the physical quantity used during the calibration of the device. V_f is the last or final value of voltage observed corresponding to the last value of the physical quantity during the calibration of the device.

The data through these calibrated measurement devices was acquired at a sampling frequency of 20 Hz through National Instrument DAQ 16 and 32 I/O cards, with BNC 2090 and SC2345 as data conditioning devices using National Instruments LABVIEW as developing software.

3.3.2 Remote Monitoring of the Compact Separator Rig

It was one of the objectives of this thesis to make this rig accessible to the remote user through internet and mobile devices so that a CALTEC can remotely access the rig experimental data and can also actually see the working of the rig through web cam live on internet. The idea of remotely accessing the rig was implemented and tested on a two phase flow rig during the initial phase of this thesis (Qazi and Yeung,2006). Following that approach a Web and WAP based multi tier application was developed using active server page technology and wireless mark up language , through which a user can access the rig either with a mobile device or through internet. A web server was created which connects the internet and mobile user to the DAQ application. The data acquired from the rig was displayed live through a web page to the internet and mobile user. The web server also accepts the command signal through the mobile device to activate a web cam takes the online photo of the rig and

then sends back that picture to the user. The detailed methodology about this application is given in Appendix A.

3.4 I-SEP Separation Efficiency

The separation efficiency definition used in this thesis is based on fraction of inlet mass of liquid and gas recovered at tangential and axial outlet of the I-SEP respectively and expressed in percentage. The liquid and gas rich streams were found to contain small portion of gas and liquid at the tangential and axial outlet of I-SEP respectively which are named as Gas Carry Under (GCU) and Liquid Carry Over (LCO) in this thesis. On this basis four terms are defined to analyze the separation efficiency of the separator. They are liquid separation efficiency η_l, gas separation efficiency η_g, GCU and LCO represented in equation 3-3 to 3-6 respectively.

$$\eta_g = \frac{m_a^g}{m_a^g + m_t^g} \qquad (3\text{-}3)$$

$$\eta_l = \frac{m_t^l}{m_a^l + m_t^l} \qquad (3\text{-}4)$$

$$\text{LCO} = \frac{m_a^l}{m_a^l + m_t^l} \qquad (3\text{-}5)$$

$$\text{GCU} = \frac{m_t^g}{m_a^g + m_t^g} \qquad (3\text{-}6)$$

Where

$m_t^g(kg/s), m_a^g(kg/s)$ is the mass flow rate of the gas at tangential and axial outlet of the separator.

$m_t^l(kg/s), m_a^l(kg/s)$ are the mass flow rates of the liquid at tangential and axial outlet of the separator. The mass flow rate of the gas at the respective outlet using the

general gas equation and definition of density can be calculated from the following relationship.

$$m = \frac{Q * P}{R * T} \qquad (3\text{-}7)$$

Following the above relationship the mass of gas at the tangential and axial outlet can then be given by following relationships:

Gas mass flow rate at tangential outlet: $$m_t^g = \frac{Q_t^g * P_t}{R * (T_t + 273)} \qquad (3\text{-}8)$$

Gas mass flow rate at axial outlet: $$m_a^g = \frac{Q_a^g * P_a}{R * (T_a + 273)} \qquad (3\text{-}9)$$

Where $Q_a^g, Q_a^g, P_a, T_a, P_t, T_t$ are the volumetric flow rate (calculated in m^3/s), pressure measured in bar (converted into corresponding SI unit of Pascal in the calculation) and temperature in Kelvin of the gas at the axial and tangential outlet of the I-SEP respectively. Q_t^g is the gas volume flow rate at tangential outlet of I-SEP and was measured by V-cone gas flow meter FM07 and FM08 while Q_a^g is the gas volume flow rate at axial outlet of HI-SEP and measured by V-cone gas flow meter named as FM05 and FM06. The value of the gas constant R was taken as 287.05 J/kg-K.

Liquid mass flow rate was calculated by multiplying the liquid volumetric flow rate to water density which is taken as 1000 kg/m^3 as all these experiments were conducted at room temperature.

Liquid mass flow rate at axial outlet $m_a^l = Q_a^l * 1000$

Liquid mass flow rate at tangential outlet $m_t^l = Q_t^l * 1000$

Where Q_a^l was measured by FM03 or FM04 in litre /sec connected at liquid outlet of HI-SEP and Q_t^l is the liquid volumetric flow rate at tangential outlet of the I-SEP and was measured indirectly by FM04 or FM09 in litre /sec connected at gravity

separator (unit 3) which was linked to the underflow of the I-SEP as described above.

3.5 Techniques to Infer Mass Flow at I-Sep Outlets

The gas volumetric flow rate as discussed above was being measured by the gas flow meters which are not directly connected to the I-SEP, these means if the above definitions of efficiency along with the definitions of the masses are used then these may not be the accurate efficiency of the I-SEP due to damping effect of liquid level in the respective gravity separators, this problem leads to infer the mass at the respective end of the I-SEP. Two approaches were used to solve this problem:

- Mass Balance approached
- Non linear estimating technique using KALMAN filter.

3.5.1 Mass Balance Approach

The mass flow rate at the axial outlet of the I-SEP can be inferred by subtracting the mass flow rate of gas and liquid at tangential outlet of I-SEP from the inlet mass flow rate.

- Gas mass flow rate at axial outlet of I-SEP $m_a^g = m_{in}^g - m_t^g$
- Liquid mass flow rate at axial outlet of I-SEP $m_a^l = m_{in}^l - m_t^l$

This approach however may be affected by the fluctuating liquid level inside the gravity separator, due this reason the effect of liquid level inside the gravity separator in this method is also investigated which is discussed in the next section.

3.5.1.1 Effect of Liquid Level Inside the Gravity Separator

The accurate measurement of the volumetric liquid flow rate of liquid is necessary to infer the correct mass flow rate of the liquid at the I-SEP outlets. The volumetric liquid flow rate at inlet is directly measured using the FM02 however at the tangential and axial outlet of the I-SEP it was measured after further separation through another gravity separator named as unit 3 in the P&ID diagram. The liquid level inside the gravity separator was controlled using the manual control valve (CV7) attached to the liquid leg of these gravity separators.

The measurement of the liquid flow rate after the gravity separator may not represent the exact liquid flow rate coming out through the tangential outlet due to the fluctuating liquid level inside the gravity separator. This could however be estimated by considering the change in liquid level inside the gravity separator. If Q_t^l is liquid flow rate at tangential outlet of I-SEP and Q_{ta}^l is the actual liquid flow rate measured after the gravity separator, then following equation could be used to represent the relationship between liquid coming out through the tangential outlet and measured through FM09 at the liquid leg of gravity separator.

$$Q_t^l - Q_{ta}^l = \Delta V \qquad (3\text{-}10)$$

Where ΔV is the change in the liquid volume per second inside the gravity separator and it can be determined using the change in the liquid level Δh and radius r of the gravity separator. This gives the following form of the equation.

$$Q_t^l - Q_{ta}^l = \pi r^2 \Delta h \qquad (3\text{-}11)$$

Thus equation 3-11 can be used to calculate the liquid coming out from the tangential outlet of the I-SEP and is given by the following equation:

$$Q_t^l = Q_{ta}^l + \pi r^2 \Delta h \qquad (3\text{-}12)$$

If liquid level does not change throughout the recoding of the experimental data this mean that the liquid coming out from the gravity separator and measured by liquid flow meter FM09 is same as liquid coming out from the tangential outlet of the I-SEP. This value of Q_t^l obtained from the equation (3-12) can then be used to determine mass flow rate of the liquid at tangential outlet i.e. m_t^l which can then be used to determine the mass flow rate of the liquid at the axial outlet of the I-SEP using the equation $m_a^l = m_{in}^l - m_t^l$.

The inferred liquid flow rate at the axial outlet was calculated with or without the liquid level fluctuation in the gravity separator attached to the tangential outlet of the I-SEP. The effect of the changing liquid level inside the gravity separator on the inferred instantaneous value of the liquid flow rate is shown in Figure 3.4.The legend WH in Figure 3.4 represents the liquid flow rate as calculated considering the liquid

level fluctuation inside the gravity separator and legend WOH represent that was calculated without the effect of liquid level.

Following the same approach the mean value of the liquid flow rate at the axial outlet of the I-SEP is compared in Table 3.4. The mean value of liquid flow rate calculated with or without the liquid level fluctuation although is similar in most of the experiments, however for some experiments the liquid level fluctuation has produced a slight difference as can be seen in the Table 3.4 .

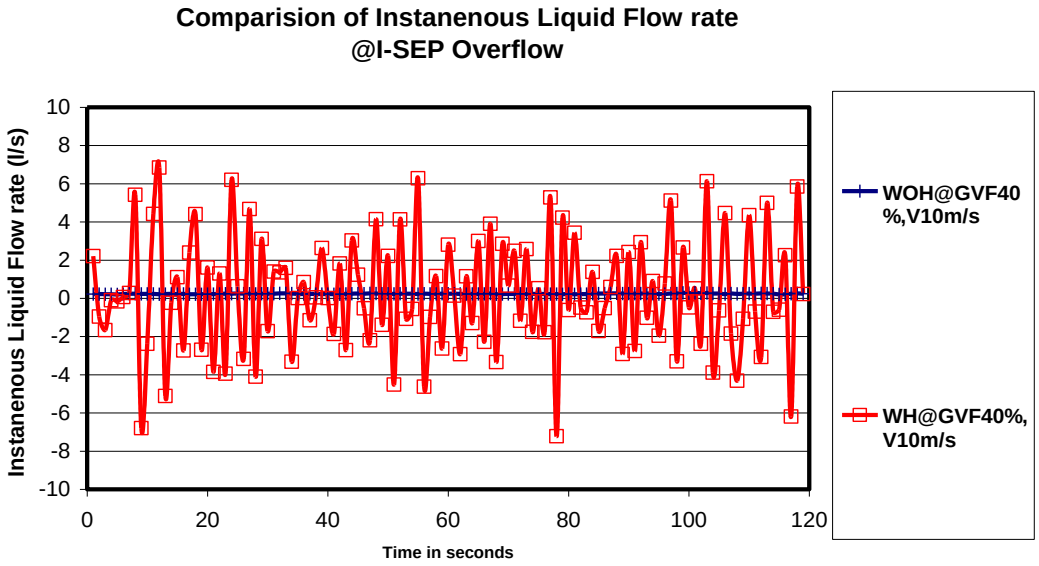

Figure 3.4 Comparison of Instantaneous liquid flow rate at I-SEP Axial Outlet

This may be because of the lack of dynamic control of the liquid level inside the gravity separator as during the recording of the data the liquid level may change which could give rise an difference in calculating the mean value of the liquid flow rate at the axial outlet. One of the other possible reasons is the short sampling time, as for the long sampling time the effect of the level fluctuation would be even out.

This mean the fluctuation in the liquid level during the data recoding may lead to some error in calculating infer liquid flow rate at the I-SEP outlets and hence may affect the exact and accurate efficiency of the I-SEP, therefore it was further investigated by applying estimating technique such KALMAN filter.

3.5.2 KALMAN FILTER

The KALMAN filter developed in 1960 is an efficient recursive filter consisting of sets of equations that estimate the state of a dynamic system from a series of incomplete and noisy measurements. It has been used in areas such as aerospace, marine navigation, nuclear power plant and many other applications. The KALMAN filter completes in two steps:

Table 3.4 Comparison of mean liquid flow rate at I-SEP axial outlet

Experiment matrix	Liquid flow rate (l/s) without liquid level fluctuation	Liquid flow rate (l/s) with liquid level fluctuation	Difference
GVF 40%,V10(m/s)	0.23	0.22	0.01
GVF 45%,V10(m/s)	0.15	0.15	0.00
GVF 50%,V10(m/s)	0.12	0.12	0.00
GVF 65%,V15(m/s)	0.08	0.07	0.01
GVF70%,V15(m/s)	0.08	0.09	-0.01
GVF 80%,V5(m/s)	0.10	0.10	0.00
GVF 85%,V25(m/s)	0.05	0.07	-0.02
GVF 90%,V5(m/s)	0.08	0.08	0.00
GVF 90%,V10(m/s)	0.08	0.08	0.00
GVF 98%,V30(m/s)	0.04	0.02	0.02

1. Prediction Step
2. Correction Step

The state and its associated error covariance matrix is predicted using a dynamic model of the process in the prediction step, this estimated state is then corrected in the correction step using the observation model. This procedure is repeated for each time step using the state of previous time step as initial value as shown in the Figure 3.5.

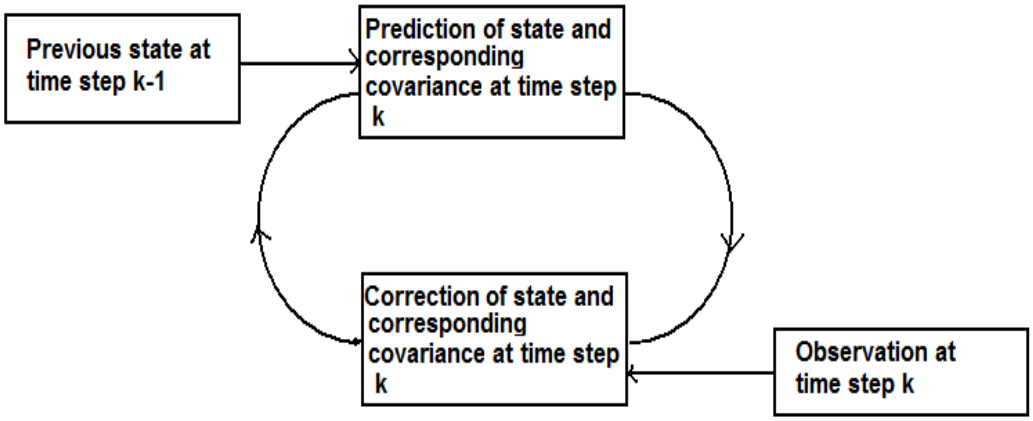

Figure 3.5 KALMAN filter Single Iteration

The state vector, the dynamic model and observation model thus becomes the basic component of the KALMAN filter.

The state vector describes the state of the dynamic system and represents the degree of the freedom. It consists of the variables of the interest in the dynamic system, for example the state vector of a moving train on a straight rail with constant velocity would constitute of its distance and velocity. The variables in the state vector however are not measured directly but they can be inferred from the measurable values. The state vector has two values at the same time, the predicted value in the predictor step which is called priori value and the corrected value in corrector step which is called as posteriori value.

Dynamic model defines the transformation of the state vector over time, whereas the observation model represents the relationship between state and the measurement. When the states are linearly related to the previous state and with the measurement vector i.e. when both the dynamic and observation model is linear then the estimation of the state can be achieved using a simple KALAN filter.

The estimation of new state vector based upon previous state vector using a simple KALMAN filter algorithm can be represented by the following two equations:

$$X_k = AX_{k-1} + BU_{k-1} + W_{k-1} \qquad (3\text{-}13)$$

$$Z_k = JX_k + V_k \qquad (3\text{-}14)$$

Where ,

X and Z is the state and measurement vector respectively

W and V represent the white noise in process and measurement respectively. The white noise means that these are not linked with their last values and is independent of any other variables.

The matrix 'A' relates the current state vector with the previous time state vector

The matrix 'B' is the matrix relating input to the state vector of the process.

The 'U ' is the input vector to the process

The matrix 'J' relates the state vector with the measurement vector Z.

Q and R are covariance in the measurement and process noise.

The output of the KALMAN filter is thus the state vector 'X' and uncertainty associated with it which is also called as error covariance matrix and usually represented by 'P'.

3.5.3 Extended KALMAN FILTER

The extended KALMAN filter is used in the situation when the process to be estimated is non-linear and (or) is non-linearly related with the measurement. The state estimation for such situations using the extended KALMAN filter can be represented by the following set of equations.

$$X_k=f(X_{k-1},U_{k-1},W_{k-1}) \qquad (3\text{-}15)$$

$$Z_k=h(X_k,V_k) \qquad (3\text{-}16)$$

Where,

W_k and V_k is the process and measurement noise respectively.

f is the non-linear function that relates the state at the previous time k-1 to state at the current step k. This function also contains as parameter the input U_{k-1} and zero mean process noise $W_{k-1.}$

h is non-linear function that relates the state x_k to the measurement z_k

3.5.3.1 Extended KALMAN Filter Algorithm

The extended KALMAN filter like the simple KALMAN filter algorithm completes in two steps the predictor step and the corrector step.

In the predictor step a priori estimation of state vector and covariance of error matrix is calculated represented by $\hat{X}_k^-$ and P_k^- respectively as shown in the equations below.

$$\hat{X}_k^- = f(\hat{X}_k, U_{k-1}, 0)$$
$$P_k^- = A_k P_{k-1} A_k^T + W_k Q_{k-1} W_k^T$$

In this case the A is called as Jacobean matrix which by definition is a matrix which contain partial derivatives of the function with respect to state vector X.
The KALMAN gain is then determined using the following equation during the corrector step.

$$K_k = P_k^- H_k^t (H_k P_k^- H_k^t + V_k R_k V_k^t)^{-1} \qquad (3\text{-}17)$$

Where H, V is the Jacobean matrix of partial derivate of h with respect to state vector X and measurement noise vector V.
The KALMAN gain thus calculated is then used to calculate the posteriori estimate of the state vector and covariance represented by $\hat{X}_k$ and P_k according to the equations.

$$\hat{X}_k = \hat{X}_k^- + K_k(Z_k - h(\hat{X}_k^-, 0)) \qquad (3\text{-}18)$$

$$P_k = (I - K_k H_k) P_k^- \qquad (3\text{-}19)$$

The state vector and covariance vector obtained in the corrector step is then feed back to predictor step for the next iteration. The overall cycle of the extended KALMAN filter algorithm is shown in the Figure 3.6

3.5.4 Infer Liquid and Gas flow rate using Extended KALMAN FILTER

The liquid level is non-linearly related to the incoming liquid and gas into the HI-SEP so an extended KALMAN filter given by equations (3-15 and 3-16) was used to estimate the liquid and gas flow rate coming out at the axial outlet of the I-SEP.
This system has two states i.e. the liquid level height and the separator pressure which were measured through a differential pressure transducer and pressure transducer

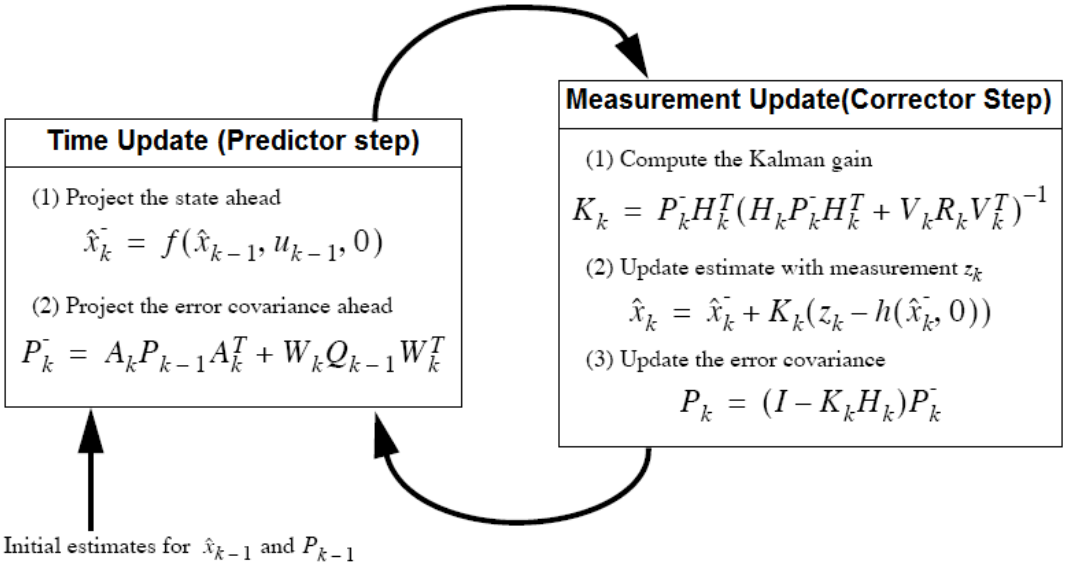

Figure 3.6 Extended KALMAN filter algorithm

respectively. Therefore the liquid level height and the pressure of the HI-SEP constitute the measurement vector (Z) of the process.

The relationship between the state and measurement vector was established by defining a model of HI-SEP using basic general gas equation. A mixture of high gas and low liquid emerging from the I-SEP axial outlet enters in the HI-SEP tangentially, HI-SEP acting as knock out vessel performs the full separation and gas was exited through gas outlet and liquid through the liquid outlet of the HI-SEP as shown in the Figure 3.7.

Let

- H_t is Total height of separator in metre
- h is height of the liquid level measure in metre
- V_g is Volume of gas in separator measured in m^3
- Q_{lin} is the input flow rate of liquid measured in m^3/s
- $Q_{lout}$is the output flow rate of liquid measured in m^3/s
- Q_{gin} is the input flow rate of gas measured in m^3/s
- Q_{gout} is the input flow rate of gas measured in m^3/s
- p is pressure (of gas) inside separator being measured by PT09 in bar
- A is the area of cross section measured in m^2
- ρ_g is the density of gas measure in kg/m^3
- M_g molecular weight of the gas
- N_g number of moles of the gas

- T is temperature in Kelvin
- m is mass of the gas in kg

Rate of change of liquid level

The volume of liquid in vessel or tank is Ah

$$\frac{dh(t)}{dt} = \frac{Q_{lin}(t) - Q_{lout}(t)}{A} \qquad (3\text{-}20)$$

Pressure Rate of Change

The equation of state for the gas in separator is given by:

$$pV_g = N_g RT \qquad (3\text{-}21)$$

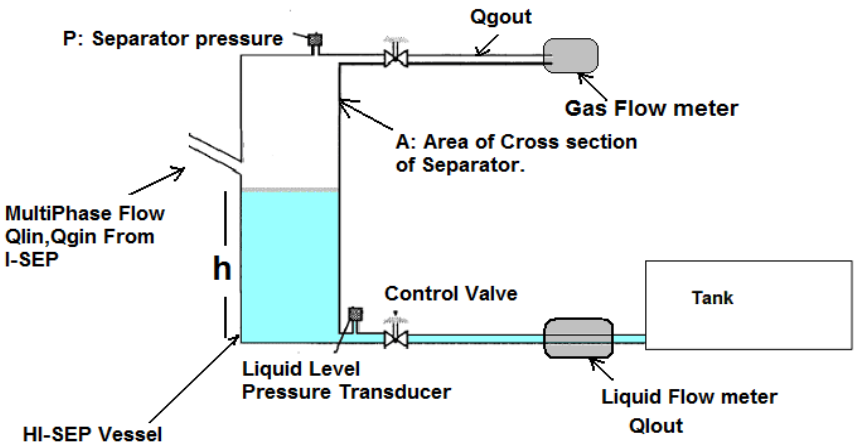

Figure 3.7 The HI-SEP.

Differentiating w.r.t to time:

$$V_g \frac{dp}{dt} = RT \frac{dN_g}{dt} - p \frac{dV_g}{dt} \qquad (3\text{-}22)$$

Where V_g =total volume of separator- volume of liquid in separator.
From the definition we know that number of moles of a gas is some time given as:

$$N_g = \frac{m}{M_g}$$

Where m can be found as: $\rho_g = \frac{m}{V_g}$ and $N_g = \frac{\rho_g V_g}{M_g}$

$$\frac{dN_g}{dt} = \frac{\rho_g}{M_g}(Q_{gin} - Q_{gout}) \qquad (3\text{-}23)$$

$$\frac{dV_g}{dt} = -\frac{dV_l}{dt} = -(Q_{lin} - Q_{lout}) \qquad (3\text{-}24)$$

Putting these equations in equation 3-12, 3-13 in 3-14

$$\frac{dp}{dt} = \frac{1}{A(H_t - h)}(RT\frac{\rho_g}{M_g}(Q_{gin} - Q_{gout}) + p(Q_{lin} - Q_{gout})) \qquad (3\text{-}25)$$

The equations (3-20) and (3-25) define the measurement vector for the extended KALMAN filter with Q_{gin}, Q_{lin} being unknown parameters which need to be determined. The two states of system i.e. height and separator pressure however may be expanded by incorporating the unknown parameter as states such that the two state of system i.e. height h and separator pressure p can be written in the following form.

$$h_{k+1} = h_k + f_1(h, Q_{lin}, Q_{lout}).\Delta t \qquad (3\text{-}26)$$

$$p_{k+1} = p_k + f_2(h, Q_{lin}, Q_{gin}, Q_{lout}, Q_{gout}).\Delta t \qquad (3\text{-}27)$$

Where Δt is the sampling time.

The next state of Q_{lin} and Q_{gin} are related to past values of the state as:

$$Q_{lin\_k+1} = Q_{lin\_k} \qquad (3\text{-}28)$$

$$Q_{gin\_k+1} = Q_{gin\_k} \qquad (3\text{-}29)$$

Since the height and pressure are also being measured therefore the measurement equations for extended KALMAN filter of these two states of the model i.e. height and the pressure can be given by the following equations:

$$h = g_1(h) \quad (3\text{-}30)$$

$$p = g_2(p) \quad (3\text{-}31)$$

The equation 3-26 and 3-27 were rearranged to determine the unknown parameters Q_{lin}, Q_{gin} .The initial guess for Q_{lin}, Q_{gin} was passed to KALMAN filter algorithm to estimate the next values of Q_{lin}, Q_{gin} .A programme was written in the MATLAB for this purpose and then two minutes time series data of every experiment are used to determine the actual values of the amount of the liquid and gas coming out from the I-SEP and going into the HI-SEP.

Cao (2008) has implemented the extended KALMAN filter using MATLAB, this code was incorporated with the developed MATLAB program to estimate the inferred gas and liquid flow rate at the I-SEP axial and tangential outlet respectively.

3.5.5 Results comparison

The instantaneous liquid and gas flow rate inferred at the I-SEP axial outlet through the KALMAN filter and mass difference is plotted in Figure 3.7 and 3.8 respectively. The legend starting with letter 'KM' in the figures represents the estimated value of gas and liquid flow rates resulted from KALMAN filter method, whereas the legend starting with letter 'MD' represents the result from mass difference method. It can be seen that estimation through the KALMAN filter is more stable than that of mass difference method as more fluctuation were observed both in liquid and gas flow rate when estimated through mass difference method. This difference is as discussed in last section is due to lack of proper dynamic control of the liquid level. These new values of Q_{lin} and Q_{gin} then used to determine the efficiency of the I-SEP separately. The efficiency calculated out using inferred value of Q_{lin} and Q_{gin} inferred from mass difference and KALMAN filter method showed that LCO is more realistic and consistent when calculated from KALMAN filter method, as mass difference method resulted zero and negative LCO % for some of the experiments as can be seen in Figure 3.9.

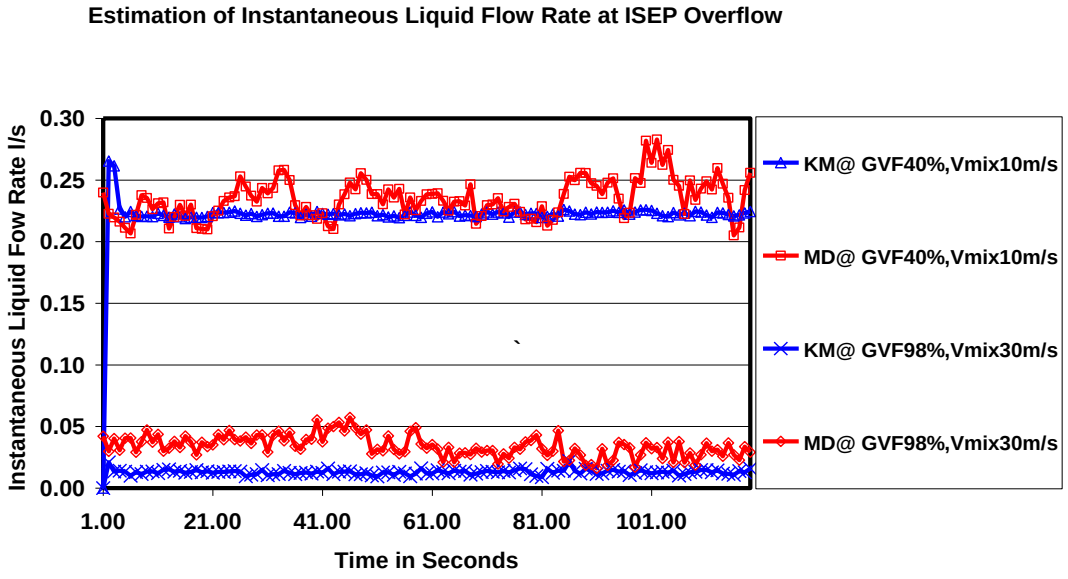

Figure 3.7 KALMAN Filter estimation of Liquid flow rate.

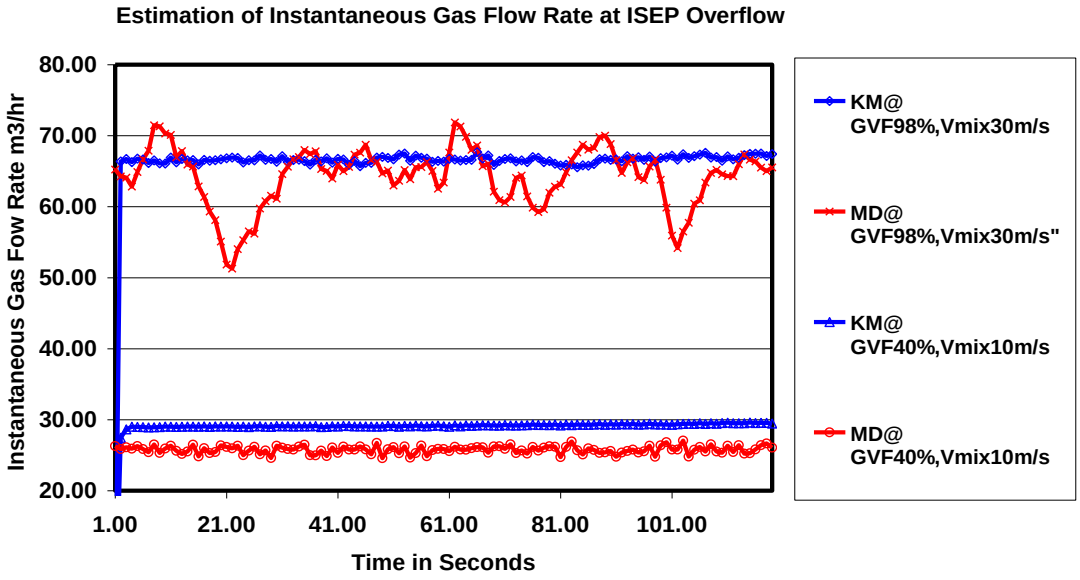

Figure 3.8 KALMAN Filter estimation of gas flow rate.

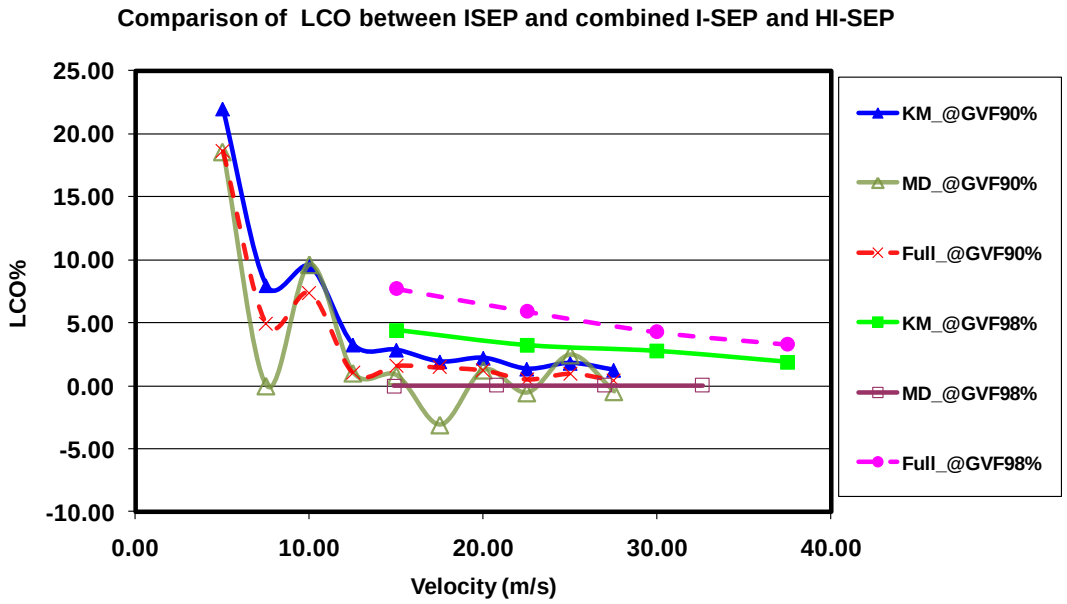

Figure 3.9 LCO% Comparison for Mass Difference and KALMAN filter method.

For example at 90% GVF and mixture velocity between 10 to 30 m/s the estimated LCO % from the mass difference method was found to be 0% and negative which is practically not possible. It is because the liquid measured through the tangential outlet of the I-SEP was greater than that of inlet. However it should be noted that this increased in flow rate of water at the tangential outlet could also be due to more water stored in the tank named as unit 3 in P&ID shown in Figure3.3a. However the KALMAN method estimated the correct situation and result more consistent and realistic LCO as can be seen in the figure. Therefore it is recommended to use this method to infer the efficiency of the I-SEP.

The infer LCO and GCU of I-SEP as observed with both the methods i.e. mass difference method and KALMAN filter method is compared with GCU and LCO of the combined I-SEP and HI-SEP in Figures 3.9 and Figures 3.10 respectively. The LCO and GCU for the combined efficiency of I-SEP and HI-SEP is shown with dotted lines using legend 'FULL' in the figure. It can be seen that LCO for combined I-SEP and HI-SEP for GVF90%, GVf98% is positive and in range of between 5 to 20% where mass difference method has inferred the LCO for I-SEP is negative, this

means that mass difference method completely failed to infer the LCO, whereas the KALMAN filter method for same case estimates positive LCO follows the trends same as observed in the LCO% of the combined I-SEP and HI-SEP. However it is either below or higher than the combined LCO. For example the infer LCO% of the I-SEP is lower than that of combined LCO% of both I-SEP and HI-SEP, it could be explained on the basis since the liquid level inside the HI-SEP is controlled manually so it is due to this reason more liquid comes out through liquid leg of the HI-SEP and measured by the liquid flow meter attached to the it and the liquid level actually inside the HI-SEP is dropped because less liquid is coming into the HI-SEP as compared to liquid going out through the HI-SEP liquid outlet.

The higher value of the infer LCO% for the I-SEP than that of combined I-SEP and HI-SEP could also be explained on the same basis, however in this case the valves is open too less so that the outgoing liquid level is less than that of the incoming liquid and resulted an increase in liquid level inside the HI-SEP. However the value of the infer LCO for the I-SEP is not very much different than of the combined LCO%.

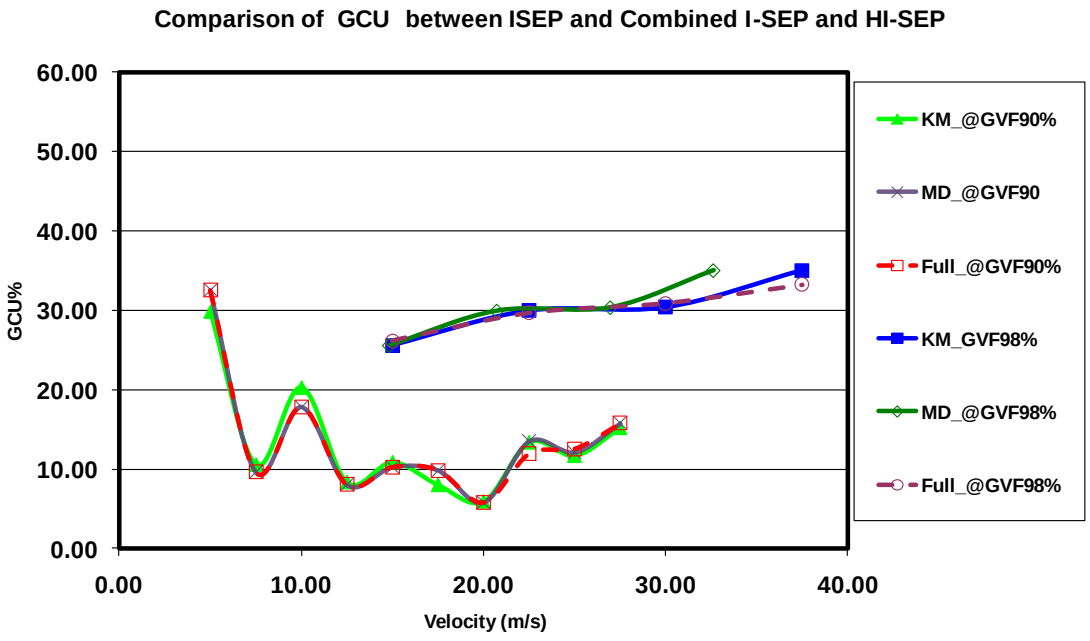

Figure 3.10 GCU% Comparison between I-SEP and Combined I-SEP and HI-SEP.

However the trend in the infer GCU resulted from the mass difference and KALMAN filter was found to more or less similar as can be seen in the Figure 3.10. The standard deviation in the inferred GCU from the mass difference method was found to be 15.37% while for the KALMAN method it was found to be 14.9% which shows the GCU as inferred from the KALMAN filter method is less scattered than that mass difference method. On this basis it was decided to use the KALMAN method to infer the separation efficiency of the I-SEP

Figure 3.8 compares the infer GCU for I-SEP using both the methods with that of the combined I-SEP and HI-SEP. It can be seen that mass difference method in most of the cases estimates almost equal GCU as obtained with the combined I-SEP and HI-SEP. It may not be very true as there is possibility that due to manual liquid level control the gas may escape through the liquid outlet of the HI-SEP and thus may be not similar to what is actually coming into the HI-SEP. On the other hand the KALMAN filter estimates although follows the same trends as combine GCU% of HI-SEP and I-SEP but with small difference. For example at GVF of 35%,90%,98% the estimation from the KALMAN filter method for the infer GCU % is slightly higher than that of combined I-SEP and HI-SEP GCU% and at other GVF values such as 70% for some of the experiments it is lower than the combined GCU% of both I-SEP and HI-SEP. This difference in infer GCU could be because of the manual liquid level control as when the liquid level goes down it may allow to release the gas through liquid outlet resulting a change in GCU%. Thus in this thesis the experimental analysis of the experiments uses the KALMAN filter method approach to infer the GCU and LCO % of the I-SEP.

3.6 Data Repository System

The data acquired from the DAQ is in text file format, this data was then exported into a relational database using Microsoft access. A data repository system was then developed using Microsoft access and Visual Basic that stores the efficiency calculated for both I-SEP alone and using both the separator (I-SEP & HI-SEP) in series. This system provides an online facility to retrieve the efficiency of the separator for any test experimental data. The details such as gas and liquid separation

efficiency, GCU, LCO ,loss coefficient, pressure drop across the I-SEP, estimated cut size diameter of the liquid drop, liquid and gas superficial velocity, mixture velocity along with gas density at all the three location of the I-SEP and many more can retrieved by running a simple query. This system thus makes it easy to analyze the experimental data at different operating condition.

3.7 Experiment Objectives

The Separation efficiency and the pressure drop across the gas cyclones are two major criteria used to evaluate the efficiency of the separators. These two parameters however depend upon the velocity distribution inside the cyclone which is affected by the inlet flow condition, the geometry and the resistance at the outlets of the separator. The inlet flow conditions are mainly related to the flow rates of the fluids, operating pressure and inlet flow regimes. These factors thus lead to define three different types of the experiments:

- Single Phase Experiments
- Multiphase Experiments
- Back Pressure Experiments

The objectives of the experiments were based upon to investigate the relationship between the operating condition with the separation efficiency and the pressure drop across the I-SEP to check the energy requirement of the I-SEP at the given inlet condition. It was also one of the objectives to find out most important parameter that dictates the separation efficiency of the I-SEP.

The inlet conditions during the experiments were generated using two independent but inter linked variables which are the mixture velocity (V_{mix}) of the fluid the gas volume fraction GVF of the mixture and inlet pressure (P_{inlet}).The mixture velocity V_{mix} was calculated at the inlet of the I-SEP rectangular section. The gas and liquid flow rates in Sm^3/hr and l/s respectively were then calculated at desire V_{mix}, GVF

and P_{inlet}. The experiments were then conducted introducing this calculated flow rate of air and liquid into the compact separator rig using the Delta V system of the Cranfield multiphase facility.

3.8 Single Phase Experiments

The single phase experiments were consisted of passing the single phase i.e. liquid and gas separately through the compact separator rig to know how single phase is split between the tangential and axial outlet of the I-SEP.

3.8.1 Gas Only Experiments

The GVF for the gas experiments was chosen to obvious 100% for the gas superficial velocity range V_{gs} between 5 to 10 m/s which corresponded to the gas flow rates between 75 Sm^3/hr to 750 Sm^3/hr at (interval of 75 Sm^3/hr) with inlet pressure monotonically increased from 1.14 bar to 4.85 bar respectively. Gas flow rates at the axial and tangential outlet were measured through gas flow meters FM05 and FM07 respectively due to high gas flow rates. The data was recorded for two minutes through DAQ system as defined in section 3.3.1. The time series data was used to calculate the infer gas and liquid flow rate at I-SEP tangential and axial outlet i.e. (Q_a^g) and (Q_a^l) using KALMAN method as discussed above.

3.8.1.1 Gas Splitting and Pressure Drop in the I-SEP

The amount of the gas that was split between the tangential and axial outlet was then calculated using the equation 3-3 & 3-6 and is termed as G_OF and G_UF respectively for single phase. The mass difference % of the gas between the inlet and two outlets of the I-SEP was found to between 0.2 to -6%. These experiments showed that the gas preferably flows more into the axial outlet than the tangential outlet as more than 80% of the inlet gas was found to exit through the axial outlet (according to our used definition it is G_OF) which increased up to 97.8% with the increased in the gas superficial velocity from 5.43 m/s to 10.80 m/s as shown in Figure 3.11. The percentage of inlet gas coming out through tangential outlet i.e. G_UF for the single phase gas experiments was found to be decreased monotonically from 18 to 2 %.

This can be explained on the basis of the observed pressures at the tangential and axial outlet, of which pressure at tangential outlet was always found higher than that of the axial outlet. The lower pressure at axial outlet created more pressure drop between inlet and axial outlet (which is termed as P_{13} in this thesis) than that of between inlet and tangential (which is termed as P_{12} in this thesis) as shown in Figure 3.12, thus creating an easier path for gas to escape through the axial outlet as compared to the tangential outlet. This phenomenon is similar to a side arm T junction where fluid is divided into side arm and run arm on the basis of pressure at these end and greater proportion of the fluid is passed through outlet having less pressure. It should also be noted here that due to relatively high pressure at the tangential outlet the density of air at this outlet will be higher than that at axial outlet. The ratio of pressure drop between inlet and axial outlet to that of between inlet and tangential (P_{13}/P_{12}) outlet was calculated and was found to increase with the amount

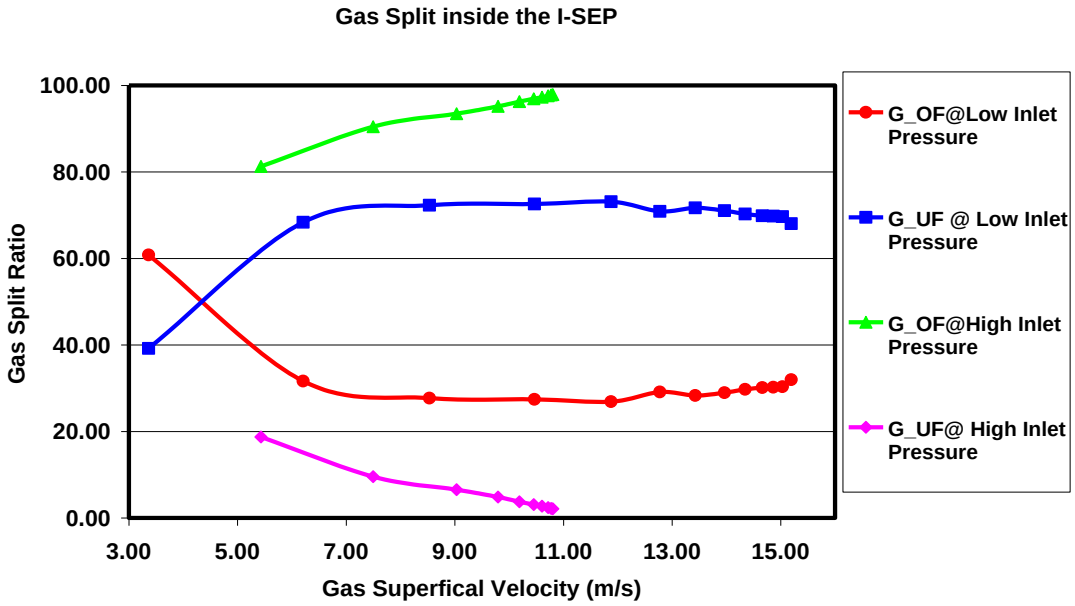

Figure 3.11 Splitting of the Gas Flow inside I-SEP

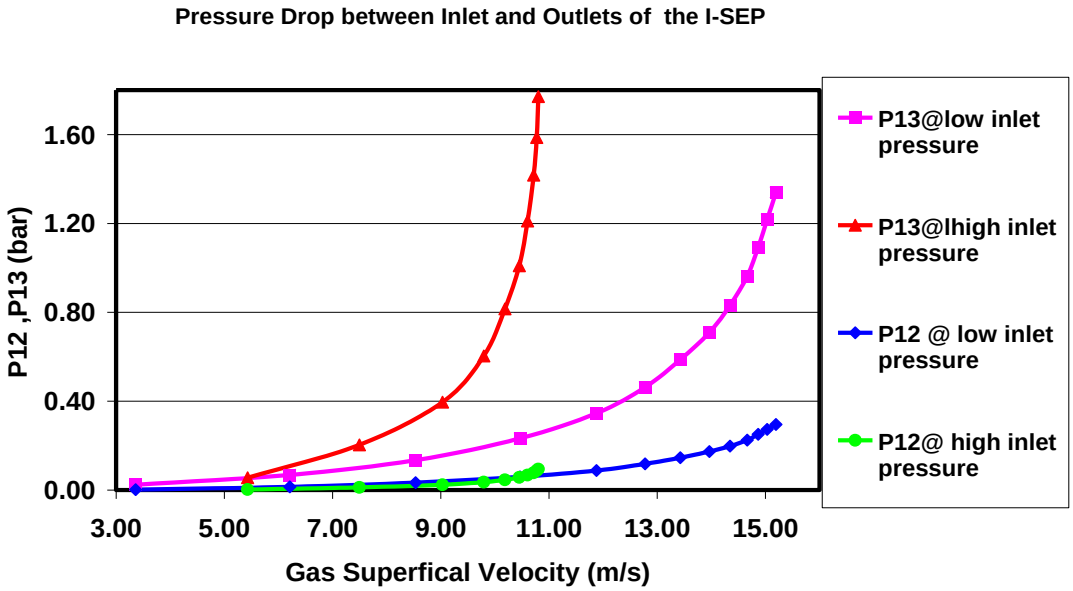

Figure 3.12 Pressure Drop for Single Phase (Gas) in I-SEP

of gas coming out at axial outlet i.e. G_OF as can be seen from Figure 3.13. This led to assume that it could be more effective parameters to define the split of the gas, inside the I-SEP. A greater value for this parameter means that more gas would be passing through the axial outlet of the I-SEP. In order to check this hypothesis another set of experiments for the single gas phase flow was performed with almost same flow rates but this time the inlet pressure was varied from 1.07 bar to 2.67 bar for air flow rate of 100 Sm^3/hr to 675 Sm^3/hr corresponding to gas superficial velocity from 3.3 m/s to 15 m/s. The same trend was observed again as axial pressure was found to be higher than that of tangential pressure. The pressure drop between axial and inlet i.e. P_{13} was once again found to be higher than that of between inlet and tangential outlet of I-SEP which will be called as P_{12}. However this time surprisingly the proportion of input gas coming out from the axial outlet was very less than that was coming out from tangential outlet, it was a ratio of about 30 to 70 % respectively i.e. 30 % was coming from the axial and rest from the tangential outlet. Moreover the this time the G_OF and G_UF were found to have slightly non linearly related with the gas superficial velocity as G_OF first decreased sharply

with the increase in gas superficial velocity then almost becomes constant but then again started increasing on further increasing gas superficial velocity.

However this time the ratio of pressure drop between inlet to axial outlet and that of between inlet to tangential outlet (P_{13}/P_{12}) was much lower than last time as can be seen from the Figure 3.13 and was found to increased with the increased in gas superficial velocity causing more gas to pass through the axial outlet. This showed that P_{13}/P_{12} is directly related to G_OF and using three important parameters i.e. gas superficial velocity, inlet pressure and ratio P_{13}/P_{12} may possibly be used to predict the splitting of the gas in single phase experiments.

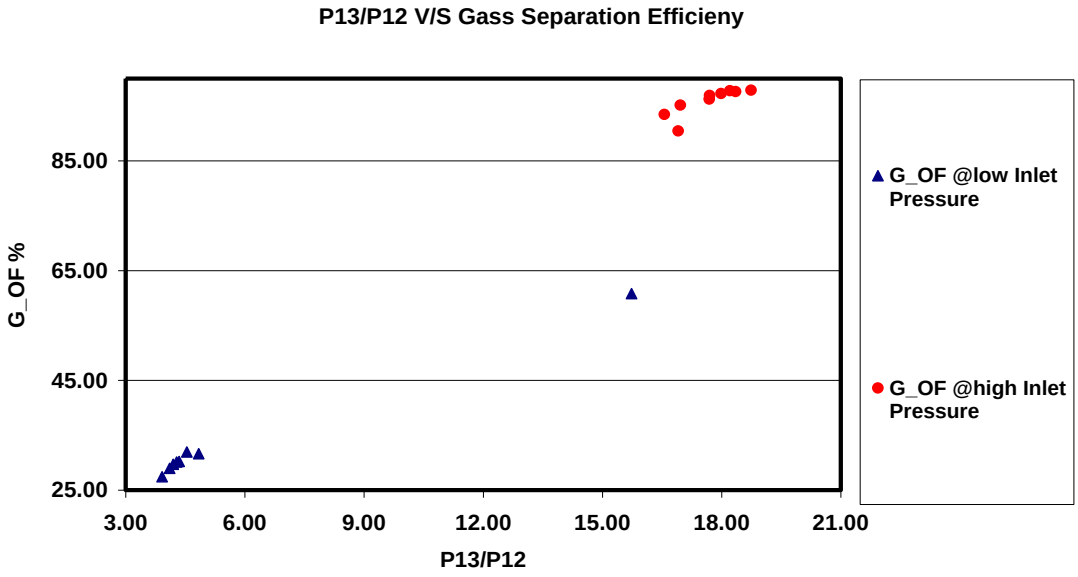

Figure 3.13 Effect of P13/P12 on Gas Split Ratio

3.8.1.2 Loss Coefficient of the Gas Phase

Loss coefficient is a dimensionless obtained by dividing static pressure with dynamic pressure. Loss coefficient between the inlet and axial outlet of I-SEP (K_{13}) was calculated according to the definition given in equation 2-13, and it was found to lie between 10 and 11 for low inlet pressure, however came out between 10 and 21 at high inlet pressure as shown in Figure 3.14. It was also observed that this number in

general chases the amount of the gas coming out through axial outlet i.e. G_OF , and as the more gas was directed towards the axial outlet, the loss coefficient value was also increased which means a more energy is need to push the gas towards axial outlet.

3.8.1.3 Back Pressure Gas Experiments

As stated in the beginning of this chapter that the gas splitting ratio is also affected by the resistance at the tangential and axial outlets of the separators, this was investigated by performing further experiments. The resistance at the tangential outlet of the I-SEP was varied by throttling the control valve attached to this end named as CV4 in P&ID diagram in Figure 3.3. These experiments were performed with 100% GVF having gas flow rates 175 Sm^3/hr, 275 Sm^3/hr and 375 Sm^3/hr corresponding to

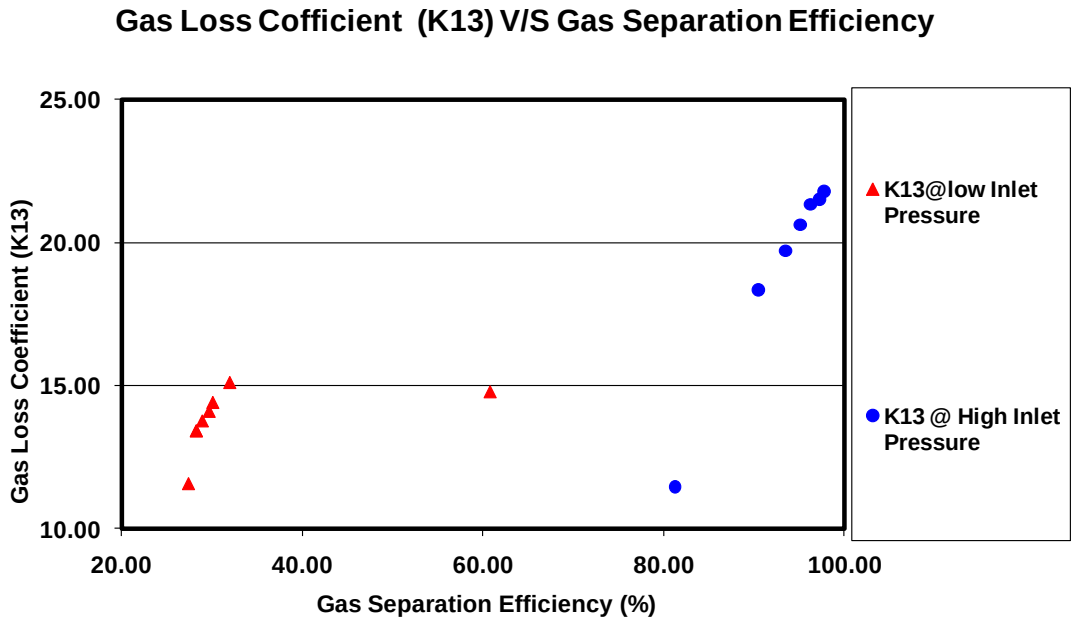

Figure 3.14 Loss Coefficient (K13) for Single Phase Gas inside I-SEP

superficial gas velocity 9m/s, 12m/s and 14 m/s respectively. The inlet pressure was kept at 1.2, 1.5 and 1.8 bar respectively. Gas flow rates at the axial and tangential outlet were measured through gas flow meters FM05 and FM07 respectively.

Each experiment was performed in four steps, the experiment started with introduction of desired gas flow rate into compact separator rig with control valve

CV4 fully opened the data was recorded for 2 minutes for fully opened control valve, then the resistance on the tangential outlet was varied by gradually closing the control valve CV4. The data was recorded for every experiment and corresponding gas G_OF and G_UF % was calculated. This procedure was repeated for other gas flow rates used in these experiments.

The throttling of control valve increased the inlet pressure which caused to increase the pressure at the tangential and axial outlet, however this increase in pressure was more mainly observed during third and fourth turns of the CV4 closing cycle. Like before the tangential pressure was more than axial pressure creating more pressure drop between axial and inlet than that of between tangential and inlet and due to this higher pressure drop more gas was diverted towards the axial outlet with the throttling of the valve. Thus throttling of the valve attached to the tangential outlet resulted in reduction of G_UF % and increased of gas separation efficiency with higher pressure drop between inlet and axial i.e. P_{13}

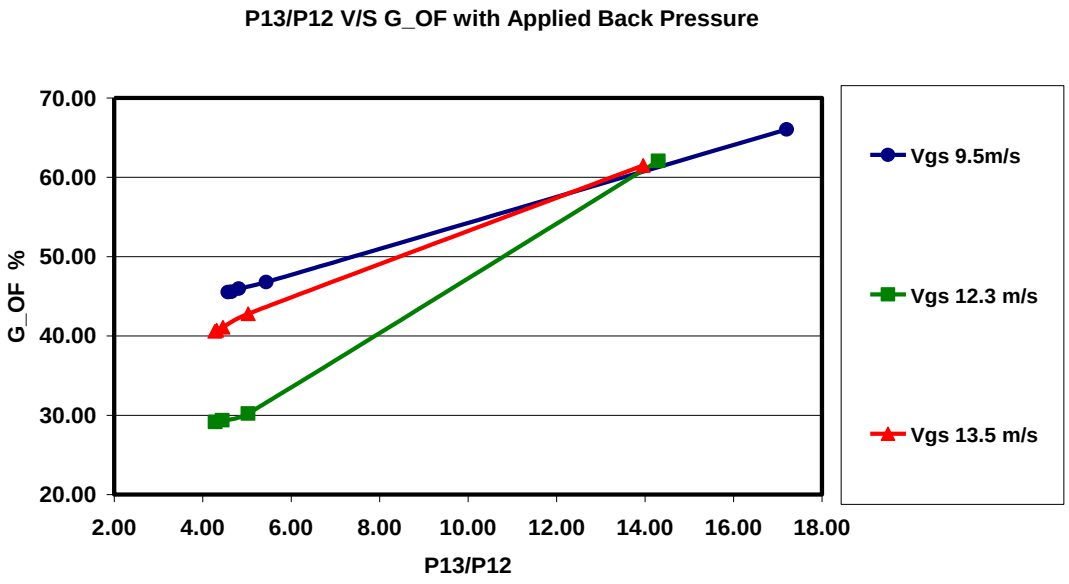

Figure 3.15 Effect of P_{13}/P_{12} on Gas Separation Efficiency during Back Pressure

It was further investigated which one of the operating variable could be used to best describe this splitting of gas during the throttling of the valve. P_{13}/P_{12} was checked again as it was found more related to the phase splitting during the single gas phase experiments. It can be seen from the Figure 3.15 that higher value of the P_{13}/P_{12} was observed for higher value of G_OF. For example the separation efficiency was increased due to the throttling of the valve from 45% to 66% with a reduction in G_UF % from 54 to 33%. The pressure between tangential and axial outlet during this throttling of the valve was increased from 0.15 bar to 0.25 bar and ratio of axial and tangential pressure drop to inlet i.e. P_{13}/P_{12} was found to increased from 4.57 at gas separation efficiency 45% to 17.20 with a corresponding increase in separation efficiency to 66%. This trend of P_{13}/P_{12} was repeated in other experiments when P_{13}/P_{12} was increase from 4.28 to 14.30 when gas separation efficiency was increased from 29.15 to 62.07%. Further comparison can be observed from the figure. These observations again strength the hypothesis that higher value of P_{13}/P_{12} creates more gas to pass through axial out let at given gas superficial velocity and inlet pressure.

3.8.1.4 Linear Regression to Predict Gas Splitting

The above analysis showed that P_{13}/P_{12} along with gas superficial velocity V_{gs} and inlet pressure P_{in} could possibly be used to predict the fraction of the gas coming out through axial outlet i.e. G_OF of I-SEP both with and without any back pressure. Following this approach a linear regression was done on the data obtained during these experiments using full set of low pressure experiment and only one third of the high pressure experiments and back pressure experiment so that the relation could be checked on unseen data. Following equation were obtained using Excel software. The testing of this equation is presented in Table 3-5. This is an empirical relationship that could be improved using more data points to make it more generalized.

$$G\_OF = 4.07 + 0.218V_{gs} + 5.27P_{in} + 3.6\frac{P_{13}}{P_{12}} \qquad (3\text{-}32)$$

The equation (3-32) is an empirical relationship obtained through the regression analysis. The data used for the regression covers gas superficial velocity i.e. V_{gs} from 3 to 15 m/s and inlet pressure i.e. P_{in} from 1 to 5 bar. The equation could be used for the extrapolation for values of Vgs and Pin less than 30 m/s and 15 bar respectively otherwise the gas efficiency would be calculated out more than 100% which is not practically possible. The regression could be more reliable by adding more experimental points.

3.8.2 Liquid only Experiments

Liquid phase experiment was performed in the same way. Liquid flow rate was varied from 1 l/s to 4 l/s corresponding to liquid superficial velocity value 0.2 to 1.03 m/s respectively. The experimental data was recorded as before using the DAQ system after the steady state for two minutes and KALMAN filter method was applied to

Table 3-5 Gas separation efficiency prediction using Regression Analysis

V_{gs} m/s	P_{in} bar	P_{13}/P_{12}	η_g (actual) %	η_g (predicted) %	Error%
10.61	3.49	17.99	97.26	89.00	8.50
10.72	4.01	18.35	97.62	93.00	4.73
10.77	4.48	18.21	97.80	95.00	2.86
10.80	4.85	18.74	97.88	99.00	-1.15
8.58	1.40	17.20	66.03	75.00	-13.58
10.55	1.78	14.30	62.07	67.00	-7.94
11.16	1.96	13.96	61.50	66.00	-7.32

infer the gas and liquid flow rate at axial outlet of the I-SEP. The amount of liquid split between axial and tangential outlet like the gas split ratios were calculated using the equation 3.4 and 3.5 and termed as L_OF and L_UF respectively.

These experiments showed the liquid has tendency to flow into tangential outlet more than axial outlet as the L_UF observed in all of these experiments were more than 90% as can be seen in the Figure 3.16. However, it was found to decrease slightly with the increase in the liquid superficial velocity as can be seen in the Figure 3.16. As the liquid flow rate was increased the inlet pressure also increased monotonically from 1 bar to 1.85 bar also causing the pressure at axial and tangential outlet to increase. However the pressure at the tangential outlet was initially found little lower than that of axial outlet but it then became higher than that of tangential pressure. It is due to this reason the pressure drop P_{13} initially was found little higher than P_{12} but following the trend of tangential pressure it than became less than P_{12}. This higher pressure drop between inlet and axial outlet sucked more liquid towards axial end hence slightly increasing the proportion of the liquid flowing through the axial outlet (which is termed as L_OF for single phase experiment). The interesting thing to note here is the effect of P_{13}/P_{12} on L_OF, as this number is increased L_OF was found to be decreased comparing to the gas split ratio i.e. G_UF, in gas experiment where it was found to increase with higher gas split ratio,. Alternatively P_{13}/P_{12} is directly linked with G_UF and inversely related with L_OF.

3.8.3 Loss Coefficient for Liquid

The loss coefficient between tangential and inlet for liquid phase was also calculated using the Euler Number and it was found that it was lower than that was observed for the gas however unlike the gas loss coefficient it decreases with the increase in liquid superficial velocity as shown in Figure 3.17.

One of other device that can also be used for separation is the T- junction, out of many types of the T-junction the side arm Type of T-junction can be considered to have similarity with the I-SEP as inside the I-SEP there is also two outlets one in the

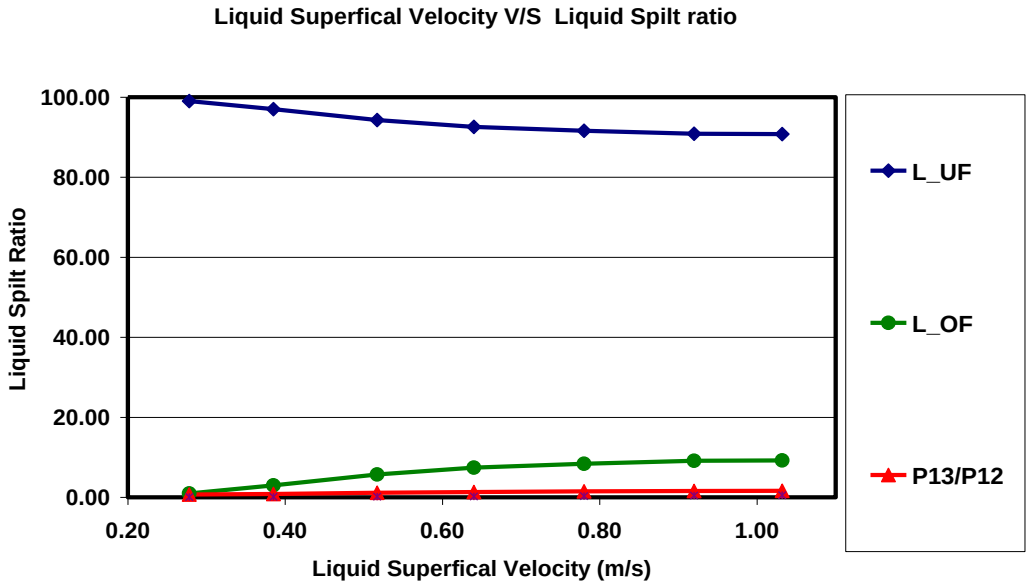

Figure 3.16 Effect of Liquid superficial Velocity on Liquid Split Ratio

direction of the flow and other perpendicular to it. Thus the behaviour of the single phase liquid flow in I-SEP was compared with that of a T-junction. The loss coefficient of the liquid phase was than compared with Buel et al. (1994b) who used a 37.6 mm ID side arm T-junction and calculated out the liquid loss coefficient for mean inlet liquid velocity of 0.18 m/s for the branch leg which could be taken as tangential outlet of I-SEP. The loss coefficient was plotted against the mass extraction ratio which is ratio of mass of the liquid at the branch to that of inlet. Figure 3.18 compared the loss coefficient for liquid phase for I-SEP with Buel et al. (1994a) experiments. It can be seen that the mass extraction for Buel et al. (1994a)data is from 0 to 1 while in I-SEP case it ranges from 0.8 to 1.0, it is due to high phase split of liquid in the I-SEP without actually any applied pressure, this gives an I-SEP an edge over T-Junction but at the same time the value of loss coefficient for Buel et al. (1994a) data lies under 2 while for I-SEP it above 4 and increases with the mass extraction ratio this shows that T junction usually consume less energy than I-SEP. However I-SEP has more tendencies to push more liquid toward the tangential outlet even without any applied pressure.

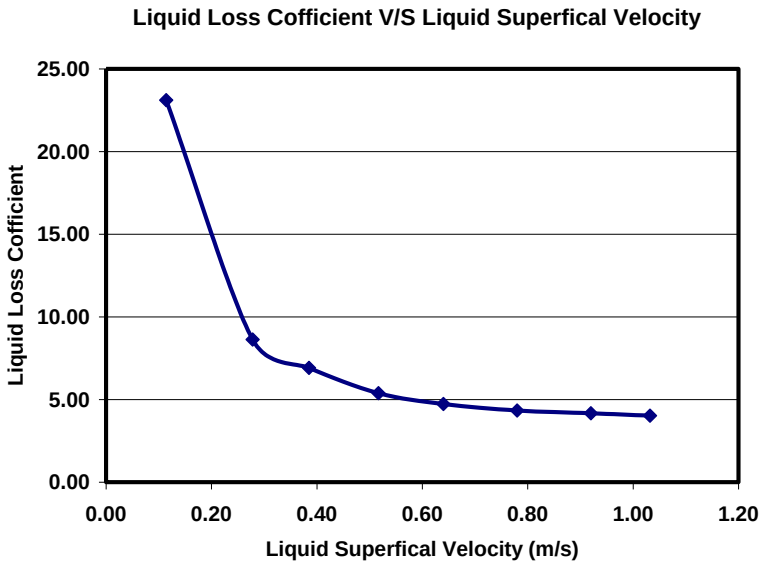

Figure 3.17 Loss Coefficient V/S Liquid Superficial Velocity

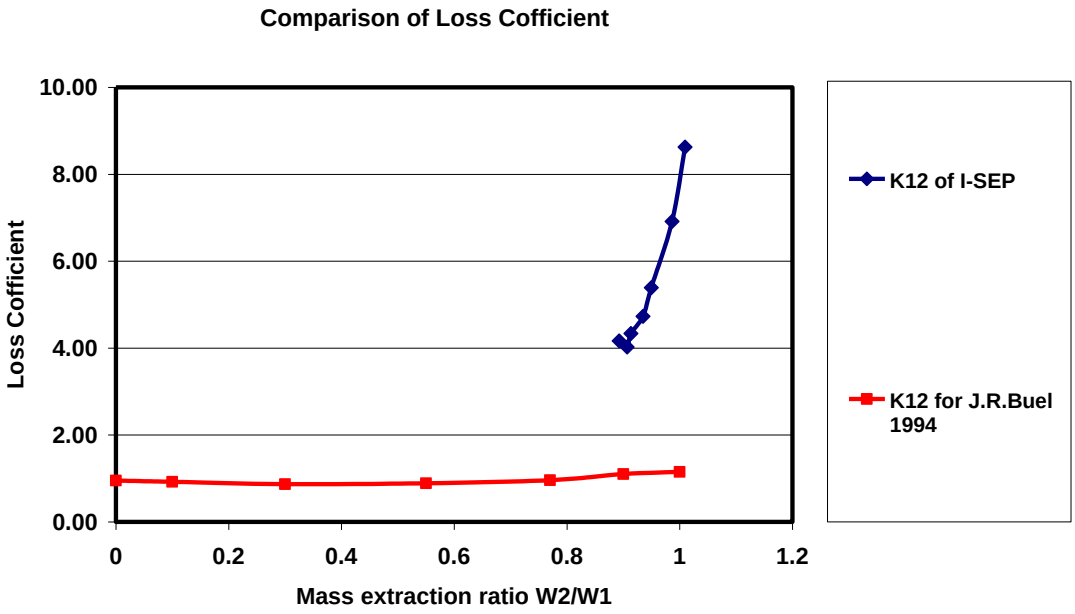

Figure 3.18 Comparison of Liquid Loss Coefficient

3.9 Conclusion

- Internet and wireless access protocol can be successfully used to access the information of the rig remotely.
- Separation Efficiency parameters i.e. GCU and LCO for I-SEP should be determined by applying KALMAN filter technique as they gave more consistent and better result than the mass difference method.
- The liquid level inside the HI-SEP seems to affect the combine efficiency of HI-SEP and I-SEP as due to this factor the combine efficiency was found to be different than I-SEP as calculated with the help of KALMAN filter technique.
- More proportion of the inlet gas was exit through the axial outlet than the tangential out let of the I-SEP at relatively high inlet pressure, reverse effect was observed for low inlet pressure during single phase gas experiment.

- Gas separation efficiency increased and G_UF% decreased with the increase in gas superficial velocity during single phase gas experiments.
- Liquid separation efficiency decreased and L_OF % increased with the increase in liquid superficial velocity.
- The L_OF and G_UF depend upon the pressure drop between inlet and axial outlet.
- Loss Coefficient for the gas between inlet and axial outlet was calculated out between 11 and 20 and it increased with the increase in gas superficial velocity.
- Loss Coefficient for the liquid between inlet and tangential outlet was calculated out between 4 and 8 and it was found to decreases with the increase in liquid superficial velocity which means the I-SEP would be more efficient requiring less energy to push the liquid to the tangential outlet with the increasing single phase liquid flow rate.
- The ratio of pressure drop between inlet and axial outlet to that of between inlet and tangential outlet i.e. P_{13}/P_{12} was found to have direct relationship with the gas separation efficiency, a high number mean more gas separation

efficiency and inversely related to liquid separation efficiency. This mean there exits an optimal value of this parameter where maximum efficiency for the both phase can be achieved.

- The gas separation efficiency was increased with the throttling the valve.
- Gas superficial velocity, inlet pressure and the ratio of pressure drop between axial and inlet to that of between tangential to inlet can be used to predict the splitting of gas both with and without the external pressure.

Chapter 4

Multiphase Flow Experiments

4.1 Introduction

Gas volume fraction of the mixture and mixture velocity were two independent operational input parameters that were chosen to study the efficiency performance of the I-SEP. These multiphase experiments were conducted by varying one parameter and keeping the other parameter constant which leads to two set of different experimental matrix i.e. Fixed GVF experiments in which mixture velocity were varied against the fixed GVF of the mixture while fixed velocity experiments were conducted keeping GVF constant and changing the inlet mixture velocity.

4.2 Experiment Methodology

The methodology of these multiphase experiment was similar as was used for the single phase experiment, the required gas flow rate was introduced into the compact separator rig using the Delta V system, while liquid flow rate was controlled using the manual control valve CV2 in the P&ID in chapter 3. The data sampled at 20 Hz was recorded for 2 minutes, after the steady state was achieved, which was defined by two constraints:

1. The liquid coming in to I-SEP (measured by FM02) should be equal to the liquid coming out from the tangential outlet through the unit 3 and from axial outlet through HI-SEP measured by FM09 and FM04 respectively. This was ensured by keeping the value of FM02 and sum of FM04 and FM09 almost equal.
2. There is enough liquid inside the both tanks i.e. unit 3 and HI-SEP attached to tangential and axial outlet respectively. The liquid level for the HI-SEP was maintained below its inlet which was around 600 mm to 700 mm and that for unit 3 was maintained between 1000 mm to 2000 mm.

The fixed GVF experiments matrix was performed with gas volume fraction of the mixture varied between 25-98% and for each of this value the inlet mixture velocity was varied from possible lowest value to possible highest attainable value i.e. 5 m/s to 60 m/s. This actually caused to change the gas flow rate from 5-850 Sm^3/hr and liquid flow rate from 0.1-4.7 l/s which actually produced gas and liquid superficial velocity in the range of 0.53 - 10.7 m/s and 0.03 - 1.24 m/s respectively. The minimum pressure recorded for fixed GVF experiments was 1.5 bar at 25% GVF having 5 m/s mixture velocity, and the maximum inlet pressure was recorded 3 bar for GVF of 70% at 20 m/s mixture velocity.

The experimental matrix for the fixed velocity experiments covered the *GVF* values from 35% to 97 % at mixture velocity between 5 -15 m/s and then for higher mixture velocity between 20 and 25 m/s the GVF was varied between 70% and 98%. This produced the gas and superficial velocity in the range of 0.25 - 6.25 m/s and 0.02 m/s - 1.82 m/s respectively. The minimum pressure during fixed velocity experiments was recorded as 0.75 bar at 80% GVF and 15m/s mixture velocity, and 4.75 bar at 40% GVF of 15 m/s mixture velocity.

4.3 Flow Regime at the I-SEP Inlet

Mandhane flow regime map for horizontal multiphase flow was used to estimate the possible flow regime at the I-SEP inlet using liquid and gas superficial velocities observed in both of these experiments. These liquid and superficial velocities are plotted over the Mandhane flow regime map and as it can be seen from the Figure 4.1 that majority of these experiments fall in slug flow although some data points also lied in wavy flow and transition between slug and annular flow. The data points in the slug to annular region corresponded to 98% GVF having mixture velocity more than 50 m/s and that for the wavy flow corresponded to 98% GVF having mixture velocity up to 15 m/s. The slug at the inlet became more aerated with the increase in GVF of the mixture and mixture velocity. This increasing degree of aeration in the slug may cause to develop a shorter length slug as compared to regular slug Drahos et al. (1996).

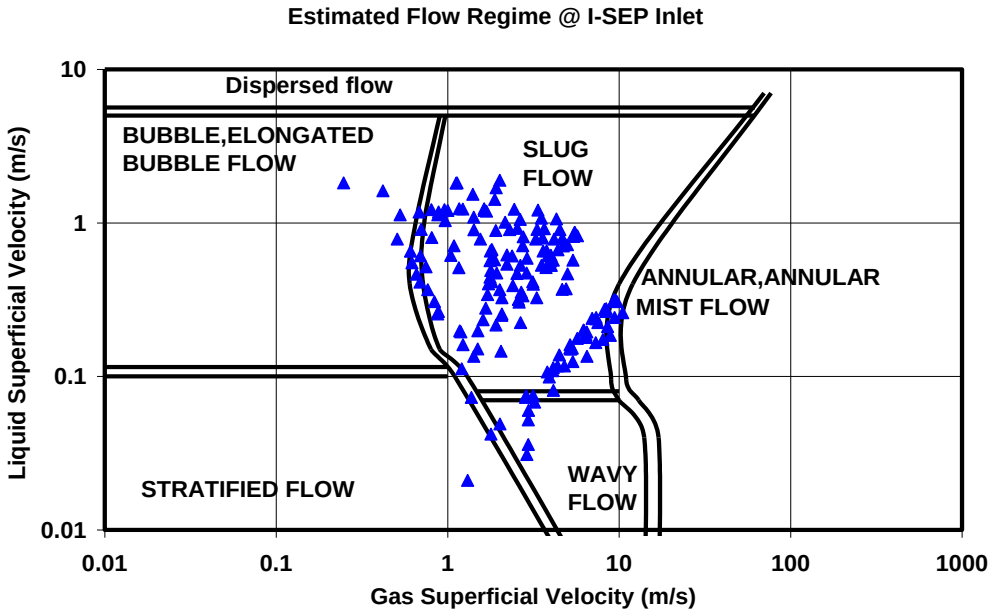

Figure 4.1 Estimated Flow regime at Inlet.

The liquid and gas superficial velocity inferred at tangential and axial outlet of the I-SEP are then also mapped on the horizontal flow regime map to estimate the possible flow regime at the respective outlet. It can be seen from the Figure 4.2a that slug flow at the I-SEP inlet after the separation through I-SEP was changed to mostly bubbly and stratified flow at the I-SEP tangential outlet along with a large number of data point still lying in slug region which initially corresponded to 98% GVF having mixture velocity greater than 30 m/s at inlet. However after separation these points emerged with relatively lower gas superficial velocity at tangential outlet. The wavy flow at inlet with high GVF 98% but having mixture velocity less than 15 m/s actually changed into stratified flow at underflow. The inferred flow regime at overflow or axial outlet at Mandhane horizontal flow regime as shown in Figure 4.2b map was found to be stratified and wavy indicating a low LCO with high amount of gas separation efficiency at axial outlet of I-SEP. It can be said that the inlet flow slug flow regime having high gas volume fraction moving with high mixture velocity has emerged again at tangential outlet whereas slug flow moving relatively lower

mixture velocity and less gas volume fraction has changed to bubbly flow at tangential outlet and wavy flow at axial outlet.

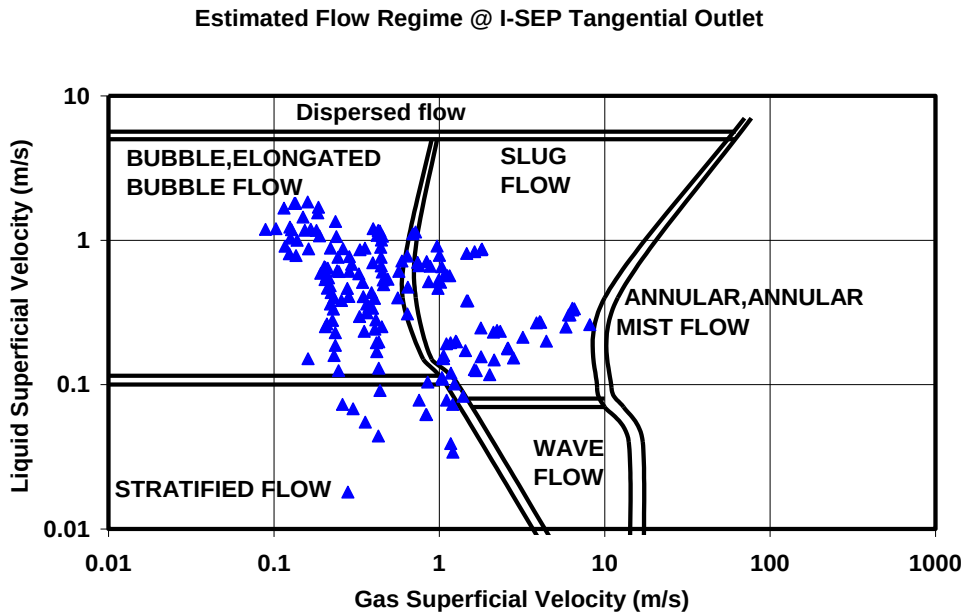

Figure 4.2a Estimated Flow regime at Tangential Outlet.

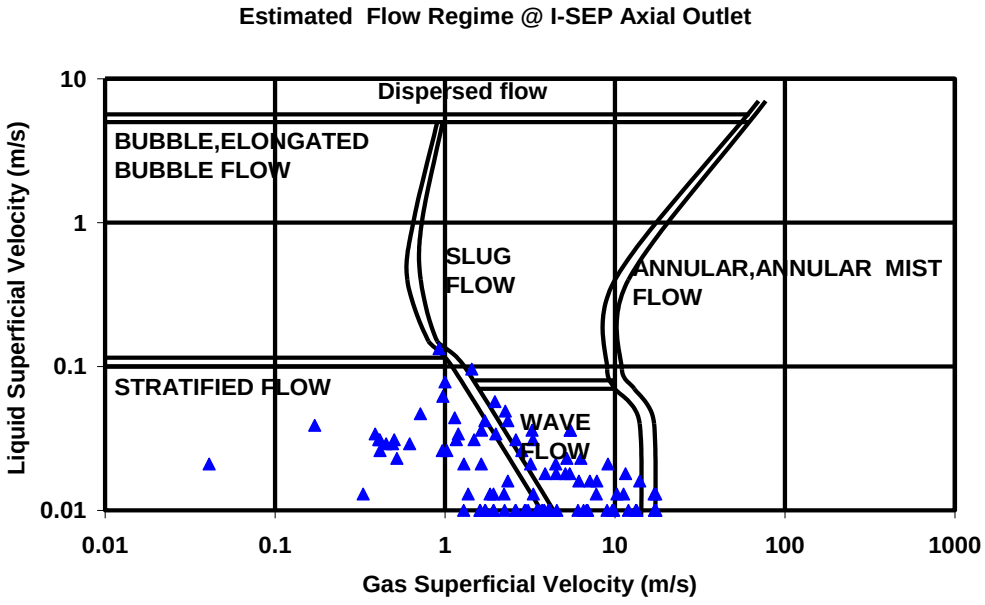

Figure 4.2b Estimated Flow regime at Axial Outlet.

The PDF of time series signal of pressure signal PT02, PT20, PT04 at the inlet, underflow and overflow respectively was also performed in order to investigate the flow regime at inlet and respective outlet of the I-SEP shown in Figure 4.4 to 4.6.

These PDF both at inlet and underflow of the I-SEP showed twin peaks with one smaller than other and a single peak at the overflow. It can also be observed that the left peak or the smaller peak at relatively lower pressure in the PDF get smaller as velocity is increased at the same GVF and became shortest at highest velocity. These two peaks could be because of both the alternative liquid and gas flows in the pipe. This smaller peak at inlet and underflow at lower pressure could be because of the liquid flow inside the pipe and higher peak at higher pressure could be assume to be because gas flows which indicated the proportion of bubbles flowing is getting larger and larger making the slug flow more aerated spreading all inside the pipe as can also be seen the visual picture of the inlet flow regime taken during the experiments as shown in Figure 4.3.

One of the important noticeable features in all of these PDF shown in Figure 4.4 to 4.6 are that the single peak at overflow is always having lower pressure than underflow for low GVF values, however at the higher GVF reversed effect can be seen at higher GVF more than 75%. The PDF in Figure 4.6 at GVF 97.5 % at lower mixture velocity of 7.5m/s and 15 m/s has shown a single peak with positive skewness and lower variance. This is different from all the other PDF observed during other tests. A visual observation along with the PDF and Mandhane Map criteria suggested that this test actually showed a wavy flow regime at inlet. The mixture mass difference observed during these experiments is in most of cases found to between -5.0 % and 0.5%. The negative mass difference is mainly due to negative liquid mass difference means sum of the liquid masses at overflow and underflow of I-SEP was found to be slightly greater than that of inlet mass. The mixture mass difference at the low GVF from 45 to 60 % was found to increasing with the increase in the inlet velocity but at high GVF of 75 to 98 % it increases initially with the increase in the inlet mixture velocity but then found to be decreasing with further increasing in inlet mixture velocity. However, it was found that observed GCU or

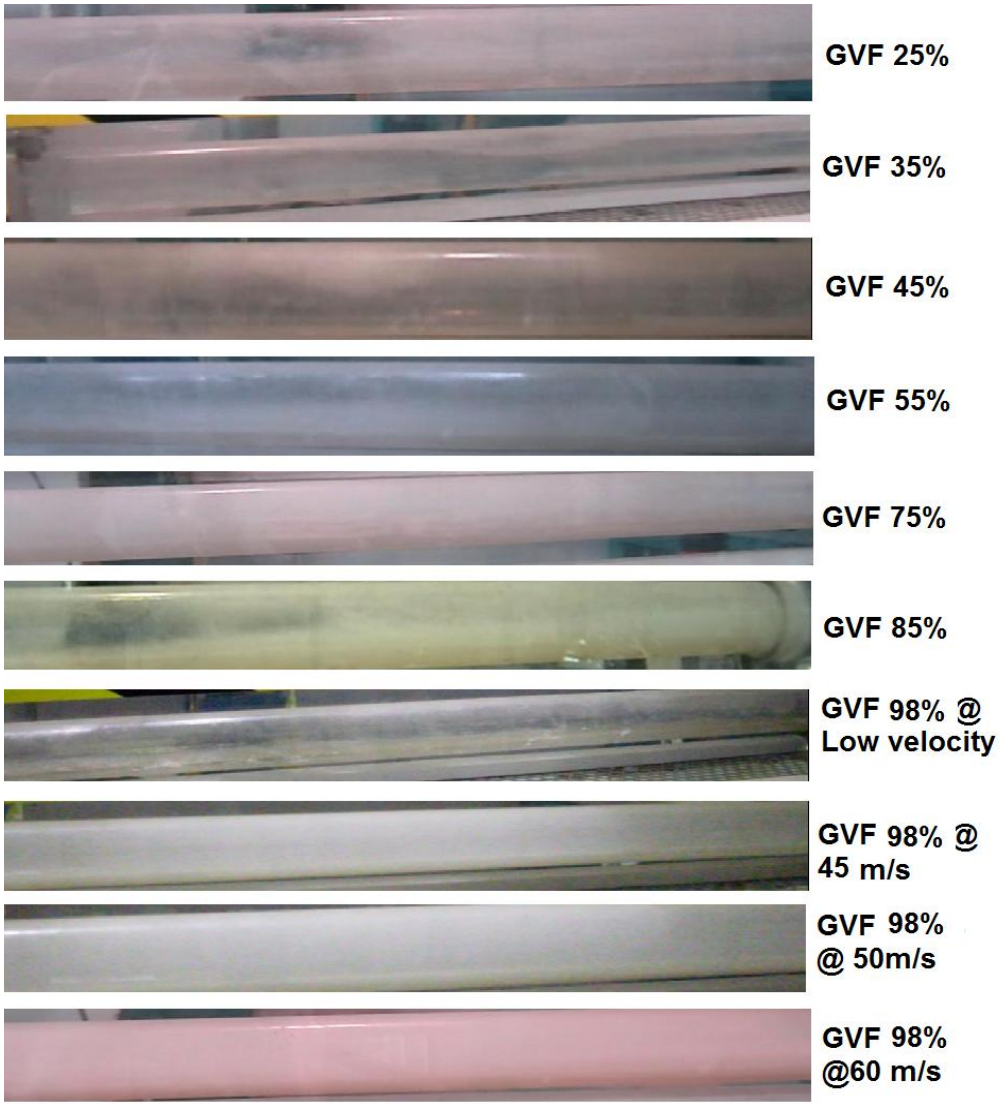

Figure 4.3 Observed flow regime at I-SEP Inlet.

LCO does not seem to be influenced very much by this variation in the mass difference percentage.

4.4 Statistical Analysis of Experiments

The statistical analysis of resulted GCU and LCO observed in these experiments revealed that under no applied back pressure the proportion of the gas found in the tangential outlet was higher than that of the liquid found in the axial outlet indicating

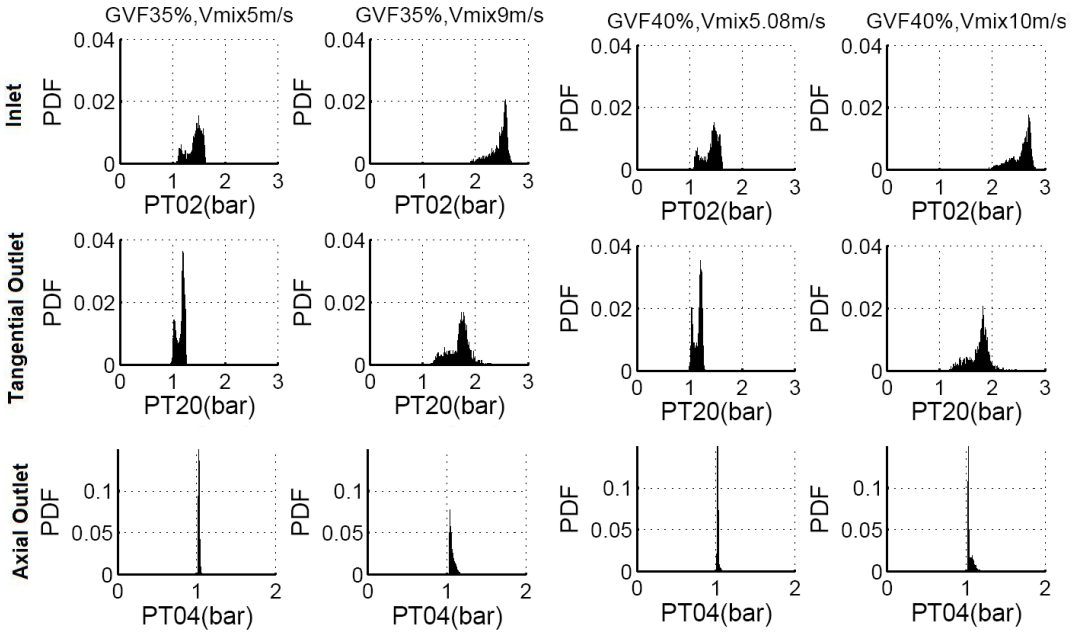

Figure 4.4 PDF of Pressure Signal at Inlet, Tangential and Axial outlet.

that the axial outlet was more purified due to less content of the LCO than tangential outlet. The average GCU in all experiments was found to be 18% with a standard deviation of 15 % and that of LCO was found to 4.87 % with the standard deviation of 4.5% indicating more dispersion in the GCU than LCO. The maximum and minimum GCU was found to be 71.2% and 2.02% at 45% and 25% GVF having mixture velocity 5 m/s respectively and that of LCO was found to be 0.47% and 23 % at 90% and 98% GVF having mixture velocity 25 and 7.5 m/s respectively. The pressure drop between inlet and axial outlet and that of between inlet and tangential outlet had their maximum value 1.7bar and 1.1bar with an average value of 0.35 bar and 0.38bar respectively with more dispersion recorded for pressure drop between axial and inlet having value of 0.41 bar than that of between inlet and tangential outlet with 0.31bar.

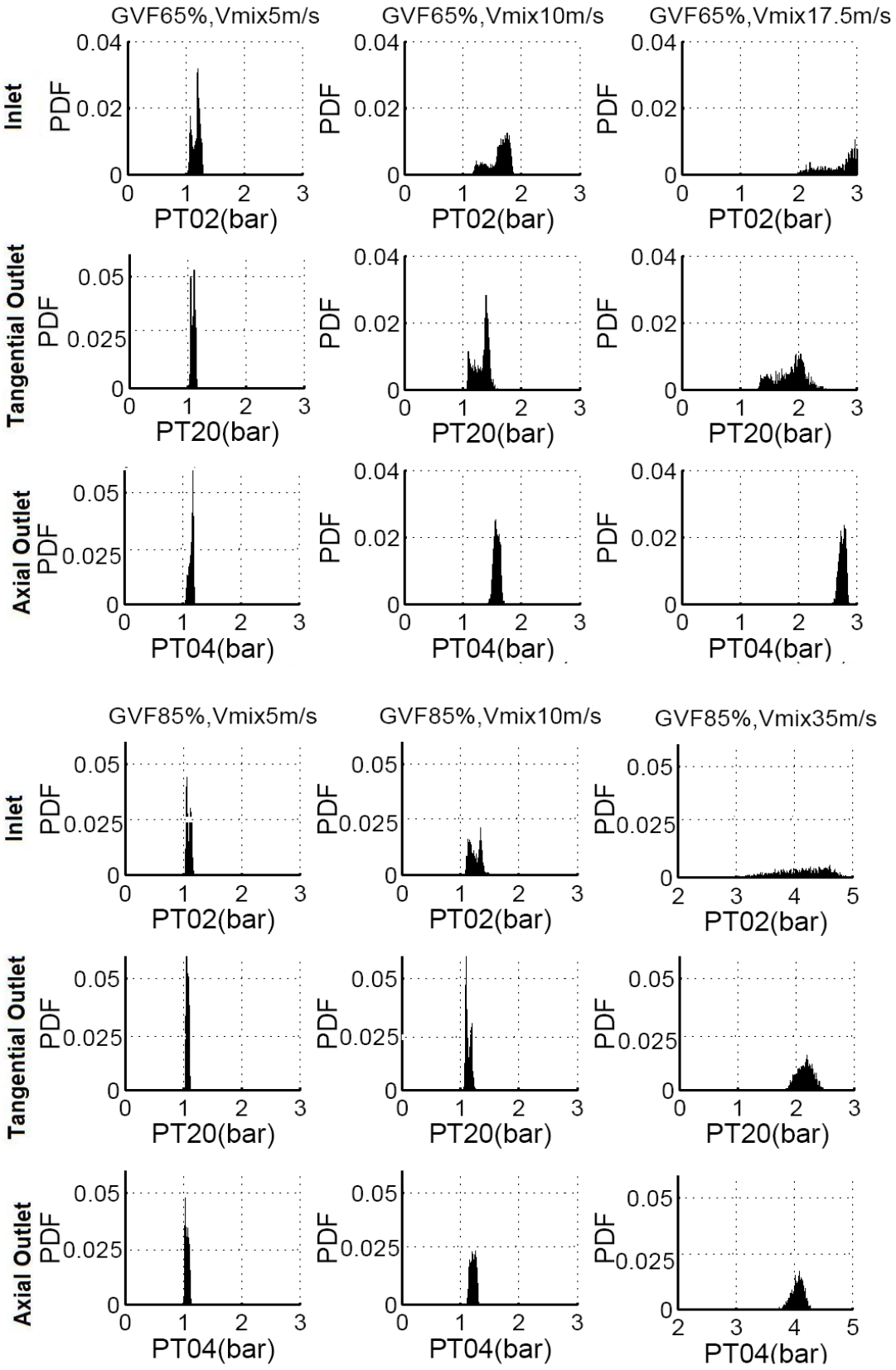

Figure 4.5 PDF of Pressure Signal at Inlet, Tangential and Axial outlet.

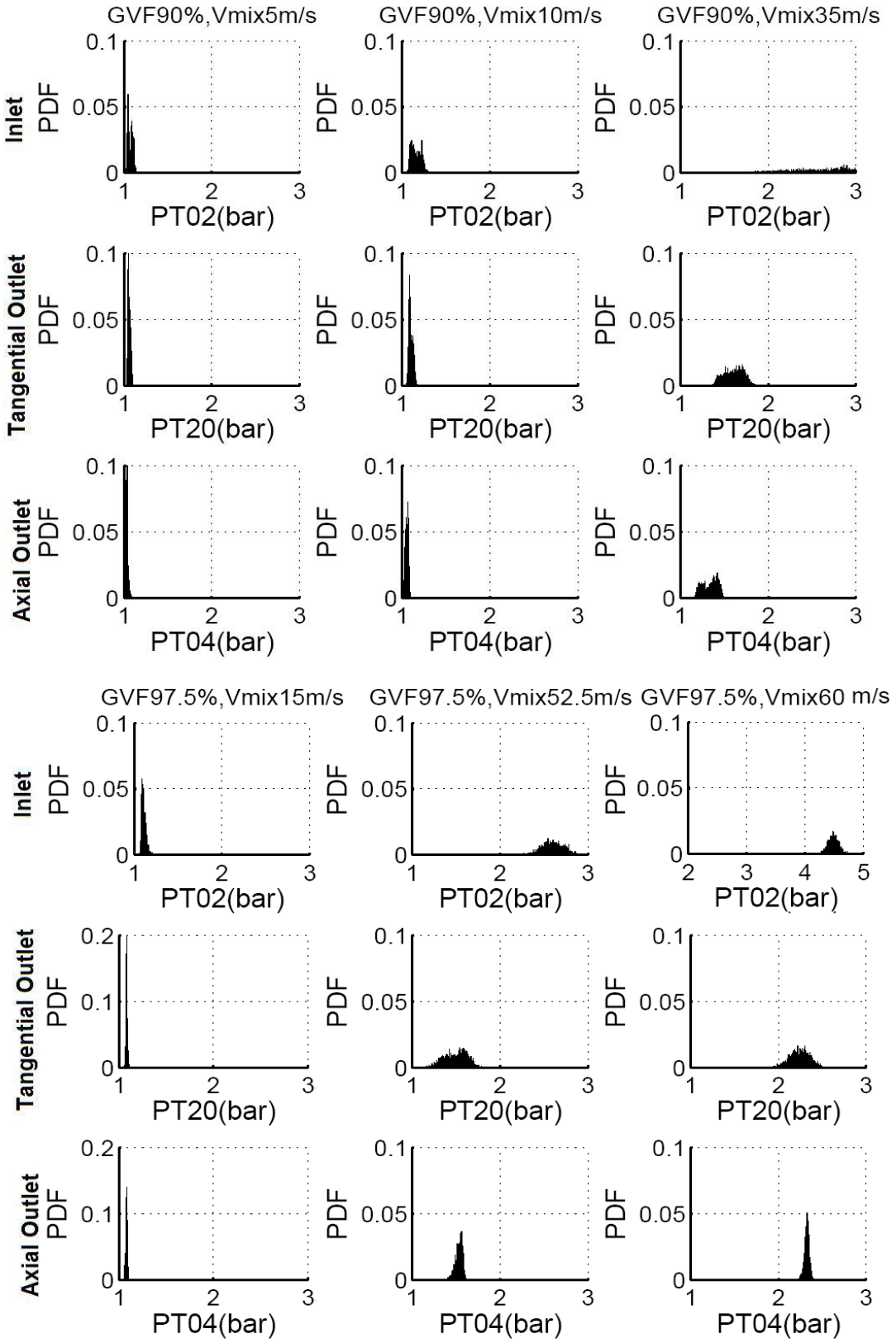

Figure 4.6 PDF of Pressure Signal at Inlet, Tangential and Axial outlet at high GVF.

A statistical analysis of GCU and LCO results are presented in a form of histograms in Figure 4.7a and Figure 4.7b respectively to investigate their frequency distribution for all data sets. The shape of both of these histogram is skew positive means that majority of the distribution has occurred towards lower range of the GCU and LCO respectively. It can be seen that about 27% of all these experiments has produced GCU between 6 to 12% followed by 13 % of total observation produced GCU between 16 to 20%. If we look at commutative relative frequency distribution curve in the Figure than it is found about 60% of experiments has recorded at least 20% GCU at underflow of I-SEP for GVF values ranging from 65% to 98 % with inlet mixture velocity ranges between 5 to 25 m/s. Only 4% experiments ended with a GCU between 50 to 72% of which just 0.86 % showed 72% GCU. The probability of an event in long run is also defined as commutative relative frequency therefore it may be concluded that the probability of producing at least 20% GCU by I-SEP is 60% and that of 72% is 0.86%. Similarly the probability of producing at least 6% LCO as observed during this experiment was found to be 82% and that of 22% is 0.86%. This shows I-SEP has tendency to produce more clear gas in axial outlet than clear liquid in the tangential outlet.

It was also tried to investigate how the produced GCU% is related to the combination of the gas volume fraction and mixture velocity. In statistic a cross classification table or the contingency table is usually created to establish the relationship between two interacting variables. This table was developed by grouping the experimental data in low, medium and high groups as shown in Table 4-1. The contingency or cross classification table consisting of observed GCU% along with the frequency of each combination of GVF and mixture velocity is compared in Table 4-2. It was found that combination of low mixture velocity with mid range GVF and that of mid range velocity with high GVF has same relative frequency producing less 6% GCU with 12% probability.

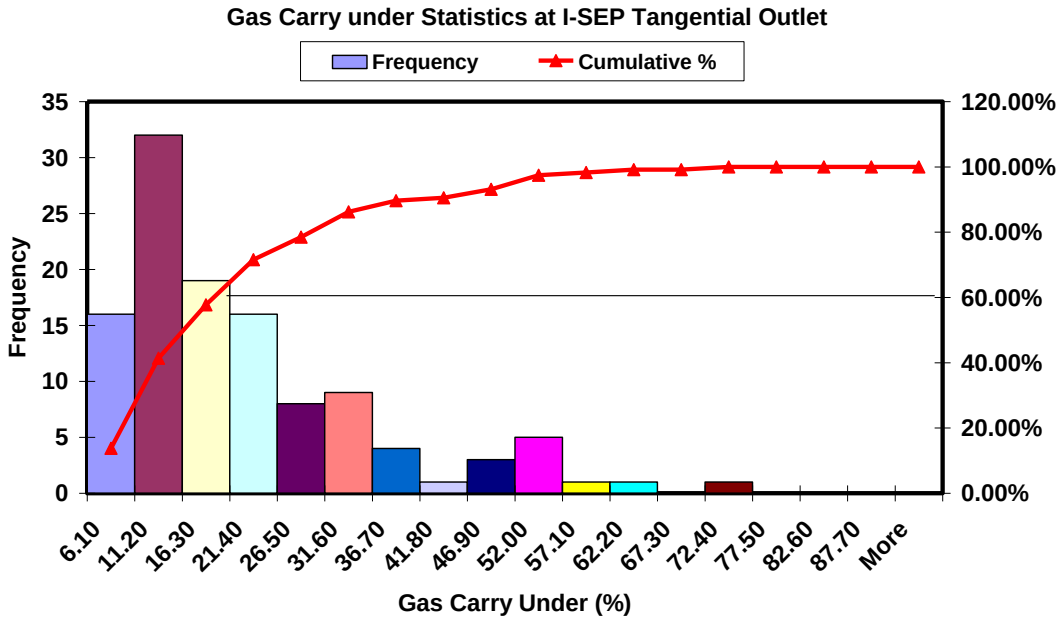

Figure 4.7a Statistical distribution of GCU as Observed in Experiments.

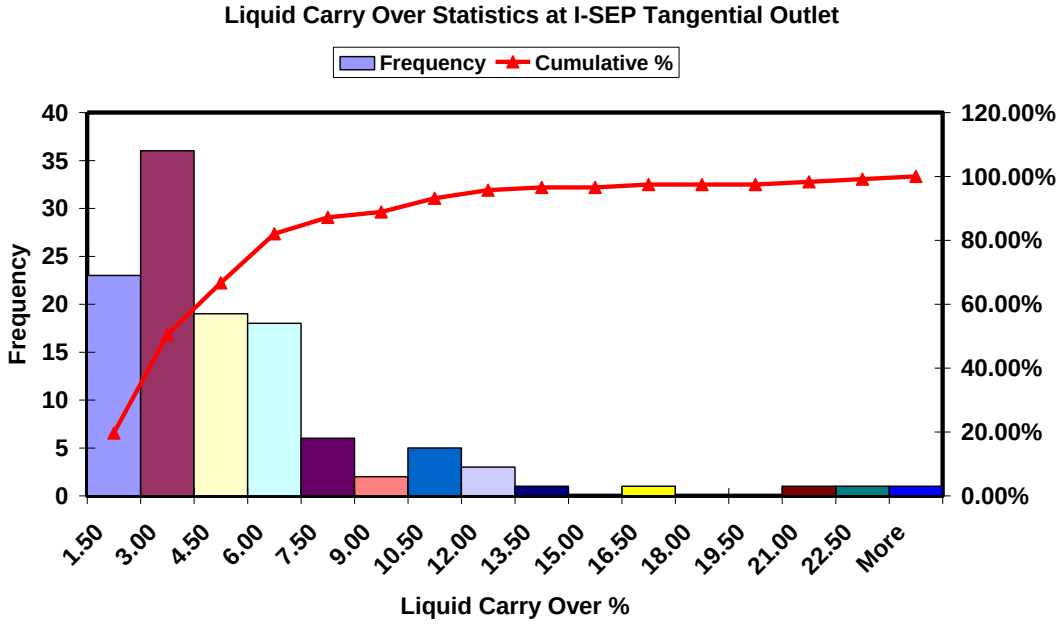

Figure 4.7b Statistical distribution of LCO as Observed in Experiments.

Table 4-1 GVF and Velocity arranged in groups.

GVF Range		Inlet Mixture Velocity
Low	Between 25% and 45%	Less than 12 m/s
Medium	Between 46% and 75%	Between 13 and 24 m/s
high	Greater than 75%	Greater than 24 m/s

Table 4-2 Contingency Table for GCU.

GCU %	Commutative Relative frequency	Relative frequency					
		LOW GVF	Mid GVF	High GVF	Low Velocity	Mid Velocity	High Velocity
0-6.10	12.12	0.00	0.19	0.11	0.15	0.13	0.00
6.10-11.20	21.21	0.00	0.19	0.26	0.12	0.33	0.10
11.20-16.30	12.12	0.00	0.14	0.14	0.09	0.21	0.00
16.30-21.40	15.15	0.18	0.14	0.14	0.15	0.08	0.30
21.40-26.50	9.09	0.00	0.00	0.17	0.06	0.08	0.20
26.50-31.60	10.61	0.18	0.05	0.11	0.06	0.08	0.30
31.60-36.70	3.03	0.09	0.00	0.03	0.03	0.00	0.10
36.70-41.80	1.52	0.09	0.00	0.00	0.03	0.00	0.00
41.80-46.90	3.03	0.18	0.00	0.03	0.09	0.00	0.00
46.90-52.00	7.58	0.09	0.19	0.00	0.09	0.08	0.00
52.00-57.10	1.52	0.00	0.05	0.00	0.03	0.00	0.00
57.10-62.20	1.52	0.09	0.00	0.00	0.03	0.00	0.00
62.20-67.30	0.00	0.09	0.00	0.00	0.03	0.00	0.00
81-92.80	0.00	0.00	0.05	0.00	0.03	0.00	0.00

The higher GCU % up to 21% has occurred for experiments at low mixture velocity combine with any GVF value whether low or high with a probability of 15%.There is another similarity found in the relative frequency of low velocity and mid GVF for the GCU between 27 to 32 % with the probability of about 10%. Next similarity is found for low mixture velocity and high GVF producing GCU between 32 to 37% with probability of about 4%.Therefore looking at the similarities in the relative frequencies of the combination of low mixture velocity with the other combination of GVF, it is observed that I-SEP tends to produces relatively a higher GCU at the lower mixture velocity. The relative frequency to produce GCU with the combination GVF with high mixture velocity is found very less leading to conclude that I-SEP has lower tendency to produce GCU at higher inlet mixture velocity which is taken as greater 24 m/s in this analysis.

4.5 Flow Split

T-junction is another device that could also be used for the separation and new research is ongoing to use T junction a separator Azzopardi (1993) Azzopardi and Rea, (2000). I-Sep on the basis of its geometry could be thought to more similar to branching T-junction with tangential outlet acting as branch arm and axial outlet could be treat as side arm of the T junction. Many researchers have investigated on the flow split i.e. fraction of the amount of the gas and liquid flow through the branch arm of various diameter T junction using different flow regime at the inlet. The work of Buel et al., (1994a); Shoham et al., (1987) on 38mm and 50 mm ID T junction with gas superficial velocity of 6.2-10 m/s respectively showed that for constant gas superficial velocity the preference of the gas to pass through the branch arm increases with the increase in the liquid superficial velocity and resistance of the branch arm. However I-SEP exhibited a reversed trend for this situation under no applied pressure. Figure 4.8a represents effect of the increasing liquid superficial velocity at constant gas superficial velocity for the performed experiments and it can be seen that the fraction of the gas flowing into the tangential arm decreased and that of liquid increased with the increase in the liquid superficial velocity which is the reverse trend as observed in the T junction. This may be use to conclude that the tangential outlet of the I-SEP may have more clear liquid as compared to the T junction branch arm.

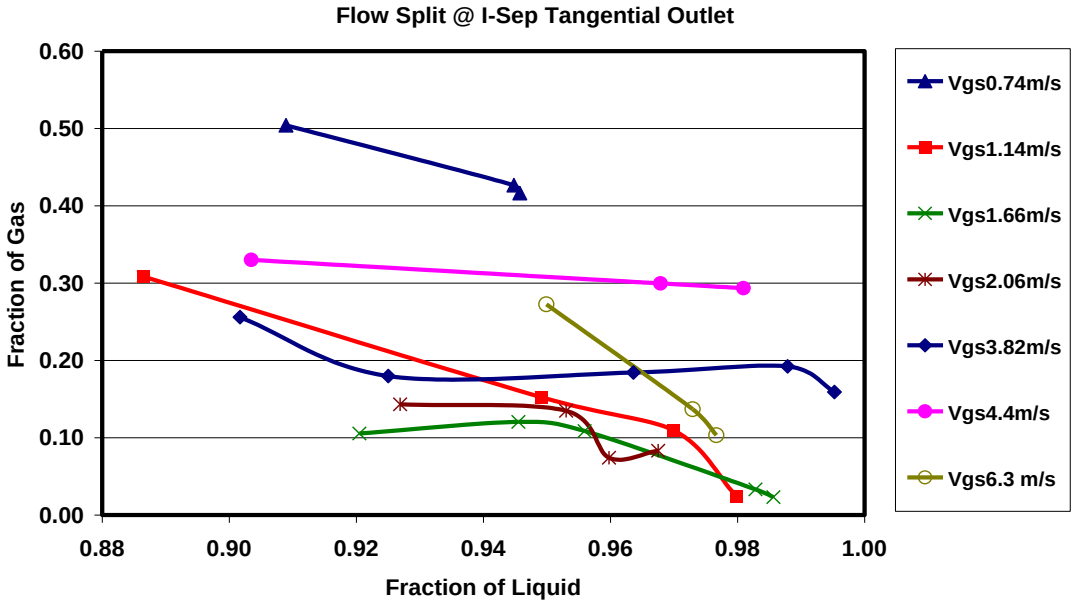

Figure 4.8a Flow split at I-SEP tangential Outlet

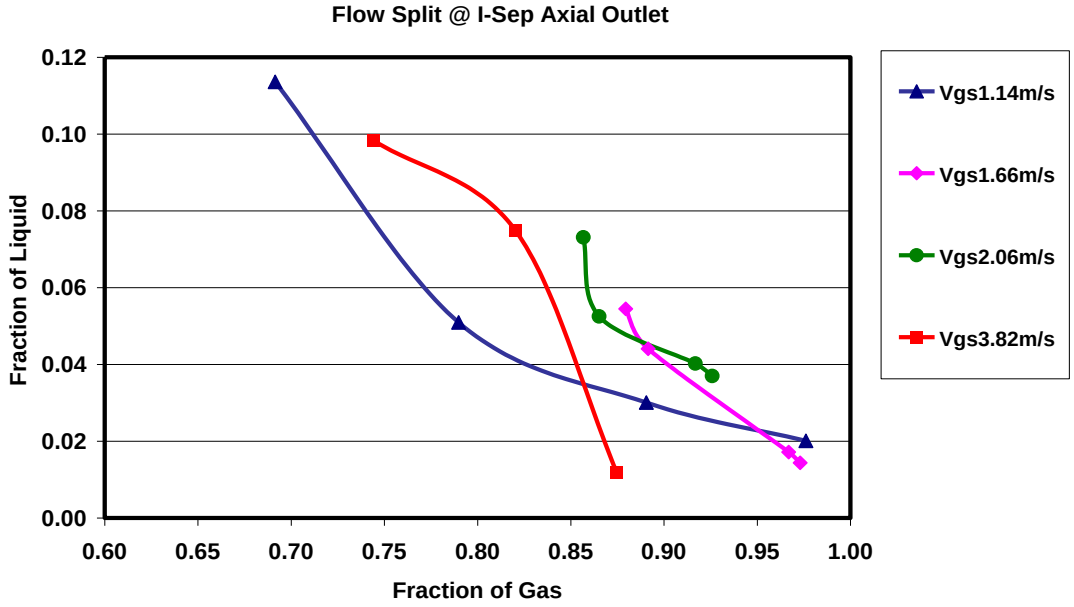

Figure 4.8b Flow split at I-SEP Axial Outlet

Similarly in T junction of 32mm Id Azzopardi, (1993) with annular flow at inlet, both the liquid and gas fraction in the side arm increases with the increase in the liquid flow rate at constant gas flow rate, however the liquid fraction increases more than that of gas fraction. This effect when investigated in the current experimental data has

showed a reverse trend. The liquid fraction decreased and gas fraction increased with the increase in the liquid flow rate as shown in Figure 4.8bThis shows that axial outlet of I-SEP give more purified separation than does perform by the T junction.

4.6 Degree of Separation

Azzopardi and Rea, (2000) have defined a parameter to define the degree of the separation in T junctions. This parameter is based on fraction of the liquid and gas flowing through a particular arm of the T junction. An optimal separation means that only one phase is coming out from each of the outlet either T junction or in our case I-SEP. This definition in our case means that for underflow arm the liquid fraction should be 1 and gas fraction should be zero and other wise for the overflow outlet of the I-SEP. The degree of the separation can then be defined using the following simple equation which gives the deviation of any data points from the optimal separation.

$$S = \sqrt{(1 - F_l)^2 + F_g{}^2} \qquad (4.1)$$

Where ,

S is named here as minimum separation parameter as minimum value of this parameter defines the best separation for the given inlet condition.

F_l is the amount of the liquid fraction coming out from the underflow.

F_g is the amount of the gas fraction coming out from the underflow.

The minimum value of S defines the best separation efficiency at the give inlet condition. The value of the S in both cases was found interestingly very close to the observed GCU % which means the GCU % should be considered main criteria to define the performance of I-SEP. The minimum separation parameter for both cases is presented in Figure 4.9a and Figure 4.9b respectively.

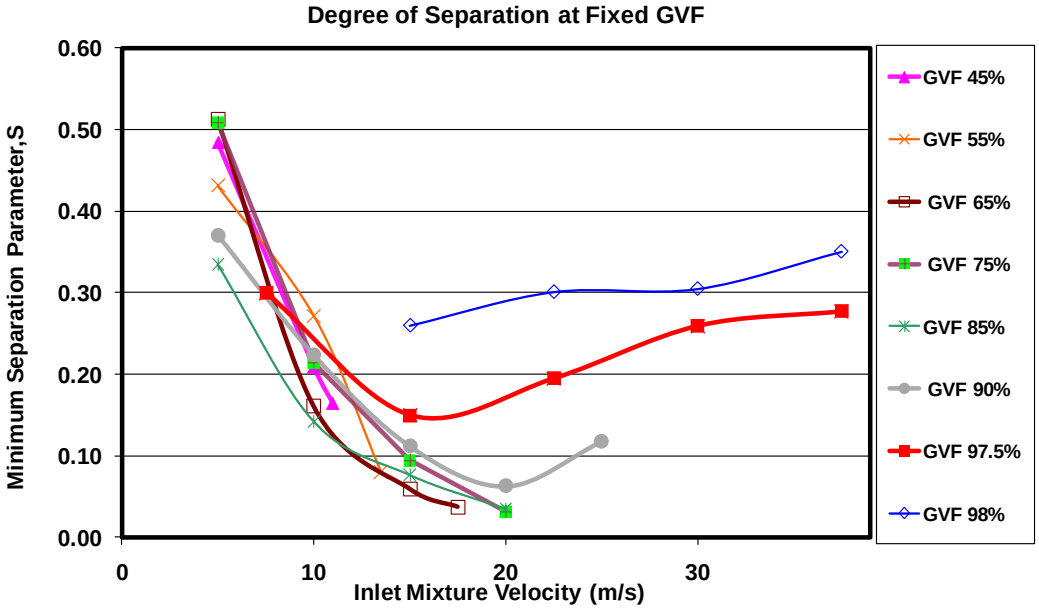

Figure 4.9a Degree of Separation at Fixed GVF.

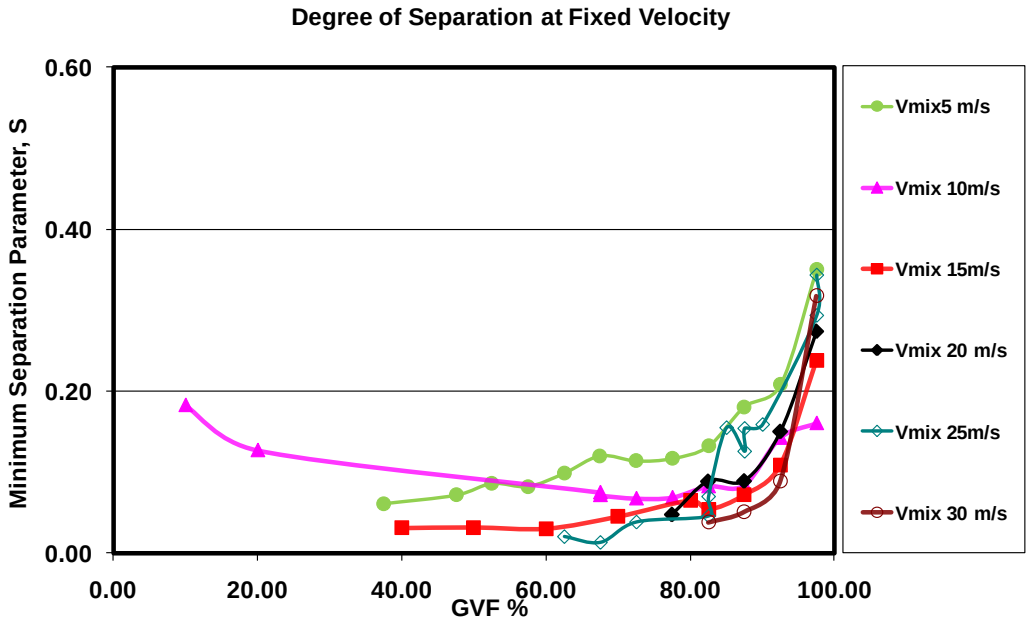

Figure 4.9b Degree of Separation at Fixed Velocity.

It can be seen from the figures that this parameter has decreased with the increase in the inlet mixture velocity at fixed GVF, and with the increase in GVF at fixed velocity approaching about less than 0.05 showing about 99% efficiency. However in both cases this parameter started slightly increasing again at high value of GVF

higher than 85% at mixture velocity greater than 20 m/s. This trend indicates that I-SEP performance is relatively lower at high velocity and high GVF greater than 85%.

This approach was then used to further investigate separation efficiency as function of gas and liquid Reynolds number in order to check the degree of separation could be achieved with a particular flow flowing in the I-SEP. The value of S less than 0.15 actually corresponded to GCU of 15%, any value of S less than this is taken as good separation and above this is taken as relatively poor separation. It was observed that value of S lies more than 0.15 or GCU was greater than 15% for all the flow having liquid Reynolds number less than 1.0×10^5 as shown in the Figure 4-10. This trend indicates that at low gas Reynolds number less than 2×10^9 GCU would be greater on high and increasing liquid Reynolds numbers.

4.7 Effect of Mixture Velocity and GVF on I-SEP Performance

These experiments showed that under no applied pressure and all values of gas and liquid superficial velocities both the gas and liquid both showed tendency to pass through both the outlet of I-SEP without actually needed any threshold of either gas or liquid to enter into a specific outlet of the I-SEP. In general the GCU and LCO was found to be decreased with increased in mixture velocity at constant GVF and increased with the increase in GVF of the mixture at the fixed velocity. It is discussed in more detail in the next section.

4.7.1 Effect of Mixture Velocity on Gas Separation Efficiency

Figure 4.11a and Figure 4.11b shows the gas separation efficiency and GCU respectively for fixed GVF experiments. It can be seen that gas separation efficiency increased and GCU decreased non linearly at GVF less than 85 % with the increase in mixture velocity up to 20 m/s, the trend is then reversed at higher mixture velocity greater than 20 m/s for higher GVF greater than 85% when gas separation efficiency fall down due to increased in GCU.

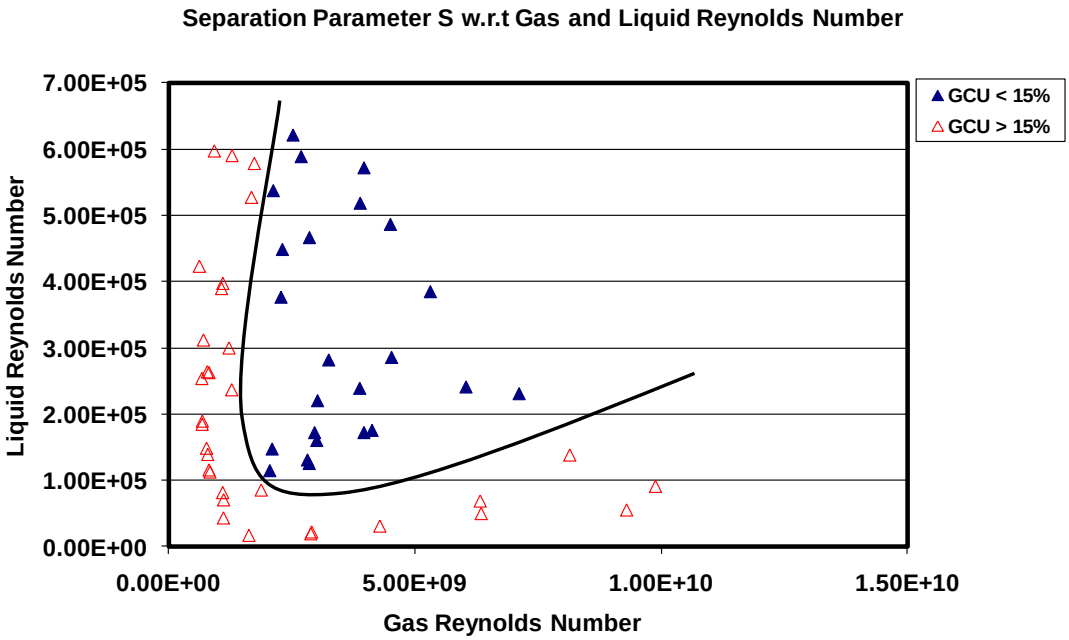

Figure 4.10 Separation Parameter vs. to Gas and Liquid Reynolds Number.

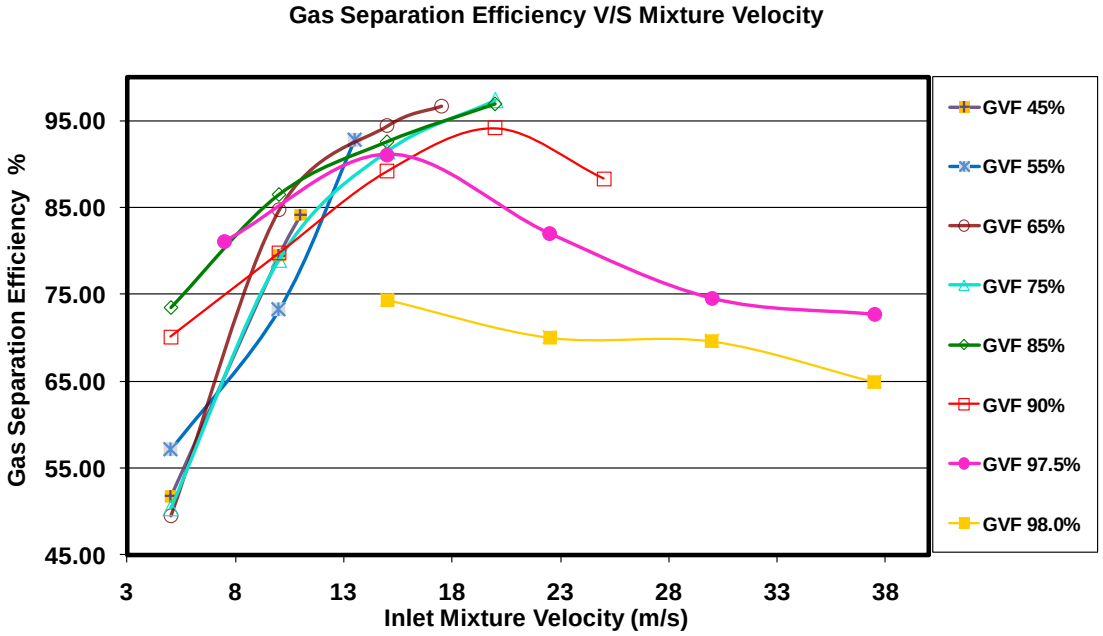

Figure 4.11a Effect of Mixture Velocity on Gas separation Efficiency.

.

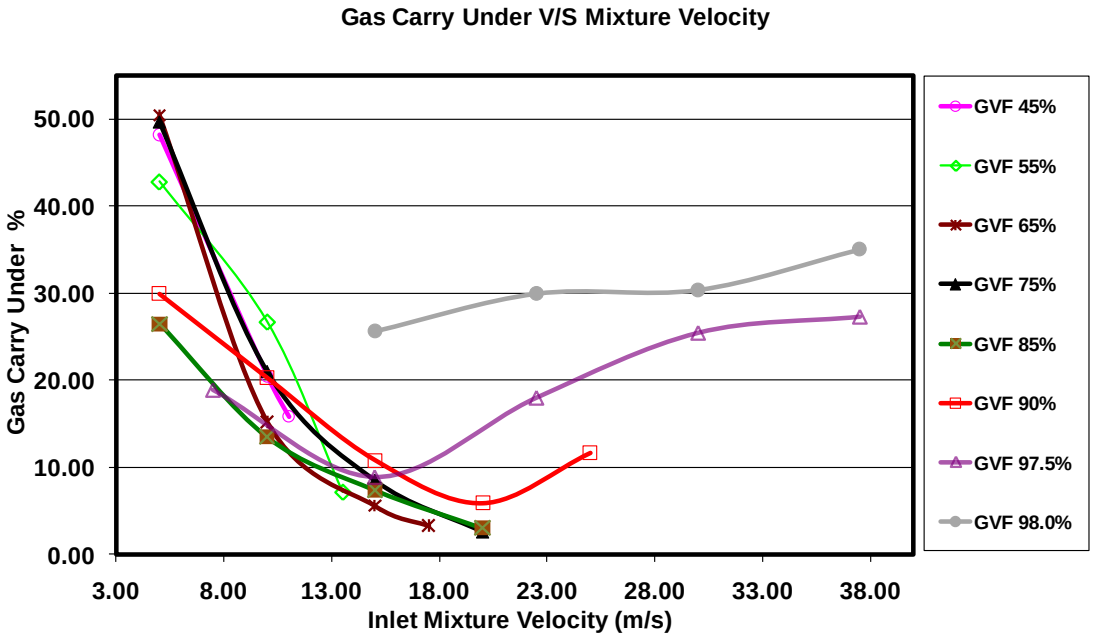

Figure 4.11b Effect of Mixture Velocity on GCU.

The increase in the GCU at higher GVF can be explained by increasing amount of gas due to high amount of GVF at the inlet and hence causing more GCU. This trend shows that the optimal velocity for the I-SEP is 20 m/s as according to GOMEZ et al., (1998) there should be an optimal velocity for any cyclone to operate and the performance of the cyclone would be affected when the inlet velocity is changed from this optimal velocity.The rate of change in gas separation efficiency with respect to mixture velocity was found higher for GVF value less than 45% and lowest for the high GVF greater than 80% and while remained same for other values of GVF. This mean increase in mixture velocity at higher GVF does not affect the separation efficiency very much. The region of maximum separation efficiency ranges between 85 to 95 % with mixture velocity between 15 to 20 m/s having GVF values between 65 to 85%.The efficiency dropped to 65% for highest GVF of 98% at highest mixture velocity of approx 40 m/s. For example at GVF 45 % under slug flow the gas separation efficiency has increased from 51% to 84% with corresponding decreased in GCU from 49 to 16%,with the increase in mixture velocity from 5 to 11 m/s. However at high GVF of 90% in the region of aerated slug the mixture velocity

greater than 20 m/s actually caused to decreased the separation efficiency from 94 to 84 % and increase the GCU from about 6 to 16% as can be seen in figure 4.12a and 4.12b respectively. This trend is again visible in high GVF values of 97.5% where gas separation efficiency is increased from 81 to 91 % with positive change in mixture velocity from 7.5 to 15m/s, however at 22.5 m/s it is decreased to 82 % and continuously decreased up to 74 % with the increased in the mixture velocity from 37.5 m/s. Similarly the gas separation was found to decreased again at 98% GVF from 74 to 64 % with the increased in mixture velocity from 15 to 37.5. A corresponding increased in GCU for this change can be seen in Figure 4.11b. Thus it can be said that the separation efficiency increases and GCU decreases with the increase in mixture velocity for GVF value less than 90% but after this GCU has increased and gas separation decreased at higher mixture velocity.

4.7.2 Effect of GVF on Gas Separation Efficiency

The effect of increasing GVF at fixed velocity on gas separation efficiency and GCU is shown in Figure 4.12a and Figure 4.12b. The gas separation efficiency is decreased non-linearly with the increase in GVF at fixed mixture velocity due to corresponding increase in the GCU. However at mixture velocity of 10m/s the trend is reversed again as GCU is decreased and gas separation efficiency is increased. It can also be seen from these Figures that change is gas separation efficiency and GCU is sharper at higher GVF values greater than 80%.

4.8 Effect of Mixture Velocity and GVF on Liquid Efficiency and LCO

The liquid separation efficiency and LCO like their counter part gas separation efficiency and GCU showed a non linear relationship with the GVF and mixture velocity. However amount of the Liquid separation efficiency was always found more than 75% for any combination of the GVF and mixture velocity. Likewise the LCO was always found lesser than GCU.

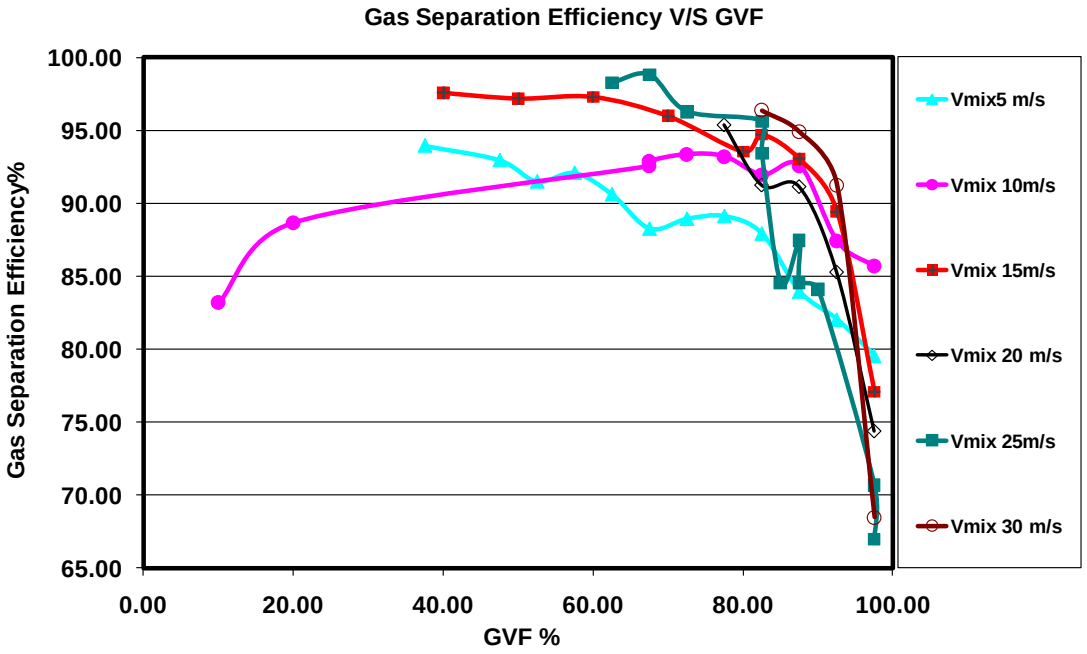

Figure 4.12a Effect of GVF on Gas Separation Efficiency.

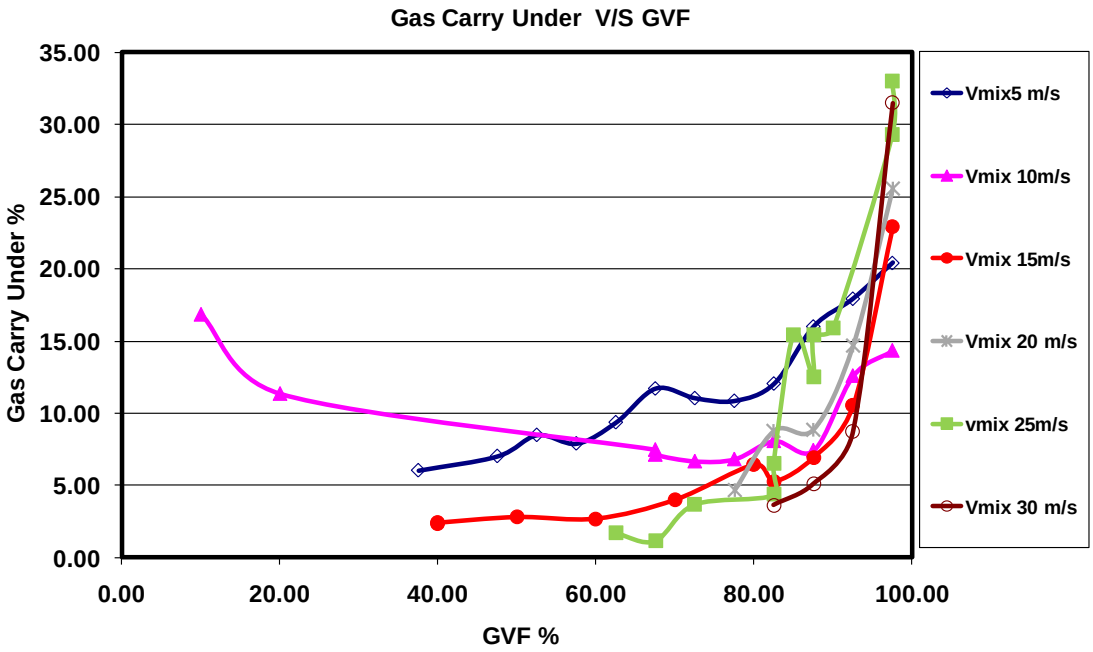

Figure 4.12b Effect of GVF on Gas Separation Efficiency.

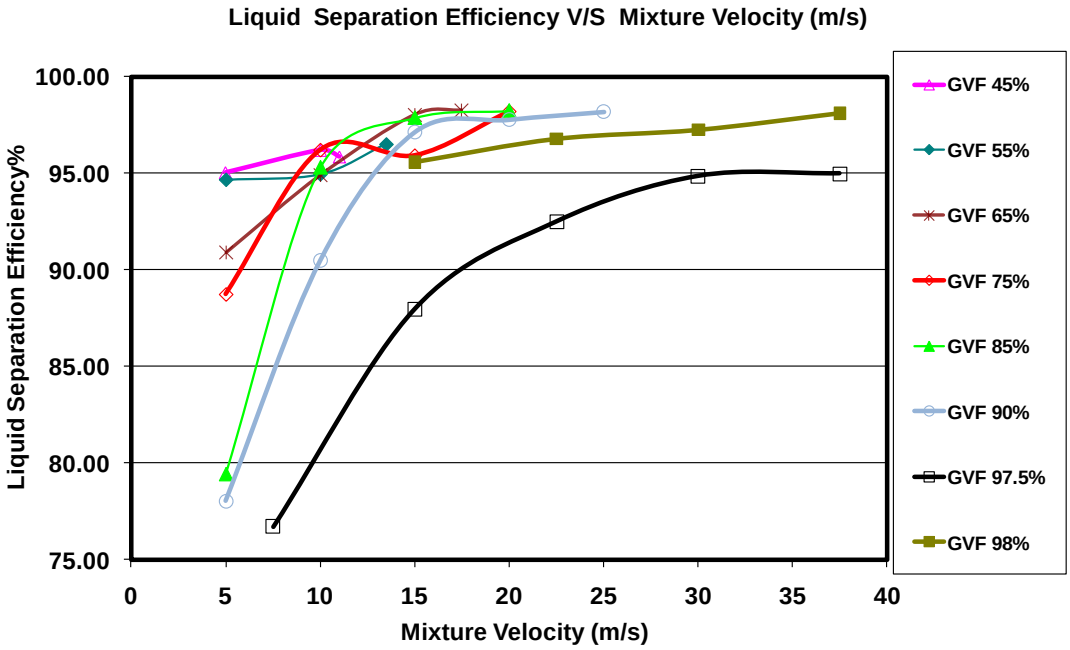

Figure 4.13a Effect of Mixture velocity on Liquid Efficiency.

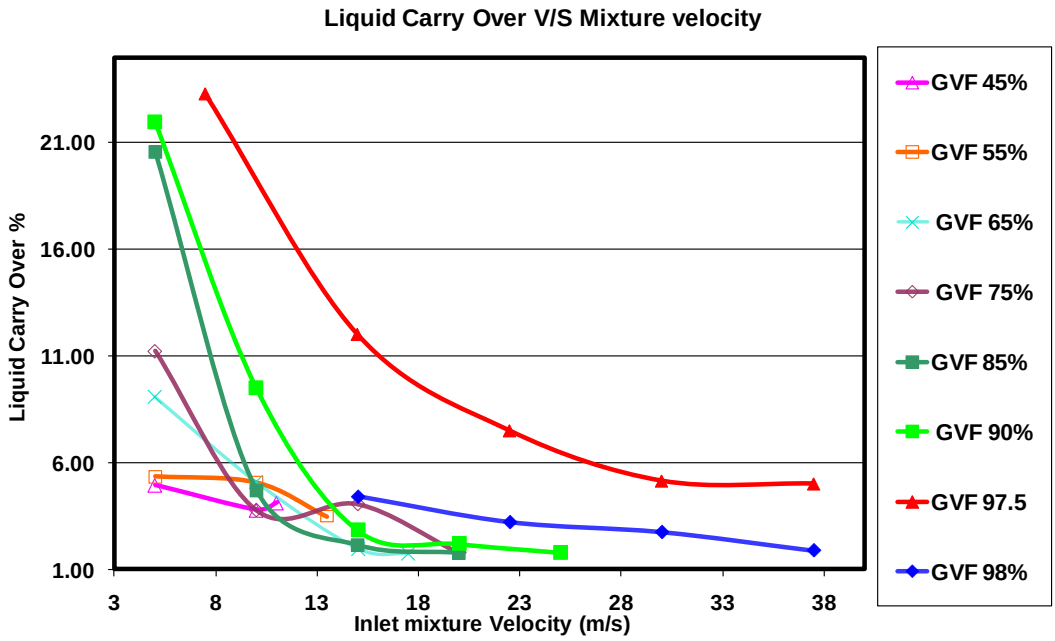

Figure 4.13b Effect of Mixture velocity on LCO.

4.8.1 Effect of Mixture Velocity on Liquid Separation Efficiency

The liquid separation efficiency and LCO to some extent exhibited similar trend like gas separation efficiency the liquid separation efficiency increased and LCO decreased sharply at fixed GVF with the increase in mixture velocity as can be seen in Figure 4.13a and Figure 4.13b respectively. However the change in both liquid efficiency and LCO seems to be almost constant for GVF greater than 85% after mixture velocity has increased more than 20 m/s. It should be noted that gas separation efficiency was found to be decreasing at fixed GVF for mixture velocity greater than 20 m/s. This means that at a higher GVF the increasing the mixture velocity does seem to affect the separation efficiency very much.

4.8.2 Effect of GVF on Liquid Separation Efficiency

On the other hand the liquid separation efficiency was founded to decrease and LCO increased surprisingly with the increase in the GVF as can be seen in the Figure 4.14a and Figure 4.14b respectively.

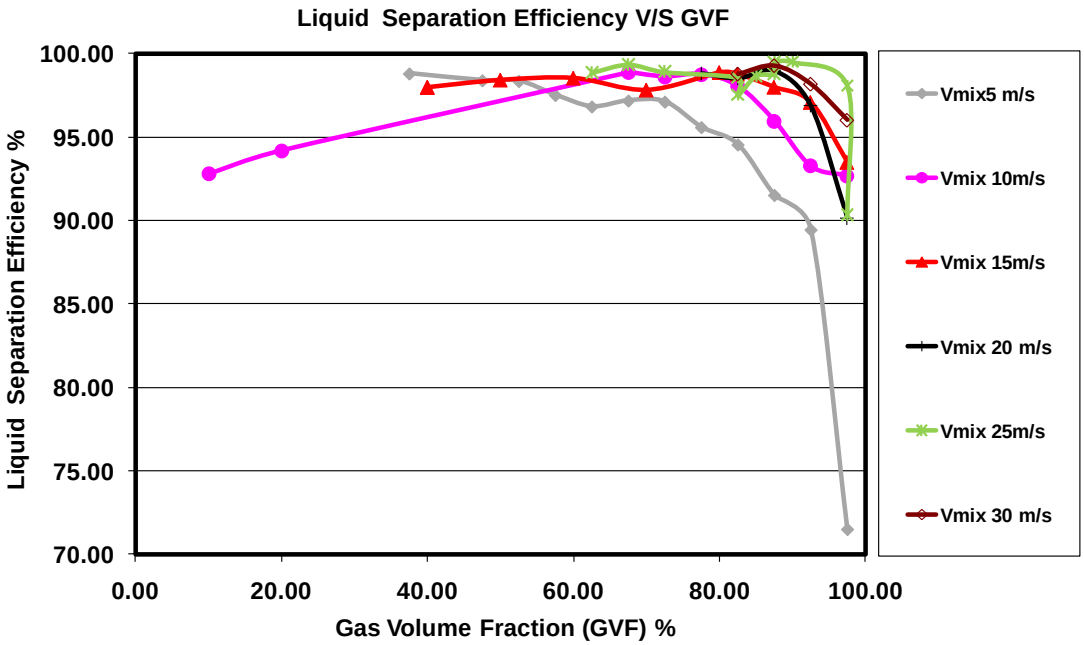

Figure 4.14a Effect of GVF on Liquid Efficiency.

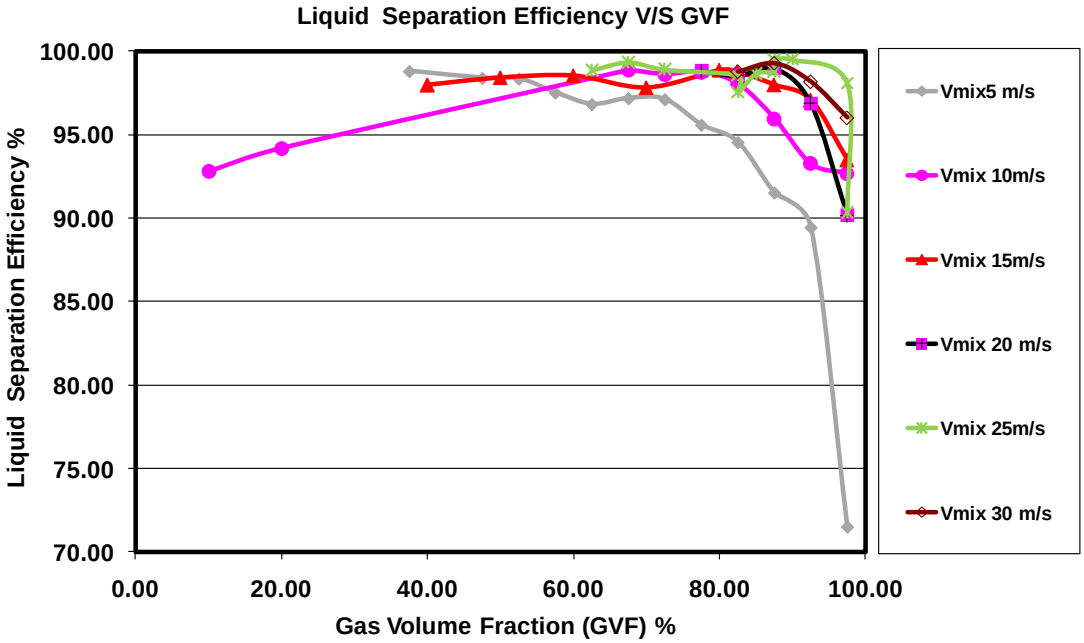

Figure 4.14b Effect of GVF on LCO.

However at 10 m/s the LCO was observed decreasing with the increasing in GVF. It can be seen in the Figure 4.14b that at 5 m/s mixture velocity the LCO % was recorded as 3.20% for GVF value of 35% having liquid inlet flow rate of 2.5 l/s, but was increased to 5% at same mixture velocity when GVF was raised to the 45% with the inlet liquid flow rate of 4.3 l/s. This trend continued for almost all value of GVF at mixture velocity of 5 m/s but then changed on higher velocities for example LCO was decreased when GVF was increased from 60 to 65% or from 75 to 80% at 10, 15 and 20 m/s. However GVF composition of 80%, 85% 90% and 97.5% showed that LCO was increased with the increase in GVF at the same inlet mixture velocity.

The increasing liquid efficiency and decreasing LCO with the increase in the inlet mixture velocity can be theoretically explained with the help of equilibrium model of separation efficiency. According to this model there are two forces acting on the particle one is centrifugal force acting away from the centre and other one is the drag force acting towards the centre and tries to move the particle in the axial direction. The centrifugal force can be given by the following equation:

$$F_c = \frac{\pi d^3(\rho_p - \rho_f)V_t^2}{6r} \qquad (4\text{-}2)$$

Where

ρ_p is the density of the particle (kg/m^3)

ρ_f is the density of the fluid in this case gas (kg/m^3)

V_t is the tangential velocity component of the mixture velocity (m/s)

r is the radius of the separator (m)

d is the diameter of the particle (m)

Looking at this equation it can be seen that the an increase in the inlet velocity would cause to increase centrifugal force resulting the more liquid to move towards the wall of separator thus allowing more liquid to pass through the underflow producing less liquid to pass through the overflow of I-SEP thus decreasing the LCO and increasing the liquid separation efficiency.

4.9 Effect of Liquid Superficial Velocity on GCU and LCO

It was also investigated how does liquid superficial velocity affects the GCU and LCO at fixed gas superficial velocity. It was observed that both the LCO and GCU in general had decreased with the increased in liquid superficial velocity at constant gas superficial velocity as shown in Figure 4.15a and Figure 4.15b. This means that efficiency of the I-SEP would be increasing on increasing liquid flow rate keeping gas velocity constant.

4.10 Effect of LCO on GCU

The LCO and GCU resulted values are further compared to each other for every increment of inlet mixture velocity at fixed GVF to understand how these two quantities relate to each other and presented in Figure 4.16. It was revealed that from 45% to 85% GVF for all inlet mixture velocity both GCU and LCO varied similarly means if GCU is increased on increasing the mixture velocity same effect was observed in LCO and vice versa. This means if more gas is passing through axial

outlet due to decrease in GCU than it does not cause to carry more liquid with it and vice versa. Likewise if amount of the liquid increased in the axial outlet indicating decease in liquid separation efficiency then it does not cause to carry more gas in the axial outlet thus reducing GCU. However a change in this trend was observed at GVF values greater than 90% when at higher velocity GCU was increased it resulted in a reduction of LCO, as can be seen for GVF 97.5, and 98% in the Figure 4.16. This indicates that when higher proportion of gas enters into tangential outlet at high inlet GVF and mixture velocity than it also cause to take with more liquid thus causing to decrease LCO%.

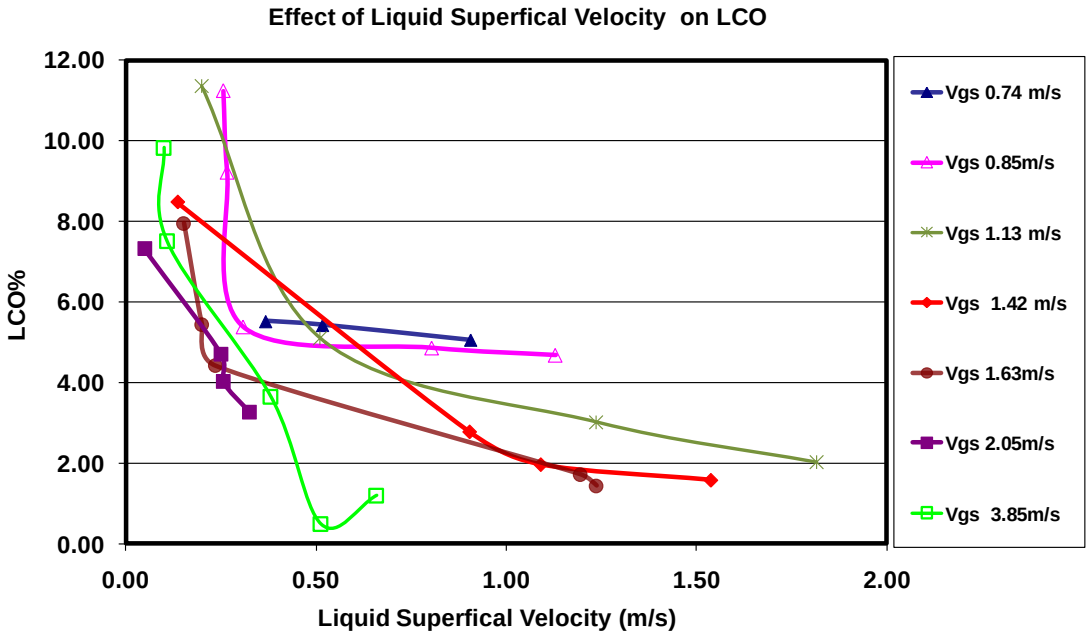

Figure 4.15a Effect of Liquid Superficial Velocity on LCO at constant Gas superficial velocity.

4.11 Effect of Pipe Diameter Connected at I-SEP Outlets

The effect of the diameter of pipe connected to tangential and axial outlet of the I-SEP was also investigated. The experiment discusses so far used gas flow meter FM06 and FM08 which were installed to pipe having one inch diameter connected to the tangential and axial outlet of I-SEP. However experiments was also conducted using the gas flow meter FM05 and FM07 which were installed on 2 inch and 3 inch

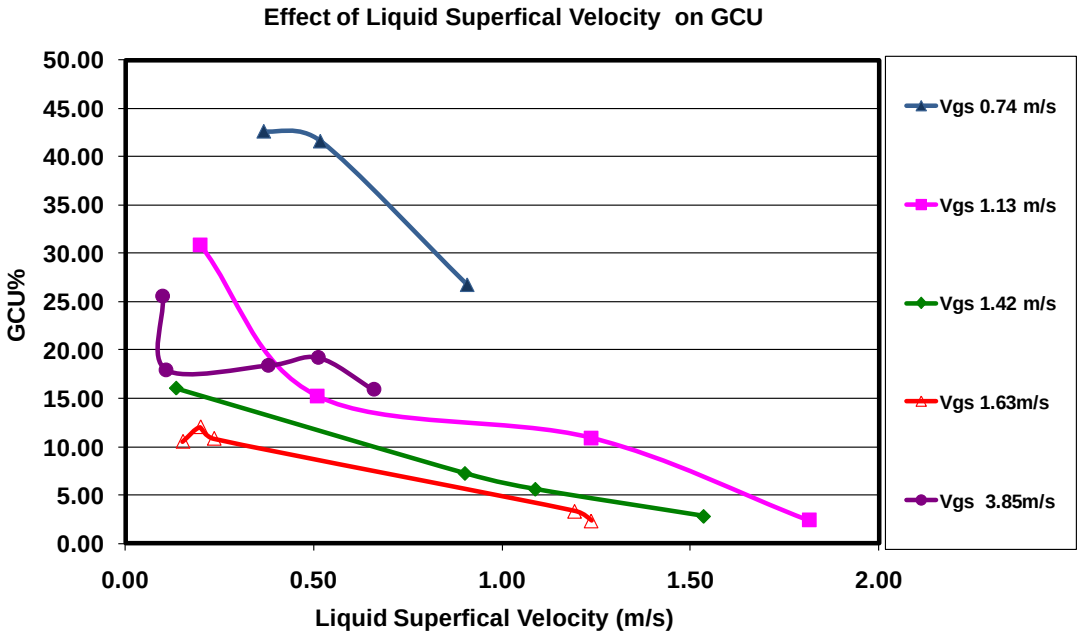

Figure 4.15b Effect of Liquid Superficial Velocity on GCU at constant Gas superficial velocity.

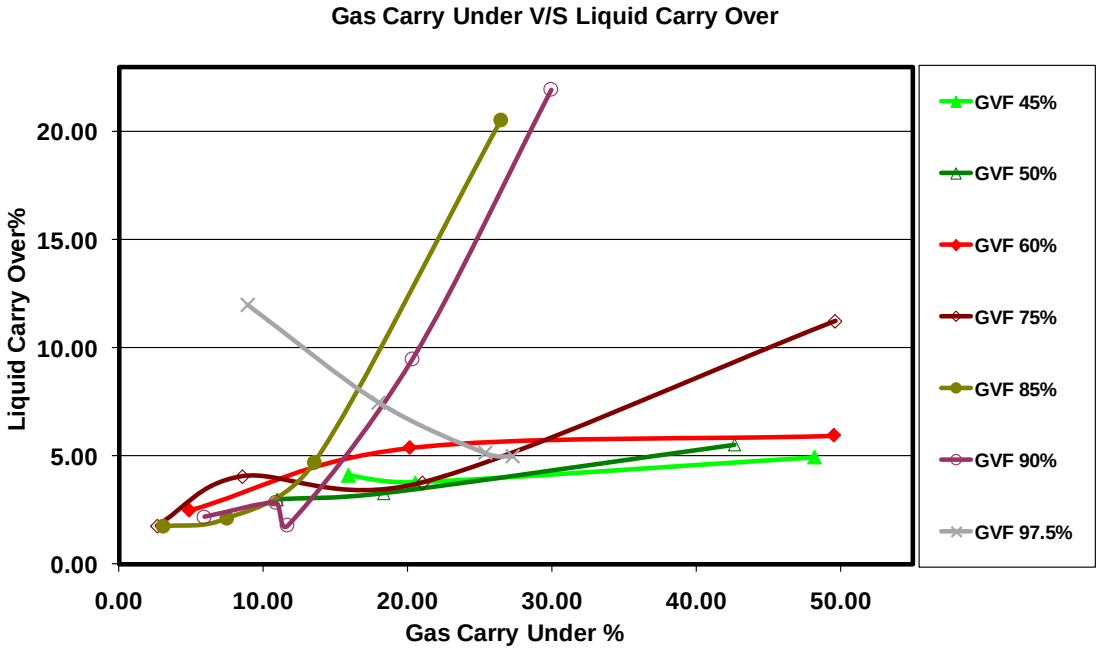

Figure 4.16 Effect of GCO on LCO.

pipe connected at axial and tangential outlet of the I-SEP respectively. Identical set of experiments were performed using FM06 ,FM08 and FM05 ,FM07 separately in order to understand the effect of the pipe size on the separation efficiency. The result is compared in the Figure 4.17. These experiments are conducted using the GVF 97.5 with velocity range from 7.5 - 60 m/s in slug flow regime region. The separation efficiency is compared in the Figure, it can be seen that while the trend in similar in both cases, the difference lies in the maximum velocity after which the GCU start again. When same size pipe was used on the tangential and axial outlet, GCU initially decreased with velocity but then increased for the velocity greater than 15 m/s, the same trend is repeated for FM05 and FM07 but this time the GCU start increasing after mixture velocity has reached to 37.5 m/s. This means I-SEP separation efficiency range would be increased if a large diameter size pipe is used at its tangential outlet as then optimal velocity would be increased and GCU would be low even at higher mixture velocity. However LCO does not affected by pipe size as can be seen from the Figure 4.17

4.12 Pressure drop and its Effect on Efficiency

The separator uses the fluid pressure energy to gain the separation power which appears as a loss in pressure across the unit. This pressure drop is usually taken immediately before the inlet and immediately after the axial outlet. Thus in our case P_{13} defines the pressure drop across the cyclone. The pressure drop between inlet and tangential outlet i.e. P_{12} and that is between inlet and axial outlet P_{13} was found less than 1.0 and 1.5 bar respectively for all the performed experiments as shown in Figure 4.18a. A close observation of experimental data for every GVF and comparing the pressure changes at inlet, tangential and axial outlet of the I-SEP, it was observed that inlet pressure was always higher than tangential and axial pressure for all range of performed experiments and all of these pressure were directly related to inlet liquid flow rate or inlet liquid superficial velocity. The pressure drop between inlet and axial outlet P_{13} and that of between inlet and tangential outlet P_{12} were always increasing with the increasing mixture velocity at fixed GVF which produced an increasing

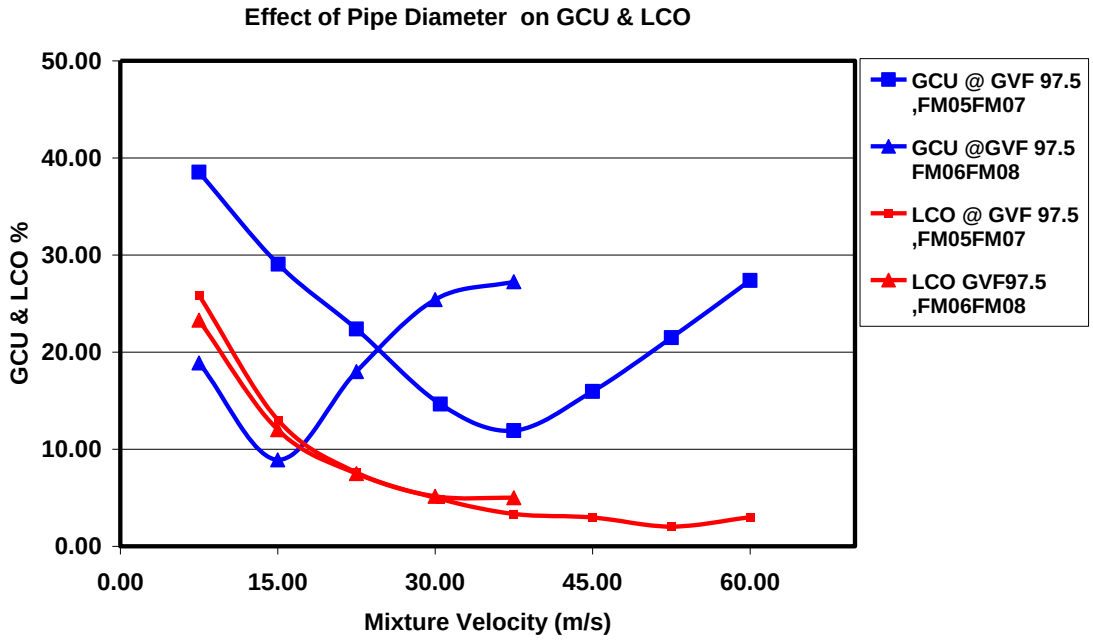

Figure 4.17 Effect of mixture velocity on GCU and LCO with large diameter pipe at outlets.

pressure difference between these two outlets P_{23} of the I-SEP. However all these pressure were found to be decreasing with the increase in GVF. The tangential outlet pressure P_2 for all GVF values less than 55% was found higher than that of axial pressure P_3 which caused to produce a higher pressure drop between inlet and overflow as compared to that of between inlet and underflow for all experiments having GVF less than 55%. On the other hand the axial pressure went ahead than tangential for GVF higher than 55% causing the pressure drop between inlet and overflow lower than that of between inlet and tangential outlet.

It was investigated that how the dimensionless pressure drop behaves with the GVF and mixture velocity. Loss coefficient or Euler number as defined in equation 2-10 was calculated between inlet and axial outlet called L_{13} and between inlet and tangential outlet called as L_{12} and are presented in Figure 4.18b and Figure 4.18c respectively. It was observed that L_{12} at fixed GVF increased with the increased in velocity, L_{13} however increased for lower GVF values but then decreased for GVF values between 60 to 85% and almost became constant for further increased of

velocity at these GVF values. However at high GVF it is increased with the increase in velocity. This means I-SEP is more efficient on mid value of GVF as compared to high GVF values greater than 85%.

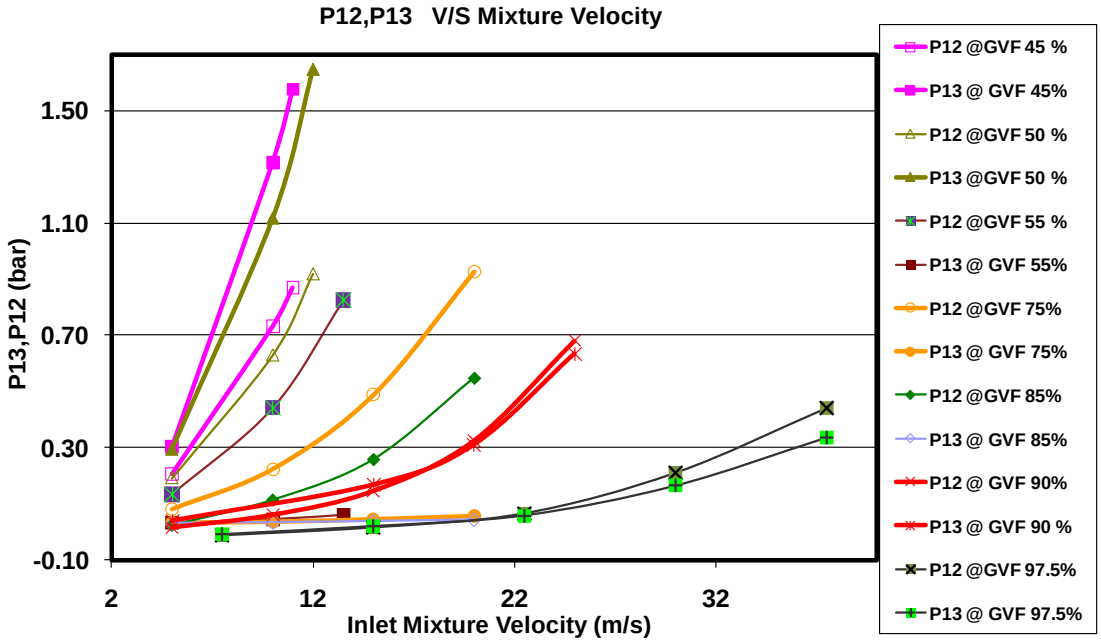

Figure 4.18a Effect of Mixture velocity on Pressure Drop.

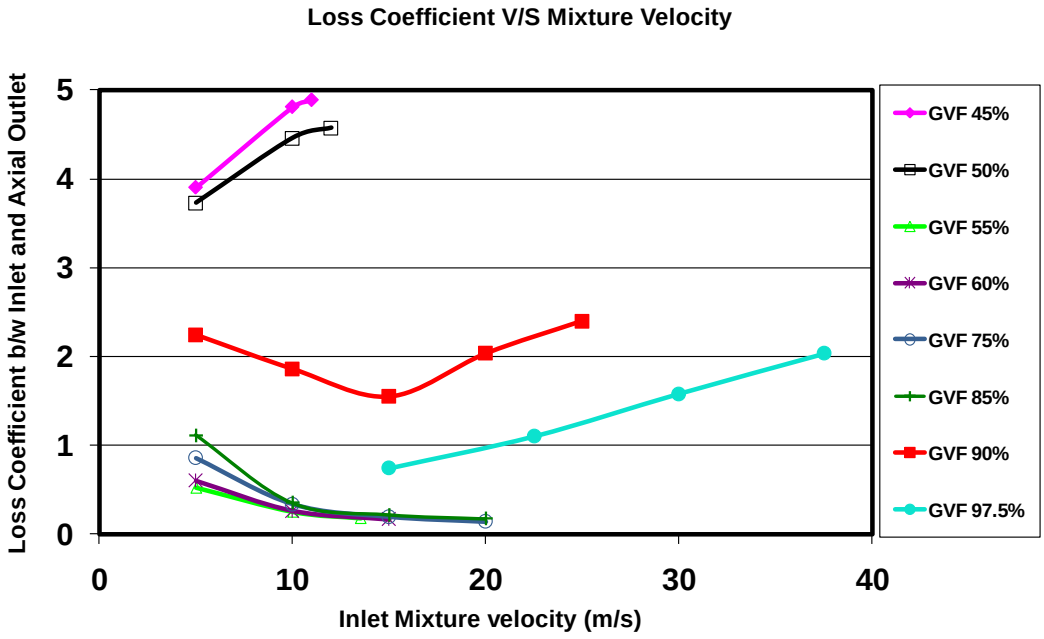

Figure 4.18b Effect of Mixture velocity on Loss Coefficient between inlet and axial outlet of I-SEP.

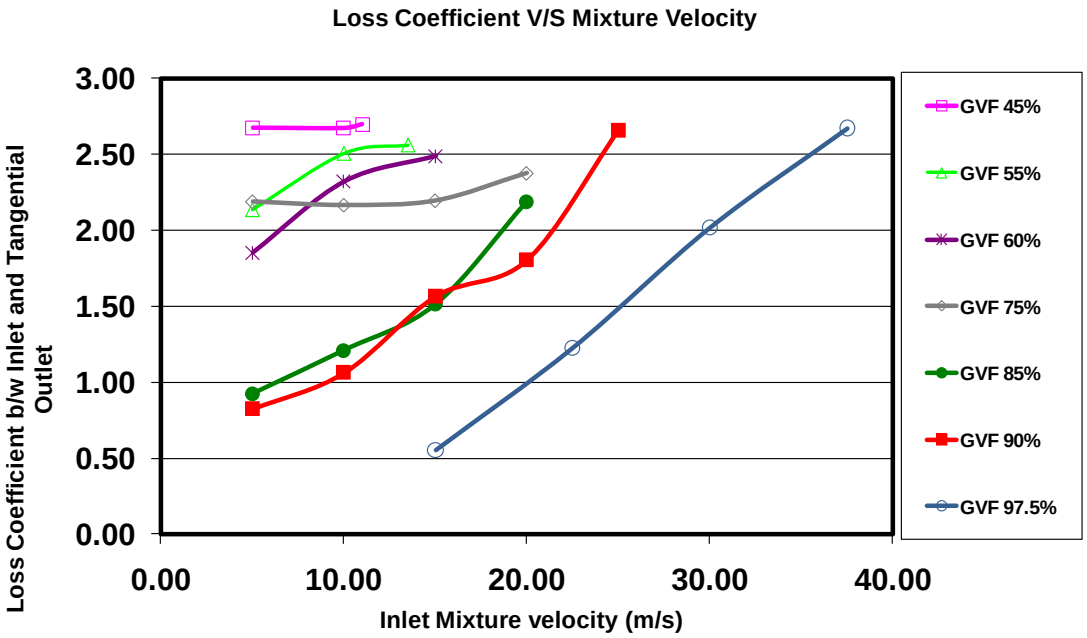

Figure 4.18c Effect of Mixture velocity on Loss Coefficient between inlet and tangential outlet of I-SEP.

4.12.1 Effect of Pressure Drop on GCU

The pressure drop between inlet and tangential and axial outlet is compared with the observed produce GCU in Figure 4.19a and Figure 4.19b. It can be seen that GCU is decreased with the increased in pressure drop at all value of GVF except at 90% GVF where further increased in pressure drop has actually caused to increased the GCU slightly. The change in pressure drop between inlet and axial outlet i.e. P_{13} for GVF between 55% and 85 % is very sensitive as here a small change has caused to decreased relatively high amount of GCU as can be seen in the figure 4.19a, indicating that relatively less energy is required to get the clear liquid. For example P_{13} was observed less than 0.06 bar or (600 mbar) for GVF between 55% and 85% corresponding to GCU% between 6 to 50%. However it went more than 1 bar at lower GVF values as can be seen in the Figure4.19a. This means decreasing GCU at lower GVF requires relatively greater energy. The pressure drop at underflow through all tests was found more than 0.1 bars as can be seen in the Figure 4.19b.

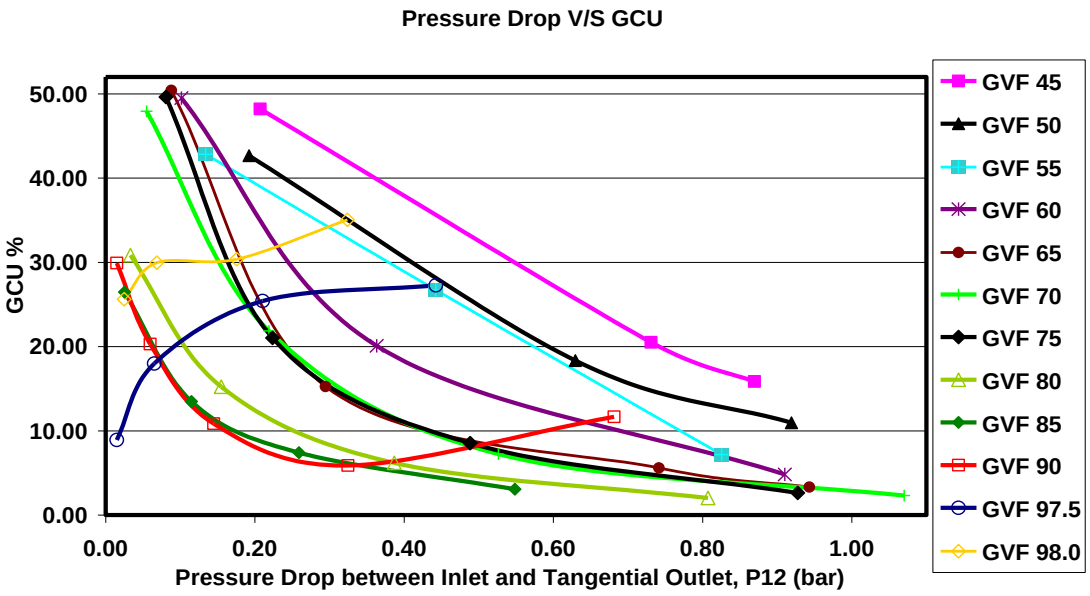

Figure 4.19a Effect Of Pressure Drop Between Inlet And Tangential Outlet on GCU & P12.

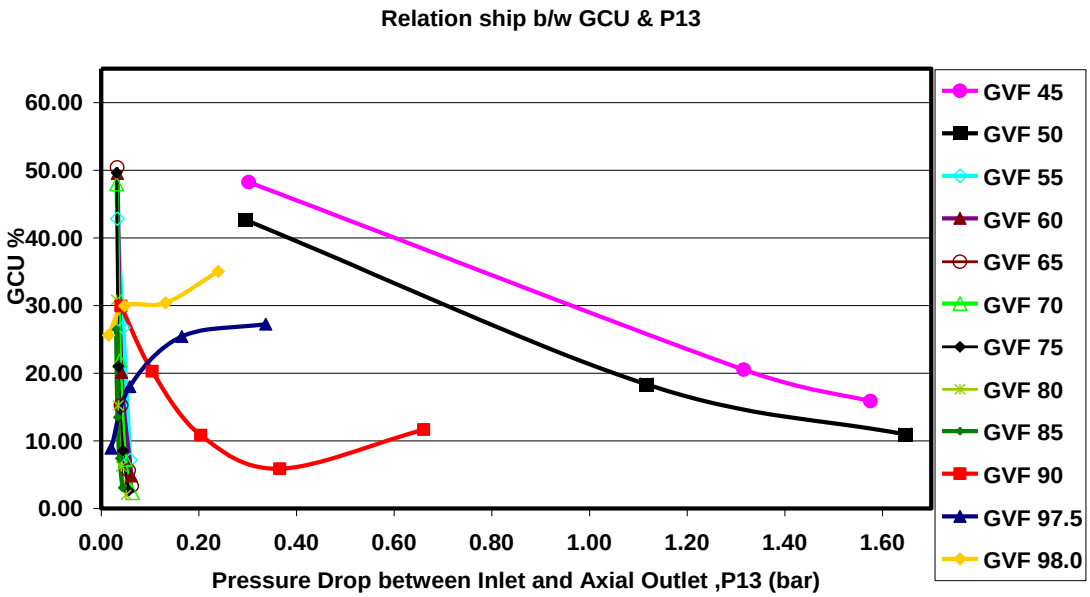

Figure 4.19b Effect Of Pressure Drop Between Inlet And Axial Outlet on GCU & P13.

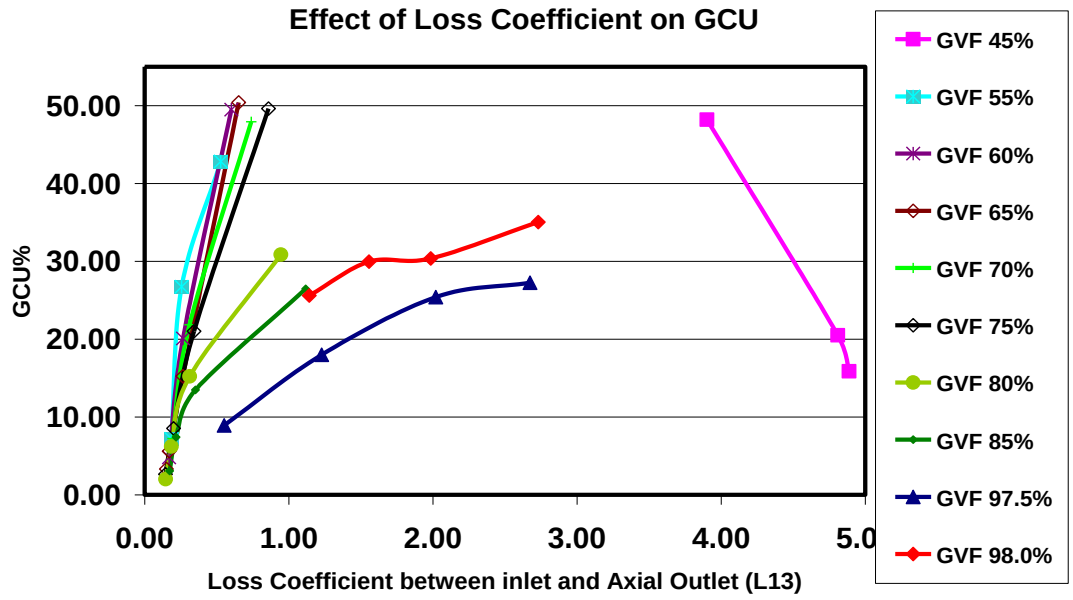

Figure 4.19c Effect of Loss Coefficient L13 on GCU.

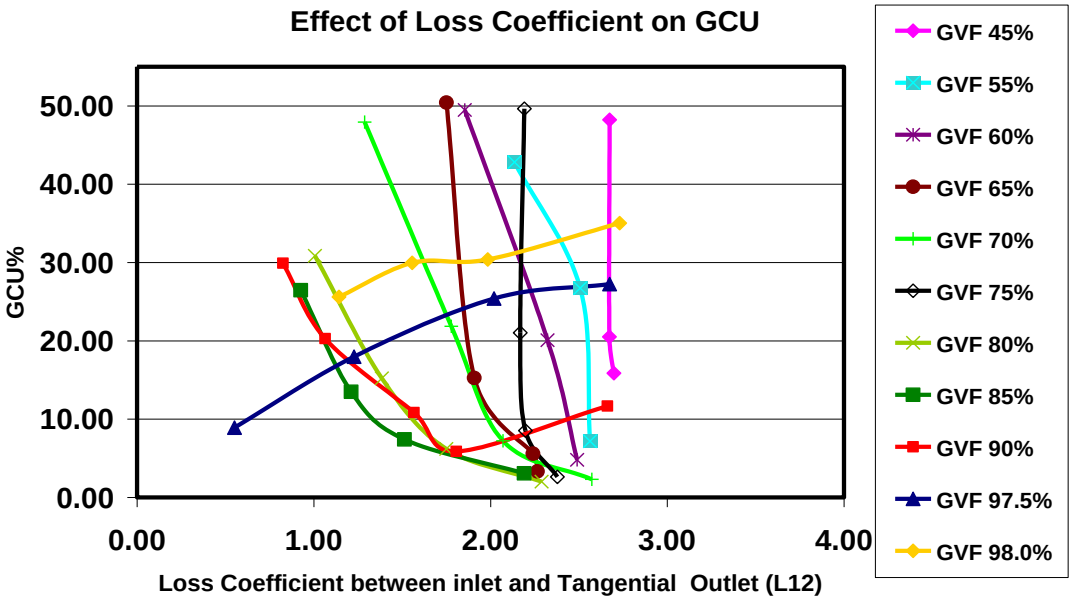

Figure 4.19d Effect of Loss Coefficient L12 on GCU.

The relationship of GCU was also explored with the loss coefficient and presented in Figure 4.19c and Figure 4.20d for loss coefficient between inlet and axial outlet i.e. L_{13} and loss coefficient between inlet and tangential outlet i.e. L_{12}. It can be seen that GCU has decreased with the increase in loss coefficient L_{12} value, however it has

increases with the very small increment in the loss coefficient L_{13} for all the GVF values greater than 50%. This means at lower GVF it requires more energy as L_{13} is in the range of 4 and 5 (see Figure 4.19c) and GCU has decreased with the increases in the L_{13} and at the mid value GVF i.e. from 65 to 85% the L_{13} is very low even less 1 and GCU increased sharply with the increase in the L_{13} This indicate that it works better in this region due to less L13 but a small change in L_{13} can produced large change in GCU so control of is needed in this region..

4.12.2 GCU and Pressure Difference between Tangential and Axial Outlet

The pressure at the tangential and axial outlet reciprocate each other, means while one is increased other is decreased as observed during these experiments which means that pressure drop between inlet and these two outlets would be opposite to each other. Therefore pressure difference between these two outlets i.e. P_{23} is usually used to control and quantify the GCU. However in this study it was found P_{23} is not very linearly related to the observed GCU and also went negative when tangential pressure went ahead than axial pressure.

Therefore some new parameter was investigated to define this behaviour. It was observed during the single phase experiment that ratio of axial and tangential pressure drop P_{13}/P_{12} was directly related to the observed GCU and had indirect relationship with the LCO. This non dimensional parameter was also investigated in these multiphase experiments and was found it was more linearly related to observe GCU than P_{23}. It was found GCU deceased with the increase P_{13}/P_{12} until GVF is less than 55%, but between 55%GVF to 85% trend is changed and it started increasing with the increasing in P_{13}/P_{12} as can be seen from Figure 4.20a.The same trend was observed between GCU and P_{23}. However the relationship between GCU and P_{23} is more non linear as in that case GCU also behaved non linearly for GVF 35% when it first increased and then decreased with the increase in P_{23} as can be seen in the Figure 4.20b. Since P_{13}/P_{12} showed more linear relationship with single phase

experiment therefore it seems to be a good choice to related GCU with P_{13}/P_{12} than P_{23}.

4.13 Pressure Drop Comparison

The pressure drop data observed in these experiments were then tried to compared with similar data in literature, T junction being in principle more similar to the I-Sep was selected for this comparison other than some commercially available separator. However most of work done on T junction was found in Annular and stratified flow regime. The Table 4-3 represents this comparison. The ID of T junction used in Buel et al. (1994a) is 38 mm with having same inlet and branch radius, whereas Walters et al. (1998) used T junction had inlet diameter of 38mm but branch arm diameter was reduced to 17.5 to make D3/D1=0.5. It can be seen in the Table 4-3 that although the pressure drop in I-SEP is relatively larger but ratio of quality of the gas x_3/x_1 is much less than others showing that much purified liquid streams having less gas compared to both the T junction.

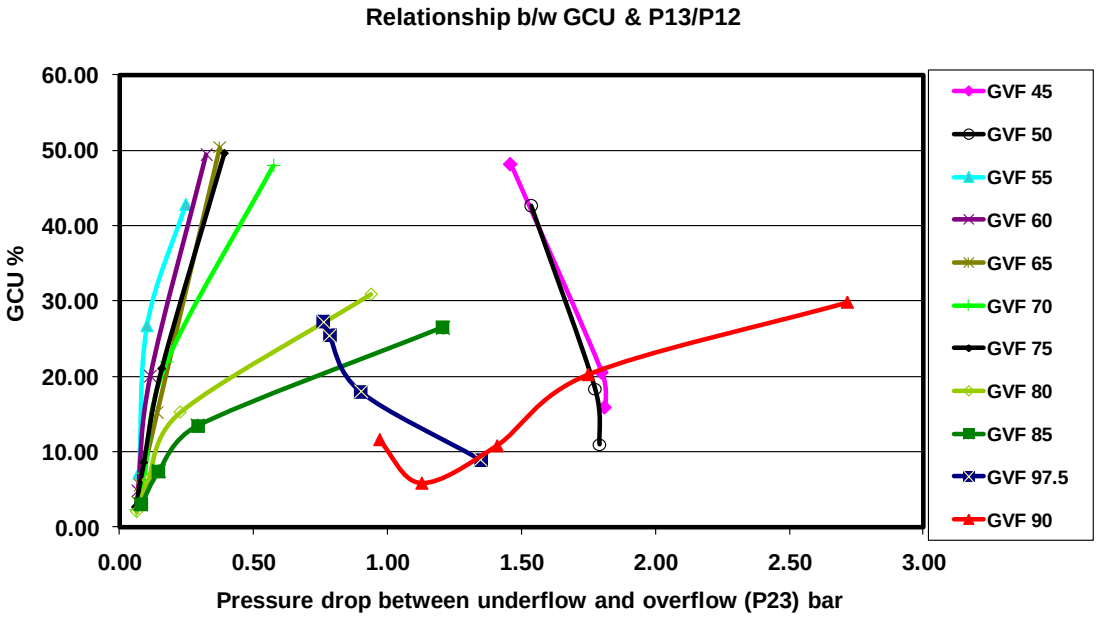

Figure 4.20a Effect of P13/P12 on GCU.

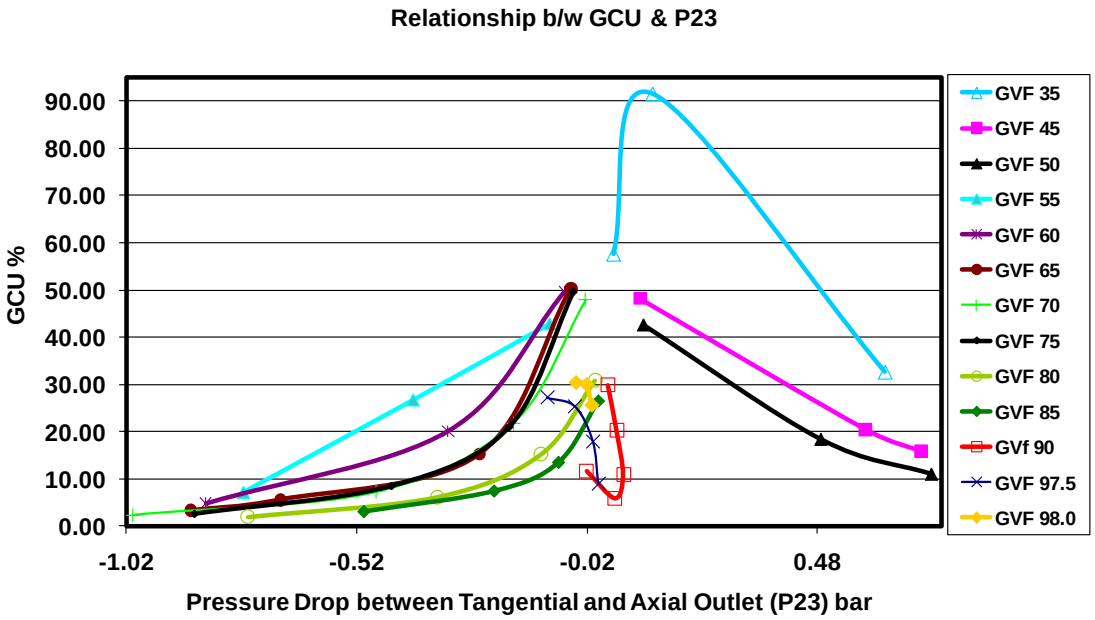

Figure 4.20b Effect of P23 on GCU.

The pressure drop model used to predict the pressure drop between the branch and inlet of the T junction Buel et al., (1994a) was also applied on the observed pressure drop data of I-SEP. The static pressure at the junctions are given by Buel et al., (1994a)

$$\Delta P_{13} = \frac{\rho_{h3}}{2}\left(\frac{G_3^2}{\rho_3^2} - \frac{G_1^2}{\rho_1^2}\right) + K_{13}\frac{G_1^2}{2\rho_l}\phi \qquad (4\text{-}3)$$

$$\Delta P_{12} = K_{12}\left(\frac{G_2^2}{\rho_2} - \frac{G_1^2}{\rho_1}\right) \qquad (4\text{-}4)$$

Where G_1, G_2, G_3 are the mass flux, ρ_1, ρ_2, ρ_3 are the mixture densities at inlet, branch and run arm of the t junction, ϕ is two phase multiplier obtained using the homogeneous flow model. It should be noted the branch arm is taken as tangential outlet of the I-Sep. however this model did not confirm the observed experimental data of I-Sep.

Table 4-3 Comparison of Pressure drop of I-SEP and T-junction.

Device	Reference	Pressure (bar)	V_{gs} (m/s)	V_{ls} (m/s)	P_{12} (mbar)	P_{13} (mbar)	x_1 (%)	x_3 / x_1
I-Sep		1.3	2.6	0.3	170	160	1.4	0.1
Reduce-Tee	(Walters et al., 1998)	1.5	2.7	.18	1.84	1.19	2.6	7.8
T junction	(Buel et al., 1994a)	1.54	2.7	.18	0.93	1.83	2.6	1.7
I-Sep		1.3	4.4	0.14	160	130	4	0.3
T junction	(Buel et al., 1994a)	1.5	4.4	0.18	.64	2.07	4.2	2.9
Reduce-Tee	(Walters et al., 1998)	1.5	4.3	0.18	2.46	0.95	4.0	3.12

4.14 Back Pressure Effect on GCU

The resistance at the outlets of the separator also affect the produced GCU and LCO. This was further studied by applying the external back pressure through the throttling of the valve attached to the tangential outlet of the I-Sep. The objective of these experiments was to find a quantitative relationship between the GCU and the applied back pressure. These experiments were conducted at mixture velocity of 10, 15 and 25 m/s with GVF value between 65 and 95%. The control valve at the I-SEP tangential outlet was throttled from the fully open position up to 90 % close position and data was recorded during every successive turn after the steady state was achieved. The throttling of the valve increased the back pressure at the tangential outlet along with the increase in inlet pressure and axial pressure. However the tangential pressure increased more than that of the axial pressure creating more pressure drop between inlet and the axial outlet during the each successive turn due to which more gas was shifted towards the axial outlet causing to decrease in the GCU. The increased in the resistance at the tangential outlet however also caused to push the liquid towards the axial outlet and hence LCO was found to increase as a result of this applied back pressure.

The pressure difference between the two outlets is usually used to measure the cost of the eliminating the GCU, however the relationship between this two parameters is observed very non linear as shown in Figure 4.21a. The other parameter that is considered was the ratio of pressure drop between inlets and axial to that of between inlet and tangential outlet, it was also found to be non -linearly related with the GCU, as can be seen in Figure 4.21b.

4.15 Proposed Control Strategy

I-SEP was used in these experiments with the combination of a gravity separator i.e. HI-SEP. The liquid level inside the HI-SEP needs to be control such that it should not

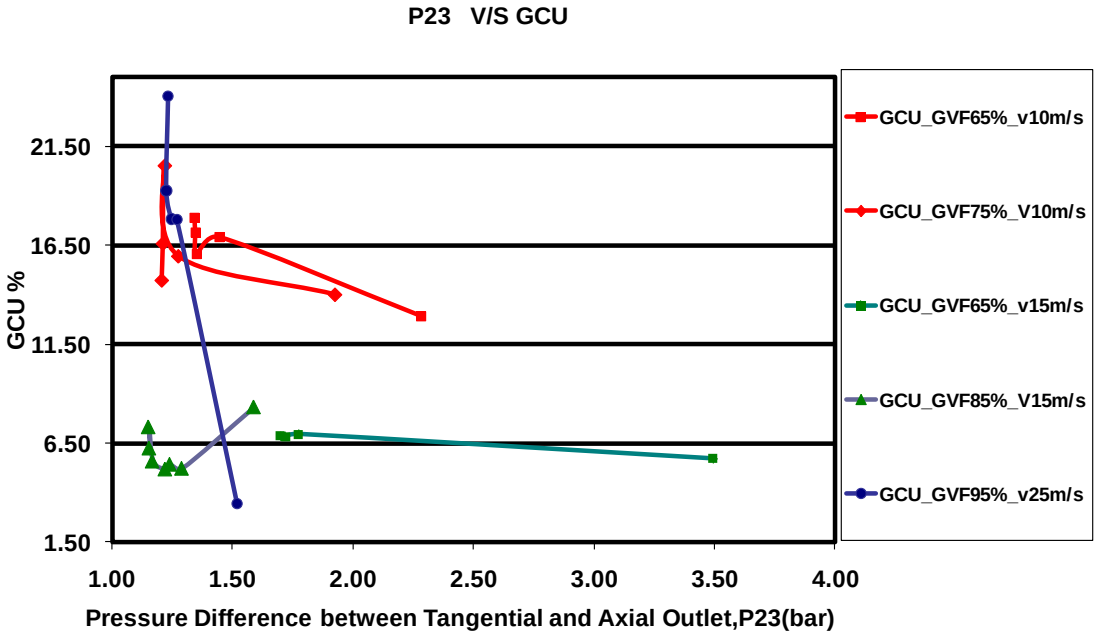

Figure 4.21a GCU & P23 under applied Back Pressure.

go more than the height of inlet section of HI-SEP for better performance of the separator. This liquid level control inside the HI-SEP depends upon the incoming liquid and gas coming out from the I-SEP axial outlet. The liquid level inside the HI-SEP could be control either using a liquid control valve (LCV) attached at the liquid leg or using a gas control valve (GCV) attached at the gas outlet of the HI-SEP or using the combination of the both valve. However the result of these experiments may be used to chose the more appropriate control valve.

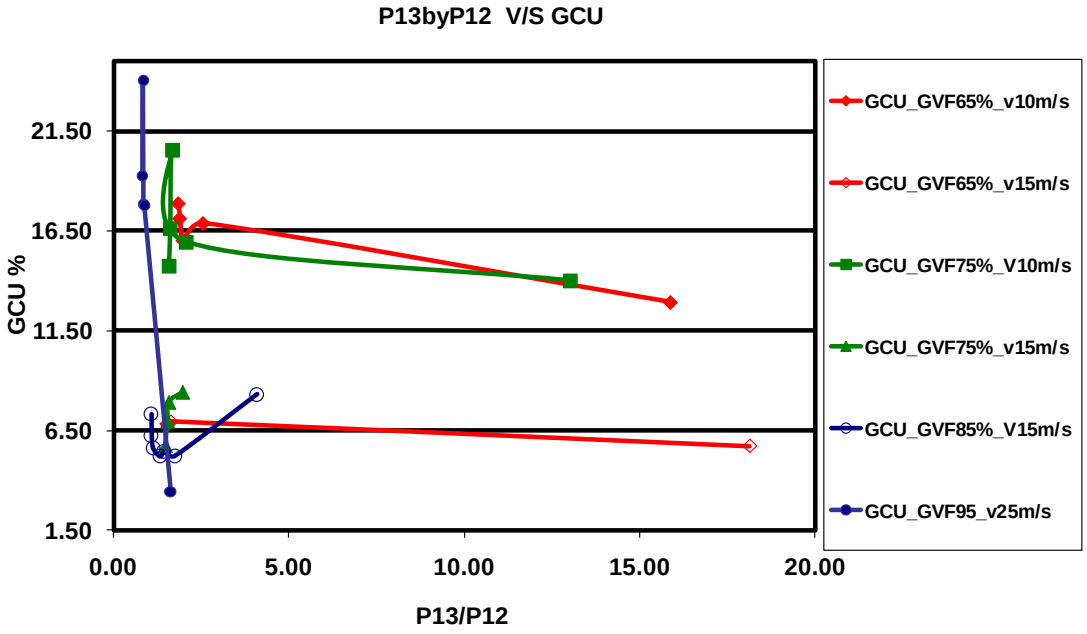

Figure 4.21b GCU &P13/P12 under applied Back Pressure.

The LCO % as discussed in section 4.4 was found lower as compared to GCU% with average value of 5%. However there is high probability of producing high LCO% at low mixture velocity at relatively high GVF between 75 to 85% as shown in Figure 4.13b.The GCU on the hand at this data values is also higher as can be seen from the Figure 4.11b. The LCO at high GVF was once again found lower than 5% at high GVF value greater than 85% while GCU was increased at these GVF.

It should also be noted that the flow at I-SEP axial outlet is most of the time is wavy or stratified and not slug as can be seen in Figure 4.2b.The lower production of LCO% suggests that liquid control valve attached with the liquid leg of the HI-SEP would be sufficient to control the liquid level under normal condition. A simple feedback control loop consisting of controller, a LCV, a DP to measure the liquid level, gas and liquid flow rate coming out from the I-SEP axial outlet and entering into the HI-SEP as input and liquid level height measured through DP as feedback signal may be used to control the liquid level inside the HI-SEP. The liquid control

valve would be relatively more opened at low mixture velocity and high GVF due to relatively high LCO% as compared to rest of the GVF and mixture velocity composition.

4.16 Conclusion

- When multiphase flow in the slug region is passed through the I-SEP, then slug flow regime does not appear at the axial outlet , however the tangential outlet may have slug but having less strength than at inlet.
- I-SEP has tendency to produce more GCU then LCO. The average GCU % was found 18% and LCO % was found below 5% for all the experiments.
- The multiphase experiment showed that the relationship of the observed GCU and LCO with either of the mixture velocity and GVF of the mixture is nonlinear.
- The GCU and LCO decreased with the increase in mixture velocity at fixed GVF non-linearly, however at higher GVF of 90 % GCU was increased with further increased in mixture velocity, while LCO remain constant.
- The increase in mixture velocity at GVF greater than 90% does not affect very much on GCU.
- LCO and GCU were found to increase non-linearly with the increase in GVF at fixed mixture velocity.
- GCU and LCO were both found to decrease with the increased in liquid superficial velocity at the constant gas superficial velocity.
- The LCO and GCU does not affect very much on each other, however at GVF greater than 90% increase in GCU also increased LCO.
- The Pressure at inlet was increased with the increased in mixture velocity and GVF
- The pressure at tangential outlet was higher than that of at axial outlet for GVF value less than 55 % but than got higher when GVF was increased more than 55%.
- Loss coefficient between inlet and tangential outlet increased with the increase in mixture velocity.

- Loss coefficient between inlet and axial outlet showed that I-SEP would perform more efficient between GVF values 60% to 85% as during this region Loss coefficient was found to decrease.
- Loss coefficient indicated that reducing GCU at lower GVF values requires more energy as compared to GCU reduction at high GVF values.
- The ratio of pressure drop between inlet and axial to that of between inlet and tangential was found relatively more linearly related to the GCU than pressure difference between tangential and axial outlet.

Chapter 5

I-SEP and Severe Slugging

5.1 Introduction

Flow assurance is one of the most important objectives for the design engineers in oil and gas industry. One of major challenge in the flow assurance during the transport of the multiphase flow in pipelines is the handling of sever slugging due to its potential to produce system instability. Severe slugging produces cyclic periods of no liquid and gas production into the separator followed by very high liquid and gas production. This rapid change in liquid production rate also becomes a problem for the downstream separator to maintain the liquid level. The large fluctuations in pressure and flow rates not only can severely reduce production capacity but also in the worst case may shut down or damage topside equipment, such as separator vessels and compressors.

The next phase of I-SEP performance was to test its behaviour in severe slugging condition. The objective was to test whether a compact cyclonic separator of this size could be use to eliminate or reduce the instabilities in pipe line riser flow. This chapter describes experiments performed to test I-SEP under severe slugging and compares the performance of I-SEP during severe slugging under same condition with a gravity separator.

5.2 Severe Slugging Mechanism

Severe slugging is produced in a situation when multiphase flow of low flow rate is allowed to flow either in a downward inclined pipe or an undulating horizontal pipe that meets a vertical riser at the other end. Taitel, (1986); Jansen et al. (1996); Kjetil and Morten, (2002) has described severe slugging as a periodic process of four stages:

1. Liquid accumulation
2. Slug production

3. Bubble penetration
4. Gas blow out

The liquid is accumulated at the bottom of the riser due to the lower flow rate of liquid to initiate the slug formation cycle. This accumulation of liquid at the bottom of riser blocks the passage of the incoming gas which results in the compression of the gas and increases pressure at the bottom of the riser. The liquid level continues to grow up in the riser until it reaches to riser top and start entering into the separator at which point the second step of the severe slugging is started which is termed as production or slug movement, this causes the expansion of the gas and it starts moving into the riser initiating the third stage bubble penetration (some authors has called it as gas blow out), causing to decrease the hydrostatic pressure and increase the gas flow rate. The gas energy is lowered and is not sufficient to carry the liquid causing the liquid to fall back in the riser, thus starting the cycle again.

This process hence produces period of no liquid and gas production into the separator followed by high liquid and gas flow rates causing large pressure and flow rate fluctuation. This situation is undesirable as high liquid flow rate may cause to shut down the separator due to over flow and fluctuation in the pressure which may decrease the production capacity.

5.2.1 Slugging Mitigation Methods

Several researches has worked out to find the remedy of this problem and proposed many method and devices by the researchers to suppress or avoid the severe slugging. These methods/devices adopted to reduced/eliminate severe slugging can be categorized in two different types: Non-control method/devices and control method/devices. The non control methods mainly involve use of gas lifting /gas injection, separator/slug catchers, and modification of the pipe line geometries, whereas the control method include back pressure control, choking, separator control, gas lift and choking combination, and flow rate control.

Gaslift is one of most used methods to eliminate the severe slugging. In the gaslift the liquid is pushed out from the riser and further accumulation is prevented to avoid any gas blockage by the injecting the gas at the base of the riser. The injected gas flow rate must be sufficient enough to carry the liquid up to riser top. Pots (1985) concluded on his work on gas injection that severe slugging was not fully eliminated even with 300% injection. Wyllie (1995) following gas injection technique patented an invention that uses the small diameter pipe inserted into the riser thus creating an annulus which is then used to inject the gas into riser to eliminate the severe slugging. The disadvantage of this method is high cost, and increased frictional pressure drop especially for deep waters.

Barbuto (1995) working on the idea of the modification of geometry of the pipe line to reduce the severe slugging connected pipeline and riser with each other to transmit the pipe line gas to the riser at predetermined position which is set to be 1/3 of the height of the riser. This arrangement thus causes to inject the gas in the riser which then mixed with the liquid slug coming into the riser and thus reducing the severe slugging process.

Separator has been used as a slug catcher working as a passive device to suppress the severe slugging. A slug catcher actually temporarily stores intermittent slug which is treated after the slugging period. Song and Kouba, (2000) proposed used of separator for under sea gas liquid separation as a method to eliminate the severe slugging. They have conducted a proof of study based on the OLGA simulation.

Schmidt et al. (1980) demonstrated that choking of the riser top valve could eliminate the severe slugging. He explained that due to the increase in back pressure through the choking of the valve the flow condition could be force to move out from the severe slugging condition towards stable condition. He was supported by Taitel (1986) with his slug flow model. However this relatively low cost method of reducing severe slugging causes to produce some unfavourable effect on fluid production. The system gets a bit over pressurized due to applied back pressure as compared to normal

steady flow. Since then worker in this area have been developing new method to applied back pressure technique in many ways in order to keep the system pressure resulted due to applied choking as much as possible. Severe feed-forward and feed-back system have been proposed. All these methods detect the severe slugging with proper mean then manipulate the pipeline chokes, pressure or liquid level to eliminate the severe slugging. Steeg (1991) presented a method using riser top side control valve to prevent slug growth in a pipeline system for gas-liquid two-phase fluid transportation. He identified the slug measuring the total flux using two meters in liquid and gas line and controlled the mixture velocity by manipulating control valve to eliminate the severe slugging.

Separator with the proper control has also been used as active device for slug mitigation. Hill (1996) demonstrated that controlling gas flow rate at the separator can damp the flow line fluctuation and bring the system in stable state. Hollenberg and DeWolf (1998) used the same technique as used by Steeg (1991) but rather than controlling the top side valve they actually control the gas flow rate at the separator output to damp the severe slugging.

5.3 Experiments Objectives

The role of I-SEP was also explored as an active/passive device to mitigate the severe slugging. The main objectives were to observe the effect of I-SEP as a separator in severe slugging condition and to see how much does it increase the riser base pressure in reducing or eliminating the severe slugging during choking as compared to the other gravity separator. The result of these experiments produced performance comparison of I-SEP with a gravity separator under same flow condition during severe slugging. The experiments were performed by incorporating the I-SEP and HI-SEP in Cranfield University multiphase test facility which is discussed briefly in the next section.

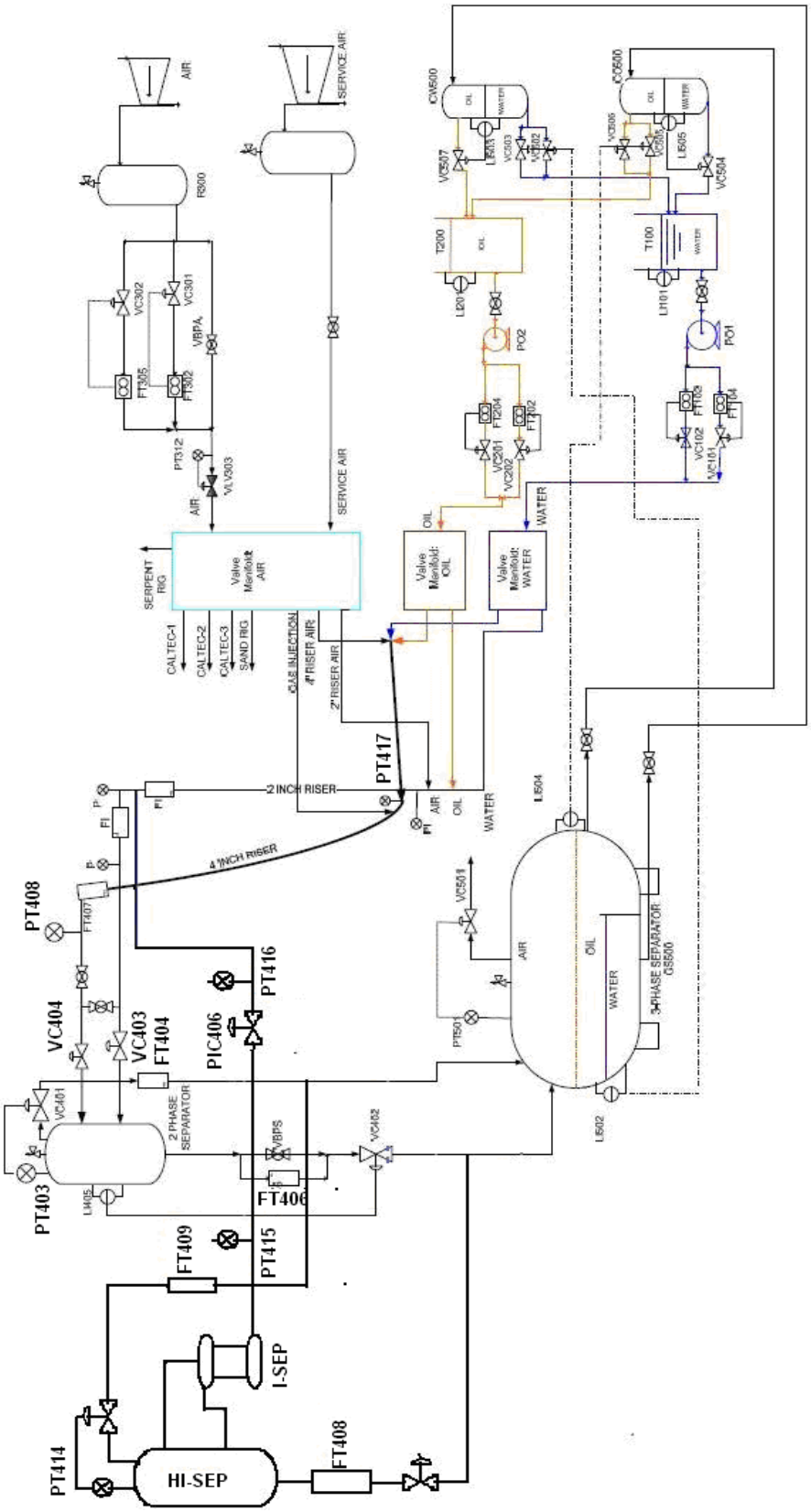

Figure 5.1 I-SEP used installed on Cranfield three phase facility

5.4 Multiphase Flow Test Facility

Cranfield University has a state of art fully automated high pressure multiphase flow test facility, which is being used for flow assurance, multiphase metering and control system research. A latest Field bus based supervisory, control and data acquisition (SCADA) software named as DeltaV by Emerson Process Management is in operation to control this facility. This facility is designed for maximum operating pressure of 20 barg with air, water and oil as testing fluids. This facility as shown in the Figure 5.1 can be divided into fluid supply and metering section, testing and fluid separation section.

5.4.1 Fluid Supply Section

Air is supplied from bank of two compressors connected in parallel capable of producing maximum air flow rate of 2550 m^3/hr FAD @ 7 barg. This air is then passed to a receiver to reduce the compressor loading and unloading cycle pulsations. Two controlled valve named as and VC301 are used to pass the air either in the ½-inch (0 – 100 Sm^3/h) or 1-inch (95 – 1275 Sm^3/h) respectively.

5.4.2 Water and Oil Supply

Water is supplied from a 12,500 litres capacity water tank, and oil is supplied from a bunded oil tank of similar capacity. The water and oil are supplied into the flow loop by two multistage Grundfos CR90-5 pumps remotely controlled by DeltaV. There are two water supply pipelines, the low flow rate line is capable of producing the water flow rate 0-1 kg/s controlled by VC102 on 1-inch line, whereas the higher flow rate line having flow rate greater than 1 kg/s is controlled by VC101 in a 1-inch line. The water flow rate is metered by a 1" Rosemount 8742 Magnetic flow meter (up to 1 kg/s) and 3" Foxboro CFT50 Coriolis meter (up to 10 kg/s) while the oil flow rate is metered by a 1" Micro Motion Mass flow meter (up to 1 kg/s) and 3" Foxboro CFT50 Coriolis meter (up to 10 kg/s). The air is metered by a bank of two Rosemount Mass Probar flow meters of ½" and 1" diameter respectively. The smaller air flow meter measures the lower air flow rate (up to 120Sm^3/hr) while the larger one meter's the higher air flow rate up to 4250Sm^3/hr.

5.4.3 Test Section

I-SEP HI-SEP combination was incorporated to 2“flow loop of the test section of the Cranfield multiphase test facility.

The 2” loop is a 55 m long horizontal pipeline connected to a 10.5 m long vertical riser which is connected to a 1.2m high and 0.5m of diameter vertical two-phase separator here after will be referred as LAB Separator. Water was introduced into the system through the long horizontal pipe whereas air was supplied at the base of the riser. Liquid level and separator pressure is controlled by DeltaV system using pressure and liquid level controller PIC401 and LIC402 respectively. The air from the vertical two-phase separator is metered by a 1” Rosemount Vortex flow meter while the water mixture is metered by a 2” Micro Motion Mass flow meter. The riser outlet valves VC403 for the 2” loop that connect riser to the vertical separator was used to throttle riser outlet to make the flow stable during instability. Pressure transducers were installed at the top and base of the riser which were used to measure the liquid level inside the riser. An additional line was joined into the two phase loop so that the riser was linked with the I-SEP and HI-SEP combination via control valve PIC406 as shown in Figure 5.1. This valve is also used as throttling valve to change the flow regime inside the riser during the severe slugging. Like the vertical separator the HI-SEP has liquid level and pressure controller to control separator pressure and liquid level inside the separator. FT409 and FT408 were used to measure the liquid and gas flow rate coming out from the HI-SEP. The air and water from the two phase separator or from HI-SEP are then transported back to three phase separator, where after further cleaning air is exhausted into the atmosphere and water from the three-phase separator enter to its coalescers for further filtering before returning to storage tanks.

5.4.4 Data Acquisition System

All instrumentation in the multiphase flow test facility is interfaced with the DeltaV system which was configured to record instrument output values at a rate of 1 Hz. Historical data could be downloaded from the DeltaV cache after experimental work for reference purposes.

5.5 Experiment Methodology

Experiments were conducted to investigate the behaviour of I-SEP/HI-SEP for low flow rate of liquid and gas flowing capable of producing severe slugging in two inch inclined pipe ending up with 10 m high vertical riser. Low flow rates of air and water were used with water flow rate varied from 0.5 kg/s to 2 kg/s with an interval of 0.25 kg/s and for each of these water flow rate the air was then varied from 6 to 20 Sm^3/hr with an interval of 2.5Sm^3/hr. This matrix was used to observe the severe slugging using Lab separator as top separator and I-SEP & HI-SEP combination by fully opening their respective valves while keeping the other one fully closed.

5.6 Severe Slugging Flow Map

The DP signal over the riser base was used to identify the severe slugging for all the performed experiments. A value of one bar for the DP signal means the riser is full of the liquid level before the gas blow down phase and hence could be used to indicate the presence of severe slugging in the pipe. Severe slugging was observed in both cases i.e. with both Lab separator and I-SEP used at the top of the riser separately. The observed severe slugging (SS) and non severe slugging (NSS) i.e. stable flow was identified through the DP signal over the riser base and is shown in the Figure 5.2a and 5.2b for both the separator. The gas and liquid superficial velocities that caused to produced the severe slugging were plotted which produced a flow regime map of severe slugging for both separators i.e. LAB separator and I-SEP as shown in the Figure 5.3a and Figure 5.3b respectively.

A comparison of these two flow regime revealed that I-SEP is more effective in maintaining the stability of the flow inside the pipe as severe slugging boundary for I-SEP was found to be shifted more towards less gas and liquid superficial velocity as compared to the LAB separator.

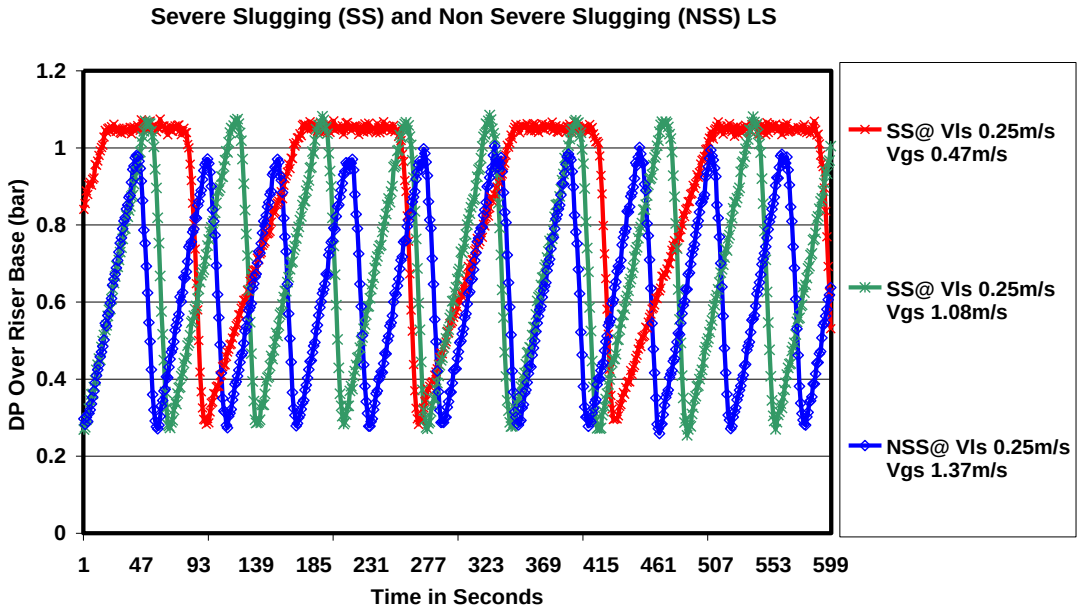

Figure 5.1a Severe Slugging boundary on 10 m high vertical riser for LAB Separator

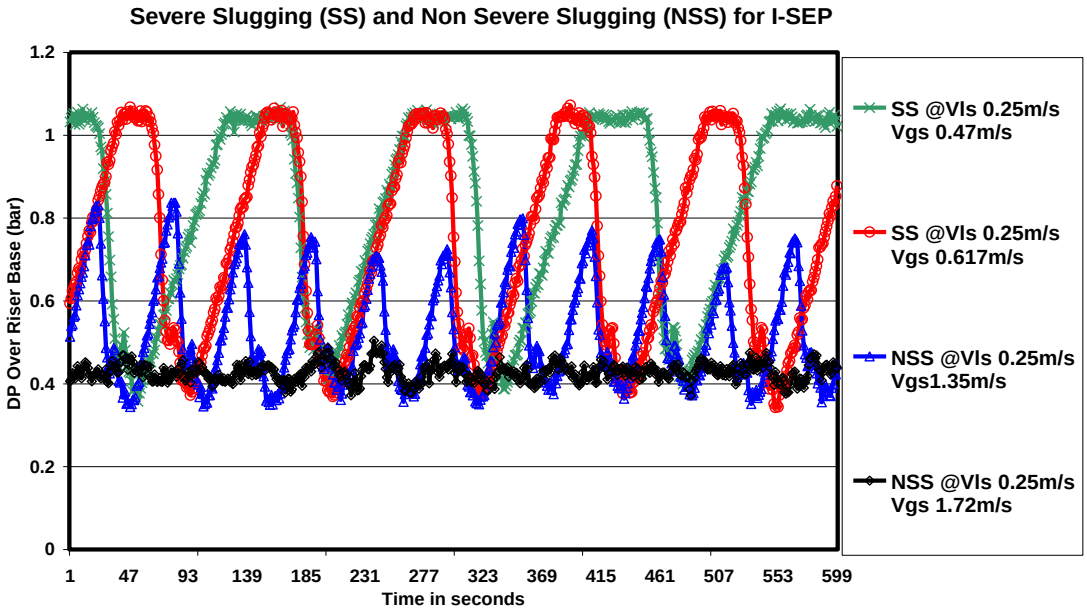

Figure 5.2b Severe Slugging boundary with I-SEP used at Top of Riser

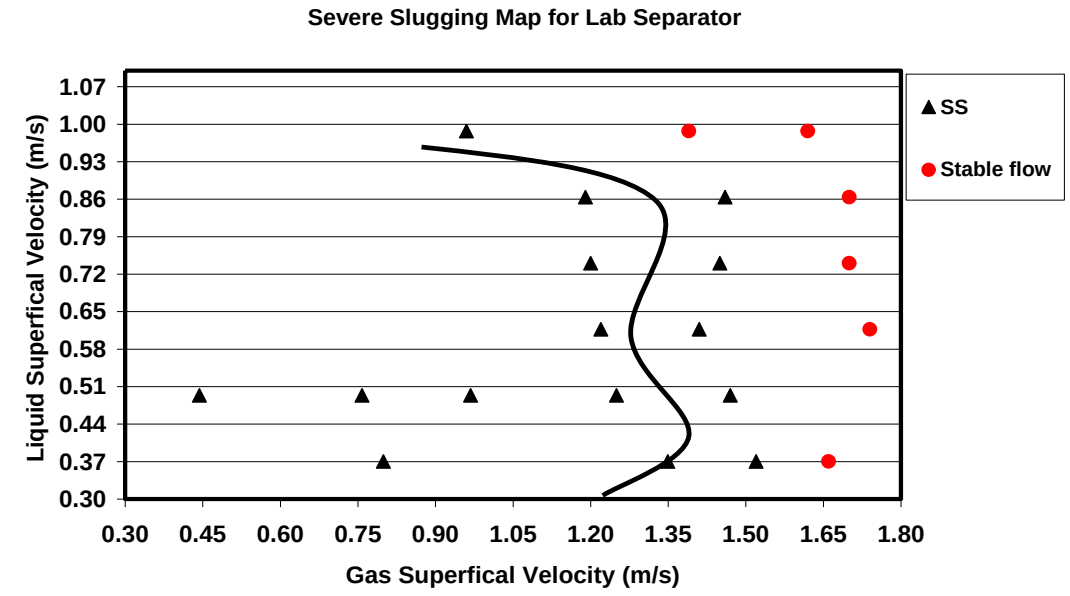

Figure 5.2a Severe Slugging Flow Regime Map for Lab Separator.

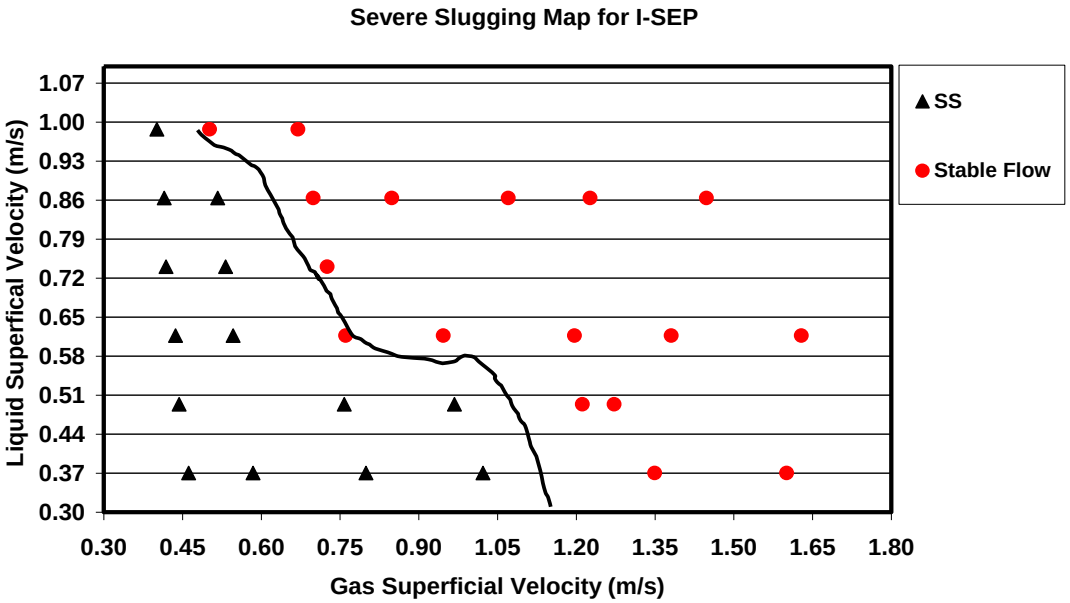

Figure 5.3b Severe Slugging Flow Regime Map for I-SEP.

For example severe slugging was not observed for gas superficial velocity greater than 1.35m/s at fixed liquid superficial velocity of 0.37m/s when I-SEP was used at

the top of the riser but the same point was found to lie in the severe slugging region for LAB separator where for liquid superficial of 0.37m/s severe slugging was observed until gas superficial velocity reaches 1.60m/s. This means I-SEP was able to avoid the severe slugging at relatively lower gas and liquid superficial velocity as compare to the LAB separator and thus can be used to mitigate the produced slug even without the use of any choking. These results are very promising and demonstrate that I-SEP can be used favourably to design the slug control system for producing maximum oil production.

5.7 Comparison of Severe Slugging Cycle

The severe slugging cycle observed for the I-SEP and LAB separator under the same flow condition having gas superficial velocity 0.47m/s and liquid superficial velocity of 0.25 m/s are compared using the pressure difference signal over the riser in Figure 5.4 The line A, B, C and D in red and blue colour are used to mark the liquid accumulation, liquid production, bubble penetration and gas blow down stage of the severe slugging cycle for I-SEP and LAB separator respectively. It can be seen due to longer liquid formation time observed for the LAB separator about 100 seconds as compared to 60 second for I-SEP, it takes more time to fill the riser fully before the maximum pressure is reached at the riser base, indicating that slug size would be greater for the LAB separator. The next stage i.e. liquid production stage was also observed to last longer for LAB separator which means that in LAB separator case, it took longer by the compressed gas at the riser base to overcome the liquid hydrostatic head to push the liquid into the separator. This is due to the longer slug formed hence more gas is needed to push out of blocked base area. A slight drop in the pressure difference can be noted in both case which indicates the start of bubble penetration and acceleration of gas into the riser to start the gas blow down followed by the last stage of liquid fall back. However the liquid fall back in the I-SEP is characterised by two small peaks which was not found in the liquid fall back of the lab separator. The another important thing to note is that the minimum pressure difference over riser after the liquid fall back stage is higher in I-SEP case, which mean that there is more liquid fall back left in the riser when I-SEP was used on the top of the riser which

explains the shorter liquid accumulation time for the I-SEP. This means the compressed gas in the I-SEP case did not hold much energy to fully empty the riser. This less energy could be because of the fact that the liquid accumulation time was found shorter than that for LAB separator. The two peaks during the liquid fall back in I-SEP may be thought to indicate a temporary blockage or liquid accumulation which was soon over come and probably due to this some energy was lost by the gas and it was not able to empty the riser fully.

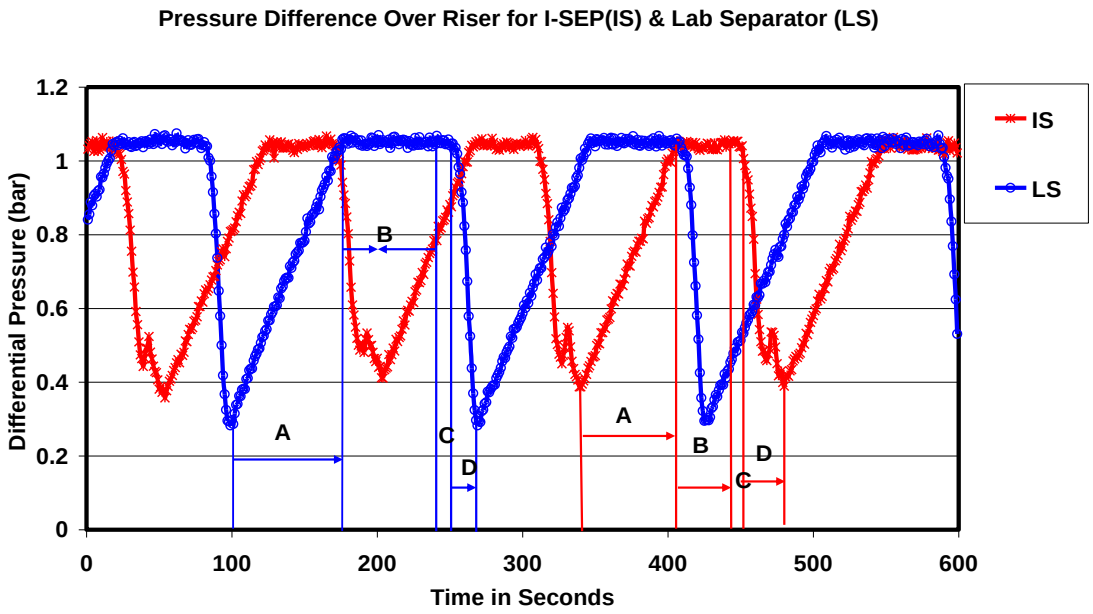

Figure 5.3 Pressure Difference over Riser Base for both Separators.

The severe slugging cycle for increasing gas and liquid superficial velocity is shown in the Figure 5.5, it can be seen from the figure that as discussed above the time for liquid accumulation and production in I-SEP was always found less than that of LAB separator and the minimum DP value in the liquid fall back stage was always found greater than that of LAB separator with two or multiple peaks. One another interesting feature is that the liquid production time was found to be reduced with the increase in the gas superficial velocity for both the separator which mean as gas superficial velocity is increased then the compressed gas at the riser base overcome the riser hydrostatic pressure more rapidly to push the liquid from riser to the separator.

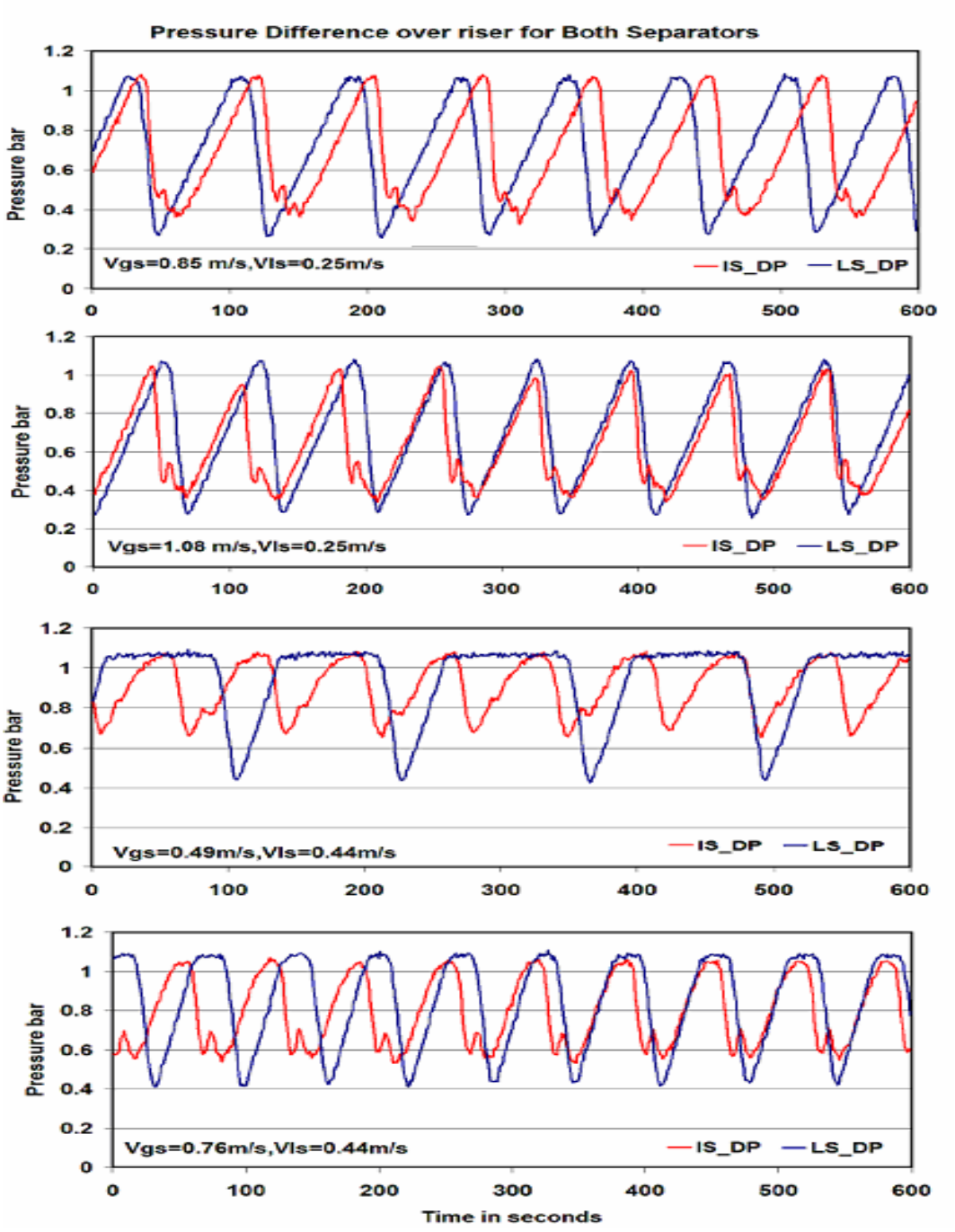

Figure 5.4 DP over Riser Base for Higher Gas Flow Rate.

5.8 I-Sep Effect on Severe Slugging

This section defines the time sequence of the event as appeared during the severe slugging process when the I-SEP was used as a separator on the top of the riser. One set of data point consisting of liquid superficial velocity of 0.25m/s and gas superficial velocity of 0.47 m/s (corresponding to water 0.5kg/s and gas 6Sm^3/hr) is chosen here from the whole experimental data matrix to define this process, the other data points were observed to behave the same during the severe slugging. The time diagram of 10 minutes (600 seconds) is shown in the Figure 5.6. It can be seen from the Figure that water flow rate has been almost constant while air flow rate has shown minor fluctuation.

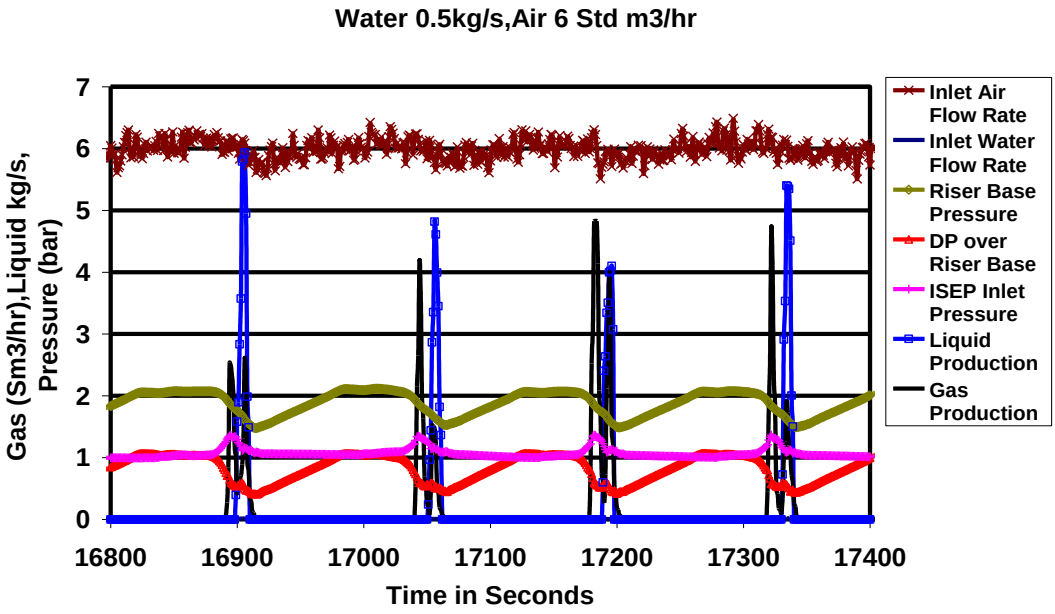

Figure 5.5 Severe Slugging with I-SEP.

The riser base pressure is following the trend in differential pressure (DP) over riser. The rise in DP or riser base pressure indicated the start of the severe slugging cycle with liquid accumulation stage. This rise time as can be seen in the Figure 5.6 is about 65 to 70 seconds followed by about 50 seconds of constant value of DP of 1 bar indicating that riser is full of water and slug formation stage is started. It is then followed by bubble penetration and gas blow down indicated by dip in the riser base

pressure or DP signal along with the gas coming out from riser as a result of which both the riser base pressure and the DP is started decreasing reaching to their minimum value at which point the liquid is started coming out from the riser and falling into separator. However multiple peaks can be seen in the gas flow rate indicating that gas flow rate at riser outlet is not smooth and it is coming in sequence of small packets. This short duration of gas production through the I-SEP has caused to increase a little rise at the inlet pressure of the I-SEP which is found to be increasing during the gas blow down and then start decreasing during the liquid accumulation phase then almost becomes constant until the gas blow down is occurred again. it can be seen that during the gas blow down period the gas is exited first from the riser followed by liquid for very short time of about 30 second after which the liquid accumulation process is started again. The minimum DP value observed during the gas blow down is about 0.6 bar which means that the riser is not fully empty during the gas blow down period.

This time sequence of event was observed repeated when the gas flow rate was increased from 6 to 7.5Sm^3/hr as shown in the Figure 5.7, however with a slight difference now the gas production at the I-SEP is found to be higher than gas production observed the last test. In the last test the average gas production was recorded as 0.21 Sm^3/hr but now it is about 0.62 Sm^3/hr whereas the average liquid production rate is increased from 0.2 kg/s to 0.23 kg/s. One observation can also be made here and it is that as the gas flow rate at inlet is increased then the rise time in the DP signal pressure is get lowered from 70 to about 60 seconds indicating a reduced in the slug length due to increase in gas superficial velocity. This trend continues with air flow rate of 10 Sm^3/hr with multiple small peaks of small duration observed in gas flow rate at the I-SEP. One can draw the conclusion that as the gas flow rate is increases with I-SEP using as a separator on the riser, the gas tends to exits from the riser in packets which cause to break the slug and stop severe slugging this behaviour can also be observed due to the short rise time in the riser base pressure and the DP signal.

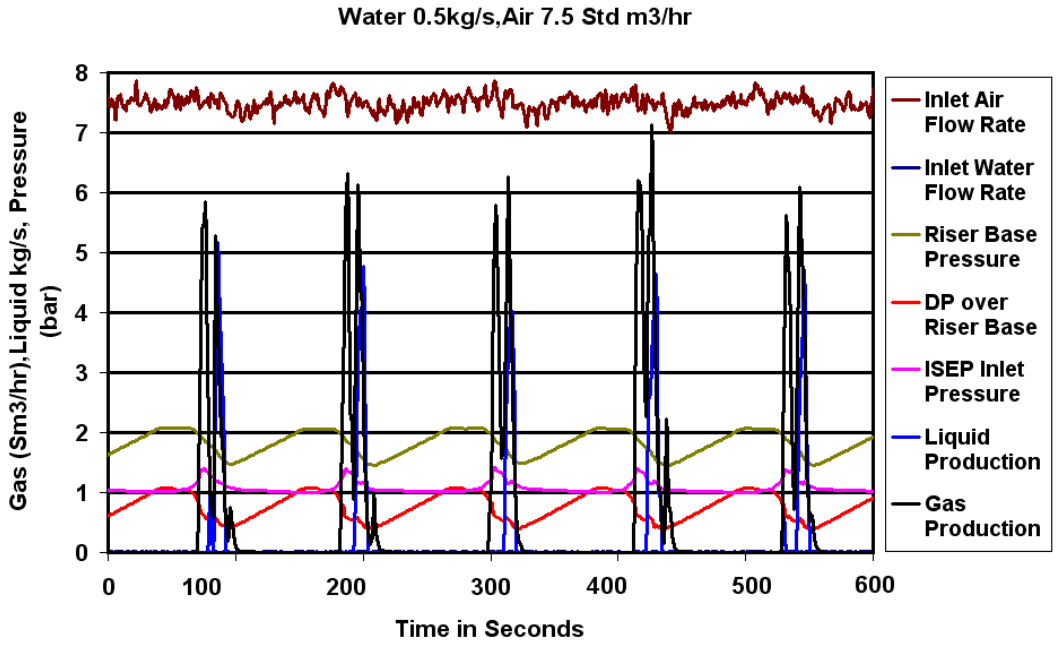

Figure 5.6 Severe Slugging cycle for Higher Gas Flow rate.

5.8.1 Effect of Gas and Liquid Superficial Velocity on Severe Slugging

The stability curve in the observed severe slugging flow regime map (Figure 5.3b) is shifted more toward lower gas superficial velocities on increasing the liquid superficial velocity , where as for this phenomenon was not observed for the LAB separator case. This mean ability of I-SEP in maintaining the stability of the flow increases with increase in liquid superficial velocity and decreases with gas volume fraction of the flow which is not visible for LAB separator in the flow regime map. It can be also seen from the Table 5.1 and flow regime map for both the separator that at fixed liquid superficial velocity, on increasing the gas superficial velocity both the separators showed the tendency to move from instability region to stable region as then the severe slugging seems to be disappeared. However I-SEP exhibited this trend with at lower gas superficial velocity than LAB separator. For example at for liquid superficial velocity of 0.25 m/s I-SEP was able to produce the stable region at gas superficial velocity 1.37m/s while lab separator was still unable to eliminate sever until the gas superficial velocity was 1.72 m/s as can seen from the flow regime map

Figure 5.3a and Figure 5.3b. This trend is persistent for other experimental data points as can be seen from the Table 5.1.

5.8.2 Riser Base Pressure Comparison

Riser base pressure has been defined by many researchers as one of the basic parameter to investigate the severe slugging. A higher valued and more fluctuated riser base pressure witnesses the instability of the flow inside the pipe and thus was used by many researchers to define the process of severe slugging. A comparison of riser base pressure for both the separators is presented in the Table 5.1. This comparison revealed that riser base pressure was always more stable whenever I-SEP was used as a separator on the top of the riser as can be seen from the lower standard deviation values of riser base pressure observed for the I-SEP during the experiments.

These experiments showed that average rise base pressure could be less than for I-SEP during severe slugging condition, as at least one time for all the severe condition the I-SEP showed a low riser base pressure about 0.26% less than that of for LAB separator for the liquid and gas superficial velocity of 0.25 and 0.47m/s. However this trend did not repeated for other values of liquid and gas superficial velocity. The riser base pressure for I-SEP during stable flow or non server slugging case was also found lower than that for LAB separator at lower liquid superficial velocity. The reduction in riser base pressure was found to between 1 to 6% for lower liquid superficial velocity of 0.25 and 0.37 m/s as can be seen in Table 5-1. But this trend changed at higher liquid superficial velocity when I-SEP riser base pressure has found greater than that of lab separator case even in stable flow.

5.8.3 Minimum Riser base Pressure

The other interesting parameter is the increase in minimum riser base pressure which was always found higher for I-SEP and decreased with the gas superficial velocity as shown in the Figure 5.8 The relatively high minimum value of riser base pressure indicates that there would be less gas blow down with I-SEP as compared to the Lab separator and it is found to increase with the increase in gas superficial velocity as can be seen from the Figure 5.8. The high minimum DP value could also be taken as

indication of the high liquid level left in the riser after the gas blow down when I-SEP was used as main separator.

Table 5-1 The average Rise base pressure comparison for both separators.

V_{gs} m/s	V_{ls} m/s	Status		Mean RBP barg			RBP_SD		Minimum DP bar		
		CS	LS	CS	LS	diff (%)	CS	LS	CS	LS	diff%
0.47	0.25	SS	SS	1.88	1.89	0.26	0.20	0.24	0.36	0.28	26.59
0.84	0.25	SS	SS	1.77	1.74	-1.67	0.20	0.25	0.33	0.26	26.09
1.08	0.25	SS	SS	1.72	1.71	-0.68	0.19	0.24	0.34	0.25	33.01
1.37	0.25	NSS	SS	1.62	1.65	1.81	0.12	0.22	0.34	0.26	33.00
0.80	0.37	SS	SS	1.86	1.82	-2.38	0.04	0.24	0.40	0.33	20.32
1.35	0.37	NSS	SS	1.65	1.76	6.10	0.03	0.24	0.49	0.31	55.80
1.60	0.37	NSS	SS	1.62	1.70	4.43	0.02	0.02	0.46	0.33	38.29
0.44	0.49	SS	SS	1.99	1.98	-0.99	0.10	0.19	0.65	0.43	53.24
0.76	0.49	SS	SS	1.94	1.88	-3.61	0.16	0.23	0.53	0.41	30.19
1.27	0.49	NSS	SS	1.76	1.79	1.65	0.03	0.22	0.59	0.40	46.79
1.20	0.62	NSS	SS	1.87	1.81	-2.85	0.05	0.02	0.65	0.43	51.11
1.38	0.62	NSS	SS	1.83	1.78	-3.20	0.03	0.02	0.62	0.42	48.85
1.63	0.62	NSS	NSS	1.83	1.70	-7.62	0.04	0.02	0.59	0.44	32.49
1.07	0.86	NSS	SS	2.08	1.87	-11.30	0.07	0.05	0.77	0.58	32.96
1.23	0.86	NSS	SS	2.06	1.77	-16.02	0.08	0.05	0.74	0.63	16.74
1.45	0.86	NSS	NSS	2.05	1.74	-17.79	0.07	0.02	0.70	0.68	3.39

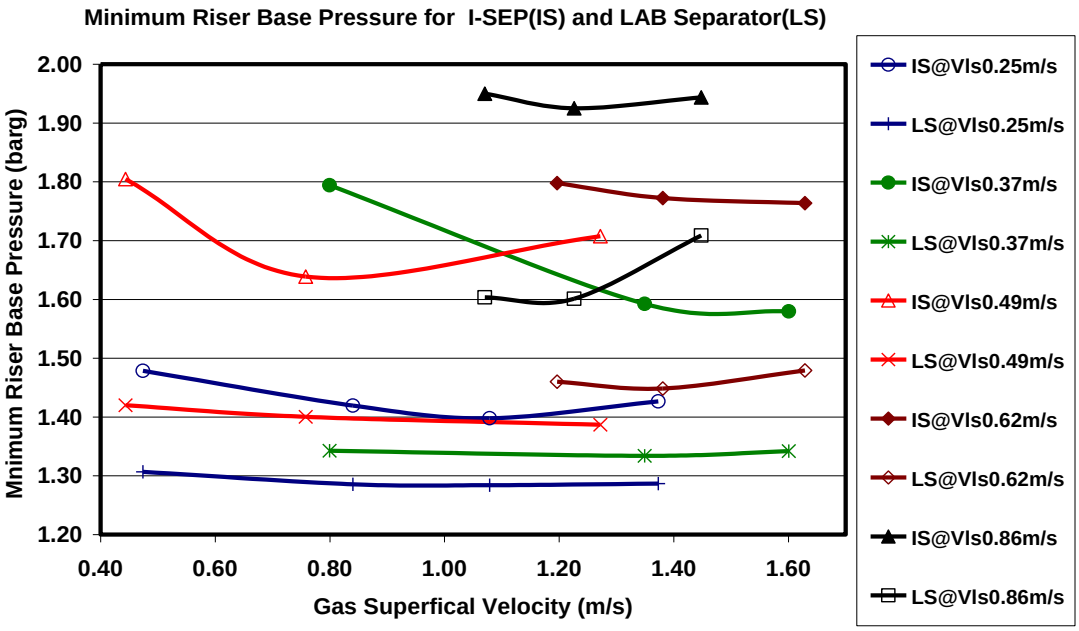

Figure 5.7 Minimum Riser base Pressure for two separators.

5.8.4 Gas Hold-up Comparison using DP Value

Figure 5.9 compares the average value of the DP observed for the same flow condition for both lab separator and I-SEP, it shows that due to lesser value of DP for I-SEP as compared to lab separator there is less liquid hold up and greater gas hold up for I-SEP, which means severe slugging for same the flow condition would not be as severe as for lab separator due to less liquid hold up inside the riser when I-SEP is used as the separator on the top of the riser. The intensity of severe slugging in both separators would be less intense due to low value of DP on in increasing the gas superficial velocity. On the other hand the liquid superficial has a direct effect on the liquid hold up which means the strength of severe slugging would be increase with the increase in liquid flow rate at same gas flow rate for both the separator.

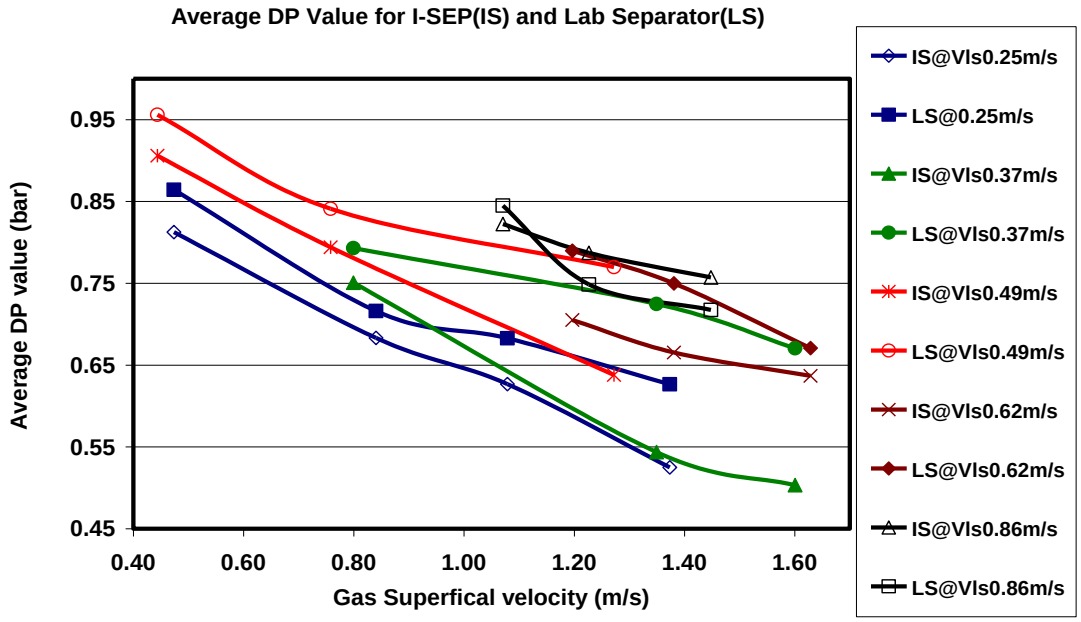

Figure 5.8 Average Pressure Difference over riser for both the separators.

5.9 Comparison of Estimated Slug Frequency and Slug Length

The periodicity of the severe slugging cycle was then further investigated by calculating the power spectrum density (PSD) of the pressure difference signal over riser. PSD is a frequency domain tool used to relate the energy in the variation of the time series signal as function of a function of frequency. The dimension of the PSD is given by power per Hertz. This means that in this case unit of the amplitude of the PSD would be bar^2 / Hz .Since the pressure difference over the riser was used to represent the height of the liquid level inside the riser this mean the amplitude of the PSD could be used to estimate the liquid length or slug length inside the riser. The frequency corresponding to the maximum amplitude may be taken as an approximate to the slug frequency.

Following this approach PSD of all the test points which produced the severe slugging (for both the separator) were calculated using the time series signal of the pressure difference over the riser. The mean value of the time series signal was subtracted from the actual time series signal in order to use only the fluctuation of the

time series signal. The recorded data was of limited range up to 10 minutes sampled at a frequency of 1 Hz, this short range of data may distort the information inside the signal, therefore in order to diminish this effect a modified periodogram method defined by Welch commonly called Welch method was used to calculate the power spectrum density of the signal. MATLAB tool box was used to estimate the PSD using hamming window of 256 data points. A Single dominant peak was observed for every test point in both the cases. The maximum frequency increases and its amplitude decreases with the gas superficial velocity as shown in Figure 5.10. Comparing the maximum slug frequency and slug length for the identical data point for both separators presented in Table 5-2 it can be seen that maximum slug frequency inside the riser with the Lab separator on the top became higher than that for I-SEP on increasing the gas superficial velocity at the same liquid superficial velocity. The estimated slug length on the other hand was also found always greater for LAB separator as can be seem from Table 5-2. This means that under the same flow condition the I-SEP has tendency to produce relatively shorter slug than the LAB separator .It can further be noted from the Table that the percentage difference in slug length in the two separator increases with the increase in gas superficial velocity at lower liquid superficial velocity but found decreased with the increased in gas superficial velocity at high liquid superficial velocity.

5.10 Liquid and Gas Production Comparison

Like any other severe slugging process the severe slugging process observed using these two separators produced spikes of liquid and gas production of varying amplitude during the gas blow down stage as shown in Figure 5.11 . It is interesting to note that time period of both gas and liquid spikes observed during the gas blow down phase is reduced with the increase in the gas superficial velocity at constant liquid superficial velocity. Thus for example the liquid production was observed four times in ten minutes at the liquid and gas superficial velocity of 0.25 and 0.49 m/s respectively but when the gas superficial velocity was increased to 1.08 m/s then liquid production was observed at about eight times in 10 minutes indicating an increasing in the frequency which is further confirmed by their PSD presented in the Figure5.12 and 5.13 respectively.

Table 5-2 Slug Frequency and Slug length comparison for both Separators.

V_{ls} m/s	V_{gs} m/s	Max Slug Frequency Hz		Estimated slug Length m		% diff in slug length
		LS	IS	LS	IS	
0.25	0.47	0.006	0.007	9.61	8.89	7.54
0.25	0.85	0.013	0.012	10.07	8.74	13.25
0.25	1.08	0.015	0.014	8.20	6.63	19.15
0.49	0.45	0.008	0.015	9.21	2.80	69.63
0.49	0.79	0.016	0.015	8.90	5.41	39.27

The PSD of both the gas and liquid production showed multiple peaks at the same liquid and gas superficial velocity and both amplitude and frequency has found to increase with the gas superficial velocity at constant liquid superficial velocity. However at higher liquid superficial velocity greater than 0.49 m/s the maximum liquid production frequency was found to be decreasing with the increasing gas superficial velocity. This phenomenon differed slightly when Lab separator was used on the top of the riser as the liquid production frequency was always found increasing with the increase in gas at constant liquid superficial velocity.

A comparison under same flow condition during severe slugging for both I-SEP and LAB separator presented in the Figure 5.14 showed that lab separator has slightly higher maximum frequency of production for both liquid and gas than I-SEP for same flow condition, which means I-SEP could be a bit more effective as compared to the Lab separator due to less number of liquid and gas production cycle during severe slugging. However increasing production frequency any way demands a robust liquid level control for the safety operation. The reduction in the time period of the gas and

liquid production indicate that as the liquid and gas superficial velocities are increased than the compressed gas at the riser base has got enough energy to overcome pressure build up due to liquid level in the riser and take less time to push the liquid slug from riser to the separator.

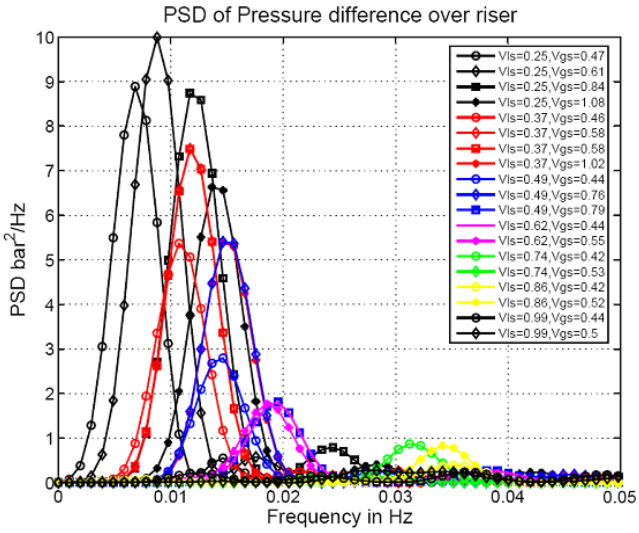

(a)

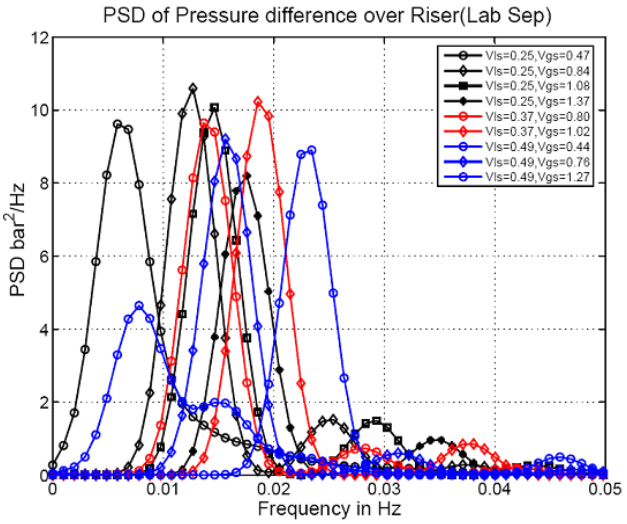

(b)

Figure 5.9 PSD of DP for Both Separator.

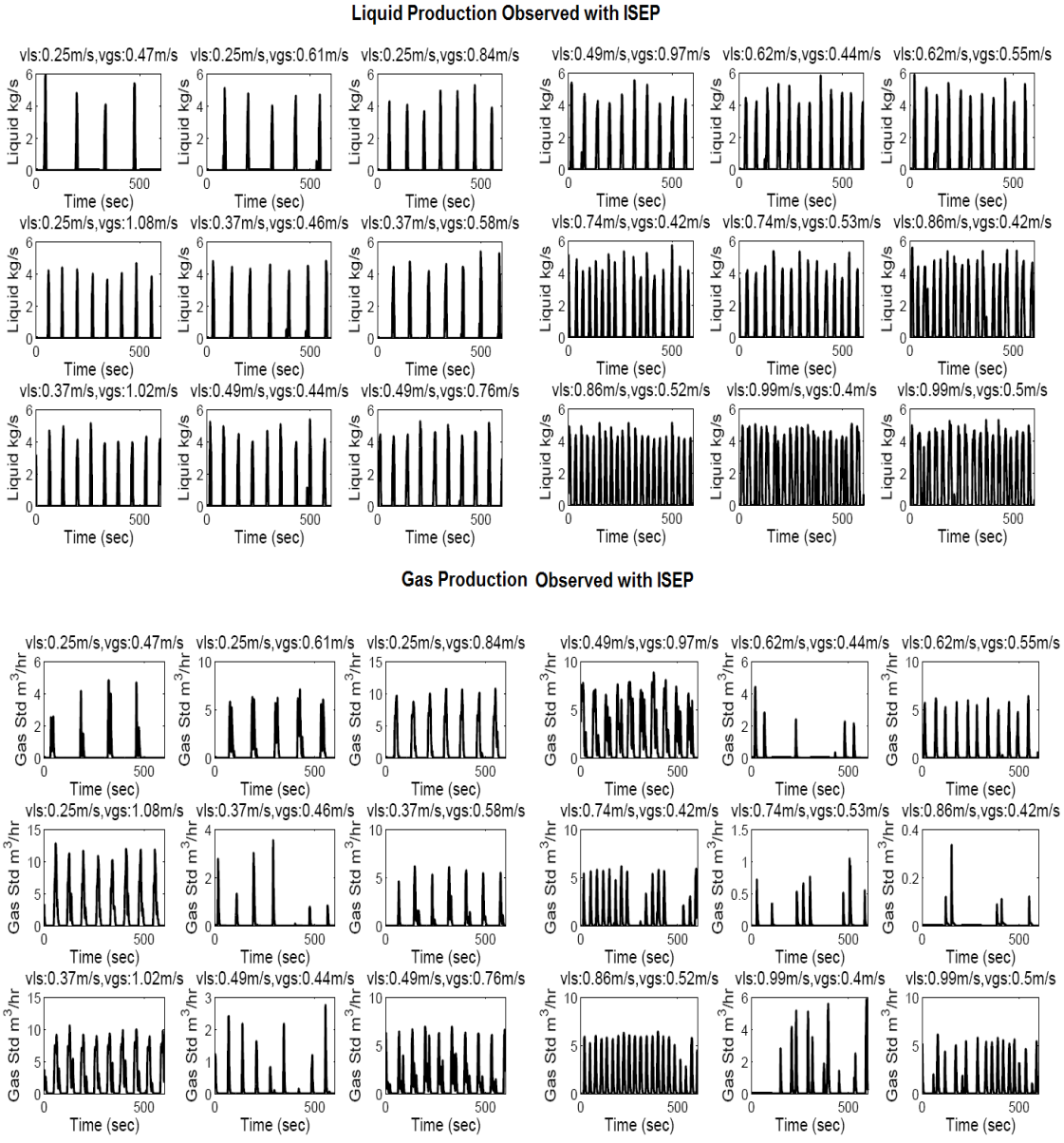

Figure 5.10 Spikes of liquid and Gas Production observed during SS (with I-SEP).

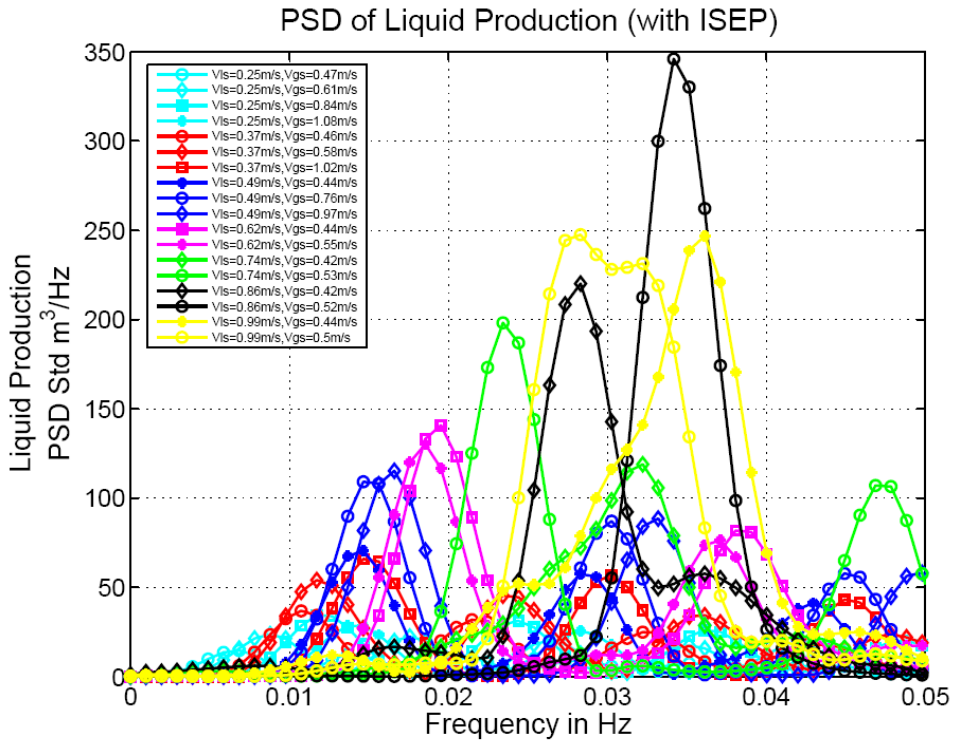

Figure 5.11 Power Spectrum density of Liquid Production (I-SEP

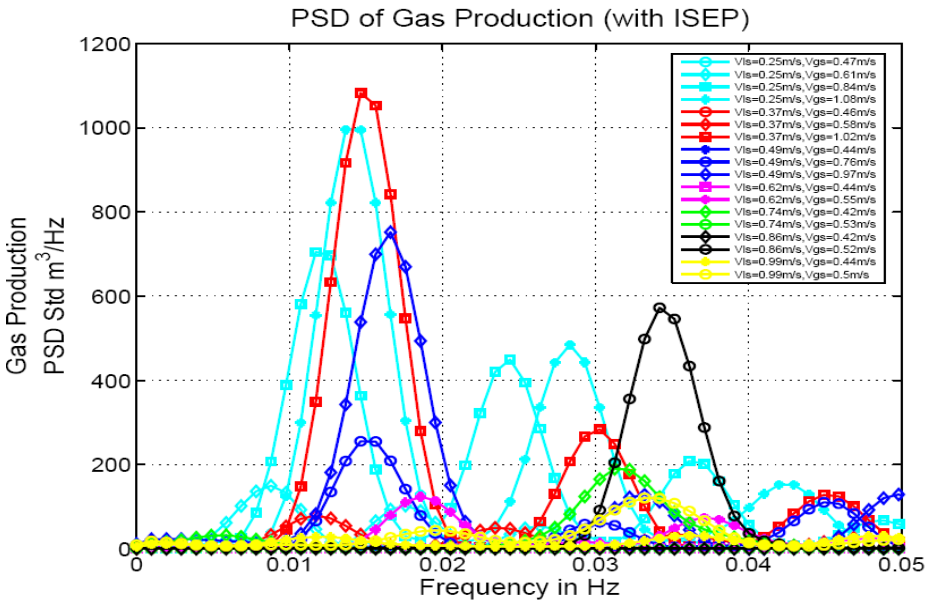

Figure 5.12 Power Spectrum Density of Gas production (I-SEP).

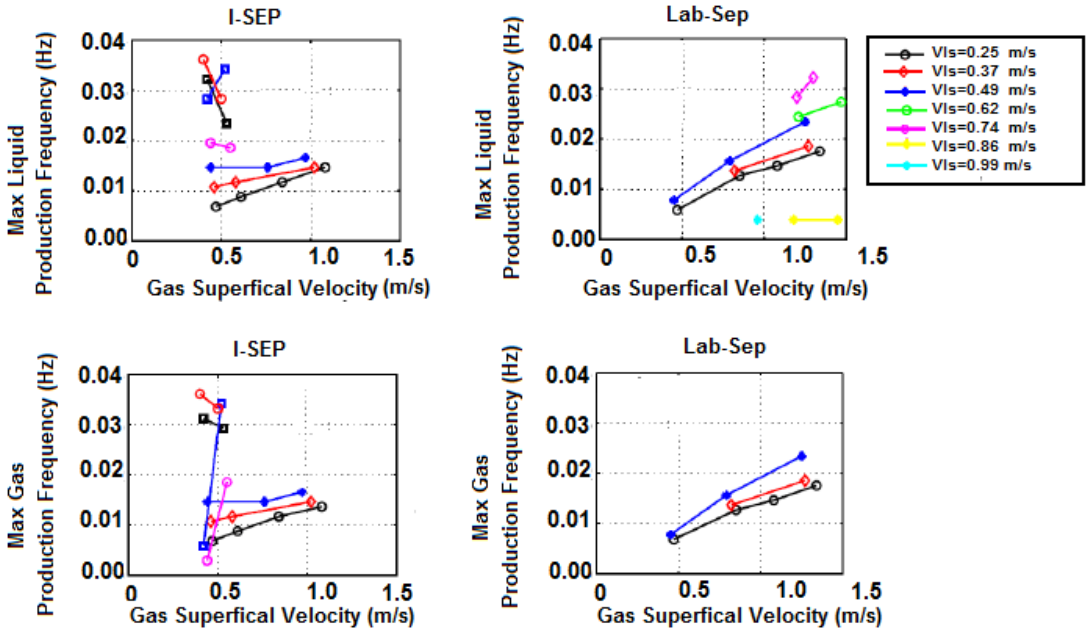

Figure 5.13 Comparison of Gas and Liquid Production frequency for I-SEP & Lab Separator

5.11 Comparison of fluctuation in Gas and Liquid Production

The fluctuation in liquid and gas during the severe slugging may reduce the production if they are increased to much by actually stopping the separator due to overflow of liquid, it is therefore worthwhile to investigate the fluctuation in the gas and production during the gas blow down stage of the severe slugging under two used separators.

The fluctuation in the gas production was recorded more than that of liquid production as can be seen from the Figure 5.15 and was found increased with the increased of both liquid and gas superficial velocity. However at higher liquid superficial velocity of more than 0.5 m/s the liquid and gas production showed more stability.

For example the fluctuation in liquid production decreased from 1.5 to 1.4 at liquid superficial velocity of 0.74m/s with the increased in gas superficial velocity, same trend can be seen in the

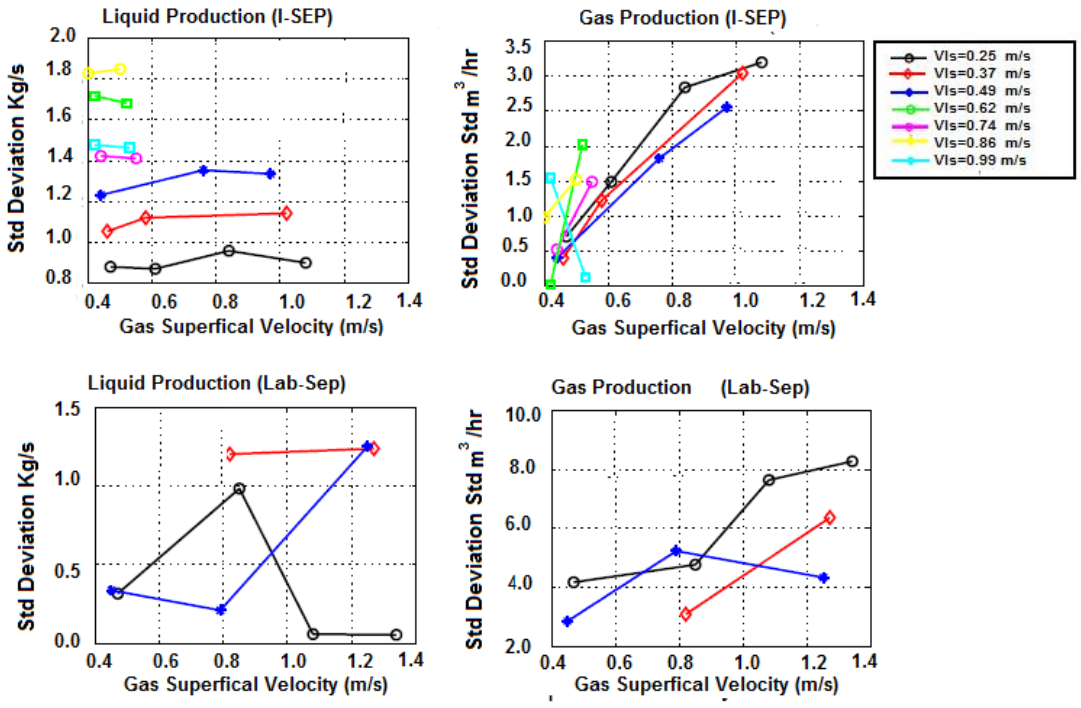

Figure 5.14 Comparison in the fluctuation of Gas and liquid Production

Figure 5.15 for the gas production. The comparison of the standard deviation for the gas production under the same flow condition for the two separators during severe slugging presented in the Figure 5.15 revealed that the gas exits from the riser was more fluctuated for Lab separator as compared to I-SEP, for example at liquid superficial velocity of 0.25 m/s and gas superficial velocity of 0.47m/s the standard deviation value or fluctuation recorded for the gas production in I-SEP was 0.6 Sm^3/hr but it was found 4Sm^3/hr for the Lab separator case and this trend is continued with the other value of gas superficial velocity as can be seen in the Figure 5.15. The liquid production as observed with the lab separator is not linear with the increasing gas superficial velocity as can be seen in the Figure 5-15 and also there is not much difference in liquid production for the both separator.

5.12 Comparison of Liquid Slug volume

The volume of the liquid slug that was accumulated inside the riser during the severe slugging condition was estimated by integrating the liquid production profile and then compared for both the separators. The liquid production was since measured in kg/s so the volume was calculated using the following relation ship:

$$V_{sl} = \frac{M_{sg}}{\rho_l} = \frac{1}{\rho_l}\int_{t1}^{t2} M_{sg} \qquad (5.1)$$

Where t_1 and t_2 is the start and end time of the severe slugging cycle and M_{sg} is the mass flow rate of the liquid observed during the cycle. The integration is done using the extended Simpson rule which says that a time series function can be integrated for given interval of time using the following relationship.

$$\int f(x)dx = h\left[\frac{1}{3}f_1 + \frac{4}{3}f_2 + \frac{2}{3}f_3 + \frac{4}{3}f_4 + ...\frac{2}{3}f_{n-2} + \frac{4}{3}f_{n-1} + f_n\right] \qquad (5.2)$$

The integration using this relationship was done using MATLAB. The resulting volume of the liquid in litres was then plotted for all the flow condition which produced severe slugging with I-SEP and the Lab separator and is shown in the Figure5.16. It can be seen from the Figure 5.16 while the liquid slug volume inside the riser increased with the increased in gas and liquid superficial velocity in both cases, it is lower for the I-SEP as compared to lab separator under the same flow condition of severe slugging. For example at liquid superficial velocity of 0.25 m/s with gas superficial velocity increased from 0.47m/s to 1.08 m/s the liquid slug volume inside the riser increased to from 41 litre to 55 litre and for the same value of liquid and gas superficial velocity the liquid slug volume was found to increased from 90 to 99 litre (which is to 50% to 43 more %)when lab separator was used on the top of the riser. This indicate the under same flow condition I-SEP generate a relatively less intense severe slugging than observed with Lab separator. The same technique was used to estimate the volume of the gas coming out during the blow down. The gas production also showed the same characteristic as it was also found to increase

with the increases in liquid and gas superficial velocity and was recorded more than for the I-SEP under same flow condition. However the overall volume of the gas was recorded nearly same for all lower liquid superficial velocity under 0.5 m/s.

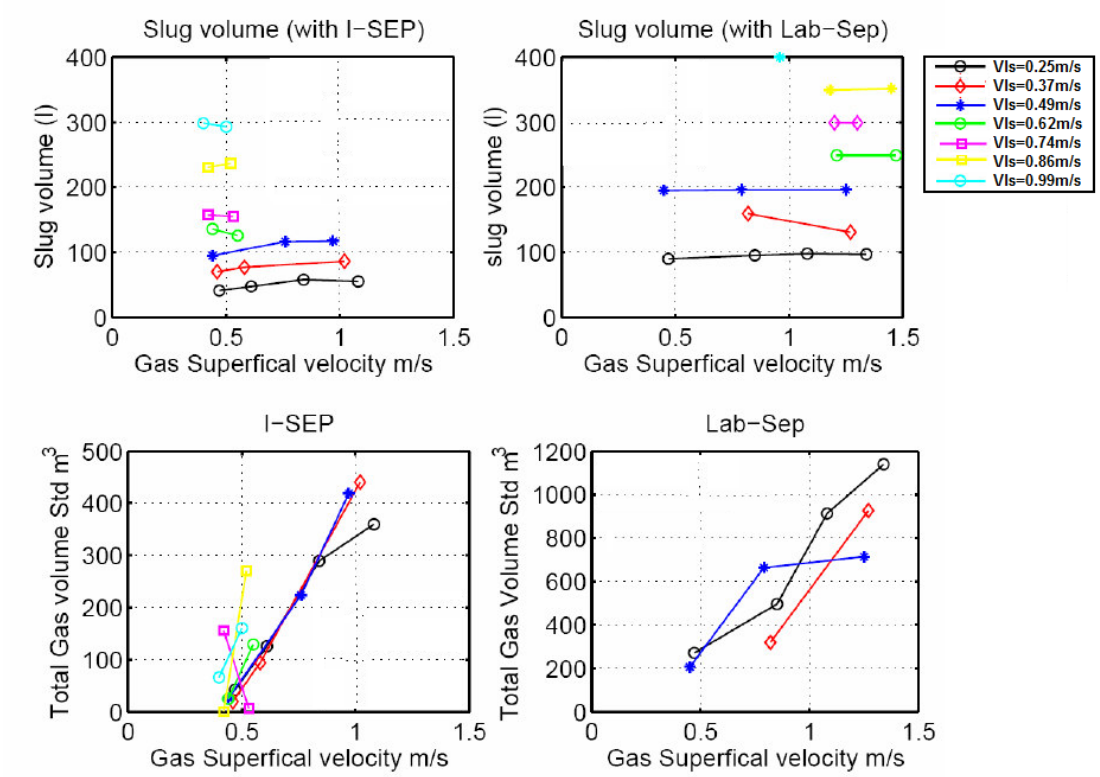

Figure 5.15 Slug Volume Comparison for two Separators

5.13 Elimination of Severe Slugging with Applied Back Pressure

Gas injection, back pressure and top side choking are the fundamental techniques used to eliminate the slugging, however the back pressure and choking produce an increase in the base line pressure and also cause to reduce the production capacity. It is one of the requirements of this technique to keep the line pressure as less possible. The experiments discussed so far had showed the I-SEP has ability to reduce the slugging, the next step was to explore the performance of I-SEP in elimination of severe slugging using the choking of the top control valve attached to separator and to compare its performance with the Lab separator during the choking. Following the

same experimental matrix as discussed above experiments were conducted in two sets, In first set of experiments Lab separator was used as main separator which means that it was fully opened in the main line and the I-SEP was fully closed when the liquid and gas was introduced into the rig, the low flow rates of water and air that produced the severe slugging were then selected form the severe slugging map. The control valve attached to Lab separator was then manipulated to eliminate the severe slugging. The pressure difference across the respective valve was also calculated to see extent of energy require suppressing the severe slugging. The pressure difference across the valve connected with the Lab separator was calculated by using the riser top pressure and lab separator pressure, whereas the pressure difference across the I-SEP was calculated using the pressure taps connected before and after the control valve with tag PT415 and PT416 respectively. These sets of experiments were repeated with I-SEP used as main separator and same steps were repeated to generate and eliminate the severe slugging.

It was observed that the riser base pressure was increased in both the cases due to applied back pressure to eliminate the severe slugging and making the flow stable. The comparison of riser base pressure for both the separators is shown in Figure 5.17. It can be seen that both the riser base pressure (RBP) and its standard deviation (SD) for I-SEP case is less than that of Lab separator. This means that I-SEP is performed better than Lab separator during the choking of the valve as the flow was more stable with less fluctuation even during the applied back pressure to eliminate the severe slugging. Thus I-SEP has got an advantage over gravity separator that it has more tendency to stable the flow as compared to the Lab separator.

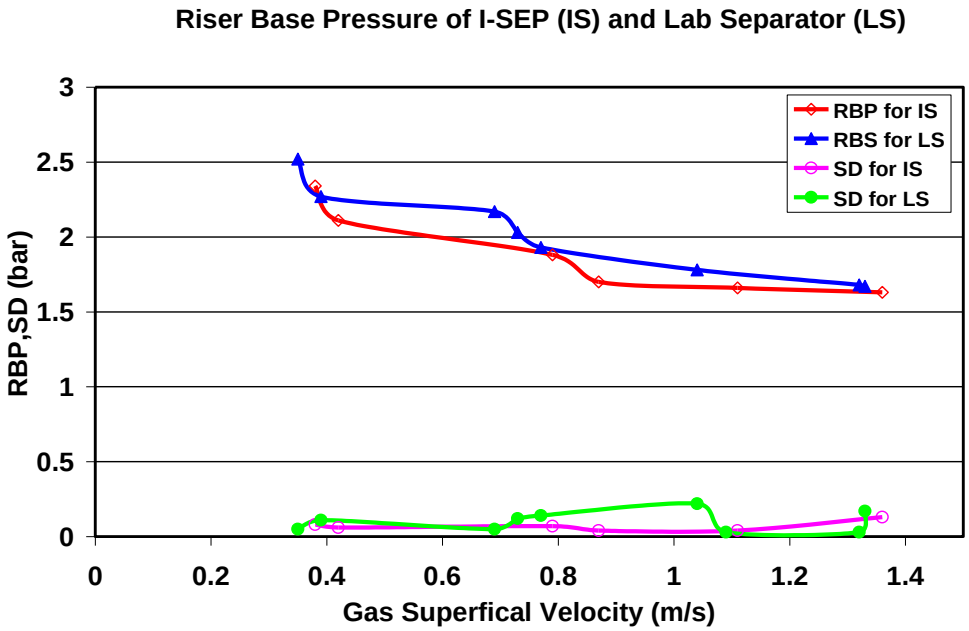

Figure 5.16 Riser base Comparison during choking for both separator

5.14 Conclusion

- It was observed during these experiments that I-SEP has better tendency to avoid the severe slugging and rise in riser base pressure is relatively low as compared to the gravity separator. The flow was found to be more stable when I-SEP was used on top of the separator due to less fluctuation as compared to the LAB separator.
- The I-SEP has tendency to avoid the severe slugging at relatively lower liquid and gas superficial velocities as compared to Lab separator.
- The minimum pressure difference over riser base was found to be higher for I-SEP indicating more liquid fall back when I-SEP was used on the top of riser. However it is decreased with the increase in gas superficial velocity indicating the intensity of the severe slugging decreased with the increase in gas superficial velocity.
- The Lab separator produced relatively longer slug with relatively high frequency than I-SEP, this mean that I-SEP would require less gas velocity to overcome the slugging and hence can be more effective slug mitigating device as compared to Lab Separator.

- Lab separator has slightly higher maximum frequency of production for both liquid and gas than I-SEP for same flow condition, which means I-SEP could be a bit more effective as compared to the Lab separator due to less number of liquid and gas production cycle during severe slugging.

Chapter 6

Modelling I- Sep Performance

6.1 Introduction

The performance of I-SEP at the varying inlet condition as discussed in chapter four was found to be very complex and nonlinear. However it was the practical requirement of its inventor CALTEC to predict its performance not only on different inlet operating condition but also for varying geometry and fluids other than gas and water. One way to achieve this objective is to repeat the experiments for every possible inlet operating condition using different fluids , which requires great time and money, the other alternative is to develop a model using the experimental results such that the model could be use to estimate the performance at different conditions. This prediction is needed because the performance of the I-SEP is dropped in the field with the change in the inlet condition and requires control of the valve attached at I-SEP tangential outlet to increase the performance. The model prediction especially the GCU and pressure prediction could be helpful in setting the value to improve the performance.

This chapter discusses the methodology used for developing the model. The main objective was to develop a realistic and easily implemented efficient method to model the performance of the I-SEP. The modelling of I-SEP performance requires predicting four parameters i.e. GCU, LCO, pressure at I-SEP tangential and axial outlet under varying inlet operating condition with or without applied pressure. However prediction of these parameters is quite difficult and complicated due to their observed complex and fuzzy relationship with the inlet operating parameters as discussed in Chapter 4. This complex mapping of the input inlet conditions to the target output can be achieved by different techniques such as fuzzy logic, artificial neural network and statistical modelling Sandhya (2007). The last two techniques were used to predict the separation performance of the I-SEP. Artificial Neural network so far has not been used in modelling the separation performance of the

separators, and it is the first attempt to develop the empirical model for a novel design compact separator I-SEP.

This chapter discusses development of the empirical model based on neural network

6.2 Requirement Specification of Model

The experimental methodology led to design two models to predict the separation efficiency both with and without applied pressure. The input and output of these models are discussed in the next section.

6.2.1 Model Output

The basic outputs of the models are GCU, LCO and pressure at the tangential and axial outlet of the I-SEP. These four outputs can then be used to further infer the required outputs such as gas and liquid separation efficiency, pressure difference between the tangential and axial outlet and ratio of pressure drop between inlet and axial outlet to that of between inlet and tangential outlet. The accuracy and performance of neural network model may be effected by the number of outputs so depending upon the modelling constrain of output parameters and the neural network accuracy the outputs of the models were group in two categories shown in Tables 6-1 and 6-2.

6.3 Feature Selection for the Neural Network Model

The model complexity and generalization ability of a neural network is directly related to the weights or free parameters that links input neurons with the hidden neurons. Additionally the selection of the appropriate inputs also depends on many

Table 6-1 Output Parameter List

Model Output without any Applied Pressure
1. GCU, LCO.
2. GCU, LCO, Pressure at tangential outlet (P_3) and at axial outlet (P_2)

Table 6-2 Output parameter list for back pressure ANN

Model Output under applied Back Pressure
1. Inlet Pressure, GCU, LCO.
2. Inlet Pressure P_{in} , Gas and Liquid flow rates at tangential and axial outlet of I-SEP

factors like their relationship with the outputs, collinearity among themselves, simplicity and cost of information. Therefore determining the most appropriate inputs to the model needs special attention in the model development. A list of the candidate variables was complied and is presented in Table 6-3 on the basis of the experiment methodology discussed in the last chapter and requirement specifications of the model discussed in the previous section.

The first seven parameters in Table 6-3 are the obvious choice for the variable selection as they defined the varying inlet conditions for the performed experiments. The statistical parameter of the inlet pressure i.e. standard deviation, kurtosis and skewness was included in this list as the separation process also depends upon flow regime and many researchers had used statistical parameter to identify the flow regime Xie et al., (2003). The definitions of these statistical parameters are given in Appendix B.

The pressure at tangential and axial outlets of I-SEP i.e. P_2 and P_3 are placed in this list for the case when the performance of the I-SEP should be predicted based on applied pressure. It was observed that the applied pressure affects the GCU as discussed in section 4.14 and this applied pressure is directly related to the pressure at tangential and axial outlet along with the inlet pressure. Therefore the pressure at tangential and axial outlet could be used to represent the strength of applied pressure as a result of throttling of the valve attached to I-SEP tangential outlet. However when performance of the I-SEP should be predicted without any applied pressure then both P_2 and P_3 would join the output parameter list.

Similarly the GCU can also be taken as input parameter for the applied pressure model. It is because when it is required to maintain the GCU during the operation of the I-SEP in the practical field then it is performed by setting the pressure difference between the tangential and axial outlet using the control valve attached to the outlet of the I-SEP. However finding the right value of pressure difference between these two outlets is not an easy process and requires operator experience and hit and trail method to achieve the right value for the required GCU %. The GCU for this situation can be thought to take as input parameter to develop an applied pressure model and therefore it placed at the last number of the candidate .input parameter list.

P_HISEP_{49} representing the pressure difference between HI-SEP inlet and its axial outlet was consider for predicting the combined efficiency of both the I-SEP and HI-SEP connected in series, however for I-SEP only case this variable will not be included in the input variable selection list.

The experiments performed in this thesis is based on air/water at atmospheric pressure, however the field condition would be different with oil and gas at high pressure. This led to include non dimensionless parameters to make the model more generalized. The first non dimensionless parameter that was chosen is the pressure coefficient or loss coefficient defined in equation 2-10 (Some authors also have called it as Euler Number). The loss coefficient between inlet and axial outlet and that of between inlet and tangential outlet can be used as input to neural network to make the model independent of the pressure factor. It should be noted that it is a calculated variable not a direct measurable from the DAQ.

The separator since separates the particles on the basic of their density difference hence a dimensionless number that relates the density difference of the particles being separated could be used for this purpose. Stokes number is a dimensionless quantity which relates the density difference of the particle being separated along with the

Table 6-3 Input Candidate input parameter list for ANN

Input candidate list
1. Gas volume fraction: GVF (%)
2. Mixture velocity at rectangular inlet of I-SEP: V_{mix} (m/s)
3. Inlet volumetric flow rate of the gas: G_{in} (Sm^3/hr)
4. Inlet volumetric flow rate of the liquid: L_{in} (l/s)
5. Superficial velocity of the gas at circular inlet V_{gs} (m/s)
6. Superficial velocity of the liquid at circular inlet V_{ls} (m/s)
7. Inlet pressure at I-SEP: P_{in} (bara)
8. Statistical parameters (P_{in}^{Sd}, P_{in}^{Krts}, P_{in}^{Skew} standard deviation, kurtosis, skewness) of inlet pressure respectively.
9. Pressure at the underflow of the I-SEP P_2 (bara)
10. Pressure at the overflow of the I-SEP P_3 (bara)
11. Pressure drop between HI-SEP inlet and its axial outlet: P_HISEP_{49}
12. Loss coefficient between inlet and axial outlet, and between inlet and tangential outlet.
13. Stokes Number Stk
14. G-Force
15. GCU%

velocity and viscosity of fluid as shown in the equation (6-1). It is a calculated parameter i.e. it is not directly measured but can be calculated from the following equation 6.1

$$Stk = \frac{\pi \Delta \rho X_{50}^{2} V_{in}}{18 \mu D} \qquad (6\text{-}1)$$

Where,

V_{in} is velocity of the fluid

$\Delta\rho$ is the difference in the densities of the particle being separated by the separator

X_{50} is the cut size diameter of particle.

D is the diameter of the separator

μ is the viscosity of the fluid.

Stk StokesNumber

The I-SEP generates high 'g' force to separate the particles of different density. This 'g' force (represented in this thesis as g-force) provides an estimate of the force applied to the fluid upon entering on the separator. It can be calculated by dividing the centrifugal acceleration by the gravitational acceleration thus giving a dimensionless figure.

$$\text{g-force} = \frac{a_c}{g} \qquad (6.2)$$

Where,

g is acceleration due to gravity

a_c is the centrifugal acceleration given by the following equation

$$a_c = \frac{V_{in}}{r}$$

r is the radius of the separator

Thus 'g' force could be a way to incorporate the effect of radius of the cyclone in the candidate input parameter. This thus provides a way to predict the separation efficiency of two I-SEP of different diameter at the same inlet condition.

The experiments are done using gas liquid mixture with the fixed geometry of the separator therefore the inclusion of the stokes number in input variable list is not very effective unless experimental data of other geometry of separator , fluids other than air and water should be used to train the network. Presently it is an option provided to make the neural network model generalized. The neural network thus would only be able to predict to the separation efficiency for gas and liquid only.

6.3.1 Relationship between Input Parameters and Efficiency

The selection of appropriate variables from the above is based upon the strength of their relationship with the output parameters. While correlation coefficient is an effective method to determine this relationship, however since correlation coefficient mainly captures the linearity in a relationship whereas in our case the trends also had some non linearity therefore more accurate relationship among these variables is a bit difficult to establish using just the correlation coefficient. Therefore new methods were searched to solve this problem. Mutual Information or (MI) is a term used in information technology to represent the quantity that measures the mutual dependence of two variables.

6.3.2 Mutual Information of the Input Parameters

Mutual Information (MI) has been proposed by many researchers for selecting input variables for a model such as (Trappenberg et al., 2006; Battiti, 1994). Mutual information measure interdependencies among attributes and is able to capture any type of functional dependency between variables and therefore can be used for both linear and non linear data. It indicates how much information one variable tells about the other. If two variables are independent then they do not contain any information about the other so the mutual information is zero.

A higher value of MI reduces the uncertainty of determining a random variable with the other related random variable. Mathematically the mutual information is given by the following formula.

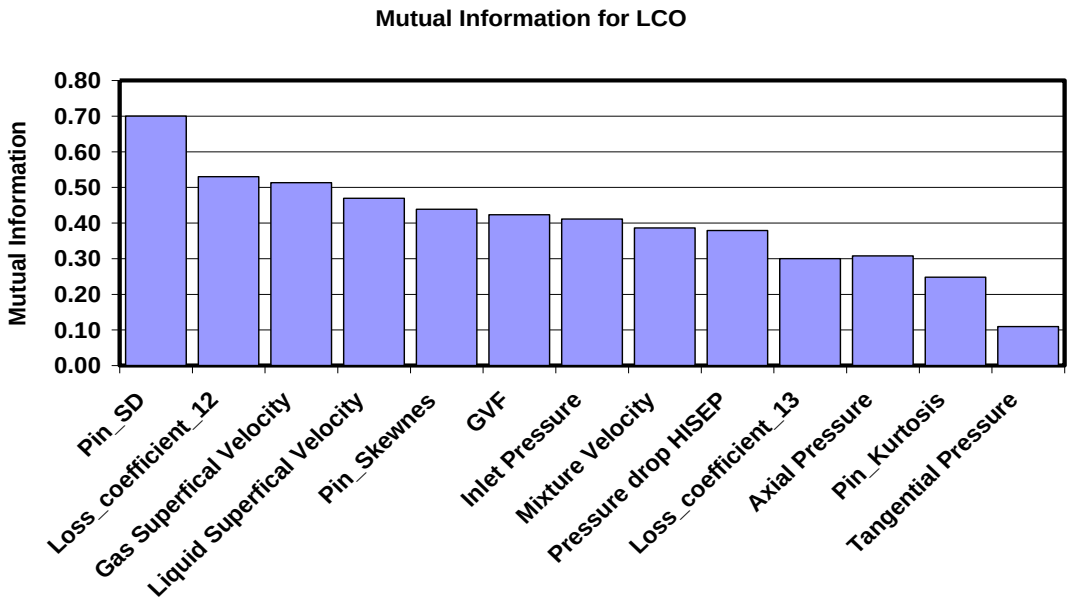

Figure 6.1a Mutual Information for LCO

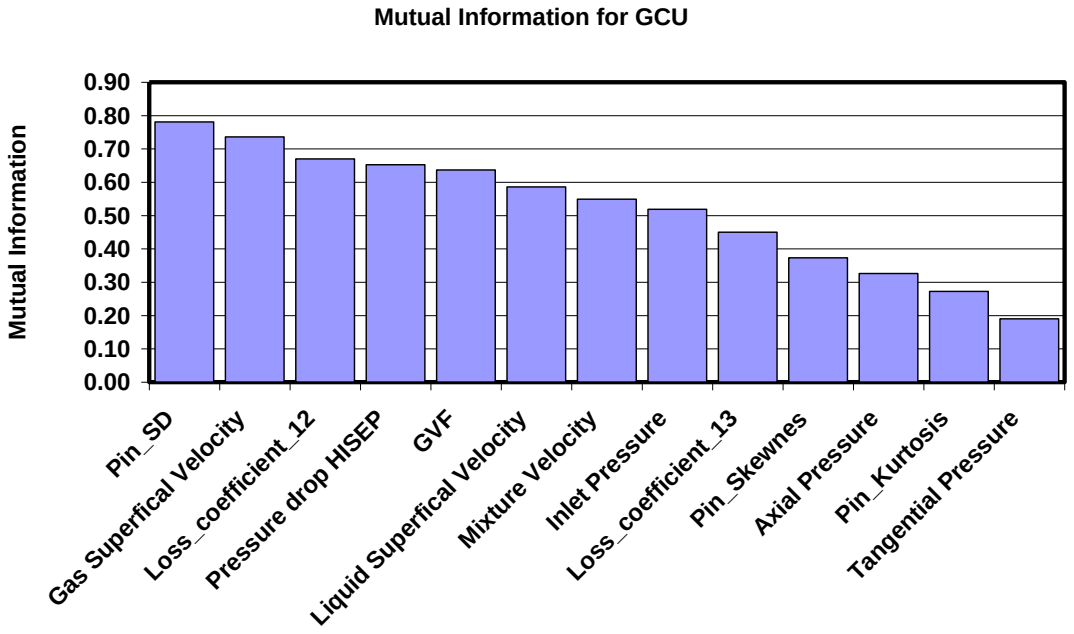

Figure 6.1b Mutual Information for GCU

$$I(X;Y) = \sum_{x}\sum_{y} p(x,y) * \log\left(\frac{p(x,y)}{p(x)\,p(y)}\right) \qquad (6.4)$$

Where

$I(X;Y)$ is mutual information of random variable X and Y.

$p(x,y)$ is joint probability distribution function of X and Y

$p(x)$ is marginal or individual probability distribution function of X.

$p(y)$ is marginal or individual probability distribution function of X.

A MATLAB program was used to calculate the mutual information between each of the variables in the candidate list and output parameters i.e. GCU, LCO liquid and gas separation efficiency for both the fixed GVF and mixture velocity experimental data.

The mutual information for all candidate variables for both GCU and LCO is shown in a graphical form in Figure 6.1a and Figure 6.1b respectively. The standard deviation of inlet pressure reflected the greater value for the MI both for LCO and GCU. The standard deviation in the inlet pressure is a statistical attribute which defines the fluctuation in the inlet pressure. This means that fluctuation in the inlet pressure comparatively has stronger relationship with both GCU and LCO. The mutual information chart in Figure 6.1a and Figure 6.1b also revealed that liquid and gas superficial velocity are more suitable candidate than inlet mixture velocity due to their high value of mutual information both for the GCU and LCO. The pressure difference between the HI-SEP inlets also has shown a high value of mutual information especially for GCU and can be used as input for predicating the combined efficiency of both the I-SEP and HI-SEP.

Once the variables are arranged in order of their relationship with GCU and LCO the next step is to select those combinations of variables which have least relationship among themselves. The existence of correlation among input variables generates multi-collinearity and should be reduced as correlated data input provides redundant

dimension to the neural network causing it to operate ineffectively. The multi-collinearity of the candidate input variables was the determined by calculating the correlation coefficient matrix for all of the possible group using all the candidate input variables and those variables were group together which showed less value of correlation coefficient. Table 6-4 shows the final group of the variable that could be used as an input to a neural network model. This combination of the input variables bear significant relationship with GCU and LCO and at the same time also have least multi co linearity among themselves and hence can be regarded more suitable choice for the input parameters. They are arranged with the most appropriate on the top of the list.

The candidate input variables for the combined efficiency of both I-SEP and HI-SEP is shown in Table 6-5 and that is for I-SEP with applied pressure is presented in Table 6-6.

6.4 ANN Framework for Modelling I-SEP Performance

The experimental data set for this work actually consists of data from two different set of experiments i.e. fixed GVF and fixed velocity experiments as discussed in Chapter 5. This means that model should be capable of predicting the performance of I-SEP and combined performance of both I-SEP and HI-SEP under these two constrains of fixed velocity and fixed GVF. However the constrains of fixed GVF and fixed velocity may not be applied in the practical field, keeping this mind a third type of model was also required which could predict the separation efficiency irrespective of the fixed GVF and fixed velocity constrain. The data set for this third type was acquired from a join set of both the fixed GVF and fixed velocity experiments. Thus in all there could be three types of input data:

- Fixed GVF experimental data which is termed as Type1.
- Fixed Velocity experimental data which is termed here as Type2.
- Combination of both which is termed here as Type5.

Table 6-4 Candidate Input parameter list to ANN for I-SEP only.

Most Appropriate input list for ANN to predict I-SEP performance only.
1. Gas volume fraction, Mixture velocity and Inlet pressure. (GVF , V_{mix}, P_{in})
2. Inlet pressure, Liquid superficial velocity and Gas superficial velocity. ($P_{in,}V_{ls}$, V_{gs})
3. Inlet pressure, Gas superficial velocity, Liquid superficial velocity, Kurtosis, Skewness of the inlet pressure. (P_{in}, V_{ls}, V_{gs}, P_{in}^{SD}, P_{in}^{Krts}, P_{in}^{Skew})
4. Mean value of inlet pressure, Gas superficial velocity, Liquid superficial velocity, Pressure at under and overflow of I-SEP. ($P_{in,}V_{ls}$, V_{gs}, P_{uf}, P_{of})
5. Gas volume fraction, Loss Coefficient between inlet and axial outlet, and between inlet and tangential outlet. (GVF,L_{13},L_{12})

Table 6-5 Candidate Input parameter list to ANN for both I-SEP and HI-SEP

Most Appropriate Inputs for ANN for predicting combined Performance of I-SEP & HI-SEP.
2. Gas Volume Fraction, Liquid superficial velocity, Pressure difference b//w under and overflow of I-SEP, Pressure difference between HI-SEP inlet and overflow.
3. Gas Volume Fraction, inlet mixture velocity, inlet pressure and pressure drop between HI-SEP inlet and overflow.

Table 6-6 Input parameter lists for ANN

Most Appropriate Inputs for ANN for predicting I-SEP Performance with applied pressure
Liquid superficial velocity, Gas superficial velocity, Pressure at tangential and axial outlet. (V_{ls}, V_{gs}, P_{uf}, P_{of})
Liquid and gas superficial velocity , GCU%

This led to design a software framework to fulfil all of these requirements. Initially a standard linear regression model was developed using the entire candidate input parameter list. However the relative percentage error found with this model was quite high ranging up to 30%. The high relative percentage error was may be due to observed non linear relationship between input and outputs. This then led to use the artificial neural network to model the performance of the I-SEP. A complete software package was written in MATLAB that offers to train the ANN neural network for a given type of experiment i.e. Type1, Type2 and Type5 both for I-SEP and combined I-SEP and HI-SEP efficiency offering the user to select any set of input and output variables shown in Table 6-1, Table 6-2 and Table 6-3. Once the neural network is trained for a given type then it can be used to predict the separation performance of both I-SEP and HI-SEP for the set of input variable on which it was trained. The user interface of this software package is shown in the Figure 6.2. The philosophy used to train these neural networks is discussed in the next section.

6.5 Model Development

The non linearity observed between performance parameters of I-SEP and inlet is modelled with a variant of MLP neural network due to its ability of approximate any nonlinear relationship between inputs and outputs Sandhya (2007) The overall model development process is shown in Figure 6.3

6.5.1 Data Pre-processing

The removal of noise and outliers from the selected data was achieved by applying z score normalization. This technique normalized the data with mean value of zero and standard deviation of 1. The multi-collinearity and dimensionality in the data was reduced using the principle component analysis. MATLAB routine Prepca with a value of 0.001 was used so that only those features that contribute to 99.9% of the variation could be used.

One of important issue that occurred during the neural network training is the generalization or over-fitting, which means that either the network is over trained or

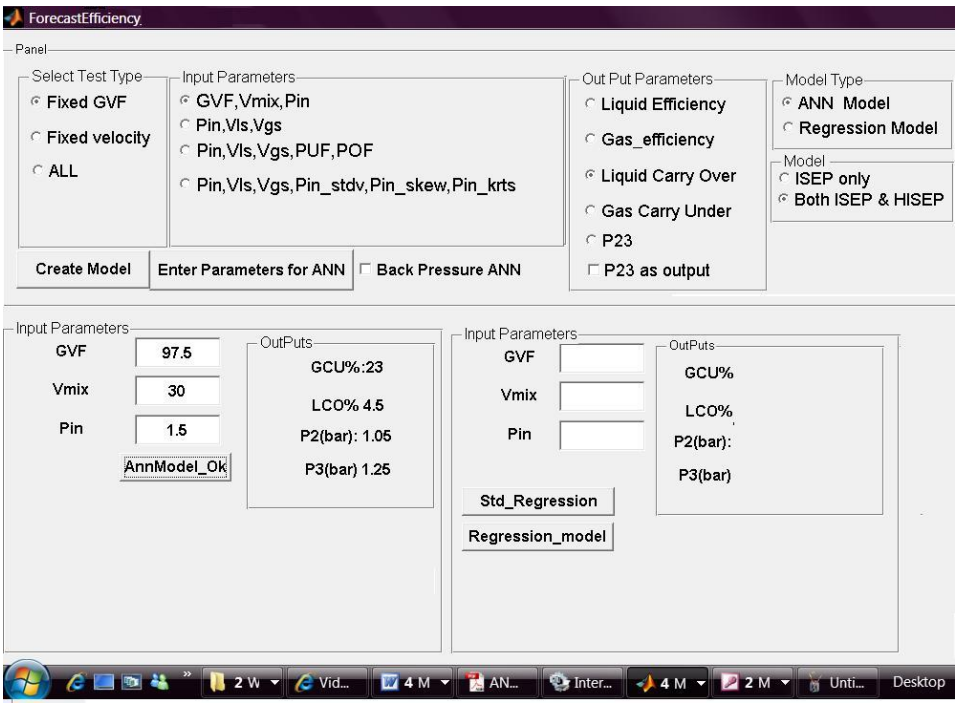

Figure 6.2 User Interface of Developed Software

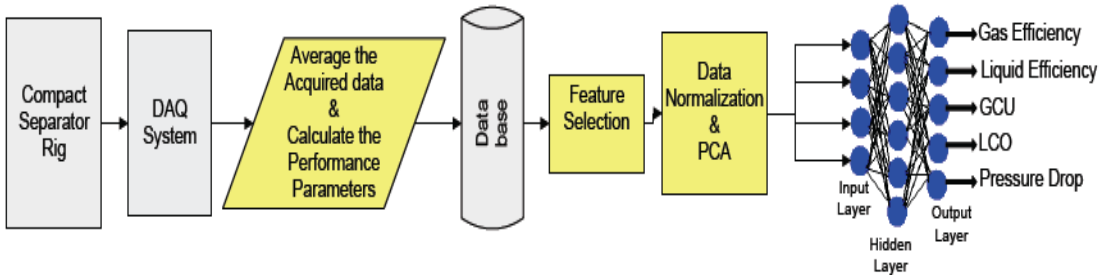

Figure 6.3 Model Development Process

under trained. An over-trained network shows large error on unseen data and vice versa, one of the solutions is to reduce the size of the network but it is hard to know before hand the optimal size of the network. The early stopping technique discussed in section 2.15.5 was chosen to overcome this problem. The early stopping technique continuously monitors the validation error and stops the training if validation error begins to rise.

The combined set of fixed GVF and fixed velocity experiment actually produces 170 data points in all. Bootstrap sampling technique was then used to generate further data set. This technique uses the sampling with replacement, data points are randomly selected from the original data set to form a list, then other data set is created by putting the last selected data points back to original data set. This means that some data points will be repeated and some will not be used at all. This technique is used by many researchers such as Zhang et al. (1997)for generating neural network training data set.

The data set was divided into three sets of training, testing and validation data sets. After testing different portioning ratio (2:1:1, 3:1:1 and 4:1:1) finally ratio of (2:1:1) was selected as it gave better result over others. One half of the data was set for the training and remaining half was divided into validation and testing data set. The testing data set was then use to evaluated the performance of the best trained model.

6.5.2 Network Architecture and Optimisation

The developed network model consisted of one input layer, one hidden layer and one output layer. The number of hidden layers was decided after doing some preliminary experiments with the network architecture. It was observed that more than one hidden layer does not produce good result hence it was decided to use one hidden layer in the model.

A number of training algorithm encounter in literature survey was tested to train the neural networks. Levenberg-Marquardt, conjugate gradient back propagation, and gradient descent momentum with an adaptive learning rate were found to give relatively good result. Therefore these algorithms were finally selected for the training. MATLAB neural tool box routines were used to implement this training algorithm. Log sigmoid in the hidden layer and Purline transfer function in the output layer can be used to approximate any function with arbitrary accuracy Sandhya, (2007). Consequently these two functions were used to train all the networks.

The number of hidden neurons depends upon the complexity of the underlying function the network is attempting to model. The model will be over fitted if too many hidden neurons are used, on the other hand it will behave poor on unseen data if trained with insufficient number of hidden neurons. Some rules of thumb were used as guides as suggested in (James and Carol,) but failing to achieve the good result the critical problem of optimising the hidden neurons in the hidden layer was tackled by following the constructive algorithms approach. The smallest possible network with one hidden neuron in the hidden layer was used at the start of the training and then numbers of neuron were increased in the hidden layer to improve the performance. The number of neurons initially had varied from 1 to 50 but the preliminary result shows that the validation error and effective parameter did not change much after 25 neurons so the total number of the neurons in the hidden layer was then reduced to 25. Figure 6.4 shows the effect of hidden neuron on the effective parameter which as can be seen became almost constant indicating that it most suitable choice for hidden neurons.

The initial value assigned to the weight and bias parameter in the network architecture is another important factor that influences the learning speed and convergence of the training process. The training process may stick in a poor local minimum for an inadequate weight initialization. This problem was solved using the Nguyen-Wirdow method which provides optimal weight initialisation for back propagation based neural network system. This method normalizes the input vectors normalized within the range of +1 and -1. A scale factor F for the input vector is then calculated using the equation:

$$F=\frac{0.7h^{\frac{1}{i}}}{R} \quad (6.5)$$

Where i is the number of input, h is the hidden neuron, and R is range of input vector. The biases are then assigned with a random value in the range of the scale factor F. The network initialisation weights are then designated by assigning random

values between -0.5 and +0.5 to the weights and then multiplying these values by the scale factor F.

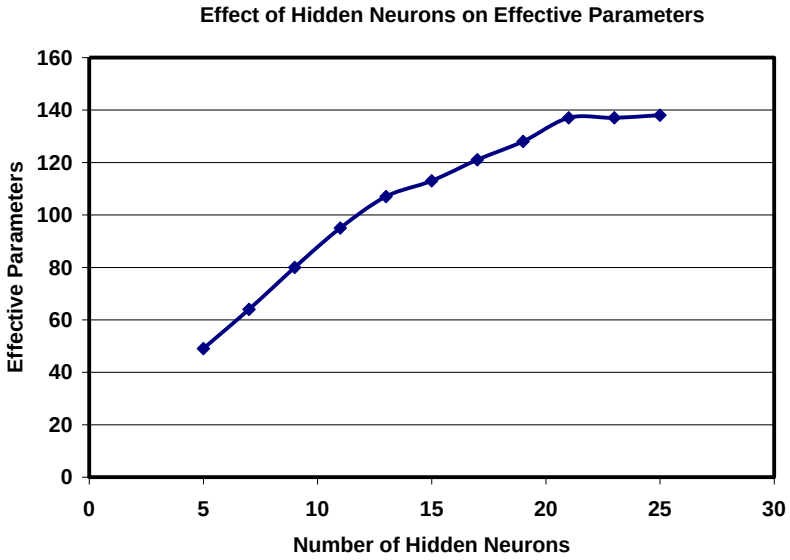

Figure 6.4 Effect of Hidden Neurons on Effective Parameter

The final weights between the input layers and hidden layer and that of between hidden and output layers of the best trained neural network for input set GVF, V_{mix}, P_{in} is shown in the Table 6-7 and Table 6-8 respectively.

Table 6-7 Final weights between Input and Hidden Layer

1.047	4.201	3.067
-1.671	2.577	5.325
1.325	0.623	1.570
-2.869	3.165	-6.504
3.304	5.095	-3.740
1.065	-5.918	2.212
-0.208	-1.313	2.129
-2.376	-0.513	3.053
0.322	-0.106	1.051
0.983	-3.151	-0.436
-0.944	-3.335	-1.856
3.720	2.501	1.724

0.163	-1.675	-0.409
-2.834	1.877	-2.711
3.547	-1.179	-0.829
-2.264	4.077	3.565
0.397	1.287	1.059
-0.273	0.652	-6.296
-1.313	-8.745	1.374
-1.101	-1.302	5.649
-0.906	-0.106	1.334

Table 6-8 Final weights between Hidden Layer and Output Layer

4.323	-1.652	-0.021	0.193
-0.418	10.428	-0.513	0.796
1.736	-0.553	0.973	-1.246
7.119	2.053	-0.067	-0.171
5.562	7.158	0.639	2.710
2.029	-0.103	-0.235	-6.625
0.327	0.545	2.423	3.853
-4.651	1.197	1.019	1.303
1.453	0.589	-1.325	-0.186
-1.615	-0.257	0.490	1.695
-2.163	1.371	-0.050	-0.746
-5.799	-0.735	-0.753	-1.987
-0.762	-2.259	0.340	0.316
-2.771	-1.753	-0.623	-3.507
3.889	1.013	-0.222	-0.571
-2.870	-1.323	-0.118	0.518
2.497	-0.046	-1.372	-1.131
3.538	1.503	0.351	1.618
-2.748	-0.822	0.219	3.839
2.914	1.045	-0.013	-4.280
2.951	-1.253	1.573	0.317

6.5.3 Post-processing of the Results

The network simulated data was then un-normalized to convert them back to their physical meaning.

6.5.4 Selection of the Best Appropriate Trained Neural Network

The method described above to train the neural network actually produced a large number of trained networks. The next most important issue was to select the most accurate trained network from the all the available trained networks. This process was accomplished in two steps, the first step searched for the best trained neural network among the entire trained networks for each input parameters list using the minimum validation error as the selection criteria for this purpose. The performances of these best selected networks were then evaluated using absolute average relative percent error (AAPE) and correlation coefficient on tested data set. The performance of the network was related to low and high value of absolute relative error and correlation coefficient for tested data set respectively. The absolute average percentage error (AAPE) was calculated using the following equations.

$$\text{AAPE} = \frac{\text{exp}erimental\_value - predicted\_value}{Range} * 100 \qquad (6\text{-}6)$$

Where, the *Range* represents the range of the experimental value calculated by subtracting maximum and minimum experimental value.

The above procedure revealed that neural network which were trained with Levenberg-Marquardt optimization with or without Bayesian regularization captured non linearity process behaviour well as compared to other training algorithms used in the training the neural networks. However the training algorithms conjugate gradient back propagation and gradient descent momentum gave better for neural network that were trained using liquid and superficial velocity along with inlet pressure as input parameters.

6.6 Combination of Best predictor into a Single Model

The GCU and LCO was predicted in general with an average relative error of under 15% and 10% respectively whereas the pressure at the under and overflow was found to have an error of under 3%. However the neural networks which were trained on the combined data of the fixed GVF and fixed velocity experiment showed a greater relative percentage error than the neural network trained separately on fixed GVF and fixed velocity experimental data.

The performance comparison of individual neural network based on AAPE% revealed that a single candidate neural network was not enough to extract all the relevant information from the data for all of the neural network outputs. If for example a neural network architecture showed good accuracy in predicting GCU then the same architecture did not showed same accuracy for other outputs i.e. LCO and pressure at under and overflow. This means that best performance of each output has found to have different number of hidden neurons and some time training algorithm. While any of these best selected network can be used, but it could affect the overall robustness of the model. This situation was observed for the all input candidate lists passed to the network which demands that there should be a single model that could best predict all the output of the network with more accuracy.

A search into neural network literature revealed that accuracy of the neural network model can be improved by combining the individual networks Clemen (1989). The combination of neural network is based on the idea that different neural network capture different aspect of process behaviour and their aggregation would reduce the uncertainty and provide a more robust and accurate model. The overall output of the combined neural network model is determined as a weighted combination of the output of the individual neural network joined in the group as shown in Figure 6.5. Mathematically this combination can be shown in the following equation

$$F(x) = \sum_{i=1}^{n} w_i f_i(X) \qquad (6\text{-}7)$$

Where

X is the input vector to the individual neural network

$F(x)$ is combined neural network predictor

$f_i(X)$ is the ith neural network output used in the combination process

w_i is the weight of the ith neural network.

If y_i represent the output vector of the individual neural networks the output vector of the combined model can be represent by following equation:

$$Y_c = \sum w_i y_i \qquad (6\text{-}8)$$

$$Y_c = [y_1 \quad y_2 \, y_3 \quad \ldots \quad y_n] \qquad (6\text{-}9)$$

While literature about the multiple combination of neural network offers many ways to combine the neural network, the combination model in this research was developed using the linear combination of all the best neural network predictor for every output. This procedure requires the determination of the weight for every included individual neural network. Equal weight, linear regression and process component regression techniques were used to calculate the weight of the individual neural network.

The mathematical equation for these methods is shown in equation 6.10, 6.11 and 6.12 respectively.

$$w_i = \frac{1}{N} \qquad (6\text{-}10)$$

$$w = (Y_c^T Y_c)^{-1} Y_c^T y \qquad (6\text{-}11)$$

$$w = P_k (P_k^T Y_c^T Y_c \, P_k)^{-1} P_k^T Y_c^T y \qquad (6\text{-}12)$$

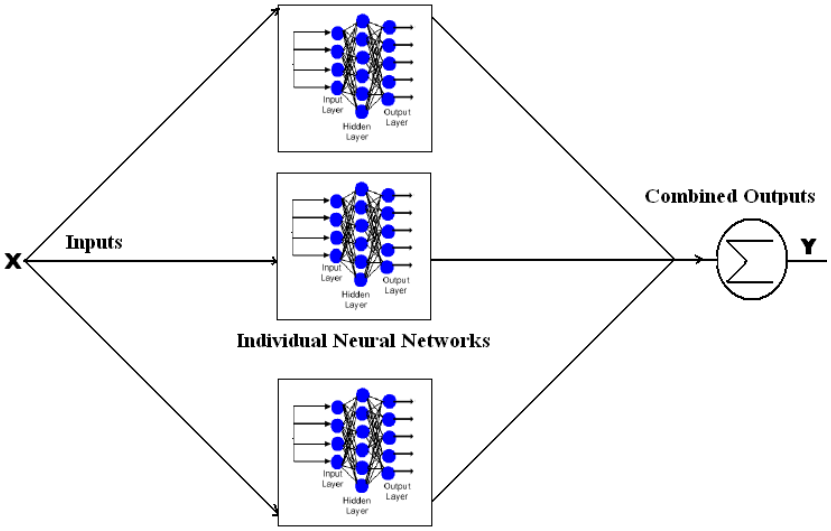

Figure 6.5 Combination of Neural network

Where

N is the total number of the participant neural network in the combined model.

Y_c is the output vector of the combined model, y is the measured output, P_k is the process component vector of the combined output vector.

This stacked neural network approached gave one more way to combine the neural network trained on fixed GVF and fixed experimental data. The best trained neural network that were individually trained on fixed GVF and fixed velocity experiment data were combined and their performance were then checked on the join set of testing data set belonging to both the fixed velocity and fixed GVF experiments data set. This thus gave one more type of trained network which is termed as Type7 in this thesis. The difference between Type7 and Type5 neural network is that in Type5 the data set for both the fixed GVF and velocity experiments were combined and then neural network was trained on this combined data set. The trained network on the combined data set of both fixed GVF and fixed velocity was then stacked using the above defined process. However in Type7 neural network trained on fixed GVF and fixed velocity data set separately were combined using above defined process and then was tested on join data set of both fixed GVF and fixed velocity experiments.

Therefore the combination of the entire trained network would result Type1, Type2, Type5 and Type7 networks.

Equal weight technique was found to be more effective in combining the neural network having two outputs i.e. LCO and GCU whereas the individual neural network having four outputs i.e. LCO, GCU, P_2 and P_3 was found to improve their accuracy through PCA. The correlation coefficient for both the cases was found to lie near 98% for all outputs.

The relative percentage error AAPE% resulted after this combination of network is presented in Table 6-9 and 6-10 both for four and two outputs respectively. The four outputs neural network showed more accuracy than the two outputs due to less AAPE%. The neural network trained for the fixed GVF experimental data i.e. Type1 showed least absolute relative error percentage under 3%, followed by the neural network trained with the combined data of both of the fixed velocity and GVF experiments i.e. Type5.

However neural network of Type7 showed greater AAPE as compared to Type5 neural network. Therefore on the basis of the accuracy and requirement specification Type5 neural network is considered more appropriate for the prediction of I-SEP performance.

It can be seen that among all the best Type5 neural network, neural network input parameter list of $\mathrm{GVF}, V_{mix}, P_{in}$ have showed relatively lower AAPE for all the outputs followed by the input parameter list of $P_{in,} V_{ls}, V_{gs}$ .This means that on the performance of neural network basis it can be said that inlet pressure along with the GVF and mixture velocity or inlet pressure along with the gas and liquid superficial velocity could be the used as the best estimator to predict the efficiency of the I-SEP using neural network.

6.7 Model Testing and Accuracy

This section discusses the model accuracy of Type5 neural network model trained with input parameter list GVF, V_{mix}, P_{in} having four outputs. It is chosen for this because of its lower AAPE as can be seen in Table 6-7. However same analysis can also be perform on neural network with other input parameter lists. The performance and accuracy of neural network model with GVF, V_{mix}, P_{in} as input list was then evaluated using statistical, graphical and finally trend analysis which is discussed below.

Table 6-9 Accuracy of four output ANN

List Candidate	Experiment Type	AAPE%			
		GCU	LCO	P_2	P_3
GVF, V_{mix}, P_{in}	Type1	0.87	0.71	0.77	0.67
GVF, V_{mix}, P_{in}	Type2	4.81	4.52	0.22	3.02
GVF, V_{mix}, P_{in}	Type5	5.43	8.29	2.12	5.42
GVF, V_{mix}, P_{in}	Type7	11.63	18.90	10.55	9.63
P_{in}, V_{ls}, V_{gs}	Type1	0.75	1.34	0.81	0.54
P_{in}, V_{ls}, V_{gs}	Type2	1.75	3.73	1.65	1.94
P_{in}, V_{ls}, V_{gs}	Type5	9.96	8.10	1.41	9.70
P_{in}, V_{ls}, V_{gs}	Type7	28.74	23.12	6.75	67.5
$P_{in}, V_{ls}, V_{gs}, P_{in}^{Sd}, P_{in}^{Krts}, P_{in}^{Skew}$	Type1	0.14	.09	0.38	0.19
$P_{in}, V_{ls}, V_{gs}, P_{in}^{Sd}, P_{in}^{Krts}, P_{in}^{Skew}$	Type2	15.63	13.90	5.64	17.75
$P_{in}, V_{ls}, V_{gs}, P_{in}^{Sd}, P_{in}^{Krts}, P_{in}^{Skew}$	Type5	6.33	3.94	1.76	5.84
$P_{in}, V_{ls}, V_{gs}, P_{in}^{Sd}, P_{in}^{Krts}, P_{in}^{Skew}$	Type7	23.56	13.60	19.54	30.74
GVF,L_{13},L_{12}	Type5	6.91	6.95	5.02	3.6

Table 6-10 Accuracy of two outputs ANN

Candidate List	Network Type	AAPE%	
		GCU	LCO
GVF , V_{mix}, P_{in}	Type1	1.57	1.81
GVF , V_{mix}, P_{in}	Type2	21.01	17.75
GVF , V_{mix}, P_{in}	Type5	8.32	3.52
GVF , V_{mix}, P_{in}	Type 7	17.60	7.94
$P_{in,}$ V_{ls} , V_{gs}	Type1	1.10	1.73
$P_{in,}$ V_{ls} , V_{gs}	Type2	7.54	3.93
$P_{in,}$ V_{ls} , V_{gs}	Type5	3.83	4.95
$P_{in,}$ V_{ls} , V_{gs}	Type 7	12.41	10.23
$P_{in,}$ V_{ls} , V_{gs} , P_{uf} , P_{of}	Type1	1.94	1.53
$P_{in,}$ V_{ls} , V_{gs} , P_{uf} , P_{of}	Type2	5.75	8.41
$P_{in,}$ V_{ls} , V_{gs} , P_{uf} , P_{of}	Type5	5.62	6.64
$P_{in,}$ V_{ls} , V_{gs} , P_{uf} , P_{of}	Type7	10.54	11.25
$P_{in,}$ V_{ls} , V_{gs} , P_{in}^{Sd} , P_{in}^{Krts} , P_{in}^{Skew}	Type1	2.21	2.14
$P_{in,}$ V_{ls} , V_{gs} , P_{in}^{Sd} , P_{in}^{Krts} , P_{in}^{Skew}	Type2	2.97	5.84
$P_{in,}$ V_{ls} , V_{gs} , P_{in}^{Sd} , P_{in}^{Krts} , P_{in}^{Skew}	Type5	7.85	4.52
$P_{in,}$ V_{ls} , V_{gs} , P_{in}^{Sd} , P_{in}^{Krts} , P_{in}^{Skew}	Type 7	11.84	7.75
GVF,L_{13},L_{12}	Type5	7.8	6.5

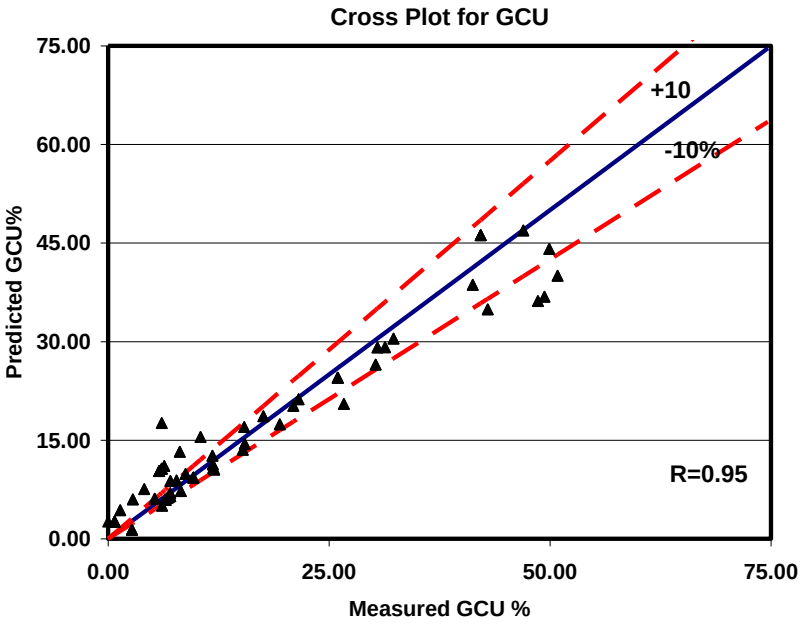

Figure 6.6a Cross Plot of GCU

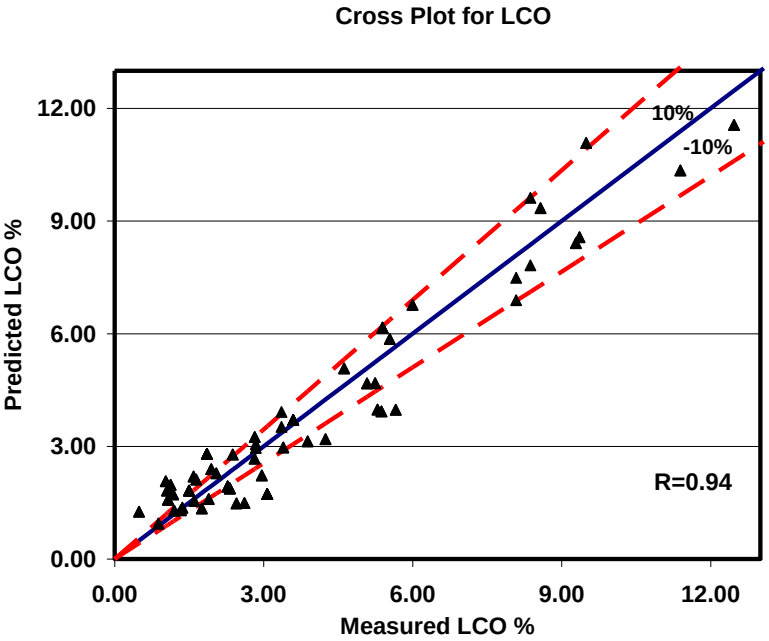

Figure 6.6b Cross Plot of LCO

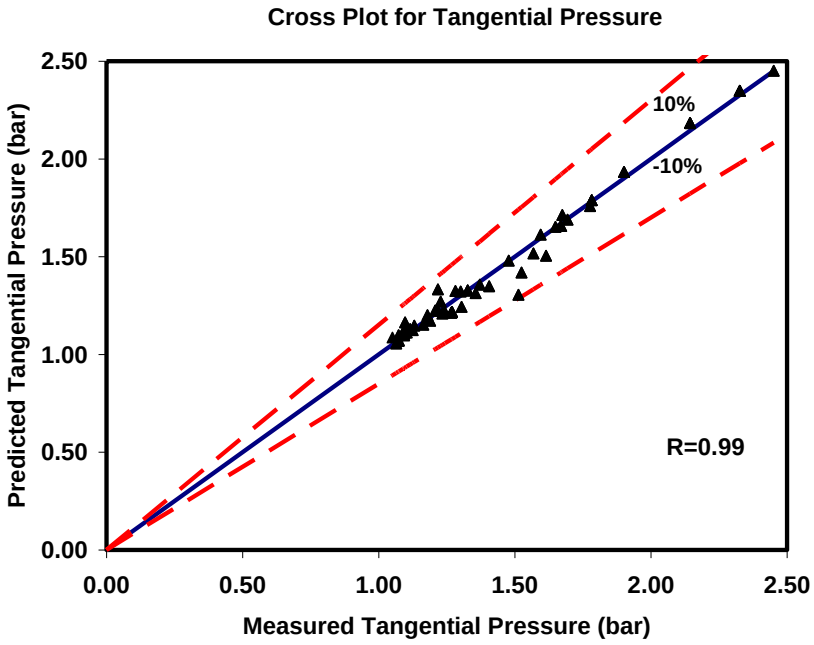

Figure 6.6c Cross Plot of Tangential Pressure

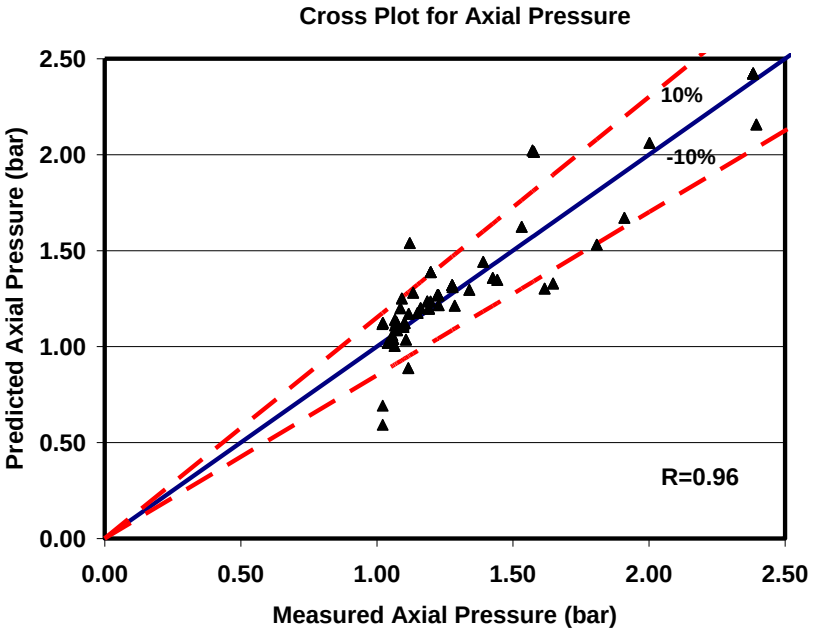

Figure 6.6d Cross Plot of Axial Pressure

6.8 Graphical Analysis of Type5 Neural Network GVF, V_{mix}, P_{in}

A graphical analysis using cross plot and residual analysis was used to visualize the accuracy of the Type5 neural network model using GVF, V_{mix}, P_{in} as input to neural network. The degree of the agreement between the predicted and measured values of the GCU, LCO, and pressure at tangential and axial outlet is presented as cross plot in the Figure 6.7a Figure 6.7b, Figure 6.7c and Figure 6.7d respectively. It can be seen that prediction of pressure at tangential and axial outlet is slightly more accurate than that of GCU and LCO due to their high correlation coefficient. The model deficiencies can be also be checked by looking the residual i.e. error between the predicated and measured values. The residual for all the four output and corresponding maximum and minimum values is shown in Table 6-11 and Figure 6.8. Looking at the mean value of the residual it can be said this model slightly over estimates GCU, LCO and P_2 while under estimates P_3.

Table 6-11 Residual Error statistics for Type5 GVF, V_{mix}, P_{in} Neural Network

	Mean Residual	**Max Residual**	**Min Residual**
GCU	0.44%	12.00%	-11.00%
LCO	0.03%	3.50%	-2.40%
P_2	0.0019bar	0.20bar	-0.11bar
P_3	-.0019bar	0.42bar	-0.44bar

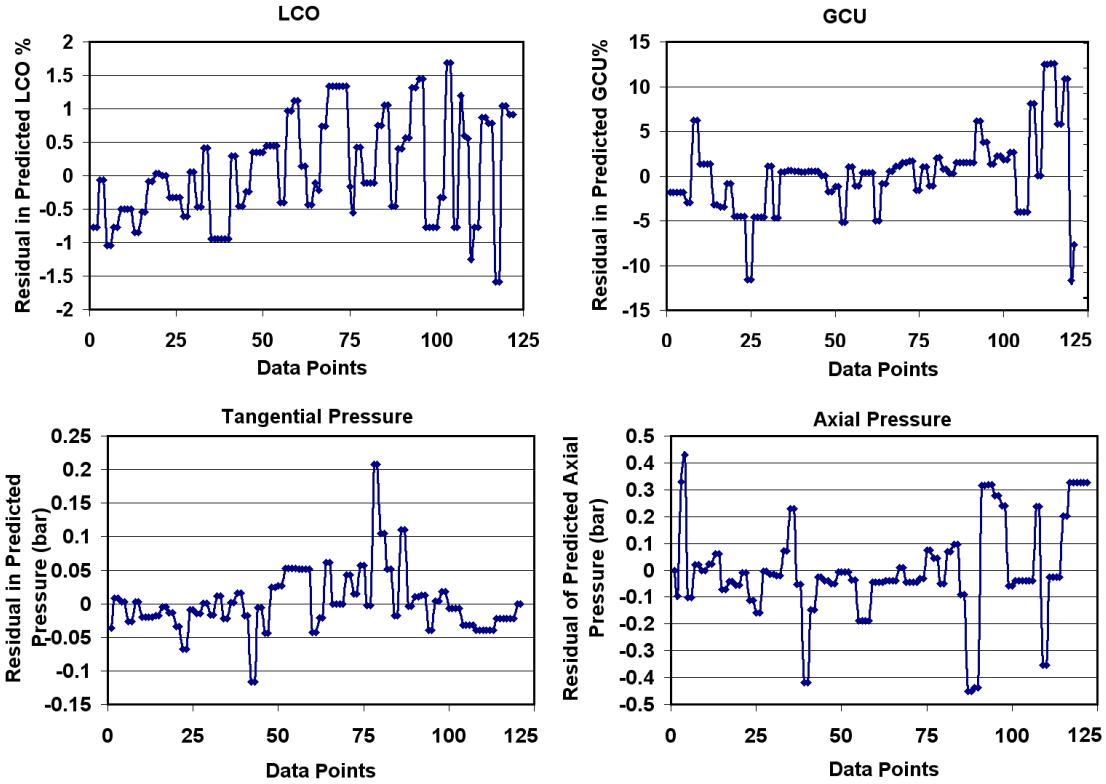

Figure 6.8 The Residual Graph.

6.9 Trend Analysis of Type5 Neural Network using GVF, V_{mix}, P_{in}

It was observed during the experiment analysis that the GCU and LCO in general was found to decrease nonlinearly with the increase in mixture velocity at fixed GVF at low mixture velocities but then GCU was increased and LCO showed non linear fluctuation with the increase in mixture velocity at higher mixture velocity and higher GVF. This trend of experimental data was tested using Type5 neural network using GVF, V_{mix}, P_{in} as input to the neural network.

In order to check these trend synthetic sets of data were prepared from the observed experimental data set. Two values of GVF i.e. 30% and 97.5% were taken for prediction. The velocity was increased from 6 to 30 m/s for fixed GVF of 30%. It should be noted that no experimental data exits for this GVF value of 30% at fixed

velocity. The experiments were conducted for GVF 35% at maximum mixture velocity of 10m/s which showed that GCU and LCO decreased with the increase in mixture velocity (see Figure 4.11b, Figure 4.13b). The prediction for the synthetic data at fixed GVF of 30% and 97% for both GCU and LCO is shown in the Figure 6.9 and Figure 6.10 respectively. It can be seen that predicted GCU decreases with the increased in mixture velocity, however then increases with the increased in mixture velocity which is in agreement of the observed trend as shown in Figure 4.11b in Chapter 4. On the other hand the predicted value of LCO for the GVF 30% also decreases with the increase in mixture velocity as expected (see Figure 4.13b), however at higher mixture the neural network model predicted higher values of LCO. The predicted value of the LCO at GVF 97% follows the same trends as was observed in during the experiments shown in Figure 4.13b.

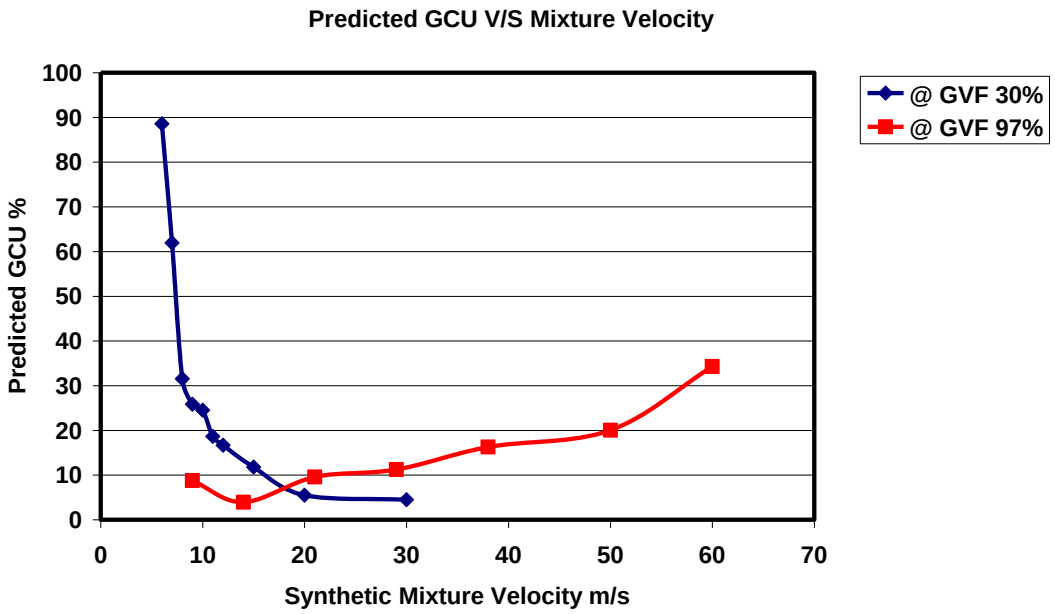

Figure 6.9 Prediction of LCO on Synthetic Mixture Velocity.

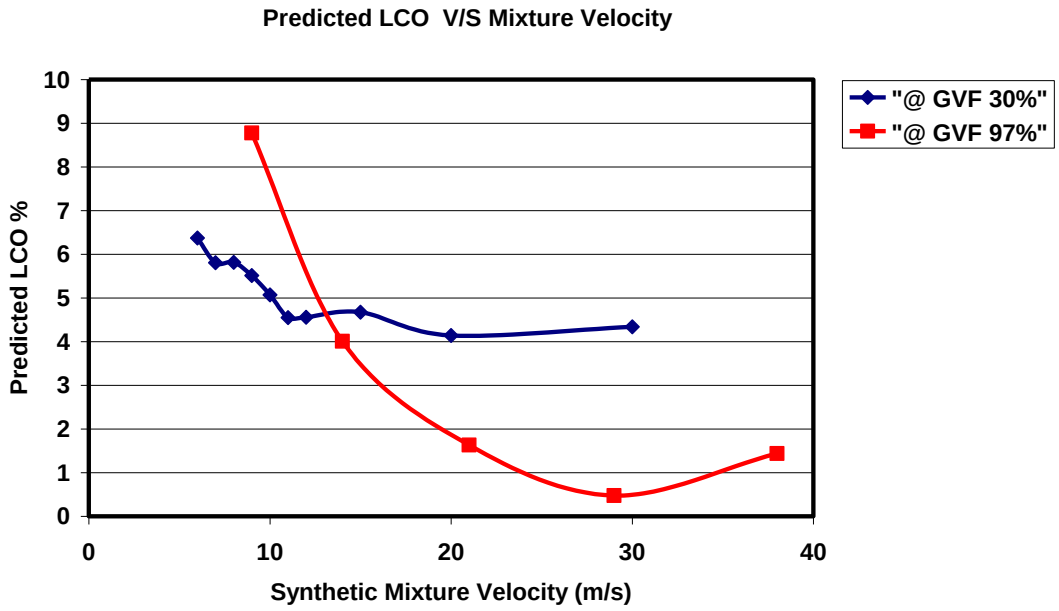

Figure 6.10 Prediction of GCU on Synthetic Mixture Velocity at Constant GVF.

6.10 Axial and Tangential Pressure

The neural network predicted values of tangential and axial pressure at GVF 30% is shown in Figure 6.11. It can be seen that predicted values both for tangential and axial pressure increases with the inlet pressure and predicted tangential pressure is higher than predicted axial pressure at low mixture velocity which is again in agreement with the observed data trend as axial pressure was higher than tangential pressure for all GVF values less than 55% as discussed in Chapter 4 section 4.12

6.11 Neural Network Model using Dimensionless inputs GVF, L_{13}, L_{12}

The performance of Type5 neural network using GVF, V_{mix}, P_{in} as input has shown satisfactory result as discussed above. However since they have been trained on input parameters that are specific to the current experimental set up therefore neural network should be retrain for different experimental condition i.e. for high pressure. It is due to this reason dimensionless input variable were also used to trained the neural network, this variable is mentioned as candidate list 5 GVF, L_{13}, L_{12} in Table

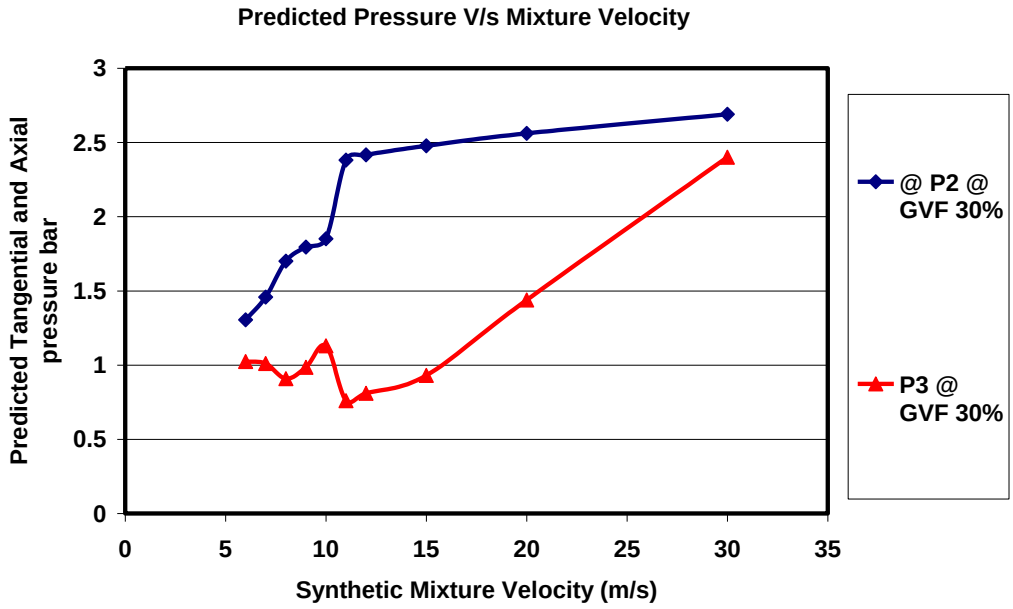

Figure 6.11 Prediction of Pressure at tangential and axial outlet on synthetic Mixture Velocity.

6-4. The performance of this neural network would be discussed now. The accuracy in term of AAPE% for Type5 neural network trained on dimensionless group was found to be fewer than 10% as can be seen in Table 6-10. The residual error statistic for this neural network model is shown in the Table 6-12. It can be seen that GCU predicted by this is model is over estimated with mean value of 1.75% and rest of other outputs i.e. LCO, P_2, P_3 are under estimated with mean value -3.30%, -1.20%, and -0.46% respectively.

Table 6-12 Residual Error statistics for Type5 GVF, L_{12}, L_{13} Neural Network

	Mean Residual	**Max Residual**	**Min Residual**
GCU	1.75%	15.50%	-9.40%
LCO	-3.30%	8.35%	-3.34%
P_2	-1.2%	-0.58%	-0.74%
P_3	-0.46%	0.57%	-0.057%

The accuracy of this model was further tested by observing the trends predicted by the model for the synthetic set of data and then compared it with the data trend as observed during the experiments. Three value of GVF 40%, 50% , 85% and 97% were selected for this purpose and loss coefficient between inlet and axial and that of between inlet and tangential outlet was synthetically increased for each value of selected GVF. Their combination was then fed into the neural network, the result so obtained is presented in the Figure 6.12. The data trend observed during experiments keeping GVF constant and increasing the loss coefficient between i.e. L_{12}, and L_{13} is shown in the Figure 6.13. It can be seen in Figure 6.13 that at low GVF value of 40% and 50% the increase in value of L_{12} and L_{13} caused to decrease the GCU and LCO. The same trend was predicted by the neural network as can be seen in the Figure 6.12 Similarly the predicted trend for the higher GVF value of 85% and 97 were also found to be similar with the experimental data trends. For example at low GVF 40%GVF the increasing value of loss coefficient between inlet and axial outlet from 2.62 to 2.78 has dropped the GCU from 52% to 18.20 %.(see Figure 6.13) Following this trend the neural network model predicts that when loss coefficient is synthetically increased from 2.73 to 2.92 the GCU will be decreased from 43% to 6.31 %. Likewise the experiments result showed that at higher GVF of 97% the increased in the loss coefficient between inlet and axial outlet from 1.34 to 1.58 has caused to decrease GCU from 21.25% to 14.29 but then was increased from to 26.59% when loss coefficient was further increased from 1.58 to 5.08(see Figure 6.13). The prediction of the neural network model for the synthetic data also follows this trend as the synthetic loss coefficient value from 1.30 to 1.5 will cause to decrease the increase the GCU from 18 to 14.5% but the predicted value of GCU will be increased to 25.73 % when the loss coefficient value is increased to 5.02 as can be seen in the Figure 6.12.

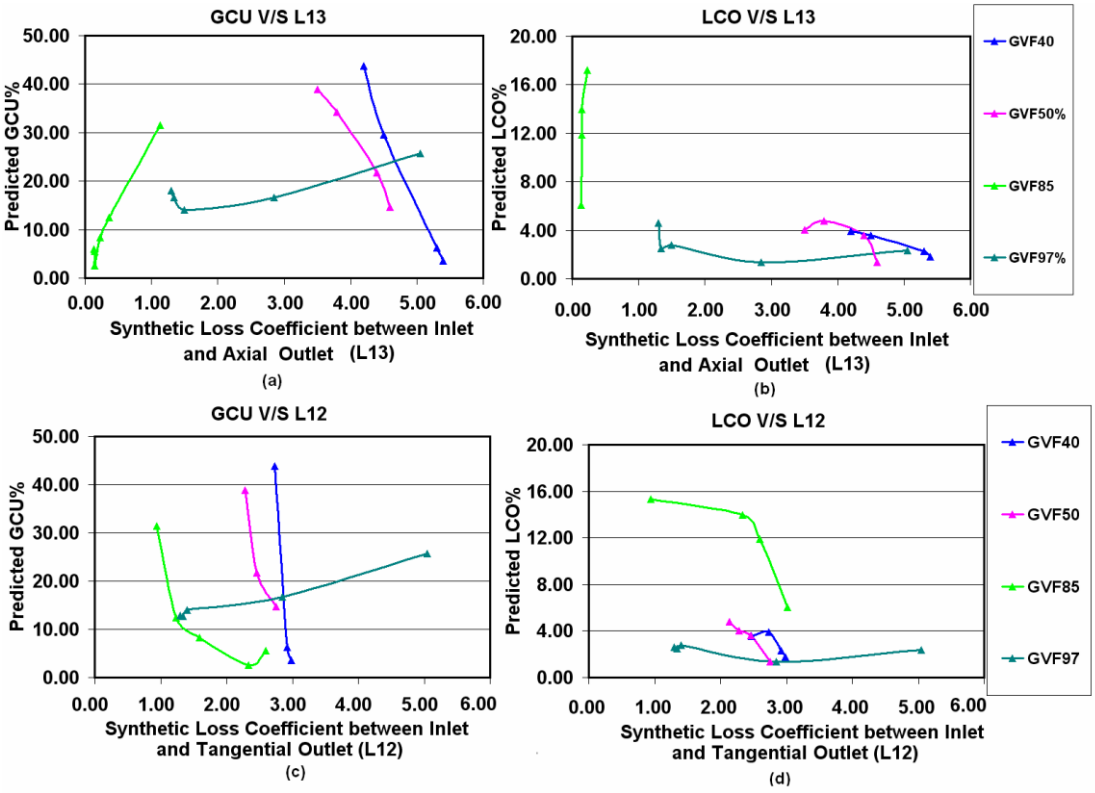

Figure 6.12 Predicted GCU, LCO on synthetic L12 and L13.

Thus on the basis of satisfactory accuracy of the trend analysis of the neural trained on dimensionless input variable and lower AAPE% ,it can be said that if neural network is trained with the dimensionless input then they may also be used to predict the gas and liquid separation efficiency for other experimental conditions which were applied in this thesis.

6.12 Back Pressure Model

A separate model is built using neural network to predict the GCU, LCO and inlet pressure at the increasing pressure at the two outlets of the I-SEP due to the increase in the back pressure. The model used four input including liquid and gas superficial velocity along with axial and tangential pressure. The model was developed using the same algorithm as discussed above. The APPE resulted on prediction from network on unseen data, was found 5% indicating a satisfactory accuracy. The cross plots of the GCU, LCO and inlet pressure as predicted by the model on unseen data set is shown in the Figure 6.15, Figure 6.16 and Figure 6.18 respectively.

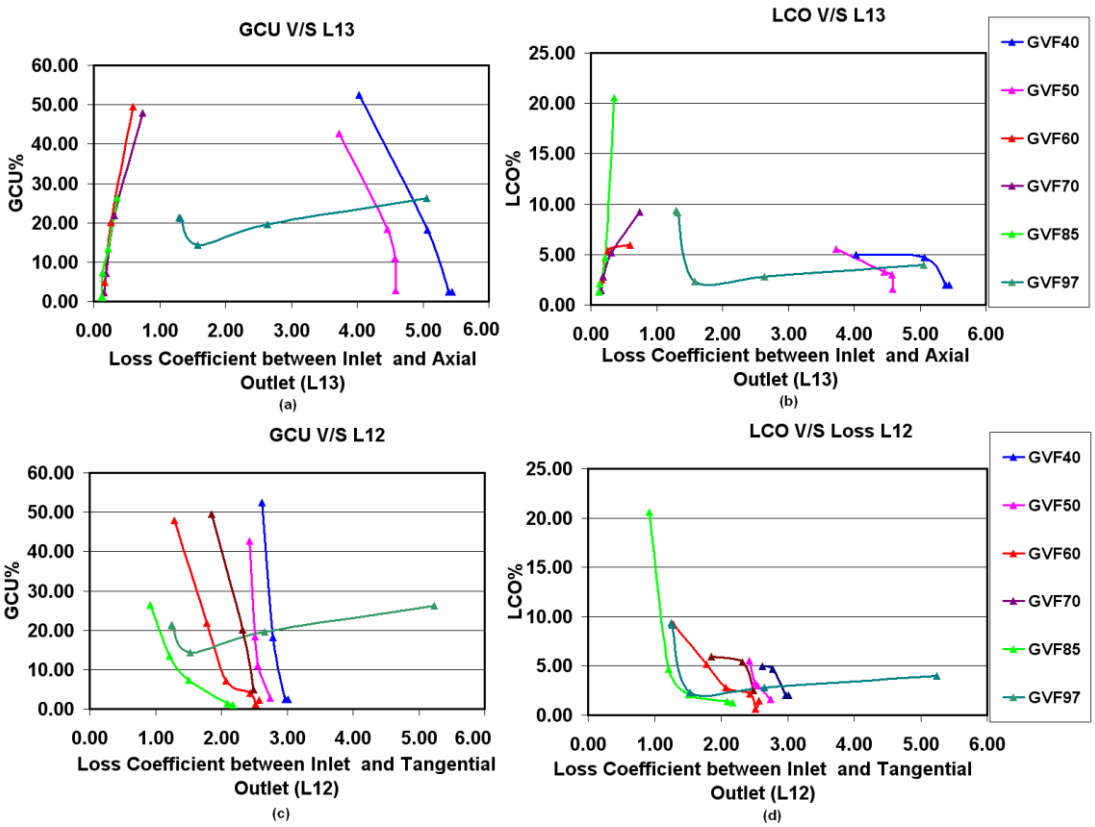

Figure 6.13 Effect of L_{12} and L_{13} on GCU and LCO as observed in experiments

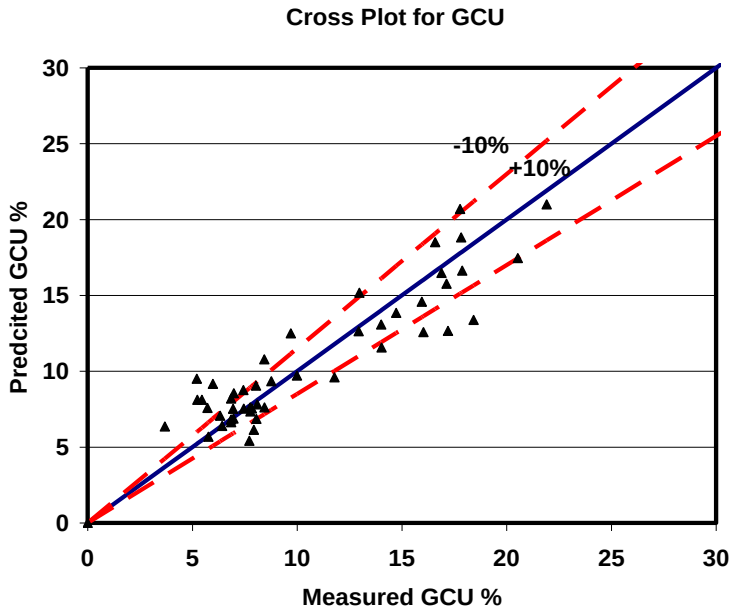

Figure 6.15 Cross Plot between Predicted and Measured GCU (Applied Pressure case)

The statistics of residual of the predicted and measured GCU is presented in the Table 6-13 which shows that this model under estimates GCU with mean value of -0.65%, over estimates the LCO and inlet pressure with mean value of 0.55% and 0.003bar.

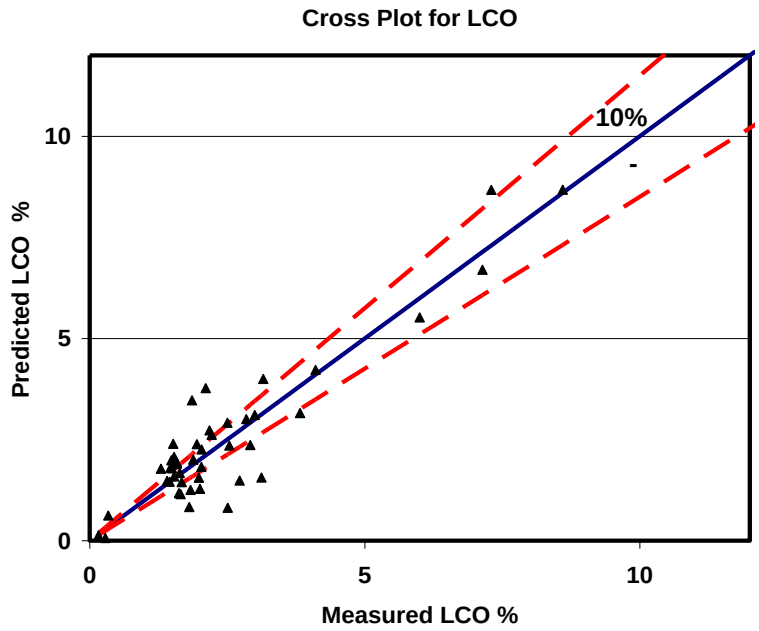

Figure 6.16 Cross Plot between Predicted and Measured LCO (Applied Pressure case)

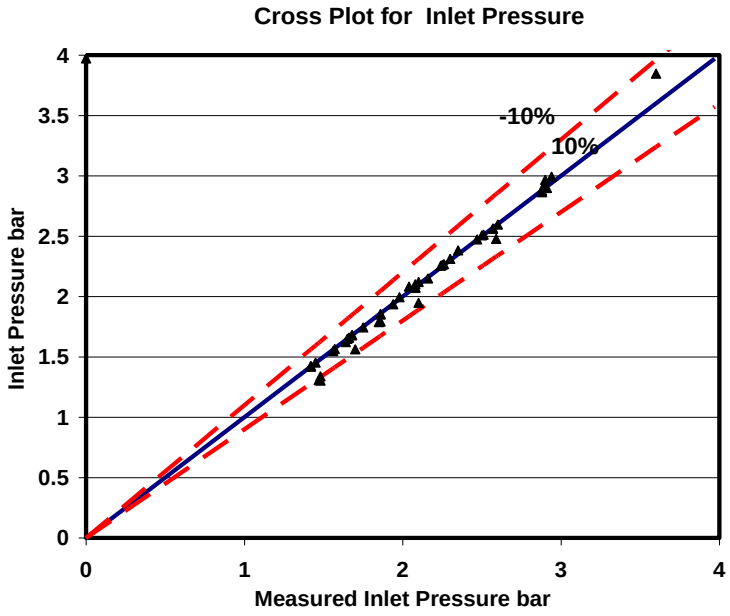

Figure 6.17 Cross Plot between Predicted and Measured Inlet Pressure (Applied Pressure case)

Table 6-13 Residual Error statistics for Applied Pressure neural network

	Mean Residual	Max Residual	Min Residual
GCU	-0.65%	17.00%	-10.00%
LCO	0.55%	13.80%	-8.75%
P_{in}	0.0083(bar)	-0.24(bar)	0.17(bar)

6.13 Controlling GCU and LCO with Inverse Function of Trained Neural Network and a PID Controller

The above discussion shows that neural network models developed using different inputs can be used to model the separation performance of the I-SEP. This neural network modelling however may also be used in controlling the important parameter of the separation efficiency i.e. GCU and LCO. The next phase of this neural network modelling was to test the appropriate neural network configuration performance in controlling the GCU and LCO on the changing inlet condition.

The Performance of the I-SEP (as observed in the experimental analysis in chapter 4) is affected by the amount of the liquid in the gas stream and amount of the gas in the liquid stream. However the performance of the I-SEP can be enhanced by applying the backpressure at the liquid outlet to remove the gas carry under in the liquid stream. The applied backpressure due to throttling of the control valve attached at the tangential outlet of I-SEP shown as CV4 in P&ID (see Figure 3.3a) has either increased or decreased the pressure at the tangential and axial outlet of the ISEP thus creating a pressure difference between the tangential and axial outlet of the I-SEP. It was found during the experiment that reduction of the GCU by the applied back pressure is a non-linear process and it requires a tedious job to set the differential pressure between tangential and axial outlet to control the GCU. This non-linear relationship was satisfactory identified by the developed neural networks as discussed in the last section. The problem of controlling GCU or LCO however can be solved

by the use of an appropriate neural network based controller to control the GCU at given set point by manipulating the pressure at the tangential or axial outlet.

Nowadays neural network have been proved to be a promising approach to control non-linear process (Anuradha,2009). The neural network control may be divided in to three main categories which are supervisory control, adaptive control and direct or indirect inverse control. In the direct inverse control the neural network is trained with observed input output of system to identify the inverse dynamics of the plant and then used as forward controller in the system. The neural network in this method is trained with current state of a dynamic system along with the next target state to produce the control action that drives the system to this target state. On the other hand in the indirect method current state and control action is used to train the neural network to predict the future state of the system. However the inverse dynamic modelling of the system may be difficult to achieve (Hussain and Kershenbaaum, 1997) for many non-linear systems.

PID controller on the other hand is also used to control the non-linearity in a process. The learning adaptation ability of neural network combined with the tracking non-linearity ability of PID controller may be used to create a novel controller to handle the severe non-linear processes such as observed between GCU and the pressure at tangential and axial outlet.

This study proposed this novel idea of the combination of PID controller with the inverse function of trained neural network to control the GCU and LCO. In this scheme neural network is trained to represent the forward dynamics of the system using the input and output of the system. However rather than predicting the output from the given input, the inverse function of the trained neural network is used to track the input for a given output of a trained neural network. In other word the inverse function of the trained neural network predicts the inputs or required manipulating variables to control the given output as shown in the Figure 6.18. This strategy thus follows the indirect control scheme of neural network controller with neural network trained to identify the forward dynamics of the system then uses

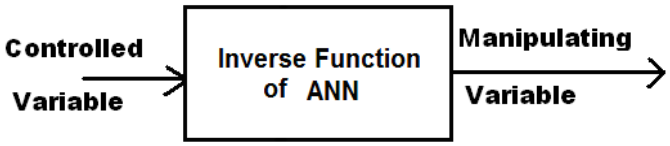

Figure 6.18 Function of Inverse Neural Network

inverse function of this trained neural network to control the output by predicting the required input or manipulating variable.

The mathematical representation to identify the forward dynamics of the neural network is given by the following equation

$$Y=NN(U,W) \qquad (6\text{-}13)$$

Where Y is the output of the trained neural network, U is the given input and W is the weight of the trained neural network. Then inverse of such trained neural network can then be given by the following equation

$$U=NN^{-1}(Y,W) \qquad (6\text{-}14)$$

The inverse function of the neural network model is then used in a closed loop along with a PID controller to control a given set point as shown in the Figure 6.19. Any input of the trained neural network may be used as manipulating variable and any output of the neural network can be used as control variable. The error signal between the output of the neural network i.e. Y and setup point is fed in to the PID controller whose control output becomes one of the input of the neural network. The PID is tuned until the manipulating variable to input of neural network gives the required set point.

The performance of this proposed control scheme is then tested on two different neural network architectures having GCU as one of the outputs but having different set of inputs variables. One of them is trained on the backpressure experimental data having following input out and output.

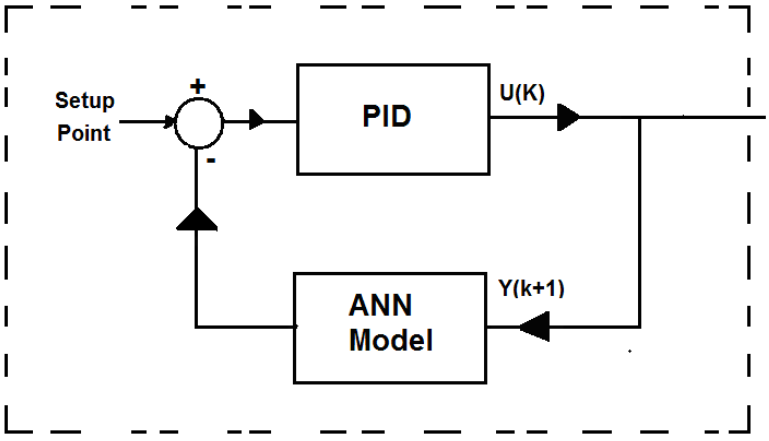

Figure 6.19 Combination of PID & Inverse Neural Network

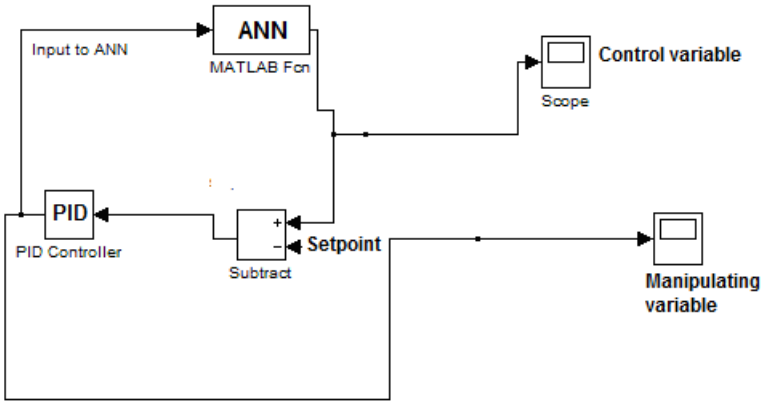

Figure 6.20 SIMULINK representation of PID controller with ANN

Input

1. Gas superficial velocity (V_{gs})
2. Liquid superficial velocity(V_{ls})
3. Pressure at underflow (P_2)
4. Pressure at overflow(P_3)

Output

1. Gas Carry Under (GCU)
2. Liquid carry over (LCO)
3. Inlet Pressure (Pin)

GCU and LCO the two outputs of the trained neural network was tested as controlled variable separately and for each of these control variable one of the input of the neural network is treated as manipulated variable keeping the other inputs

constant. The simulation shown in Figure 6.20 is done using SIMULINK using the testing data set which was not seen by the neural network during the training.

6.13.1 GCU as Controlled variable

The inverse function of the trained neural network with the PID controller in the feedback loop is tested with GCU as control variable and pressure at overflow i.e. P_2 as manipulating variable keeping all the other inputs to neural network unchanged. The loop was tested for more than one set point of the GCU. The Figure 6.21 shows the case when the GCU was set 7.58% and P2 was 1.64 bar, The simulation was run for 500 seconds, however as can be seen from Figure 6.21 that the manipulated variable P2 matched with the actual within 50 seconds. The other tested values are shown in the Table 6-14. It can be seen from this table that simulated values are either similar to actual values or very near to it to track the given set point of GCU.

Table 6-14 Test result of inverse of ANN (SP:GCU, Manipulated variable :P_2)

Set Point	**Test Point**				**Manipulated Variable P2 (bar)**		**PID Parameters**		
GCU %	**V_{ls} m/s**	**V_{gs} m/s**	**P_3 bar**	**P_2 bar**	Simulated	Difference	P	I	D
7.58	1.06	1.71	1.20	1.64	1.64	0.00	10	50	100g
17.53	.25	4.298	1.30	1.26	1.26	0.00	10	2	100
15.82	0.489	1.618	1.08	1.27	1.27	0.00	.65	3.5	100
18.00	.445	4.237	1.48	1.39	1.38	0.01	10	2	100
6.894	.699	2.271	1.20	1.33	1.33	0.00	0.9	10	500
14.14	.507	1.625	1.08	1.20	1.19	0.01	.05	1.7	100
17.46	.697	1.354	1.07	1.34	1.25	0.09	10	5	100
7.08	0.81	2.11	1.20	1.51	1.48	0.03	10	50	100

The difference in the actual and simulated values observed in results presented in Table 6-14 and Table 6-15 may be minimized by increasing the number of training dataset used during the training of neural network.

This test is repeated with the pressure at overflow i.e. P3 taken as manipulated variable, the simulation is shown in the Figure 6.22 , the results for other values are shown in the Table 6-15.This test also shows that manipulated variable successfully track the given set point with P_3 value =1.20 similar as actual value of P3.

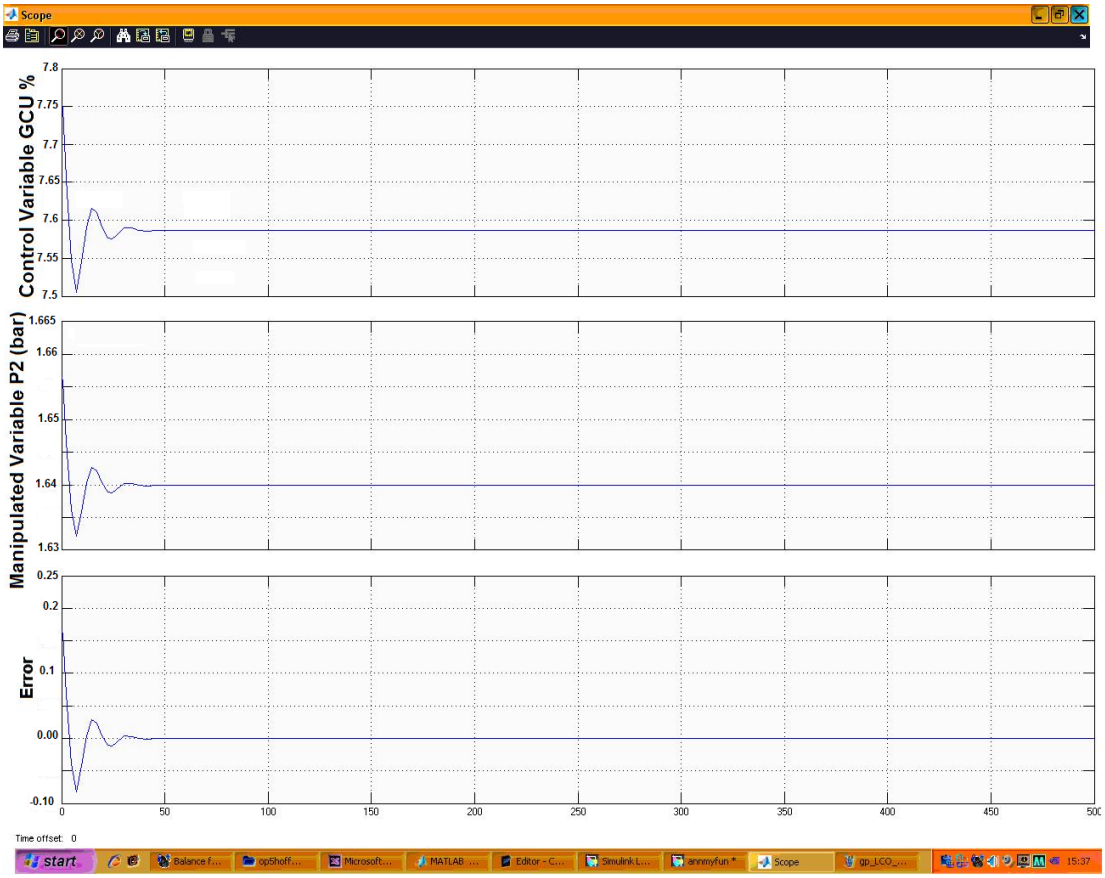

Figure 6.21 Test Result of Inverse ANN for GCU Set point :7.58%, P_2=1.64 bar V_{ls}=1.06m/s,V_{gs}=1.71m/s,P_3=1.20 bar

Table 6-15 Test result of inverse of ANN (SP: GCU, Manipulated Variable: P_3)

Set Point	Test Point				Manipulated Variable P3 (bar)		PID Parameters		
GCU %	V_{ls} m/s	V_{gs} m/s	P_2 bar	P_3 bar	Simulated	Difference	P	I	D
7.58	1.06	1.71	1.64	1.20	1.20	0	0.50	1.09	300
15.82	0.48	1.61	1.27	1.0	0.93	0.07	0.50	1.09	150
18.00	0.44	4.23	1.39	1.48	1.48	0.00	0.50	1.09	300
7.93	0.79	2.13	1.53	1.20	1.14	0.06	1.00	1.09	300
14.14	0.50	1.62	1.20	1.08	1.08	0.00	1.10	5.00	300
7.57	1.01	2.19	1.81	1.47	1.48	-0.01	10.0	3.00	500

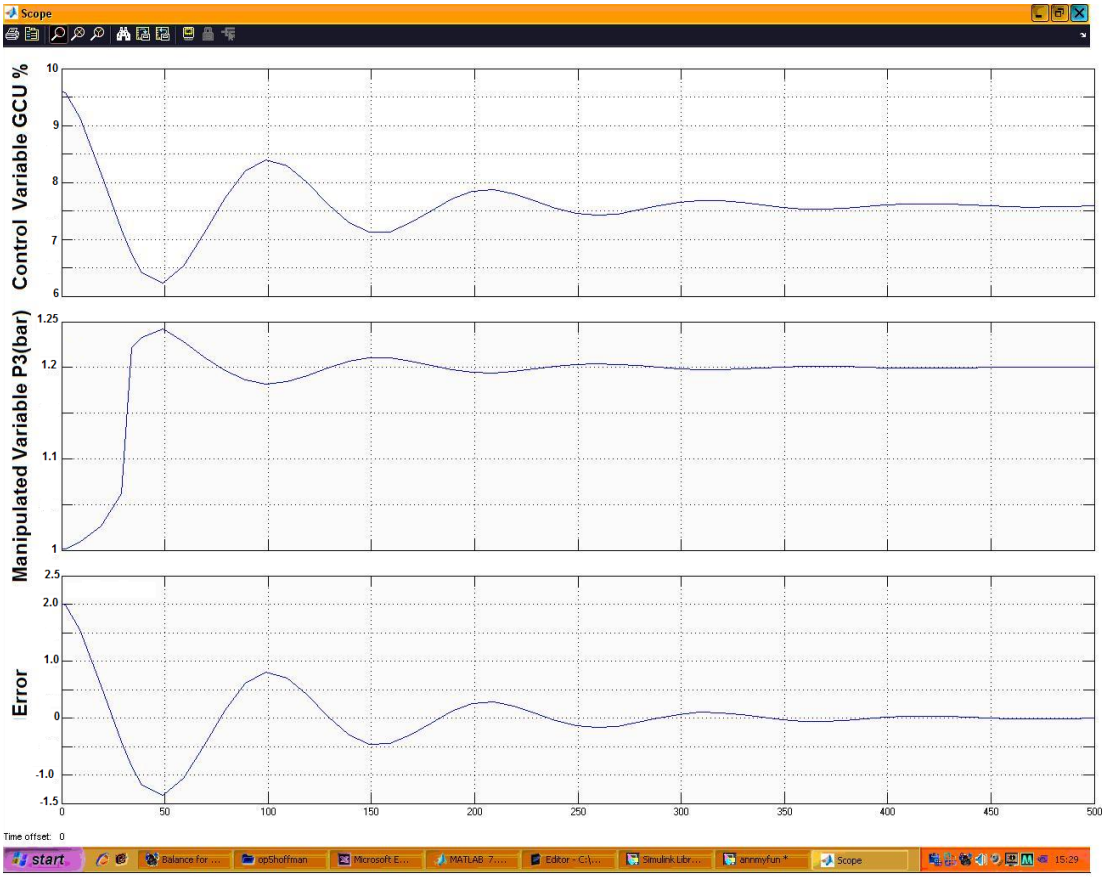

Figure 6.22 Test Result of Inverse ANN for GCU Set point :7.58%, (Manipulating variable P_3)=1.20 bar V_{ls}=1.06m/s,V_{gs}=1.71m/s, P_2=1.64 bar

6.13.2 LCO as Controlled variable

The inverse of the trained neural network function is also tested with LCO as control point and using the P_2 and P_3 as manipulated variable as shown in the Figure 6.23 and Figure 6.24 respectively for LCO set point of 2.1%, The manipulated variable P_2 was found to be 1.73 bar which is close to the actual value of 1.71 bar. The result for other values of LCO is shown in the Table 6-16 and 6-17 respectively. It can be seen that the simulated values for both the manipulated variables of P_2 and P_3 is similar or very close to their actual values.

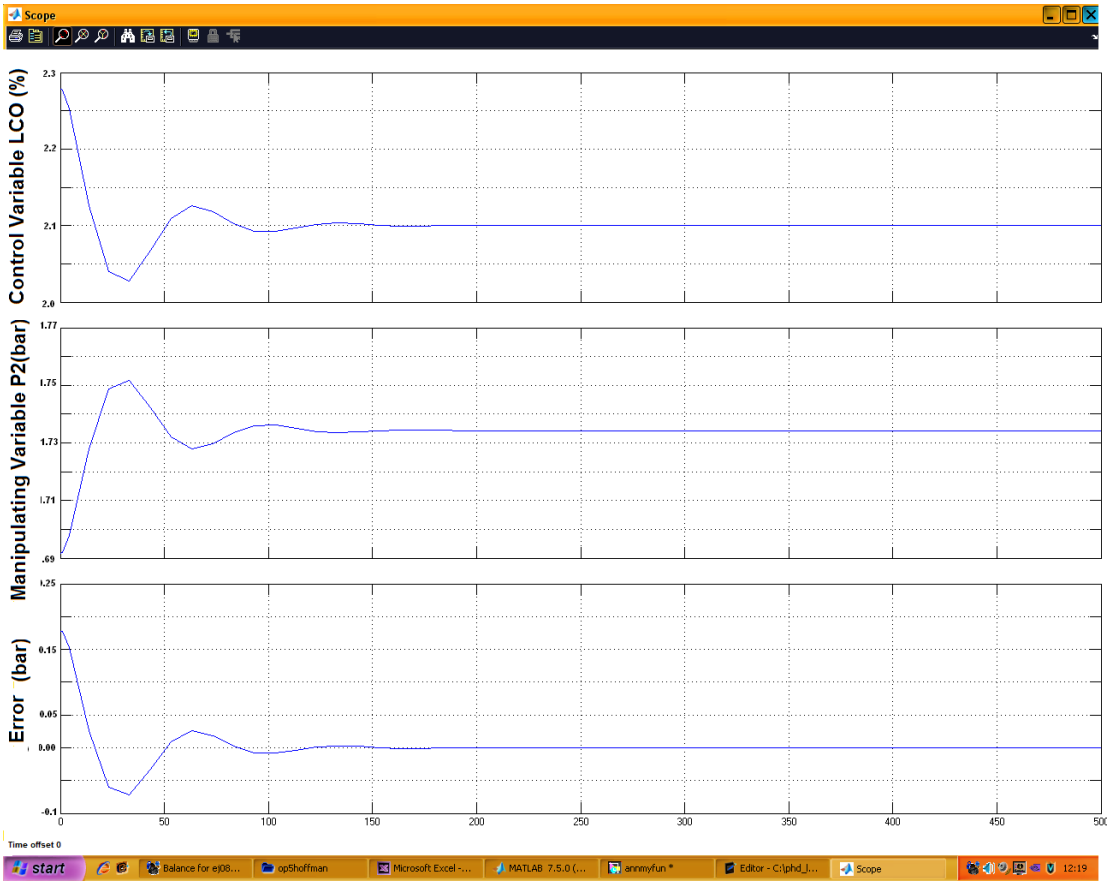

Figure 6.23 Test Result of Inverse ANN for LCO Set point : 2.10%, (Manipulating variable P_2) =1.71 bar V_{ls}=1.06m/s,V_{gs}=1.86 m/s, P_3=1.23 bar

Table 6-16 Test result of inverse of ANN (SP: LCO, Manipulated Variable: P_2)

Set Point	Test Point				Manipulated Variable P2 (bar)		PID Parameters		
LCO %	V_{ls} m/s	V_{gs} m/s	P_3 bar	P_2 bar	Simulated	Difference	P	I	D
2.10	1.06	1.86	1.23	1.71	1.72	-0.01	9.50	5.0	500
1.05	0.44	4.16	1.47	1.37	1.37	0.00	10.0	5.0	500
2.36	0.50	1.61	1.05	1.01	0.7	0.31	0.30	6.0	500
1.75	0.62	2.41	1.24	1.22	1.25	-0.03	10.0	5.0	100
1.45	0.699	2.27	1.20	1.33	1.33	0.00	0.9	10	500
0.68	.67	2.55	1.22	1.35	1.32	0.03	10.0	5.0	500

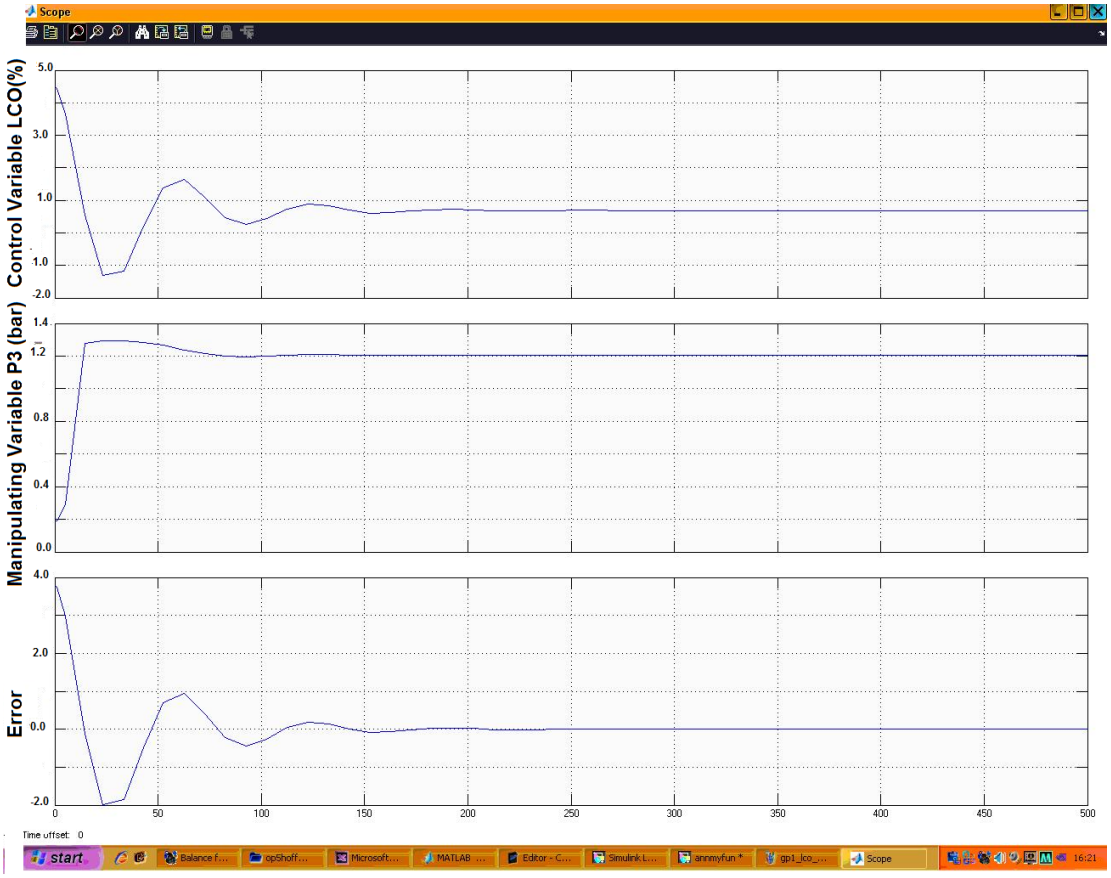

Figure 6.24 Test Result of Inverse ANN for LCO Set point :2.1%, (Manipulating variable P_3)=1.23bar V_{ls}=1.06m/s,V_{gs}=1.86 m/s, P_2=1.71 bar

After satisfactory result of this proposed control scheme to control the GCU and LCO , it was further tested on the trained neural network having inlet pressure (Pin), Gas Volume fraction (GVF) and inlet mixture velocity (Vmix) as input with LCO ,

Table 6-17 Test result of inverse of ANN (SP: LCO, Manipulated Variable: P_3)

Set Point	Test Point				Manipulated Variable P3 (bar)		PID Parameters		
LCO %	V_{ls} m/s	V_{gs} m/s	P_2 bar	P_3 bar	Simulated	Difference	P	I	D
2.10	1.06	1.86	1.71	1.23	1.20	0.03	1.00	5.00	300
.68	.57	2.49	1.30	1.20	1.2	0.00	0.05	5.00	500
1.05	0.44	4.16	1.37	1.47	1.47	0.00	1.00	5.00	500
1.38	.70	2.25	1.33	1.20	01.3	-0.1	0.90	5.00	100
2.36	.50	1.61	1.01	1.05	0.7	0.04	0.30	6.00	500

Table 6-18 Test result of inverse of ANN (SP: GCU, Manipulated Variable: P_{in})

Set Point	Test Point			Manipulated Variable P_{in}		PID Parameters		
GCU %	GVF %	V_{mix} m/s	P_{in} bar	Simulated	Difference	P	I	D
2.70	60	15	2.98	3	.02	5.0	.3	0.1
2.79	85	20	1.95	2.0	.05	5.0	.3	0.1
6.77	90	37.5	3.13	3.11	.02	45.0	10	0.1
20.01	90	10	1.15	1.13	.02	100	10	0.1

Table 6-19 Test result of inverse of ANN (SP: GCU, Manipulated Variable: V_{mix})

Set Point	Test Point			Manipulated Variable V_{mix}		PID Parameters		
GCU %	GVF %	P_{in} bar	V_{mix} m/s	Simulated	Difference	P	I	D
11.22	72.5	1.20	5.0	4.8	0.02	1	1.5	10
40.91	60	1.19	5.0	5.23	0.2	100	15	100
15.39	87.5	1.10	5.0	4.7	0.3	100	15	100
10.63	50	2.75	12.0	12.1	0.1	1	.5	1
17.56	97.5	1.25	22.5	20.54	0.04	100	52	500
11.82	97.5	1.55	37.5	37.48	0.02	100	52	500

GCU as output and results are presented in Table 6-18 and Table 6-19. It can be seen from these tables the inverse neural network function for this case also work satisfactory as manipulated variables with the proper value of PID controller were able to track the given controlled variable.

The result mentioned in the tables showed that inverse function of trained neural network has shown this tendency to track the given set point in close loop with a properly tuned PID controller. On the basis of the result it can be said that the neural network can be used to control the GCU by using the input of the trained neural network as manipulating variable.

6.14 Conclusion

- Artificial Neural network was used to model is the performance of the I-SEP. Software was developed in the MATLAB that offers to trained more than one neural network for the given variable list, once trained these neural network can be used to simulate the separator performance.

- The ANN neural network trained on the input parameter list P_{in}, GVG, V_{mix} was evaluated using the synthetic data , the predicted trends for GCU and LCO from this neural network follows the observed experimental results hence showing that ANN could be used to model the efficiency of the I-SEP
- The Neural network trained for the back pressure experiment also produced satisfactory results.
- The developed software thus provides an opportunity to simulate the separation efficiency of the I-SEP in the rig using different set of variable list. However since all of these networks are trained on less number of data points, hence the accuracy of these network can be improved by training network on more data points.
- The online control of the GCU is possible using the neural network model and remote access platform developed during this thesis.

Chapter 7

Conclusions and Future work

This chapter presents the summary of the work done in this thesis and concludes with a discussion of recommendation for future work.

7.1 Thesis Summary

The work performed in this thesis can be divided in to three main parts.

1. A literature review covering following areas:
    a. Compact separator including performance of the separator for gas liquid separations
    b. Control methods to improve the performance of the compact gas liquid cyclonic separator
    c. Methods to identified the flow regimes in gas liquid flow,
    d. Use of neural network in modelling
    e. Combination of neural network
    f. Methods to mitigate the severe slugging
2. Experimental Study of Gas liquid separation on a novel design compact axial flow separator i.e. I-SEP, Three type of experiments were performed:
    a. Single phase experiments (Chapter 3)
    b. Multiphase phase experiments (Chapter 4)
    c. Back Pressure experiments (Chapter 4)
    d. Experiments to mitigate severe slugging using I-SEP and to compare it with a gravity separator(Chapter 5)
3. Use of extended KALMAN filter to estimate gas and liquid flow rate coming out through the axial outlet of the I-SEP
4. Design and Development of a data repository system to store the experimental result in term of gas and liquid separation efficiency in a database .

5. Development of an application that could provide access to working rig and its experimental result remotely using internet (both wired and wireless internet) and mobile devices (Chapter 3, and Appendix A)
6. Development of a Neural network Model to predict the performance of novel design cyclonic separator that could offer following features (Chapter 6)
    a. Prediction of the GCU, LCO and Pressure drop with or without applied pressure
    b. Prediction of pressure drop between tangential and axial outlet for a given GCU

7.2 Conclusion

- Literature review identified that while compact separator are becoming the choice of oil and gas industry for many potential application, there is not very much literature available on these type of separators and most of the published work is on the reverse flow cyclone modelling solid gas separation. There is lack of modelling literature for the liquid gas separation using axial flow cyclone.
- I-SEP being a novel design in the compact separator needs a model to predict its separation performance at varying inlet conditions as there is no exiting model that can be used to predict its efficiency because of its design.
- An extended KALMAN filter can be used to estimate the single phase flow measurement of the gas and liquid at the axial outlet of the I-SEP using the separator pressure and height of the liquid level inside the HI-SEP. The estimated values of the liquid and gas flow rates by KALMAN filter was found to be more consistent and realistic than the mass difference method.
- They infer gas and liquid flow rate at the axial outlet of the I-SEP was then used to infer the separation efficiency of the I-SEP.
- The combined efficiency of I-SEP and HI-SEP is affected by the liquid level inside the separator, as due to this factor the combined efficiency was found to be different than the inferred efficiency of the I-SEP
- An internet based application was developed that allowed to access the experimental data both numerically and graphically ,

- The single phase gas experiment revealed that the I-SEP has more tendency to push the gas towards the axial outlet than toward the tangential outlet ,depending upon the inlet pressure.
- The proportion of the gas flowing through the axial outlet in single phase gas experiment was increased and that of flowing into the tangential outlet was decreased with the increased gas superficial velocity.
- The I-SEP has more tendency to push the single phase liquid flow towards the tangential outlet, thus more than 90% of inlet liquid was diverted to the tangential outlet of the I-SEP.
- The proportion of the liquid flow through the tangential outlet decreased slightly and that of flowing through axial outlet increases with increases in liquid superficial velocity.
- Loss coefficient for single phase gas flow was found to decrease with the increase in the gas superficial velocity
- Loss coefficient for single phase liquid flow was found to decrease with the increase in liquid superficial velocity.
- The ratio of pressure drop between inlet and axial outlet to that of between inlet and tangential outlet was found directly related to proportion of the gas flowing through the tangential outlet i.e. G_UF and inversely related to the amount of the liquid flowing in to the axial outlet i.e. L_OF.
- Gas superficial velocity, inlet pressure and ratio of pressure drop between inlet and axial to that of inlet and tangential outlet can be used to predict the splitting of the gas with or without external pressure.
- T junction usually consume less energy than I-SEP for separation however the liquid stream of the I-SEP is more purified than T junction.
- When two phase flow in the slug region is passed through the I-SEP , then slug flow regime does not appear at the axial outlet , however the tangential outlet may have slug but having less strength than at inlet.
- Two phase flow experiments revealed that I-SEP has tendency to produce more GCU then LCO. The average GCU % was found 18% and LCO % was found below 5% for all the experiments.

- The multiphase experiment showed that the relationship of the observed GCU and LCO with either of the mixture velocity and GVF of the mixture is nonlinear.
- The GCU and LCO decreased with the increase in mixture velocity at fixed GVF non-linearly, however at higher GVF of 90 % GCU was increased with further increased in mixture velocity, while LCO remain constant.
- The increase in mixture velocity at GVF greater than 90% does not affect very much on GCU.
- LCO and GCU were found to increase non-linearly with the increase in GVF at fixed mixture velocity.
- GCU and LCO were both found to decrease with the increased in liquid superficial velocity at the constant gas superficial velocity.
- The LCO and GCU does not affect very much on each other. However at GVF greater than 90 an increase in GCU also increased LCO.
- The Pressure at inlet was increased with the increased in mixture velocity and GVF .
- Loss coefficient between inlet and axial outlet showed that I-SEP would perform more efficient between GVF values 60% to 85% as during this region Loss coefficient was found to decrease.
- Loss coefficient for multiphase flow indicated that reducing GCU at lower GVF values requires more energy as compared to GCU reduction at high GVF values.
- The ratio of pressure drop between inlet and axial to that of between inlet and tangential was found relatively more linearly related to the GCU than pressure difference between tangential and axial outlet.
- The developed neural network model produced satisfactory result.
- Severe Slugging experiment showed that I-SEP could be used both as active or passive device to mitigate the slug as it has better tendency to avoid the severe slugging due to less rise in riser base pressure .
- The flow was found to be more stable when I-SEP was used on top of the separator due to less fluctuation as compared to the LAB separator.
- The I-SEP has tendency to avoid the severe slugging at relatively lower liquid and gas superficial velocities as compared to Lab separator.

- The minimum pressure difference over riser base was found to be higher for I-SEP indicating more liquid fall back when I-SEP was used on the top of riser. However it is decreased with the increase in gas superficial velocity indicating the intensity of the severe slugging decreased with the increase in gas superficial velocity.
- A set of input variables were identified to be used as input to neural network.
- A software package was developed that offers training of neural networks based on any selected input variables and then can be used to predict the I-SEP separation efficiency on unseen data.
- The online control of the GCU is possible using the neural network model and remote access platform developed during this thesis

7.3 Recommendations for Future Work

- The experiments conducted during this thesis were mostly high GVF values, the lower GVF less than 40% was not possible due to construction of the rig, it is recommended to test the I-SEP performance under low GVF less than 40%.
- The back pressure experiments were performed on the tangential outlet to reduce the GCU , however same type of experiments are recommend on the axial outlet valve to reduce the LCO.
- Conductivity probes should be used to measure the flow regime at the inlet and two outlets, it will help to understand the hydrodynamic inside the I-SEP
- CFD simulation could be performed to investigate the velocity profile inside the I-SEP it would help in better understanding the I-SEP behaviour.
- A neural network based control strategy could be developed that will control the liquid level inside the HI-SEP based on the prediction of the neural network on the changing inlet operating condition.
- The remote access application that was developed in this thesis could be further enhanced such that the valves attached to the I-SEP tangential and axial outlet could be accessed remotely, so that CALTEC can control the

performance of the I-SEP by remotely accessing these valves. This controlling process can further be enhanced by using the remote access application that was developed to access the rig remotely and discussed in Appendix A. This application is capable of accessing the experimental data of the rig using the internet and mobile devices and can also send signal using the mobile devices. The idea is that using the neural network prediction for a DP value, the control valve can be adjusted remotely using the wireless device such as mobile. The remote access of the web cam using the mobile and internet was successfully tested, however following the same approach the remote access application need to enhance to access the control valves remotely.

- This thesis has used neural network for predicting the separation efficiency, however the fuzzy logic may also be tried in the future for developing the model for the I-SEP.

References

Abro, E., Khoryakov, V. A. and Johansen, G. A. (1999), "Determination of void fraction and flow regime using a neural network trained on simulated data based on gamma-ray densitometry", *Measurement Science and Technology,* vol. 10, no. 7.

Altiparmak, F., Dengiz, B. and Smith, A. E. (2009), "A General Neural Network Model for Estimating Telecommunications Network Reliability", *Reliability, IEEE Transactions on,* vol. 58, no. 1, pp. 2-9.

Anandarajan, M., Lee, P. and Anandarajan, A. (2001), "Bankruptcy prediction of financially stressed firms: an examination of the predictive accuracy of artificial neural networks", *International Journal of Intelligent Systems in Accounting, Finance & Management,* vol. 10, no. 2, pp. 69-81.

Arpandi, I., Ashutosh, R. J., Shoham, O. and Siamack, A. S. (1996), "Hydrodynamics of Two-Phase Flow in Gas-Liquid Cylindrical Cyclone Separators", *SPE Journal,* SPE 30683, pp. 426-436.

Azzoparadi, B. J. (May 1993), "T-junction as phase separator for gas liquid flows: Possibilities and problems", *Trans IChemE,* vol. 71, Part A.

Azzoparadi, B. J. and Rea, S. (2000), "Phase separation using simple T-Junction", *Society of Petroleum engineer,* SPE annual and Technical Conference and Exhbtion-2000, Dallas, TX.

Baker, A. C. and Entress, J. H. (1992), "VASPS (Vertical Annular Separation Pumping System) Subsea separation and pumping system", *Trans. IChemE,* vol. 70, Part A, pp. 9-16.

Barbuto, F. A., (1995), "Method of Eliminating Severe Slug in Multi-Phase Flow Subsea Lines", Application for UK Patent no. 2 282 399.

Battiti, R. (1994), "Using mutual information for selecting features in supervised neural net learning", *Neural Networks, IEEE Transactions,* vol. 5, no. 4, pp. 537-550.

Blaney, S. and Yeung, H. (2007), "Investigation of the exploitation of a fast-sampling single gamma densitometer and pattern recognition to resolve the superficial phase velocities and liquid phase water cut of vertically upward multiphase flows", *Flow Measurement and Instrumentation,* vol. 19, no. 2 pp 57-66.

Buel, J. R., Soliman, H. M. and Sims, G. E. (1994a), "Two-phase pressure drop and phase distribution of a horizontal tee junction", *International Journal of Multiphase Flow,* vol. 20, no. 5, pp. 819-836.

Buel, J. R., Soliman, H. M. and Sims, G. E. (1994b), "Two-phase pressure drop and phase distribution of a horizontal tee junction", *International Journal of Multiphase Flow*, vol. 20, no. 5, pp. 819-836.

Cao,Yi (2008),"Learning the Extended Kalman Filter", www.mathworks.nl/matlabcentral/fileexchange/18189

Chen, H., Lin, Z., Liu, D., Wang, X. S. and Rhodes, M. J. (1999), "A Down-Exhaust Cyclone Separator", *Industrial & Engineering Chemistry Research*, vol. 38, no. 4, pp. 1605-1610.

Chirinos, W. A., Gomez, L. E., Mohan, R. S., Shoham, O. and Kouba, G. E. (2000), "Liquid Carry-Over in Gas/Liquid Cylindrical Cyclone Compact Separators", *SPE Journal*, vol. 5, no. 3, pp. 259-267.

Clemen, R. T. ((1989)), "Combining forecasts: A review and annotated bibliography", *International Journal of Forecasting*, vol. 5, pp. 559-583.

Coelho, M. A. Z. and Medronhob, R. A. (2001), "A model for performance prediction of hydrocyclones", *Chemical Engineering Journal*, vol. 84, pp. 7-14.

Coker, A. K. (1993), "Understand cyclone design.", *Chemical Engineering Progress*, vol. 28, pp. 51-55.

Costigan, G. and Whalley, P. B. (1997), "Slug flow regime identification from dynamic void fraction measurements in vertical air-water flows", *International Journal of Multiphase Flow*, vol. 23, no. 2, pp. 263-282.

Cowie, D. (1992), "Vertical caisson slug catcher performance", *Institution of Chemical Engineers Conference, Subsea Separation and Transport III, IChemE.*, vol. 70, part A, pp. 25-31.

Davies, E. E. (1984), "Compact Separators for Offshore Production", *Proceedings of .2nd New Technology for the Exploration and Exploitation of Oil and Gas Reserves Symposium*, Luxembourg, Belgium, vol. 1, pp. 621.

Davies, E. E. and Watson, P. (1979), "Miniaturized Separators for Offshore Platforms", *1st New Technology for Exploration and Exploitation of Oil and Gas Reserves Symposium* , Luxembourg Belgium, pp. 75.

Drahos, J., Tihon, J., Serio, C. and Lübbert, A. (1996), "Deterministic chaos analysis of pressure fluctuations in a horizontal pipe at intermittent flow regime", *The Chemical Engineering Journal and the Biochemical Engineering Journal*, vol. 64, no. 1, pp. 149-156.

Earni, S., Wang, S., Mohan, R. S., Shoham, O., Marrelli, J. D. and Kouba, G. E. (2003), "Slug Detection as a Tool for Predictive Control of GLCC Compact Separators", *Journal of Energy Resources Technology*, vol. 125, no. 2, pp. 145-153.

Eberhardt, J. (1999), "An interview with Julius Eberhardt", vol. 30, no. 9, pp. 66-69.

Gharbi, R. B., Elsharkawy, A. M. and Karkoub, M. (1999), "Universal Neural-Network-Based Model for Estimating the PVT Properties of Crude Oil Systems", *Energy & Fuels*, vol. 13, no. 2, pp. 454-458.

Gomez, L. E., Mohan, R. S., Shoham, O. and Kouba, G. E. (1998), "Enhanced mechanistic model and field application design of gas-liquid cylindrical cyclone separators", *SPE Annual technical conference*, 27th-30th September, New Orleans, pp. 533-544.

Gomez, L. E., Mohan, R. S., Shoham, Q. and Kouba, G. (June 2000), "Enhanced Mechanistic Model and Field-Application Design of Gas/Liquid Cylindrical Cyclone Separators", *SPE Journal*, vol. Vol. 5, no. No. 2, pp. 190-198.

Hill, T. J., Fairhurst, C. P., Nelson, C. J., Becerra, H. and Bailey, R. S. (1996), "Multiphase production through hilly terrain pipeline in Cusiana oilfield, Columbia", SPE Annual Technical Conference & Exhibition, Denver, 6-9 October, SPE 36606.

Hoffmann, A. C. and Stein, L. E. (2002), *Gas Cyclones and Swirl Tube: principles, design and operation*, second edition, ISBN: 3540433260.

Hollenberg, J. and DeWolf, S. (1998), "Suppression of slug flow in a multi-phase fluid stream", Application at European Patent Office EP19950924951.

Hubbard, M. G. and Dukler, A. E. (1966), "The characterization of flow regimes for horizontal two-phase flow", *Proceedings of Heat Transfer and Fluid Mechanics Institute*, Stanford Univ. Press, Stanford, CA, .

Iozia, D. L. and David, L. (1990), "The Logistic Function and Cyclone Fractional Efficiency", *Aerosol Science and Technology*, vol. 12, no. 3, pp. 598-606.

James, R. C. and Carol, E. B. (2007), "Artificial neural networks in accounting and finance: modelling issues", *Intelligent Systems in Accounting, Finance & Management*, vol. 9, no. 2, pp119-144.

Jansen, F. E., Shoham, O. and Taitel, Y. (1996), "The elimination of severe slugging-experiments and modeling", *International Journal of Multiphase Flow*, vol. 22, no. 6, pp. 1055-1072.

Jones, J. and Zuber, N. (1975), "The interrelation between void fraction fluctuations and flow patterns in two-phase flow", *International Journal of Multiphase Flow*, vol. 2, no. 3, pp. 273-306.

Kao, K. Y. and Tsai, C. J. (2001), "On the theory of particle collection efficiency of cyclones", *Journal of Aerosol and Air Quality,* vol. 1, pp. 47–56.

Kim, N. and Calise, A. J. (2008), "Neural network based adaptive output feedback augmentation of existing controllers", *Aerospace Science and Technology,* vol. 12, no. 3, pp. 248-255.

King, M. J. S., Hale, C. P., Lawrence, C. J. and Hewitt, G. F. (1998), "Characteristics of flowrate transients in slug flow", *International Journal of Multiphase Flow,* vol. 24, no. 5, pp. 825-854.

Kjetil, H. and Morten, D. (2002), "Active feedback control as a solution to severe slugging", *SPE production & facilities,* vol.17, no3, pp. 138-148.

Komura, N., Yutaka, H., Satoshi, T. and Kazuya, M., (2002), "Gas liquid centrifugal separator", Application for United States patent no. 6776812

Kouba, G. E. and Shoham, O. (1996), "A Review of Gas-Liquid Cylindrical Cyclone (GLCC) Technology", *"Production Separation Systems" International Conference,* April 23 & 24, Aberdeen, UK.

Svarovsky, L. (1984), *Hydrocyclones*. Technomic Publishing Company, London

Lapple, C. E. (1951), "Processes use many collector types", *Chemical Engineering*, vol. 58, no. 5, pp. 144-151.

Liu, B. Y. H., and Rubow, K. L. (1984), A new axial flow cascade cyclone for size characterization of airborne particulate matter. In: Liu, B. Y. H., Pui, D. Y., & Fissan, H. J. (Eds.), Aerosols (pp. 115-118). Amsterdam: Elsevier.

Lupo, J. C. (1989), "Defence applications of neural networks", *Communications Magazine, IEEE,* vol. 27, no. 11, pp. 82-88.

M-A Abia-Biteo Belope,R B Thorpe (2007) "Alba field three phase separator performance",BHR 13th International Conference on Multiphase Production Technology 13-15 2007 une Edinburg UK

M.A.HUSSAIN. and L.S.KERSHENBAUM (2000),"Implementation of an inverse-model-based control strategy using neural networks on a partially simulated exothermic reactor",Institution of Chemical Engineers Trans IChemE, Vol 78, Part A, March 2000

Marti, S., Erdak, F. and Shoham (1996), "Analysis of Gas Carry-Under in Gas-Liquid Cylindrical Cyclones", *Hydrocylone 96,* 2-4 April, St. John College, Cambridge, England, .

Matsui, G. (1984), "Identification of flow regimes in vertical gas-liquid two-phase flow using differential pressure fluctuations", *International Journal of Multiphase Flow*, vol. 10, no. 6, pp. 711-719.

Maynard, A. D. (2000), "A Simple Model of Axial Flow Cyclone Performance under Laminar Flow Conditions", *Journal of Aerosol Science*, vol. 31, no. 2, pp. 151-167.

Mothes, H. and Loffler, F. (1984), "Investigation of cyclone separator", *2nd International Conference on Hydrocyclone*, 19th -21st September, Bath, UK.

Movafaghian, S., Jaua-Marturet, J. A., Mohan, R. S., Shoham, O. and Kouba, G. E. (2000), "The effects of geometry, fluid properties and pressure on the hydrodynamics of gas–liquid cylindrical cyclone separators", *International Journal of Multiphase Flow*, vol. 26, no. 6, pp. 999-1018.

Nieuwstadt, F. T. M. and Dirkzwager, M. (1995), "A Fluid Mechanics Model for an Axial Cyclone Separator", *Industrial & Engineering Chemistry Research*, vol. 34, no. 10, pp. 3399-3404.

Nist. (2003), "NIST / SEMATECH *e-Handbook of Statistical Methods"*, (http://www.itl.nist.gov/div898/handbook).

Olson, T. (1998), "Porosity and Permeability Prediction in Low-Permeability Gas Reservoirs From Well Logs Using Neural Networks", Society of Petroleum Engineers, SPE 3996485, pp. 563-572.

Oranje, I. L. (1990), "Cyclone-Type Separators Score High in Comparative Tests", *Oil and Gas Journal*, vol. 88, no. No. 4, pp. 54.

Pots, B. F. M. Bromilow, I. G. and Konijn, M. J. W. F. (1987), "Severe slug flow in offshore flowline-riser systems", *SPE Production Engineering*, SPE 13723, vol. 2, pp. 319-324.

Qazi, N. and Yeung, H. (2006) Remote access and monitoring of two phase flow rig using Web/WAP protocol. National Instruments: LabVIEW in the Curriculum Paper Contest, pp. 80-85

Rao, D. H. (1995), "Neural network in robotics and control: some perspectives", IEEE/IAS Proceedings of International Conference on Industrial Automation and Control (IA & C '95), pp. 451-456.

Rosa, E. S., França, F. A. and Ribeiro, G. S. (2001), "The cyclone gas-liquid separator: operation and mechanistic modeling", *Journal of Petroleum Science and Engineering*, vol. 32, no. 2-4, pp. 87-101.

Rousseau,R.W "Handbook of Separation Process Technolgy ,1987

Sandhya S. (2007), “Neural Networks for Applied Sciences and Engineering: From Fundamentals to Complex Pattern Recognition”, Published by CRC Press, ISBN 084933375X.

Schmidt, Z., Brill, J. P., Beggs, H. D. (1980) “Experimental study of severe slugging in a two-phase-flow pipeline-riser pipe system”. *SPE Journal*, vol. 20, no.5, pp 407-414, SPE 8306.

Shim, W. J. and Jo, C. H. (2000,), "Analysis of Pressure Fluctuations in Two-phase Vertical Flow in Annulus", *Journal of Industrial and Engineering Chemistry*, vol. 6, no. 3, pp. 167-173.

Shoham, O., Brill, J. P. and Taitel, Y. (1987), "Two-phase flow splitting in a tee junction-experiment and modelling", *Chemical Engineering Science*, vol. 42, no. 11, pp. 2667-2676.

Song, C. H., No, H. C. and Chung, M. K. (1995), "Investigation of bubble flow developments and its transition based on the instability of void fraction waves", *International Journal of Multiphase Flow*, vol. 21, no. 3, pp. 381-404.

Song, S. and Kouba, G. :. (2000), "Fluids Transport Optimization Using Seabed Separation", *ETCE2000/PROD-10051, ETCE/OAME 2000 Joint Conference*, Feb. 14-17, New Orleans, LA, .

Steeg, V. D. J. (1991), “Methods and apparatus for preventing slug growth in a pipe line”, Application at European Patent Office EP 0410522.

Sun, Z. and Zhang, H. (2008), "Neural networks approach for prediction of gas-liquid two-phase flow pattern based on frequency domain analysis of vortex flowmeter signals", *Measurement Science and Technology*, vol. 19, no. 1.

Taitel, Y. (1986), "Stability of Severe Slugging", *International Journal of Multiphase Flow*, vol. 12, no. 2, pp. 203-217.

Trappenberg, T., Ouyang, J. and Back, A. (2006), "Input variable selection: mutual information and linear mixing measures", *Knowledge and Data Engineering, IEEE Transactions on*, vol. 18, no. 1, pp. 37-46.

Tutu, N. K. (1984), "Pressure drop fluctuations and bubble-slug transition in a vertical two phase air-water flow", *International Journal of Multiphase Flow*, vol. 10, no. 2, pp. 211-216.

Walters, L. C., Soliman, H. M. and Sims, G. E. (1998), "Two-phase pressure drop and phase distribution at reduced T-junctions", *International Journal of Multiphase Flow*, vol. 24, no. 5, pp. 775-792.

Wang, S., Mohan, R. S., Kouba, G. E. and Shoham, O. (1998), "Design and Performance of Passive Control System for Gas-Liquid Cylindrical Cyclone Separators", *Journal of Energy Resources Technology*, vol. 120, no. 1, pp. 49-55.

Wang, S., Mohan, R. S., Shoham, O., Marrelli, J. D. and Kouba, G. E. (2000), "Control System Simulators for Gas-Liquid Cylindrical Cyclone Separators", *Journal of Energy Resources Technology*, vol. 122, no. 4, pp. 177-184.

White, A. C., Molnar, D. and Aminian, Mohaghegh, S. K., Ameri, S. and Esposito, P. (1995), "The application of ANN for zone identification in a complex reservoir", Proceeding of SPE Eastern Regional Conference, Morgantown, WV, SPE 30977.

Wyllie, M. W. J. (1995), "Apparatus for inserting into a conduit", Application for UK Patent no. GB19940014802 19940722.

Xie, T., Ghiaasiaan, S. M. and Karrila, S. (2003), "Flow Regime Identification in Gas/Liquid/Pulp Fibre Slurry Flows Based on Pressure Fluctuations Using Artificial Neural Networks", *Industrial & Engineering Chemistry Research*, vol. 42, no. 26, pp. 7017-7024.

Zhang Li-Peng, Li Li-Mei and Cai Chang-Nian, (1993), *Speech recognition using dynamic recognition neural network*.

Zhang, J., Martin, E. B., Morris, A. J. and Kiparissides, C. (1997), "Inferential estimation of polymer quality using stacked neural networks", *Computers & Chemical Engineering*, vol. 21, no. Supplement 1, pp. S1025-S1030.

Zhao, B. (2005), "Development of a new method for evaluating cyclone efficiency", *Chemical Engineering and Processing*, vol. 44, pp. 447–451.

Zhao, B. (2004), "A Theoretical Approach to Pressure Drop across Cyclone Separators", *Chemical Engineering & Technology*, vol. 27, no. 10, pp. 1105-1108.

Appendix A

Remote access and monitoring of two phase flow rig using WEB/WAP protocol

The Challenge

The latest wave in high speed networks and multimedia development is shaping new forms of teaching and learning. Following this trend new virtual learning environments are being developed where students are not just spectators but are participants of their own learning process. This emerging field of virtual education requires that students could access Laboratory remotely any time any where.

The Solution

The solution lies in the development of real time remote laboratories. Remote and virtual laboratories are becoming back bone of virtual learning environments. This project work has made it possible to access the real time lab experimental data live on internet and mobile.

Introduction

This project work has used internet technology both wired and wireless to give the solutions of the two problems of the same nature. One of the problems is related to remote control of the power plant industry and other is related to distant education. In both cases it is required that scientific instrument could be used remotely. The solution lies in the development of real time remote laboratories. Remote and virtual laboratories are becoming back bone of virtual learning environments.

The basic idea behind this project is to apply the latest wireless and internet communication protocol to access, control and analysis the process information from a distributed system. The distributed system can be a power plant, a test rig, a laboratory etc.

Application Architecture

The developed system is a real time on line data acquisition and data monitoring system that allows a remote user to access the process parameters from internet and

intranet using web browser or wireless devices. This application is developed by following client server multi tier architecture. The software architecture of the system consists of multiple servers like web server, Microsoft SQL server and Lab VIEW server all installed on a single PC running Windows XP as operating system. This PC is connected to the other users of the LAN via Ethernet card using TCP/IP protocol. This application utilizes WAP protocol in conjunction with TCP/IP protocol to relay process data and control information between test rig and remote client. Wireless mark up language along with Microsoft Dot network is used to create web and WAP pages. The LabVIEW data acquisition VI is published on internet using LabVIEW remote front panels. Figure 1 shows the application architecture.

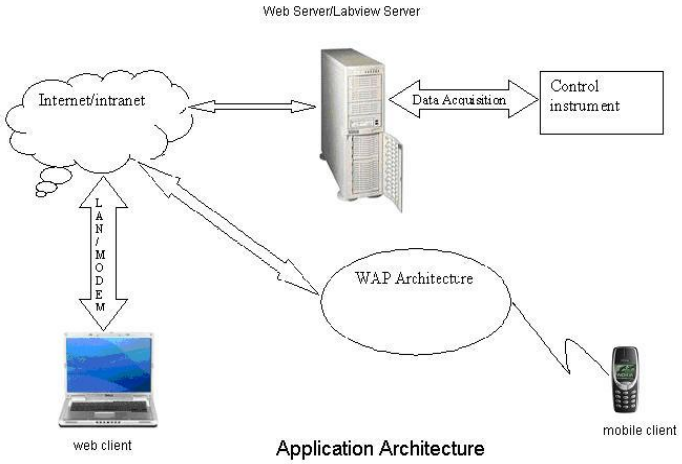

Figure 1 Application Architecture

System Features

This system provides following features:

- Live data access both numerically or graphically from any where any time using internet.
- Graphical analysis of the experimental data.
- Sending experimental data using Email to remote client.
- Any of measured process variable can be set to generate Alarms.
- Alarm notification via SMS and Email.

- Remote capturing the image of water flowing in the vertical pipe using wireless device and a web cam.
- Saving of the measured process variables in text file at following rate:
    - Every one second.
    - Every one millisecond.

The user of this system may be categorized in two categories depending upon the type of their accessing devices.

- Internet user accessing rig via internet.
- Wireless user accessing rig via mobile.

A login page as shown in Figure 2 is displayed asking user login and password. After successful login user is redirected to the option page giving the following three options:

- Live Data
- View History
- Log off

When user clicks the Live Data its request is transferred to the LabVIEW server and LabVIEW server displays the live data to remote users using remote front panel via TCP/IP. LabVIEW server should be running in order to access the rig. Users have options for alarm configuration depending upon the different numerical value of any process variables being measured. Alarm notification is sent to user via email. Figure 3 shows the remote front panel acquiring live data from the rig and displaying graphically on internet.

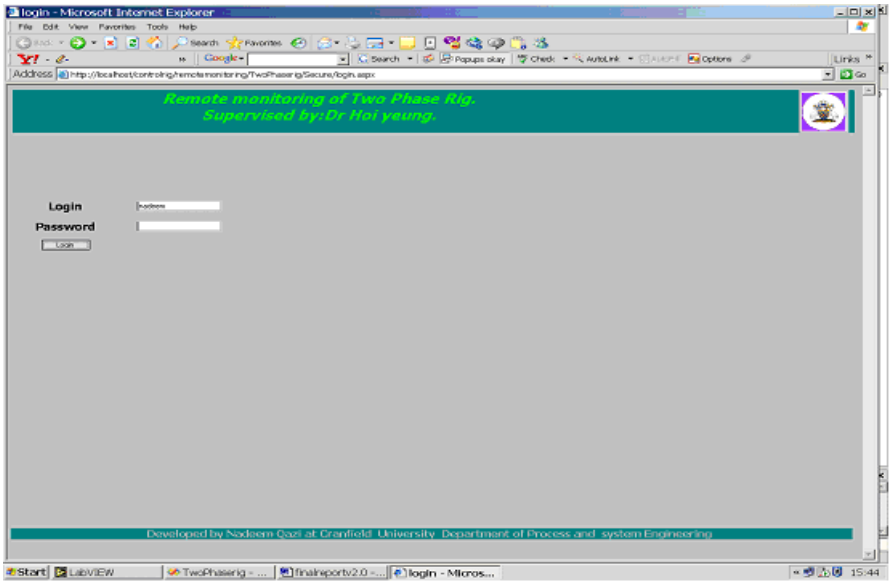

Figure 2 Login screen

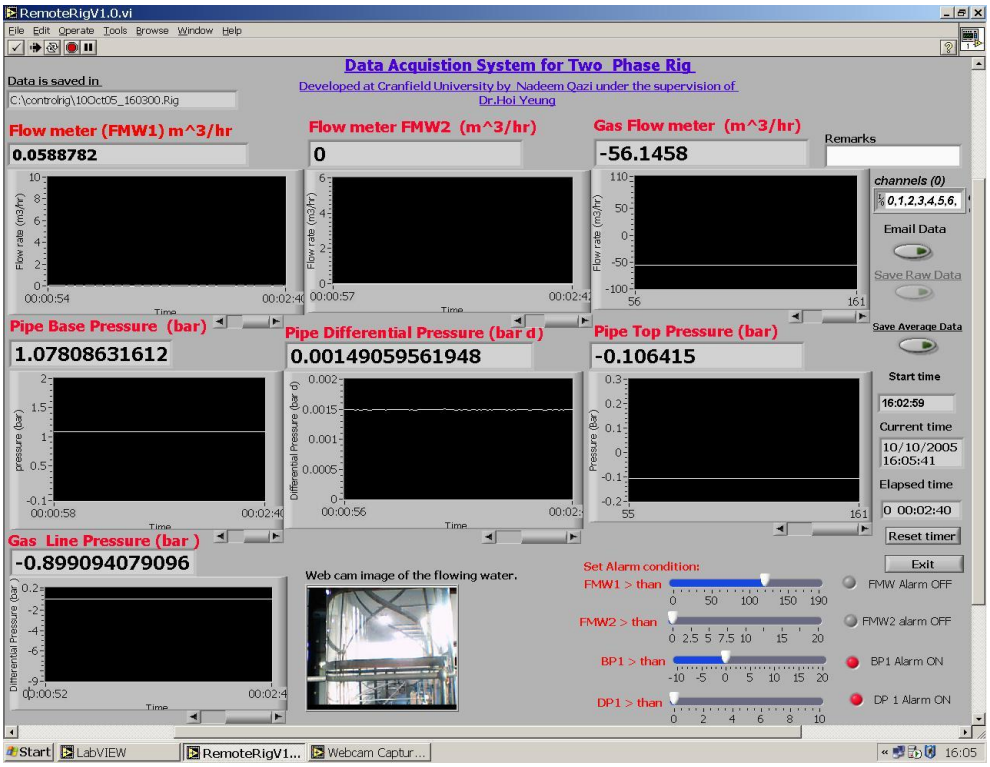

Figure 3 Remote Front Panel

Wireless user

A wireless internet client can access this system using PDA or mobile device via WAP browser. However he has limited options due to the small screen size of the devices. Mobile users can view the data numerically. However data can be viewed graphically using PDA. Alarm notification is sent to mobile user via SMS. On receiving the SMS mobile user can captured the image of the system remotely from their mobile by posting request to the WAP server. The mobile user request is then posted to web server and from here this requested is processed by the Lab VIEW VIs. This VI updates it responses to web server which then transmits this information back to the mobile user. Figure 1 shows how a request from a remote client is proceed.

The user interface for the WAP user is kept very simple due to mobile constraint. A user can request any time to access the acquire data. The numerical value of the current instant of the data would be displayed on the mobile phone. Figure 4 shows the options available for the mobile user while Figure 5 show the numerical value of the flow meter requested by a mobile user.

Figure 4 mobile user interfaces

Figure 5 Data display on mobile

Data Acquisition

It is buffered data acquisition application developed by using National Instrument LabVIEW Data acquisition VIs (virtual instrument). All the signals are acquired at a sampling frequency of 1000 Hz.

The Data acquisition of this system consists of a National instrument 12 bit E series (PCI- MIO 16 E-4) Data acquisition card, BNC 2090 accessory and Druck conditioning unit. BNC 2090 is used for its simplification in making connection between input signals and the DAQ board. All the pressure transducers and flow meters are connected to DAQ card via BNC connector as shown in Figure 6. One flow meter is connected with serial port of the PC using serial communication RS 232 protocol. A USB web cam is used for capturing the images of the flowing liquid in the vertical pipe.

The pressure variables are measured by using the pressure transducers, differential pressure transducers all of them are from Druck giving 0 to 5 volt DC signal. An electromagnetic flow meter is used for measuring flow rate of water and a vortex flow meter is used for measuring flow rate of air. The raw signal received from the sensing

devices i.e. flow meters pressure transducers and differential pressure transducer is converted to their corresponding physical quantity. All these sensing devices are first calibrated by plotting a calibration curve between the physical quantities i.e. pressure or flow rate and their corresponding voltage.

The second important task after the data acquisition is to publish this data live on internet. LabVIEW offers two solutions for this job. These are Data sockets and remote front panel. Both of them use TCP/IP to transfer the data across the network. The benefit of using remote front panel monitor is that it requires installation of Lab View run time engine at client machine to view this front panel remotely. On the other hand data sockets require full development environment whether it is LabVIEW or another programming language like Visual Basic. These remote front panels allow multiple users to view and control the VI front panels remotely from LabVIEW or from a web. Thus remote front panels are used to publish live data on internet. The data refresh rate is kept at 1 sec in order to minimize the network traffic. Figure 6 shows the Data acquisition architecture of the system.

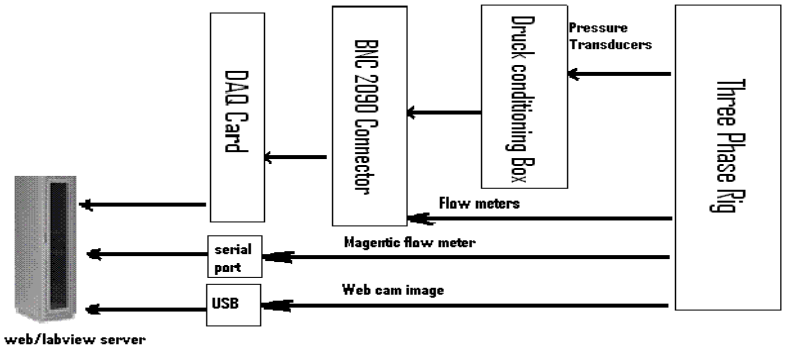

Figure 6 DAQ from Rig

Conclusion

The work developed during this research should be further extended to create real time virtual learning environment for performing real time experiments and analysis.

The provider of such virtual learning environment would be paid for the use of their facilities and user of such system would save their cost in term of building and maintaining the laboratory experiment. However the development of such a real time learning environment would in itself require a great deal of research from the perspective of ubiquitous computing and virtual reality.

Appendix B

Definitions: Below are some of the definitions used in the earlier sections of the thesis (Nist, 2003):

Mean

The mean (x) is defined as the arithmetic average value of the data points. It estimates the value around which a central clustering of data points occurs. It is expressed in mathematical terms as:

$$\bar{x} = \frac{\sum_{i=1}^{N} x_i}{N}$$

Where x is the amplitude value of the i_{th} data point and N represents the total number of points in the sampled record.

Standard Deviation

The standard deviation of the data set is the root mean square of the amplitude deviations from the arithmetic mean and is effectively a measure of the spread of the data. Mathematically, the standard deviation (SD) can be expressed by:

$$SD = \sqrt{\frac{\sum_{i=1}^{N} (x_i - \bar{x})^2}{(N-1)}}$$

Skewness

The skewness characterises the degree of asymmetry exhibited by a distribution around its mean. A positive skewness corresponds to a distribution with a greater number of large values for the parameter than one would expect if the distribution was Gaussian. Conversely, a negative value for the skewness implies a higher occurrence of smaller values. For a Gaussian distribution, the skewness is zero. The skewness is defined by the equation shown below:

$$Skewnes = \frac{\sum_{i=1}^{N} (x_i - \bar{x})^3}{(N-1) \times SD^3}$$

Kurtosis

The kurtosis characterises the degree of 'peakedness' exhibited by a distribution in comparison to that of a classical Gaussian distribution. A positive value of kurtosis

corresponds to a distribution with a greater extent of 'peakedness' than a normal distribution. On the other hand, a negative value for the kurtosis implies a lesser degree of 'peakedness'. For a Gaussian distribution, the kurtosis is 3. Mathematically, the kurtosis can be expressed as:

$$Kurtosis = \frac{\sum_{i=1}^{N}(x_i - \bar{x})^4}{(N-1)\times SD^4} - 3$$

Correlation coefficient

It is also called as linear correlation coefficient represented by r, used to measure the strength and the direction of a linear relationship between two variables. The mathematical formula for computing *r* is:

$$r = \frac{\sum_{i=1}^{N}(x_{1i} - \bar{x}_1)\cdot(x_{2i} - \bar{x}_2)}{\sqrt{\sum_{i=1}^{N}(x_{1i} - \bar{x}_1)^2 \cdot \sum_{i=1}^{N}(x_{2i} - \bar{x}_2)^2}}$$

The value of r is such that $-1 \leq r \leq +1$. The + and – signs are used for positive linear correlations and negative linear correlations, respectively.

Positive correlation: Positive values of r indicate a direct relationship between *x* and *y* variables which mean increasing value of x would also cause to increase the value of the y. The strong positive linear correlation between x and y is indicated by values of r more close to +1. A correlation greater than 0.8 is generally described as *strong*, whereas a correlation less than 0.5 is generally described as *weak.*

Negative correlation: Negative values of r indicate an inverse relationship between *x* and *y* variables which mean increasing value of x would cause to decrease the value of the y. The strong negative linear correlation between x and y is indicated by values of r more close to -1.

No correlation: A value of r equal to zero indicates that there is no relationship exists between x and y.

Appendix C